WestminsterResearch
http://www.westminster.ac.uk/westminsterresearch

The Adenylate-Uridylate-Rich element RNA binding protein ZFP36L1 suppresses replication stress-induced genomic instability

Sidali, A.

A PhD thesis awarded by the University of Westminster.

© Dr Ahmed Sidali, 2023

https://doi.org/10.34737/w2165

The WestminsterResearch online digital archive at the University of Westminster aims to make the research output of the University available to a wider audience. Copyright and Moral Rights remain with the authors and/or copyright owners.

The Adenylate-Uridylate-rich element RNA binding protein ZFP36L1 suppresses replication stress-induced genomic instability

Ahmed Sidali

A thesis submitted in partial fulfilment of the
requirements of the University of Westminster
for the degree of Doctor of Philosophy

December 2022

Abstract

The RNA binding protein (RBP) ZFP36L1, which binds to adenylate/uridylate (AU)-rich elements (AREs) (AU-RBP) in the 3' untranslated region of many messenger RNAs, has been extensively characterised for its role in post-transcriptional control of gene expression and is reported as a newly identified cancer driver gene. Replication stress (RS) threatens DNA replication fidelity and stability of the genome. Recently, a small number of AU-RBPs have emerged as key figures in the maintenance of genome integrity through mechanisms that govern the replication stress response and DNA repair. Herein, we report that treatment with low doses of aphidicolin results in hallmarks of RS-associated genomic instability in a cellular model depleted of ZFP36L1 using CRISPR/Cas9. We find that loss of ZFP36L1 results in defects in mitosis leading to chromosome segregation errors and genomic instability. Remarkably, we also identify loss of ZFP36L1 increases the prevalence of FANCD2-associated anaphase ultra-fine bridges indicating chromatid non-disjunction at intrinsically labile common fragile site loci. Furthermore, we detected an increase in RPA and γH2AX foci in S/G2 cells indicative of replication stress-induced DNA damage potentially indicating chronic replication fork stalling and double-strand break formation as demonstrated by increased γH2AX foci colocalising with 53BP1. Surprisingly, chromatin enrichment of U-2OS, HCT116 and Hela cells demonstrated that ZFP36L1 is physically bound to chromatin fractions. Here we also demonstrated the specificity of CRISPR-Cas9 mediated ablation of ZFP36L1 through the inducible expression of ZFP36L1 that demonstrated suppression of 53BP1 nuclear bodies (NBs) and micronuclei formation. Importantly, we demonstrate, by overexpression of a catalytically inactive mutant of human RNase H1 tagged with GFP that loss of ZFP36L1 induces R-loop formation. We also implicate unscheduled R-loop formation as a potential cause for replication stress associated genomic instability through the expression of wild-type RNase H1 which was able to limit the occurrence of 53BP1 NBs in G1 phase cells and RPA in S/G2 phase cells. Finally, we highlight potential ZFP36L1 interactions through mass spectrometry that uncover proteins involved in the maintenance of genome integrity and R-loop resolution. Taken together, our work highlights an important, yet previously unidentified role, for ZFP36L1 in preserving genomic stability including limiting the formation of R-loops in response to replication stress.

Table of Contents

1. INTRODUCTION 10

1.1 Key processes determine the fate of mRNA 11
  1.1.1 *Trans-acting* adenylate/uridylate-rich element RNA binding proteins . 12
  1.1.2 Classification of AREs 15
1.2 The ZFP36 family of AU-RBPs are key players in mRNA decay 17
  1.2.1 History of the ZFP36 family 17
  1.2.2 The ZFP36 family protein structure 20
  1.2.3 ZFP36 family are key mediators of mRNA destabilisation and decay...... 25
1.3 Post-translation modifications of the ZFP36 family: focus on phosphorylation 28
1.4 Subcellular trafficking and location-specific roles of the ZFP36 family 32
1.5 Expression of the ZFP36 family in normal human tissues 36
1.6 ZFP36 family target mRNAs regulate diverse physiological functions............ 39
  1.6.1 Immune response and immune cell development 39
  1.6.2 Cellular proliferation through cell cycle regulation 40
1.7 The ZFP36 family and disease: focus on cancer 41
1.8 AU-RBPs are key regulators of genome integrity 51
  1.8.1 Regulation of replication and faithful genome duplication 51
  1.8.2 The Eukaryotic DNA Damage response network 56
  1.8.3 AU-RBPs post-transcriptionally regulate key DDR genes 60
  1.8.4 DNA damage stimulates PTMs of AU-RBPs 65
  1.8.5 DNA damage orchestrates AU-RBP subcellular localisation 67
  1.8.6 Emerging role of AU-RBPs in DNA repair 68
  1.8.7 AU-RBP's association with R-loops 69
1.9 Study aim 74

2. MATERIALS AND METHODS 76

2.1 Cell lines and cell culture details 76
2.2 ZFP36L1 sgRNA plasmid construction 77
  2.2.1 ZFP36L1 guide RNA design 77
  2.2.2 Construction of sgRNA oligo duplex and ligation into PX459.................. 78
2.3 CRISPR-Cas9 targeting of *ZFP36L1* 79
2.4 Screening and validation of *ZFP36L1* mutants 80
  2.4.1 *ZFP36L1* Indel screening by agarose gel electrophoresis 80
  2.4.2 Analysis of ZFP36L1 protein expression in monoclones.......................... 81
  2.4.3 Indel verification of ZFP36L1 KO cells by amplicon sequencing.............. 83
2.5 Growth curve analysis... 84
2.6 Micronuclei, anaphase bridges and lagging chromosomes 84
2.7 Immunofluorescence assays 85
2.8 Metaphase spread preparation 87
2.9 Flow cytometry 89
  2.9.1 Cell cycle analysis 89
  2.9.2 Apoptosis assay 89
2.10 Generation of a ZFP36L1 tetracycline-inducible cell line 90
  2.10.1 Plasmid construction 90

2.10.2 Generation of a stable cell line 93
2.10.3 ZFP36L1 KO phenotype rescue 93
2.11 R-loop assays 94
2.11.1 Plasmids 94
2.11.2 Western blot detection of inducible RNase H1 expression 94
2.11.3 Detection of R-Loops 95
2.11.4 Impact of R-loops on 53BP1 NB formation in ZFP36L1 KO cells 95
2.12 Isolation of chromatin and soluble proteins 96
2.13 Mapping the ZFP36L1 interactome 97
2.13.1 Constructing a tetracycline-inducible expression plasmid encoding FLAG-StrepII in frame with ZFP36L1 97
2.13.1 Immunoprecipitation of FLAG-StrepII-ZFP36L1 for proteomic analysis. 98
2.13.2 Mass spectrometry detection of proteins 99
2.14 Statistical analysis 100
2.15 Analysis of Immunofluorescence assays 100

3. GENERATION OF A TETRACYCLINE-INDUCIBLE (T-REX) ZFP36L1 KNOCK-OUT MODEL UTILISING CRISPR-CAS9 TECHNOLOGY 101

3.1 Introduction 101
3.2 Construction of an all-in-one CRISPR-Cas9/sgRNA expression plasmid targeting *ZFP36L1* 106
3.3 CRISPR-Cas9/*ZFP36L1* sgRNA expression plasmid delivery into T-REx U-2OS cells 109
3.4 Testing editing efficiency at the CRISPR-Cas9 *ZFP36L1* target site by genomic PCR amplification screens 110
3.5 Protein expression analysis of ZFP36L1 mutants 112
3.6 NGS analysis of ZFP36L1 KO T-REx U-2OS cellular model 113
3.7 CRISPR-Cas9 mediated ablation of ZFP36L1 reduces growth rate in T-REx U-2OS cells 116
3.8 Discussion 117

4. LOSS OF ZFP36L1 CONTRIBUTES TO CHROMOSOMAL SEGREGATION IMPAIRMENTS AND GENOMIC INSTABILITY IN RESPONSE TO REPLICATION STRESS 122

4.1 Introduction 122
4.2 Loss of ZFP36L1 results in aberrations on metaphase chromosomes 127
4.3 Loss of ZFP36L1 results in chromosome segregation defects during conditions of replication stress 129
4.4 Loss of ZFP36L1 results in CFS-specific chromatid non-disjunction 132
4.5 Loss of ZFP36L1 increases micronuclei formation 135
4.6 Loss of ZFP36L1 results in DNA lesions sequestered by 53BP1 nuclear bodies in G1 cells 137
4.7 Discussion 140

5. LOSS OF ZFP36L1 LEADS TO RECRUITMENT OF DNA DAMAGE RESPONSE AND REPAIR PROTEINS UNDER REPLICATION STRESS CONDITIONS 143

5.1 Introduction 143
5.2 Loss of ZFP36L1 induces RPA accumulation in S/G2 cells 146
5.3 Loss of ZFP36L1 increases γH2AX foci in S/G2 phase cells 149

5.3 ZFP36L1 is required to limit replication stress-induced DSBs 152
5.5 Ablation of ZFP36L1 increases S-phase cells and CHK1 phosphorylation in response to low dose APH 155
5.6 Loss of ZFP36L1 does not induce apoptosis in APH -induced replication stress conditions 159
5.7 ZFP36L1 exhibits chromatin binding in human cells 161
5.8 Discussion 164
6. GENETIC COMPLEMENTATION REVERSES PHENOTYPIC ABNORMALITIES ASSOCIATED WITH LOSS OF ZFP36L1 IN T-REX U-2OS CELLS 170
6.1 Introduction 170
6.2 Generation of stable inducible expression system of ZFP36L1 172
6.3 Tetracycline-induced expression of ZFP36L1 limits micronuclei formation in ZFP36L1 KO cells 176
6.4 Tetracycline-induced expression of ZFP36L1 suppresses 53BP1 NB formation in ZFP36L1 KO cells 180
6.5 Discussion 183
7. LOSS OF ZFP36L1 INDUCES REPLICATION STRESS ASSOCIATED R-LOOP FORMATION 186
7.1 Introduction 186
7.2 Loss of ZFP36L1 increases replication stress-associated R-loop formation 188
7.3 R-loops contribute to replication stress associated 53BP1 NBs in ZFP36L1 abolished cells 191
7.4 R-loop resolution suppresses RPA accumulation in S/G2 cells in ZFP36L1 abolished cells 195
7.5 Discussion 198
8. MAPPING THE ZFP36L1 INTERACTOME 201
8.1 Introduction 201
8.2 IP-MS identifies multiple novel ZFP36L1 interactors 201
8.3 Discussion 207
9. GENERAL DISCUSSION 209
10. CONCLUSION AND FUTURE WORK 221
11. APPENDICES 222
12. GLOSSARY 236
13. BIBLIOGRAPHY 239

Table of Figures

Figure 1.1.1. Organisation of RNA binding domains in AU-RBPs 15
Figure 1.2.2A. Predicted 3D structure of full-length ZFP36L1 and CCCH-Zinc finger domains. 21
Figure 1.2.2B Sequence conservation across ZFP36 family protein domains 24
Figure 1.2.3 Mechanisms of decay for ARE-containing mRNA by the ZFP36 family. 28
Figure 1.3 Phosphorylation sites of ZFP36 family members and phosphorylation site conservation in other members respective to ZFP36. 31
Figure 1.4 Subcellular localisation of the ZFP36 family. 36
Figure 1.5 Protein expression of ZFP36 family across different human tissue types. 38
Figure 1.7 Reported ZFP36L1 association with cancers. 42
Figure 1.8.1 DNA replication in eukaryotes. 53
Figure 1.8.2A AU-RBPs coordinate the replication stress response. 58
Figure 1.8.2B AU-RBPs coordinate the DNA double strand-break response network. 59
Figure 1.8.3 Genotoxic stress facilitates post-transcriptional gene expression of DDR genes by AU-RBPs. 64
Figure 1.8.7 Emerging roles of AU-RBPs in R-loop prevention in response to replication stress. 71
Figure 3.1 Mechanisms of NHEJ and HDR following CRISPR-Cas9-mediated introduction of DNA double-strand breaks at the target site. 105
Figure 3.2 Scheme for targeted disruption of human *ZFP36L1* located on Chromosome 14: q24.11 using CRISPR-Cas9. 107
Figure 3.2.1 Construction of an all-in-one CRISPR-Cas9/sgRNA expression plasmid targeting *ZFP36L1*. 108
Figure 3.3 Experimental workflow from transfection to clonal expansion. 110
Figure 3.4 PCR amplification of target site of *ZFP36L1* gene in T-REx U-2OS cells. 111

Figure 3.5 Western blot screen for ZFP36L1 mutants. 112
Figure 3.6 NGS analysis of the ZFP36L1 KO T-REx U-2OS cellular model 116
Figure 3.7 CRISPR-Cas9 ablation of ZFP36L1 in T-REx U-2OS cells exhibits a reduced growth rate. 117
Figure 4.1 Characteristics of replication stress-induced chromosomal segregation defects and genomic instability in human cells. 126
Figure 4.2 Loss of ZFP36L1 results in chromosome aberrations. 129
Figure 4.3 Loss of ZFP36L1 results in chromosome segregation defects in response to replication stress. 131
Figure 4.4 Loss of ZFP36L1 results in CFS-specific chromatid non-disjunction. 135
Figure 4.5 Loss of ZFP36L1 results in the formation of micronuclei. 137
Figure 4.6 Loss of ZFP36L1 results in DNA lesions sequestered by 53BP1 nuclear bodies in the G1 phase. 139
Figure 5.1 Causes and consequences of replication stress. 145
Figure 5.2 Loss of ZFP36L1 increases RPA accumulation in S/G2 cells. 149
Figure 5.3. Loss of ZFP36L1 increases γH2AX foci in S/G2 phase cells. 152
Figure 5.4 ZFP36L1 is required to limit replication stress-induced double-stranded DNA breaks (DSB). 155
Figure 5.5 Ablation of ZFP36L1 increases S-phase population and induces low CHK1 phosphorylation in response to low dose APH. 158
Figure 5.6 Loss of ZFP36L1 does not induce apoptosis in response to low-dose APH. 160
Figure 5.7 ZFP36L1 expression in chromatin fractions is influenced during episodes of mild replication stress. 163
Figure 6.2A Inducible expression of exogenous ZFP36L1 in ZFP36L1 KO cells. 173
Figure 6.2B Stable inducible expression of ZFP36L1 in ZFP36L1 KO cells. 175
Figure 6.3 Tetracycline-induced expression of ZFP36L1 suppresses micronuclei formation. 179
Figure 6.4 Tetracycline-induced expression of ZFP36L1 suppresses 53BP1 NB formation. 183
Figure 7.1 Proteins involved in suppressing R-loop accumulation. 187
Figure 7.2 Loss of ZFP36L1 increases replication stress-associated R-loop formation. 190

Figure 7.3 Schematic representation of RNase H1 WT and mutant RNase H1 D210N and their action on RNA: DNA hybrids. 192
Figure 7.3.1 R-loops contribute to replication stress-associated 53BP1 NBs in ZFP36L1 abolished cells. 194
Figure 7.4. R-loop resolution suppresses RPA accumulation in S/G2 cells in ZFP36L1 abolished cells. 198
Figure 8.2 Confirmation and enrichment of ZFP36L1 with anti-flag magnetic beads for proteomic analysis.. 203
Figure 9. Proposed model for ZFP36L1's role in maintaining genome integrity in conditions of replication stress. 211

List of Tables

Table 1. Most characterised AU-RBPs in eukaryotes...13

Table 2. Classification of AU-rich elements and a brief overview of ARE-containing mRNAs...16

Table 3. The ZFP36 family in multiple cancer types...47

Table 4. Common inhibitors of DNA replication...54

Table 5. Antibodies utilised for ZFP36L1 mutant screen by western blot................83

Table 6. List of antibodies used for immunofluorescence assays........................... 86

Table 7. Table listing proteins present in FLAG-StrepII-ZFP36L1 eluates with a peptide score <1 in FLAG-EV control...197
.

Acknowledgements

I would first like to begin by saying Alhamdullilah for the opportunity to conduct this PhD programme.

I would like to spread my deepest thanks to my supervisors Dr Kalpana Surendranath and Dr John Murphy. To Dr Kalpana who placed faith in me from the first moment, I walked into her office during my master's programme. We have been through a long testing journey but without your belief in me, I would not have evolved into the person I am today. Dr Kalpana Surendranath instilled resilience in me that I will be eternally grateful for, and she continues to mould the future generation of aspiring young scientists. To Dr John Murphy for his continued support and indispensable advice throughout my PhD journey. My deepest gratitude to Dr Kanagaraj Radhakrishnan for the training, guidance, and expert knowledge in the field of replication stress. His training pushed the boundaries to what I could truly accomplish as a researcher, and I will be forever grateful. I would like to also thank Dr Emmanuella Volpi for her support starting from my undergraduate journey to a PhD graduate. I thank Dr Alastair Barr whose feedback was pivotal throughout my PhD journey and for his valuable discussion and feedback during my viva. Lasty, thank you to Dr Nitika Taneja for her expert knowledge and discussion during my viva.

To my mum who supported me during this journey and my grandmother who I lost during my PhD, I hope I have made you proud parents. Finally, a message to my wife Gerta and beautiful children Adam and Aiyla you have given me a purpose in life, and I strive to give you a brighter future. Through, my PhD journey they have sacrificed so

much and without them, I would not have made it this far. I hope daddy has made you proud.

Author declaration

I declare that all the material contained in this thesis is my own work.

1. Introduction

Gene expression is a tightly controlled mechanism coupled to factors associated with transcription and through post-transcriptional regulatory pathways (Cramer, 2019) (Reviewed in Corbett, 2018). Post-transcriptional mechanisms can be divided into processes that promote the translation of messenger RNA (mRNA) or processes that ensure a fine balance between the rate of transcription and mRNA degradation. RNA-binding proteins (RBPs) are key players in regulating gene expression at the post-transcriptional level (Glisovic et al., 2008). RBPs have been identified across multiple species, demonstrating a diverse repertoire of functions responding to specific cellular signalling. Large-scale studies and quantitative methods utilising approaches such as next-generation sequencing and modern protein mass spectrometry have enabled the identification of over 1500 RBPs (Castello et al., 2012; Kwon et al., 2013; Gerstberger, Hafner and Tuschl, 2014; Brannan et al., 2016). RBPs can interact with numerous proteins and classes of RNA, such as mRNA, non-coding RNA (ncRNA), small nuclear RNAs (snRNAs) and transfer RNA (tRNA), forming large ribonucleoprotein (RNP) complexes (Gerstberger, Hafner and Tuschl, 2014). The diverse interactions of RBPs enable the recruitment of numerous factors, forming large protein complexes to modulate the fate and function of RNA (Hong, 2017; Hentze et al., 2018).

Conventionally, RBPs play a primary role in post-transcriptional regulatory mechanisms that determine the maturation and half-life of mRNA. Post-transcriptional RNA processing by RBPs is mediated through interactions with various regions located on RNA transcripts, such as coding sequences within introns and exon domains, 5’ untranslated regions (5’ UTR) and 3’ untranslated regions (3’ UTR) of mRNA. Such interactions moderate the subsequent fate of RNA including splicing and polyadenylation of pre-mature RNA (pre-mRNA) in the nucleus and mRNA localisation, stability, translation, and degradation within the cytoplasm (Phillips, Ramos and Blackshear, 2002). RBPs that regulate post-transcriptional events through sequence-specific interactions with adenylate/uridylate rich elements (ARE) in the 3'UTR are classified as AU-RBPs (adenylate/uridylate rich element RNA binding proteins) (Baou, Jewell and Murphy, 2009). Importantly, AU-RBPs have emerged as important regulators of a plethora of physiological processes and defects to AU-RBPs have been implicated in cellular dysfunction and cancer hallmarks such as genomic instability (Hanahan and Weinberg, 2011; Reviewed in Otsuka et al., 2019).

1.1 Key processes determine the fate of mRNA

Mechanisms of mRNA decay are critical for gene expression (Ghosh and Jacobson, 2010). Regulatory sequences located in mRNAs known as *cis*-acting elements, often located within the 5’ UTR and 3’UTR untranslated regions (UTR) enable the functional organisation of multi-subunit complexes by *trans*-acting factors such as RBPs (García-Mauriño et al., 2017). These regulatory sequences located within the 3’UTR often determine mRNA stability, subcellular location, and translation (García-Mauriño et al., 2017). Furthermore, *cis*-acting elements’ length and sequence pattern in the 3’UTR influence mRNA half-life (Khabar, 2005). However, the final fate of mRNA is determined through interactions of specific *trans*-acting factors bound to mRNAs.

1.1.1 *Trans-acting* adenylate/uridylate-rich element RNA binding proteins

Multiple *cis*-acting elements comprise the 3'UTR of mRNAs, such as poly (A) tail, GU-rich elements (GREs), iron-responsive elements (IREs) and adenylate/uridylate rich elements (AREs) (Otsuka et al., 2019; Rehfeld et al., 2013; Campillos et al., 2010; Halees et al., 2011). AREs are one of the predominant *cis*-acting elements in the 3'UTR of labile mRNAs (Matoulkova et al., 2012). Early reports estimated that 8% of all mRNA transcripts possess AREs (Bakheet, 2006). However, a comprehensive investigation of AREs revealed that 3275 protein-encoding genes contain a minimum of one ARE in their 3'UTR (Halees, El-Badrawi and Khabar, 2007). Moreover, analysis of intronic regions of human genes also identified that 9114 additional genes contained AREs (Gruber et al., 2010). These reports demonstrate that approximately 50% of human genes, some of which encode for components involved in a variety of physiological processes such as signalling, transcription, proliferation, immune response, development, proto-oncogenes, and tumour suppressors, contain AREs and require tight regulation by *trans*-acting AU-RBPs (Bakheet, Hitti and Khabar, 2017). mRNA-containing AREs are specifically recognised by *trans*-acting factors known as AU-RBPS, that have also been described as turnover and translation regulatory RNA-binding proteins (TTR-BPs) (Pullmann et al., 2007). AU-RBPs, like other RBPs, maintain their roles in mRNA processing, export from the nucleus, subcellular localisation, degradation, and translation. However, unlike other RBPs, the effect exhibited on specific mRNA transcripts largely depends on the regulatory function of the mRNA-bound AU-RBP (Baou, Jewell and Murphy, 2009; Gratacós and Brewer, 2010; Cammas et al., 2014). Balancing between counteracting factors that compete with AU-RBPs for ARE binding or co-activation of AU-RBPs due to protein-protein interactions determines mRNA stability (Cherradi et al., 2006; Hinman and Lou, 2008; Kedar et al., 2012). Therefore, AU-RBP bound mRNAs can either be stabilised increasing their translation or destabilised where they are subsequently degraded and translationally repressed. The most characterised AU-RBPs are listed in **Table 1.**

Table 1: Most characterised AU-RBPs in eukaryotes

Name (aliases) of AU-RBPs	**Function**	**RNA binding domain**	**Mechanism of stabilisation/decay**
AUF1 (HNRNBP, HNRPD)	Stabilising and destabilising	RRM	RNA remodelling; recruitment of exosome (Chen et al., 2001; Zucconi and Wilson, 2013).
HuR (ELAVL1)	Stabilising and Translation silencing	RRM	Competes for ARE binding sites against mRNA destabilising modulators (Tiedje et al., 2012).
TIA1 (TIA-1)	Translational silencing/enhancer	RRM	Relocalises mRNA into stress granules; Exchange of mRNAs from stress granules to polysomes (Kedersha et al., 2000; Díaz-Muñoz et al., 2017).
TIAR (TIAL1)	Translational silencing	RRM	Relocalises mRNA into stress granules (Anderson and Kedersha, 2002).
ZFP36 (TTP, TIS11)	Destabilising/ also reported stabilising role	CCCH-type zinc finger	Recruitment of mRNA decay machinery interacting with CCR4; PARN and human exosome RRP4 (Marchese et al., 2010; Lykke-

			Andersen and Wagner, 2005; Lai, Kennington and Blackshear, 2003).
ZFP36L1 (TIS11b)	Destabilising	CCCH-type zinc finger	Recruitment of mRNA decay machinery interacting with CCR4 and human exosome RRP4 (Chiu et al., 2022).
ZFP36L2 (TIS11d)	Destabilising	CCCH-type zinc finger	Recruitment of mRNA decay machinery interacting with CCR4 (Adachi et al., 2014).
KHSRP (KSRP)	Destabilising	KH-domain	Recruitment of mRNA decay machinery PARN and exosome (Briata et al., 2013; Gherzi et al., 2004)

AU-RBPs listed in table 1 have been identified as critical players in post-transcriptional gene regulation. RNA-binding domains (RBD) of AU-RBPs interact with ARE-containing mRNAs through specific motifs and secondary structures (Castello et al., 2016). Despite significant degrees of conservation in primary sequence, RBDs can vary in organisation, some, of which are biochemically and structurally characterised (Lunde, Moore and Varani, 2007; Castello et al., 2016). These include well-characterised canonical RBDs which are composed of RNA recognition motifs (RRM), K-homology (KH) domains and Zinc finger domains (ZFD) (Lunde, Moore and Varani, 2007). The functional repertoire of AU-RBPs is exemplified through their various interactions, for example, RRM motifs recognise RNA and can also interact with proteins, KH domains can bind single-stranded DNA (ssDNA) and single-stranded RNA (ssRNA) and ZFDs can bind DNA as well as RNA (Valverde, Edwards and Regan, 2008). Importantly, some AU-RBPs have multiple RBDs to provide specificity and affinity for their binding partners (Corcoran et al., 2011). Therefore, this structural diversity of AU-RBPs enables diverse interactions, enabling AU-RBPs to exhibit multifaceted functions.

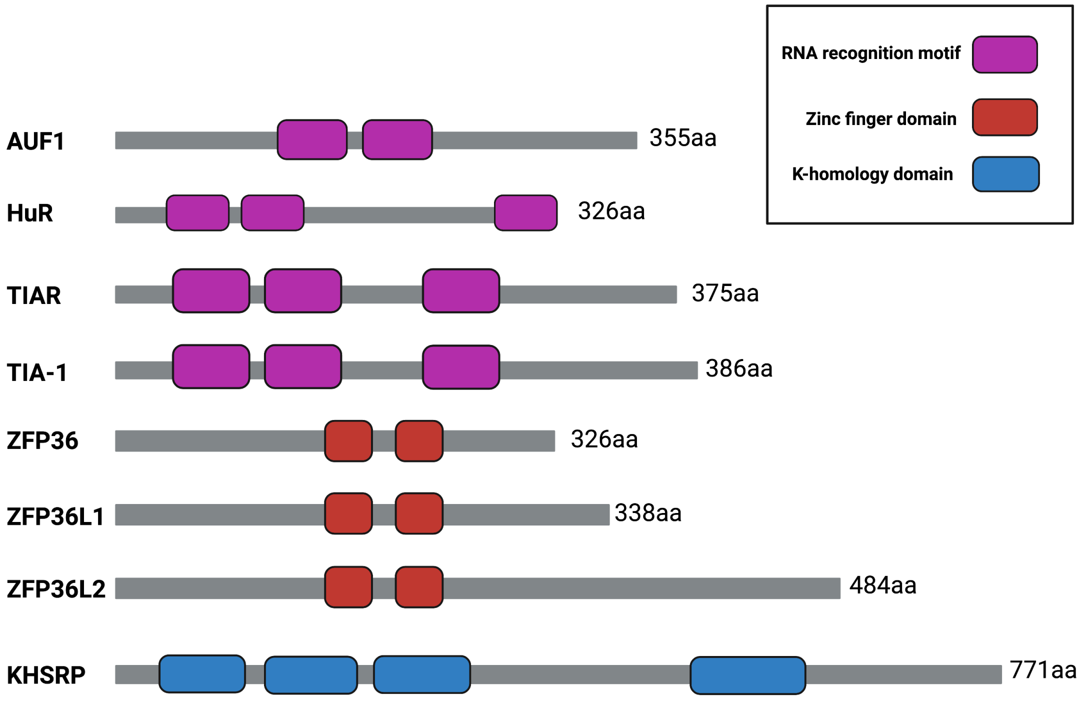
RNA recognition motif
Zinc finger domain
K-homology domain
AUF1
355aa
HuR
326aa
TIAR
375aa
TIA-1
386aa
ZFP36
326aa
ZFP36L1
338aa
ZFP36L2
484aa
KHSRP
771aa

Figure 1.1.1. Organisation of RNA binding domains in AU-RBPs
Examples of RBDs of well-known AU-RBPs. AU-RBPs contain different RBDs enabling dynamic interactions with mRNA substrates. Schematic representation of AUF1 composed of two RNA recognition motifs (RRM) (Purple), and HuR, TIAR and TIA-1 containing three RRMs. The ZFP36 family of AU-RBPs which include ZFP36, ZFP36L1 and ZFP36L2 contain two tandem Zinc finger domains (ZFD)(Red). AU-RBP KHSRP is composed of four K-homology domains (Created with Biorender.com).

1.1.2 Classification of AREs

As well as being intrinsically labile, the half-life of mRNAs containing AREs is short, usually up to a few hours (Barreau, 2005). mRNAs containing AREs vary in length based on adenylate uridylate-rich sequences that range from 40-150 nucleotides and are comprised of multiple copies of an AUUUA motif. The composition of AUUUA motifs within AREs are further divided into three classifications (Table 2). The first class of AREs belong to Class I which contain multiple AUUUA motifs flanked by U-rich sequences dispersed in the 3'UTR, usually located on mRNAs of transcription factors such as the nuclear phosphoprotein transcription factor MYC, that tightly regulate the cell cycle (Dang, 2012; Brewer, 1991). Class II AREs contain several pentamers of the AUUUA motif that overlap (Bakheet et al., 2018). Class II ARE examples are genes encoding cytokines such as tumour necrosis factor α (TNFα), Vascular endothelial growth factor (VEGF), or Granulocyte-macrophage colony-stimulating factor (GM-CSF). Lastly, class III AREs are less defined than class I and II AREs; they lack the AUUUA pentanucleotide but are U-rich and present in mRNA for transcription factor c-Jun (Wilusz, Wormington and Peltz, 2001). Significantly, all three classes of AREs can mediate the recruitment of mRNA decay machinery (Bakheet et al., 2018).

Table 2: Classification of AU-rich elements and a brief overview of ARE-containing mRNAs. TNFα (Tumor necrosis factor), VEGF (Vascular endothelial growth factor), and GM-CSF (Granulocyte macrophage-colony stimulating factor).

Classification	**Motif**	**mRNA examples**
Class I	Multiple AUUUA motifs flanked by U-rich dispersed in 3'UTR	Transcription factors e.g., MYC
Class II	Multiple, overlapping pentamers of the AUUUA motif	Cytokines e.g., TNFα, VEGF, GM-CSF
Class III	Absence of AUUUA pentanucleotide but are U-rich	c-jun

1.2 The ZFP36 family of AU-RBPs are key players in mRNA decay

1.2.1 History of the ZFP36 family

Timely and accurate regulation of gene expression is a fundamental process required to maintain a biological equilibrium. The family of zinc fingers containing AU-RBPs known as the Zinc finger proteins (ZFP) family, have been identified as imperative regulators of gene expression through post-transcriptional regulatory mechanisms and represent the most abundant protein superfamily in eukaryotes (Kim and Kini, 2017). The 14 families of ZFP proteins can be characterised based on structure and function. These families can be divided into subfamilies categorised by variation in the number of cysteine-histidine (C-H) repeats located within each zinc finger. The zinc finger protein 36 (ZFP36) subfamily (also identified as tristetraprolin (TTP), TIS11, TTP, NUP475, or GOS24), consists of four mammalian members ZFP36, zinc finger protein 36-like 1 (ZFP36L1) (also known as TIS11b, Berg36, ERF1, BRF1 or cMG1), zinc finger protein 36-like 2 (ZFP36L2) (also known as BRF2, ERF2, RNF162C or TIS11D) (DuBois et al., 1990; Lai, Stumpo and Blackshear, 1990; Taylor et al., 1991; Heximer and Forsdyke, 1993). Zinc finger protein 36-like 3 (ZFP36L3) is a fourth member that is placenta-specific and unique to mice and rats (Stumpo et al., 2016).

Early reports depicting full-length ZFP36 through cloning of ZFP36 mouse-derived complementary DNA (cDNA) from insulin-stimulated 3T3-L1 fibroblasts were initially described as a protein containing three proline repeats (pro-pro-pro-pro) and named tristetraprolin (TTP) (Lai, Stumpo and Blackshear, 1990). This initial description was followed by descriptions of the corresponding ZFP36 sequence and chromosome location in humans (Taylor et al., 1991). However, it is now accepted that the universal name for these protein members is ZFP36 (or TTP), ZFP36L1, and ZFP36L2. In contrast, the systemic name of the corresponding gene in mice is *Zfp36*, *Zfp36l1*, *Zfp36l2* and *ZFP36*, *ZFP36L1* and *ZFP36L2* in humans.

The physiological significance of the ZFP36 family of proteins was first demonstrated in ZFP36 knock-out (KO) mouse models that exhibited severe growth retardation, systemic inflammation, cachexia, and autoimmunity (Taylor et al., 1996). This was the earliest report to demonstrate a relationship between ZFP36 and the pro-inflammatory cytokine tumour necrosis factor alpha (TNFα), where ZFP36 KO mice treated with anti-TNFα antibodies prevented all defects attributed to loss of ZFP36 (Taylor et al., 1996). This observation was followed by reports of a link between ZFP36 and mRNA homeostasis. Specifically, ZFP36 KO macrophages displayed an abnormal increase of *TNFα* mRNA when stimulated with lipopolysaccharide (LPS), leading to hypersecretion of TNFα protein (Carballo, Gilkeson and Blackshear, 1997). The first physical interaction and role for ZFP36 in mRNA destabilisation were made by the same group. Specifically, Blackshear's lab demonstrated that ZFP36 interacts with AU-rich elements in *TNFα* mRNA to mediate destabilisation and inhibit TNFα expression (Carballo, Lai and Blackshear, 1998). These early reports resulted in the first clear link for ZFP36 in post-transcriptional control of gene expression. Subsequent work to characterise peptide-mRNA interactions revealed multiple conserved UUAUUUAUU binding sites in the 3'UTR of *TNFα* mRNA available for ZFP36 binding (Blackshear et al., 2003). Intriguingly, ZFP36L1 was discovered independently at a similar period to ZFP36. Initially, ZFP36L1 was described as an early-response gene whose expression can be transiently induced following growth factor stimulation in epithelial cells (Gomperts, Pascall and Brown., 1990). Sequencing of cDNA recombinants following growth factor stimulation identified a protein of 338 amino acids that shared 72% sequence homology over a 67-amino acid stretch to ZFP36 (Gomperts, Pascall and Brown., 1990). The discovery of ZFP36 and ZFP36L1 was quickly followed up by a report that identified another member of the mammalian ZFP36 family, ZFP36L2 (Varnum et al., 1991). ZFP36L2 was discovered through cDNA library screens in murine cells utilising degenerate oligonucleotide probes encoding highly conserved sequences from both ZFP36 and ZFP36L1, enabling the identification of a sequence of 67-amino acids in length that was found to be highly homologous to both ZFP36 and ZFP36L2 (Varnum et al., 1991). Although, the ZFP36 family members were identified to share sequence homology and act similarly as *trans*-acting factors in mRNA decay. Unlike early reports implicating germline knockout of *Zfp36* in mice resulting in systemic inflammatory syndrome (Taylor et al., 1996), further studies demonstrated that germline deletion of *Zfp36l1* and *Zfp36l2* in mice leads to vastly different phenotypes (Stumpo et al., 2009; Stumpo et al., 2004). Specifically, germline deletion of *Zfp36l1* was reported to be embryonic lethal in mice (Stumpo et al., 2004). Whereas deletion of *Zfp36l2* in mice results in death within two weeks following birth due to defects in haematopoiesis (Stumpo et al., 2009). Thus, these reports demonstrated that although the ZFP36 proteins share significant sequence homology their physiological functions vastly differ.

1.2.2 The ZFP36 family protein structure

The ZFP36 family members are characterised by their highly conserved tandem CCCH-zinc finger (TZF) domain located in between an N and C-terminal domain (Figure 1.2.2A). The TZF domain is composed of two CCCH zinc finger motifs and a lead in amino acid sequence (R/K)YKTEL). The TZF motifs consist of strict spacing in between zinc-binding residues CX8CX5CX3H (x being the variable amino acid) separated by an 18-residue long linker. The TZF domains enable RNA binding, characterising the ZFP36 family as RNA binding proteins (RBPs). All three members of the ZFP36 family share high sequence homology for the TZF domain enabling binding through recognition of adenylate/uridylate rich elements (AREs) (characteristically the heptameric sequence 5'UAUUUAU-3' for class II-AREs) in the 3'-UTR of mRNAs, initiating the formation of hydrogen bonds between mRNA bases, the TZF and their (R/K)YKTE(L) motifs, further sub-categorising the ZFP36 family as AU-RBPs. Mutations to one of the zinc finger motifs or a single mutation to one of the eight conserved amino acids abolish mRNA binding affinity (Lai, Kennington and Blackshear, 2002). For example, the substitution of cysteine (Cys) to arginine (Arg) in one of the zinc fingers motifs in ZFP36L1 leads to loss of mRNA binding and destabilisation (Stoecklin, 2002), possibly because of protein misfolding and destabilisation of the zinc finger domain (Figure 1.2.2A).

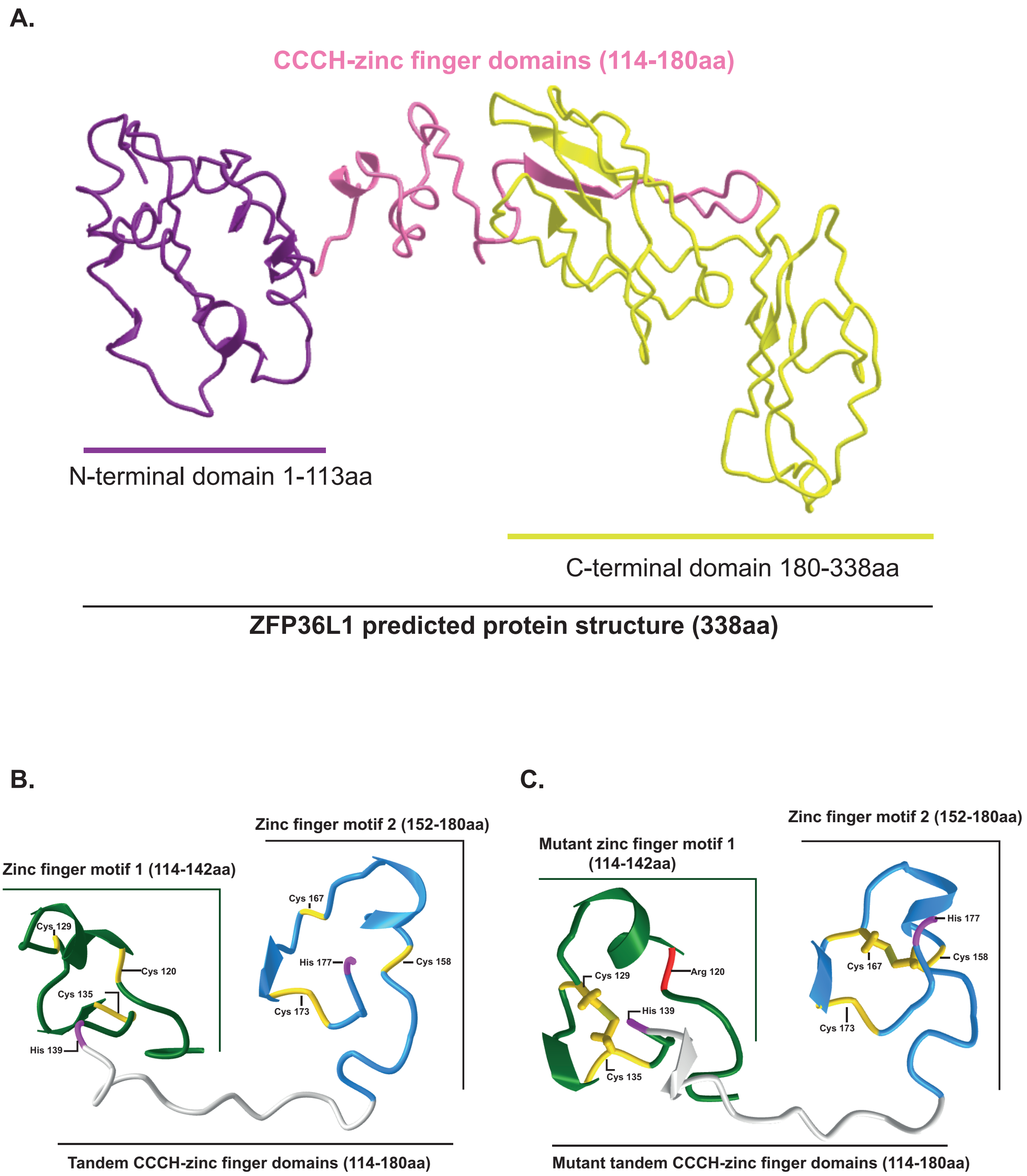
A.
CCCH-zinc finger domains (114-180aa)
N-terminal domain 1-113aa
C-terminal domain 180-338aa
ZFP36L1 predicted protein structure (338aa)
B.
Zinc finger motif 2 (152-180aa)
Zinc finger motif 1 (114-142aa)
Cys 167
Cys 129
Cys 120
His 177
Cys 158
Cys 135
Cys 173
His 139
Tandem CCCH-zinc finger domains (114-180aa)
C.
Zinc finger motif 2 (152-180aa)
Mutant zinc finger motif 1 (114-142aa)
His 177
Cys 158
Cys 167
Cys 129
Arg 120
His 139
Cys 173
Cys 135
Mutant tandem CCCH-zinc finger domains (114-180aa)

Figure 1.2.2A. Predicted 3D structure of full-length ZFP36L1 and CCCH-Zinc finger domains.

A. Predicted structure of full length ZFP36L1 with indicated N-terminal domain (1-113aa), CCCH-zinc finger domain (114-180aa) and C-terminal domain (180-338aa), Confidence score (C-score) =2.55, Template modelling-score (TM-score) =0.42±0.14 and RMSD-12.5±4.3 Angstroms (Å). **B**. 3D structure model of wild-type ZFP36L1 tandem CCCH-zinc finger domains (114-180aa), comprised of two zinc finger motifs: Zinc finger motif 1 (114-1142aa) (green) and Zinc finger motif 2 (152-180aa) (blue). Corresponding location of Cysteine (Cys) and histidine (His) residues are indicated in yellow and purple respectively; C-score=0.74, TM-score = 0.81±0.09 and RMSD = 1.8±1.5Å. **C**. Predicted 3D structure of mutant ZFP36L1 tandem CCCH-zinc finger domains following amino acid substitution of Cysteine to Arginine (Arg) (Red) at position 120 in Zinc finger motif 1; C-score=0.79, TM-score = 0.82±0.08 and RMSD = 1.8±1.5Å. All 3D models were generated using I-TASSER (Zheng et al., 2021) and annotated with NCBI iCn3D (Wang et al., 2019).

The TZF domain of all ZFP36 family members harbours two critical arginine (R) residues that comprise the nuclear localisation sequence (NLS) enabling translocation to the nucleus (Figure 1.2.2B) (Murata et al., 2002). A highly homologous stretch of 14 amino acids located in the C-terminal domain (CTD) comprises the nuclear export sequence (NES) for ZFP36L1 and ZF36L2 (Figure 1.2.2B). The same region within ZFP36 shares less sequence similarity to ZFP36L1 and ZFP36L2 and does not form ZFP36's NES (Figure 1.2.2B). Instead, ZFP36's NES is located within the N-terminal domain (NTD) (Figure 1.2.2B). The NES and NLS enable nucleo-cytoplasmic shuttling of all members of the ZFP36 family (Figure 1.2.2B) (Murata et al., 2002; Phillips, Ramos and Blackshear, 2002). Importantly, all members share the highly conserved motif known as the CNOT1 binding domain located within the C-terminus (Figure 1.2.2B) (Lai et al., 2019). In ZFP36L1 and ZFP36L2 the CNOT domain overlaps with the NES. The CNOT1 binding domain enables binding to the core subunit of the Ccr4/Caf1/Not deadenylase (CCR4-NOT) complex to mediate deadenylation of mRNA targets (Discussed in Section 1.2.3) (Lai et al., 2019). Another domain sharing high sequence homology in all members is located immediately downstream of the TZF domain comprised of the sequence PxLxxSxSFxGxPS (x represents a closely related family of amino acids) (Figure 1.2.2B). The functional significance of this domain remains largely unknown, however, ZFP36 and ZFP36L1 contain a binding site for the 14-3-3 protein (Schmidlin et al., 2004; Stoecklin et al., 2004). Sequence alignments suggest that ZFP36L1 and ZFP36L2 are of closer relation than ZFP36

(Figure 1.2.2B). Although, the ZFP36 family members contain regions with high sequence homology, notably in the TZF motifs. The presence of weaker protein homology outside the TZF motifs suggests that protein-protein interactions that lead to distinct functions of the individual members of the ZFP36 family could be attributed to these unrelated domains.

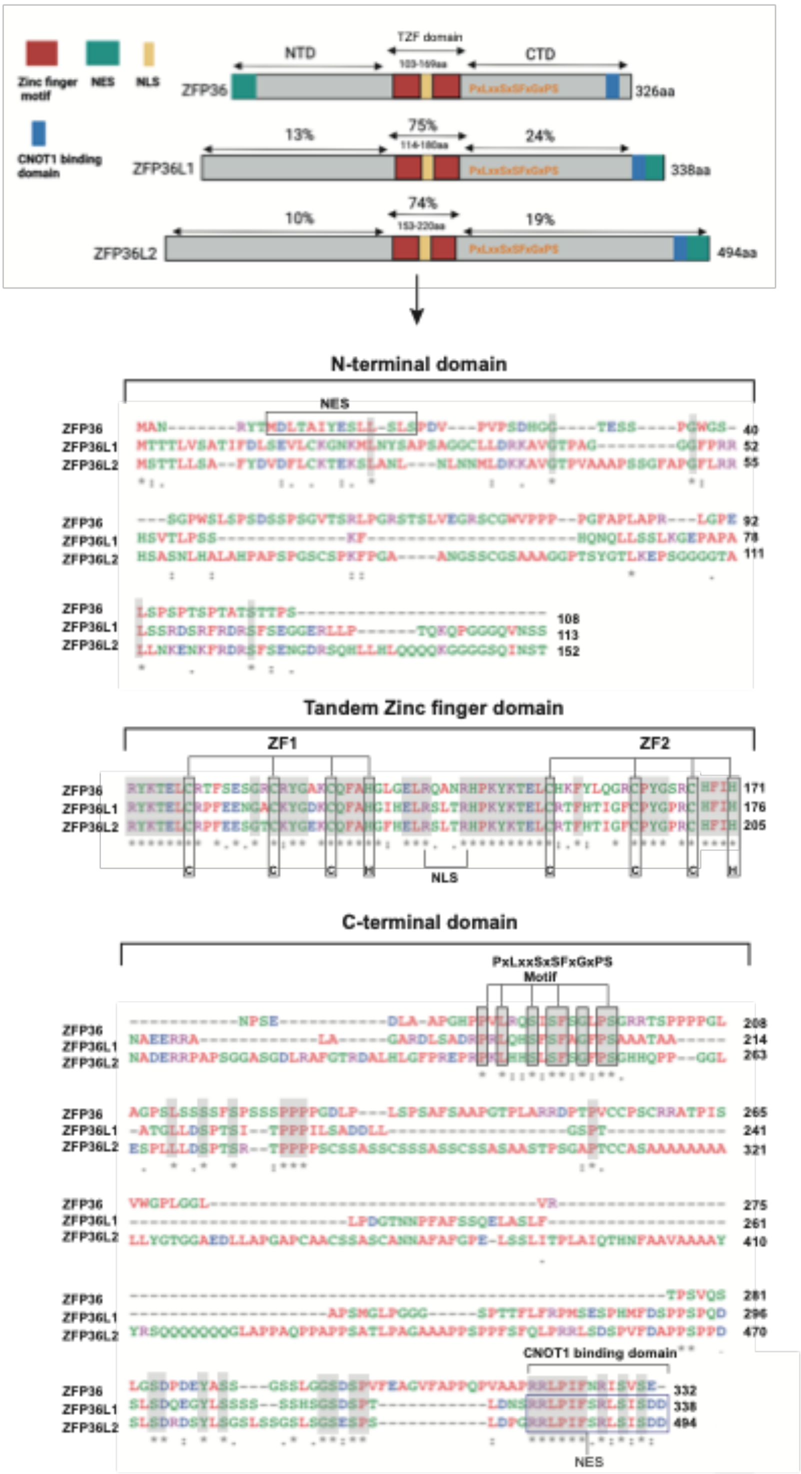
Zinc finger motif
NES
NLS
CNOT1 binding domain
NTD
TZF domain
CTD
ZFP36
326aa
PxLxxSxSFxGxPS
ZFP36L1
13%
75%
24%
338aa
ZFP36L2
10%
74%
19%
494aa
N-terminal domain
NES
Tandem Zinc finger domain
ZF1
ZF2
NLS
C-terminal domain
PxLxxSxSFxGxPS Motif
CNOT1 binding domain
NES

Figure 1.2.2B Sequence conservation across ZFP36 family protein domains
Schematic representation of ZFP36, ZFP36L1 and ZFP36L2 with domain similarities (%) respective to ZFP36. Domain features include an N-terminal domain (NTD), a tandem zinc finger (TZF) domain comprised of two zinc finger motifs (red) with an NLS located in between (yellow), a C-terminal domain (CTD) including nuclear export sequence (NES) (green), PxLxxSxSFxGxPS motif and the CNOT1 binding domain (blue). Clustal Omega alignment of N-terminal, tandem zinc finger and C-terminal

domain for human ZFP36 (CCDS ID: 12534.2), ZFP36L1(CCDS ID: 9791) and ZFP36L2 (CCDS ID: 1811) grey boxes/stars indicate conserved sequences. The NES for ZFP36 is indicated (Box) in the CTD alignment. Zinc finger 1 (ZF1) and zinc finger 2 (ZF2) for all members are indicated with emphasis on CCCH residues in the TZF domain. PxLxxSxSFxGxPS motif and the CNOT1 binding domain are in the CTD for all members of the ZFP36 family. The NES for ZFP36L1 and ZFP36L2 located in the CTD overlaps the CNOT1 binding domain (Created with Biorender.com).

1.2.3 ZFP36 family are key mediators of mRNA destabilisation and decay

Regulation of ARE-containing mRNA transcripts requires initial binding to AREs in the 3’UTR by AU-RBPs. Once bound destabilising AU-RBPs such as the ZFP36 family serve as a platform for the recruitment of important protein components of the mRNA decay machinery either through direct or indirect interactions resulting in poly (A) tail shortening (deadenylation), decapping and degradation (Baou, Jewell and Murphy, 2009). Although the underlying molecular mechanisms of mRNA decay are not completely understood, mounting evidence suggests that the ZFP36 family’s primary role in mRNA destabilisation is to mediate the recruitment of deadenylation machinery, promoting poly(A)tail shortening and subsequent mRNA destabilisation (Tudor et al., 2009; Fabian et al., 2013). Co-immunoprecipitation of ZFP36 has demonstrated interactions with various deadenylases (Marchese et al., 2010). ZFP36 mediates the deadenylation of mRNA targets through direct interactions with the central domain of the CCR4-NOT deadenylation complex and ZFP36’s CNOT1 binding domain (Fabian et al., 2013). As well as recruiting the CCR4-NOT complex, ZFP36 was also demonstrated to stimulate the activity of alternative deadenylases such as poly(A) RNase (PARN) *in vitro*, without impacting transcripts lacking AREs (Lai, Kennington and Blackshear, 2003). Similarly, ZFP36L1 and ZFP36L2’s ability to bind to ARE-containing mRNA and initiate degradation was also dependent on C-terminal binding to the CCR4-NOT complex (Adachi et al., 2014).

CCR4-NOT complex mediated deadenylation of mRNA transcripts enables subsequent steps of mRNA decay to proceed (Adachi et al., 2014). The ZFP36 family members have also been shown to facilitate the latter steps of mRNA decay through interaction with key mRNA decay components. Specifically, ZFP36 and ZFP36L1 once bound to ARE-containing mRNA act as a binding platform for decapping subunits DCP1 and DCP2 and 5′→3′ exoribonuclease XRN1, enabling 5’ cap structure removal and subsequent 5′→3′ exoribonucleolytic decay of the deadenylated mRNA respectively (Lykke-Andersen and Wagner, 2005). Alternatively, following deadenylation, mRNA can also be degraded in the 3′→5′ direction by recruiting the RNA-exosome complex (Kilchert, Wittmann and Vasiljeva, 2016). Both ZFP36 and ZFP36L1 have been reported to mediate mRNA decay through the 3′→5′ RNA-exosome RNA decay pathways by recruiting the RNA exosome complex, mediated through interactions with human exosome complex component RRP4 (Lykke-Andersen and Wagner, 2005; Chiu et al., 2022). Therefore, ZFP36 family bind ARE regions on mRNA transcripts initiate the recruitment of deadenylation complex CCR4-NOT followed by 5’ decapping by DCP1/DCP2 leading to XRN1 mediated 5′→3′ exoribonucleolytic decay or following mRNA deadenylation initiate the recruitment of the human exosome complex for 3′→5 RNA decay (Figure 1.2.3).

Interestingly, ZFP36 also seems to exhibit ARE-independent mechanisms involving negative transcriptional regulation of promoters containing nuclear factor kappaB (NF-κB) binding sites. Specifically, ZFP36 was suggested to suppress transcriptional activity of p65/NF-κB through recruitment of histone deacetylase 1 and 2 (HDAC1 and 2) on target gene promoters (Liang et al., 2009; Schichl et al., 2009). This suggests a potential ARE-independent mechanism whereby ZFP36 may inhibit transcription in the nucleus and promote mRNA decay in the cytoplasm underlining the role in maintaining stability and translational competence of mRNA. Moreover, the ability of the ZFP36 family to recruit different mRNA decay machinery infers that the ZFP36 family may also interact with different RNA substrates. For example, the recruitment of distinct exosome complexes has been reported to occur in both the nucleus and cytoplasm (Ibrahim, Wilusz and Wilusz, 2008). Furthermore, as the ZFP36 family members are known regulators of mRNA decay in the cytoplasm their emerging association with the nuclear RNA exosome suggests potential regulation or interactions with RNA substrates in the nucleus, whereby the ZFP36 family can interact with ARE-containing RNA in the nucleus and recruit the nuclear RNA exosome. However, the ZFP36 family's association with nuclear exosome recruitment is currently unknown.

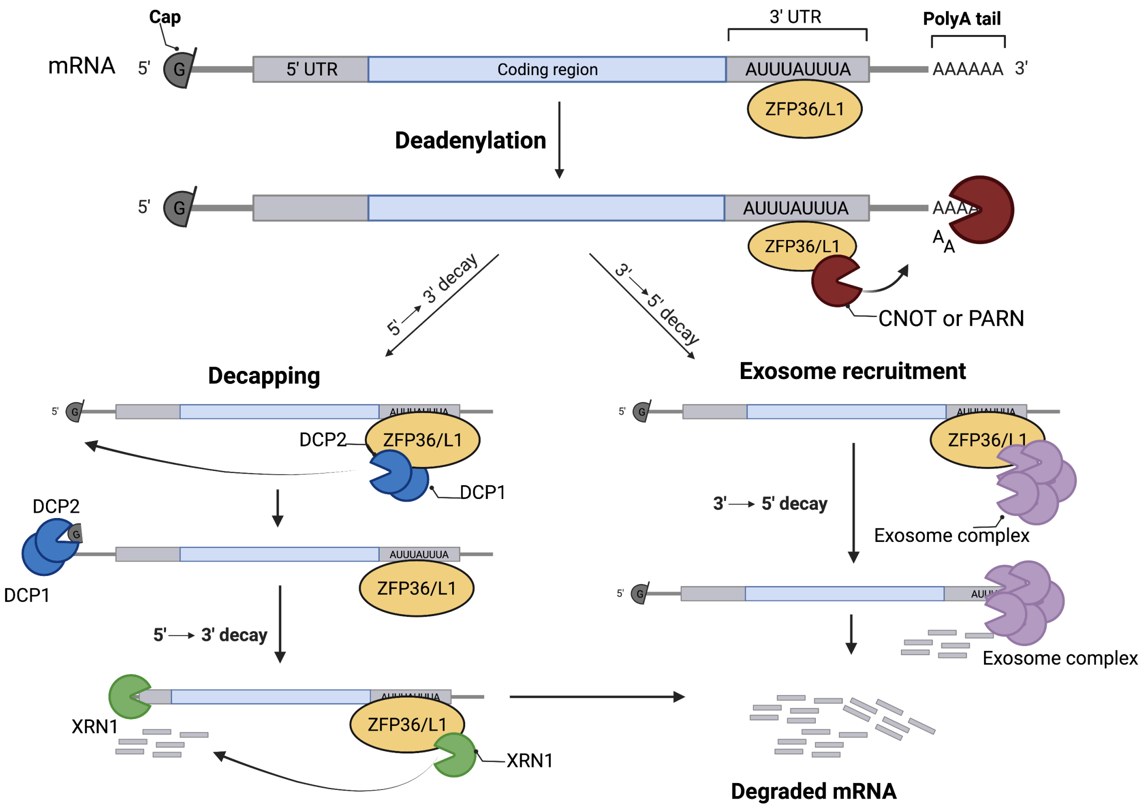
Cap
3' UTR
PolyA tail
mRNA
5'
G
5' UTR
Coding region
AUUUAUUUA
AAAAAA
3'
ZFP36/L1
Deadenylation
AAAA
A
A
CNOT or PARN
5' → 3' decay
3' → 5' decay
Decapping
DCP2
DCP1
XRN1
Exosome recruitment
Exosome complex
Degraded mRNA

Figure 1.2.3 Mechanisms of decay for ARE-containing mRNA by the ZFP36 family.
ZFP36/L1 binding to ARE (AUUUAUUUA) regions in the 3'UTR of mRNA leads to deadenylation of the PolyA tail mediated by the CNOT complex or PARN. Following deadenylation, mRNA decay can be initiated in the 5′→3' or 3′→5' direction. 5′→3' decay requires interaction with decapping complexes DCP1/DCP2 with ZFP36/L1 mediating removal of the 5' cap (G) structure. Removal of the 5' cap structure leads to recruitment of the exonuclease XRN1 which subsequently degrades the mRNA. 3′→5' mRNA decay requires the recruitment and interaction of the human exosome complex with ZFP36/L1 leading to mRNA degradation in the 3′→5' direction (Created with Biorender.com).

1.3 Post-translation modifications of the ZFP36 family: focus on phosphorylation

Post-translational modifications (PTMs) particularly phosphorylation have been elucidated to modulate ZFP36 family protein activity and function. Several putative target sites are available for phosphorylation of the ZFP36 family. Specifically, studies have elucidated multiple Serine (S) and Threonine (T) phosphorylation sites in ZFP36 such as S90, S93, S184, S186, S228, T257 and T271 which are highly conserved between species (Clark and Dean, 2016) (Figure 1.3A) (Cao, Tuttle and Blackshear, 2004; Cao et al., 2006; Cao, Deterding and Blackshear, 2014). Furthermore, *in vitro* assays have demonstrated that these sites are targeted for phosphorylation by several protein kinases that influence the biological activities of the ZFP36 families such as p38- MAPK2-activated protein kinase 2 (MK2), extracellular signal-regulated kinase 2 (ERK2), protein kinase B (PKB/Akt), and protein kinase C (PKC) (Cao and Lin, 2007; Cao, Dzineku and Blackshear, 2003). For example, MK2-mediated phosphorylation of S52 and S178 of ZFP36 prevents the recruitment of the CCR4–NOT complex and degradation of ARE-containing mRNA (Marchese et al., 2010). Major phosphorylation sites of ZFP36 do not seem to be shared by family members ZFP36L1 and ZFP36L2 (Figure 1.3B) (Clark and Dean, 2016). Specifically, phosphorylation sites S54 and S92 or S57 and S127 seem to be the most prominent phosphorylation sites for ZFP36L1 and ZFP36L2 respectively (Clark and Dean, 2016). Interestingly, ZFP36's proline-rich domain located from residues 80-90 are not present for both ZFP36L1 and ZFP36L2 demonstrating a lack of conservation of these sites across family members (Clark and Dean, 2016). Moreover, where phosphorylation sites demonstrate conservation in the ZFP36 family members amino acid residues located adjacent may not favour phosphorylation. For example, ZFP36 residue S220 is immediately followed by a proline residue, whereas ZFP36L1 or ZFP36L2 are proceeded by alanine or serine residues respectively inhibiting phosphorylation of these residues by proline-directed protein kinases (Clark and Dean, 2016; Igarashi and Okuda, 2019).

Unlike ZFP36, proteomic based screens deciphering phosphorylation sites for ZFP36L1 or ZFP36L2 are currently unavailable. However, evidence elucidating phosphorylation of either ZFP36L1 or ZFP36L2 has been reported in high-throughput studies. Reports have implicated phosphorylation of S92 and S203 on ZFP36L1 to enlist 14-3-3 proteins which influence ZFP36L1's mRNA destabilising activity, and protein stability (Benjamin et al., 2006). Specifically, PKB-mediated phosphorylation of ZFP36L1 at S92 and S203 leads to the binding of the 14-3-3 protein complex restricting ZFP36L1's mRNA destabilisation activity (Benjamin et al., 2006). Furthermore, *in vitro kinase* assays demonstrated MK2-mediated phosphorylation of ZFP36L1 at S92, S203, S54 and an unidentified site at the C-terminus inhibits ZFP36L1's ARE binding and mRNA decay activity (Maitra et al., 2008). Regulation of the ZFP36 family function through C-terminus phosphorylation may be attributed to its highly conserved nature amongst species recognisable in oyster and lamprey orthologues (Figure 1.2.2B) (Blackshear and Perera, 2014). For example, phosphorylation of ZFP36 C-terminal S316 and S318 residues stabilises ZFP36 target ARE containing mRNAs by impairing recruitment of the CCR4–NOT complex (Fabian et al., 2013). Similarly, both ZFP36L1 and ZFP36L2 were demonstrated to bind the 3'UTR of the Low-density lipoprotein receptor (LDLR) mRNA and recruit the CCR4–NOT complex to initiate mRNA decay (Adachi et al., 2014). However, phosphorylation of C-terminal residues S334 of ZFP36L1 and S493 and S494 of ZFP36L2 by p90 ribosomal S6 kinase, a kinase downstream of ERK, resulted in CCR4–NOT complex dissociation and stabilisation of LDLR mRNA (Adachi et al., 2014). Phosphorylation of specific residues of the ZFP36 family seems to play a prominent role in mediating their subsequent activities on mRNA targets. Whereby, phosphorylation promotes mRNA destabilisation or stabilisation by inhibiting the ZFP36 family's ability to recruit mRNA decay machinery.

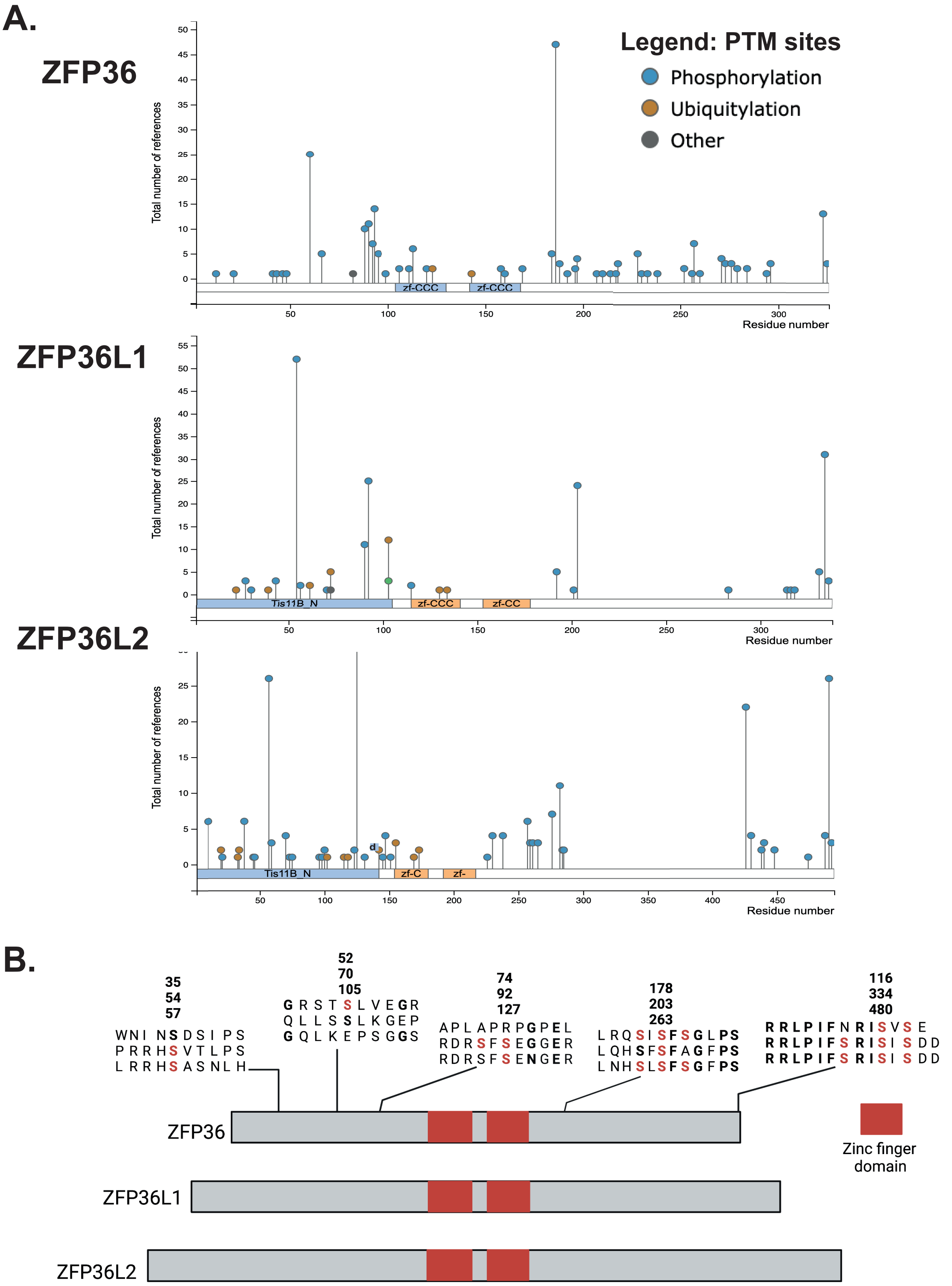

Figure 1.3 Phosphorylation sites of ZFP36 family members and phosphorylation site conservation in other members respective to ZFP36.

A. Documented post-translation modification (PTM) sites for ZFP36, ZFP36L1 and ZFP36L2 including phosphorylation (blue), ubiquitylation (orange) and other (red) (PhosphoSitePlus®, www.phosphosite.org). **B**. Phosphorylation sites demonstrate conservation and divergence in ZFP36 family members. Schematic representations of ZFP36, ZFP36L1 and ZFP36L2 including zinc finger domains (red box) are illustrated. Amino acid sequences of specific regions are represented in order (top to bottom). Amino acid sequences in bold are conserved between ZFP36 family members. Amino acid residues in red indicate known phosphorylation sites carried out *in vivo* (Created with Biorender.com; Adapted from Clark and Dean, 2016).

1.4 Subcellular trafficking and location-specific roles of the ZFP36 family

Like other reported AU-RBPs, the ZFP36 family exhibits nucleo-cytoplasmic shuttling properties that influence their physiological function (Figure 1.4). The nuclear export of ZFP36 is regulated by ZFP36's leucine-rich NES interacting with the nuclear export protein Chromosomal Maintenance 1 (CRM1) (Murata et al., 2002; Phillips, Ramos and Blackshear, 2002). Hela and human embryonic kidney (HEK) 293 cells display predominant cytoplasmic accumulation of recombinant ZFP36 tagged with a green fluorescent protein (GFP), following inhibition of CRM1, ZFP36 exhibits nuclear accumulation (Ramos and Blackshear, 2002). Therefore, this elucidates a nucleo-cytoplasmic role for ZFP36, dependent on CRM1 export from the nucleus. Inversely, contrasting mechanisms have implicated phosphorylation of ZFP36 to determine its retention within the cytoplasm mediated through mechanisms dependent and independent of 14-3-3 protein interactions (Johnson et al., 2002). One of the clearest demonstrations of nuclear localisation is reported in macrophages following inhibition of MAPK p38 (Brook et al., 2006). Specifically, inhibition of MAPK p38 causes rapid dephosphorylation of ZFP36 at residues S52 and S178, resulting in cytoplasmic to nuclear re-localisation (Brook et al., 2006), thus demonstrating phosphorylation status of ZFP36 influences its subcellular localisation. Importantly, nuclear accumulation of endogenous ZFP36 has also been reported (Sedlyarov et al., 2016). Moreover, ZFP36 was reported to interact with poly (A) elongation factor, poly(A)-binding protein nuclear 1 (PABPN1) in the nucleus inhibiting poly (A) tail synthesis of pre-mRNA, leading to pre-mRNA degradation by the nuclear exosome (Su et al., 2012). Interestingly, ZFP36 was indicated to act as a transcriptional co-repressor of nuclear factor kappa-light-chain-enhancer of activated B cell (NF-κB), indicating that ZFP36 could potentially inhibit transcription in the nucleus (Liang et al., 2009). However, if ZFP36 phosphorylation status impacts its potential role in transcription inhibition is yet to be determined. Like ZFP36, ZFP36L1 and ZFP36L2 have also been reported to exhibit nucleo-cytoplasmic functions. Recent evidence elucidated a potential cell cycle-dependent nuclear accumulation of ZFP36L1 in Hela cells. Specifically, nuclear accumulation of ZFP36L1 was demonstrated to be highest in the G1/S phase and eliminated from the nucleus in the G2 phase (Matsuura et al., 2020). Importantly, this cell cycle-dependent nuclear accumulation of ZFP36L1 was attributed to the protein's C-terminal serine-rich cluster, a region that was previously described to experience cell-cycle-dependent phosphorylation in *Xenopus* embryos (Matsuura et al., 2020; Kondo et al., 2018), indicating that nuclear accumulation of ZFP36L1 could be dependent on ZFP36L1's phosphorylation status.

The role of this family of AU-RBPs in the nucleus remains not fully understood. However, recent advances utilising transcriptome and computational biology techniques have identified ARE-rich intronic sequences on RNAs within the nucleus (Kishore et al., 2011). Suggesting a potential unexplored role for this family of AU-RBPs in binding intronic AREs in the nucleus. This is further supported by a report on mechanisms associating ZFP36 to nuclear polyadenylation of ARE-containing mRNA (Su et al., 2012). Interestingly, cross-linking and immunoprecipitation (CLIP) in human HEK293 and photoactivatable ribonucleoside-enhanced (PAR)- CLIP in murine macrophages identified ZFP36 to be bound to excised introns (Mukherjee et al., 2014;

Sedlyarov et al., 2016). Suggesting, that ZFP36 may have a potential role in pre-mRNA splicing mechanisms within the nucleus. However, further investigation is needed to understand the functional significance of the relation between ZFP36 and intronic AREs in the nucleus.

In the event of cellular stress, stress granules (SGs) and processing bodies (P bodies) are formed within the cytoplasm (Anderson, Kedersha and Ivanov, 2015; Kedersha et al., 2005). SGs form around sites of stalled translational preinitiation complexes, whereas P-bodies are distinct sites of mRNA modulation comprised of regulators of mRNA decay such as the CCR4-NOT complex (Anderson, Kedersha and Ivanov, 2015; Kedersha et al., 2005). Importantly, SG and p-bodies are spatially and functionally linked often encountering one another. The ZFP36 family members are key mediators of shuttling ARE-containing mRNAs between SGs and p-bodies and are determining factors that reflect mRNA fate leading to storage, degradation, or reinitiating translation (Kedersha et al., 2005; Murata et al., 2005). Precisely, arsenite-induced oxidative stress in murine macrophages was reported to mediate p38-MAPK/MK2-mediated phosphorylation of S52 and S178 on ZFP36, indirectly stabilising mRNAs in SGs (Rigby et al., 2005). Moreover, phosphorylation of ZFP36 results in exclusion from SGs by the 14-3-3 protein complex promoting mRNA stabilisation (Chrestensen et al., 2004; Stoecklin et al., 2004).

Contrastingly ZFP36 and ZFP36L1 have been reported to deliver ARE-containing mRNAs to P-bodies to mediate mRNA decay (Franks and Lykke-Andersen, 2007; Kedersha et al., 2005). Importantly, the ZFP36 family’s ability to direct ARE-containing mRNAs to P-bodies has been linked to their association with P-body components important for the turnover of mRNAs such as decapping enzymes DCP1A, DCP2 and exonuclease XRN1 to initiate mRNA decapping and 5′-3′ exonucleolytic degradation (Hau et al., 2007; Franks and Lykke-Andersen, 2007). ZFP36 was found to colocalise with cytoplasmic p-bodies in intestinal epithelial cells to mediate decay of ARE-containing transforming growth factor β (TGF-β) mRNA (Blanco et al., 2014). This demonstrates a pro-active role for the ZFP36 family in mediating mRNA decay in p-bodies or stabilisation in SGs. However, the precise mechanisms underlying the dynamic shift of the ZFP36 family from SGs to P-bodies remain unclear.

Perhaps the most unexpected subcellular function of ZFP36L1 was reported in its ability to form a membranelles organelle associated with the endoplasmic reticulum (ER) (Ma and Mayr, 2018). Specifically, ZFP36L1 was reported to form membranelles organelles known as TIS granules (named after ZFP36L1's alias TIS11B) forming a reticular meshwork with ER. Thus, creating a novel subcellular compartment distinct from the cytoplasm is known as the TIGER (TIS granule-ER) domain (Ma and Mayr, 2018). Moreover, the TIGER domain was found to be enriched with ARE-containing mRNAs enabling subsequent translation and increasing functional diversity of translated proteins, through novel interacting partners. However, if translation occurs within TIS granules or supports translation through association with the ER remains unclear. Further work utilising transcriptome and proteome studies could elucidate possible differential gene and protein expression within this novel subcellular compartment, uncovering novel roles for ZFP36L1.

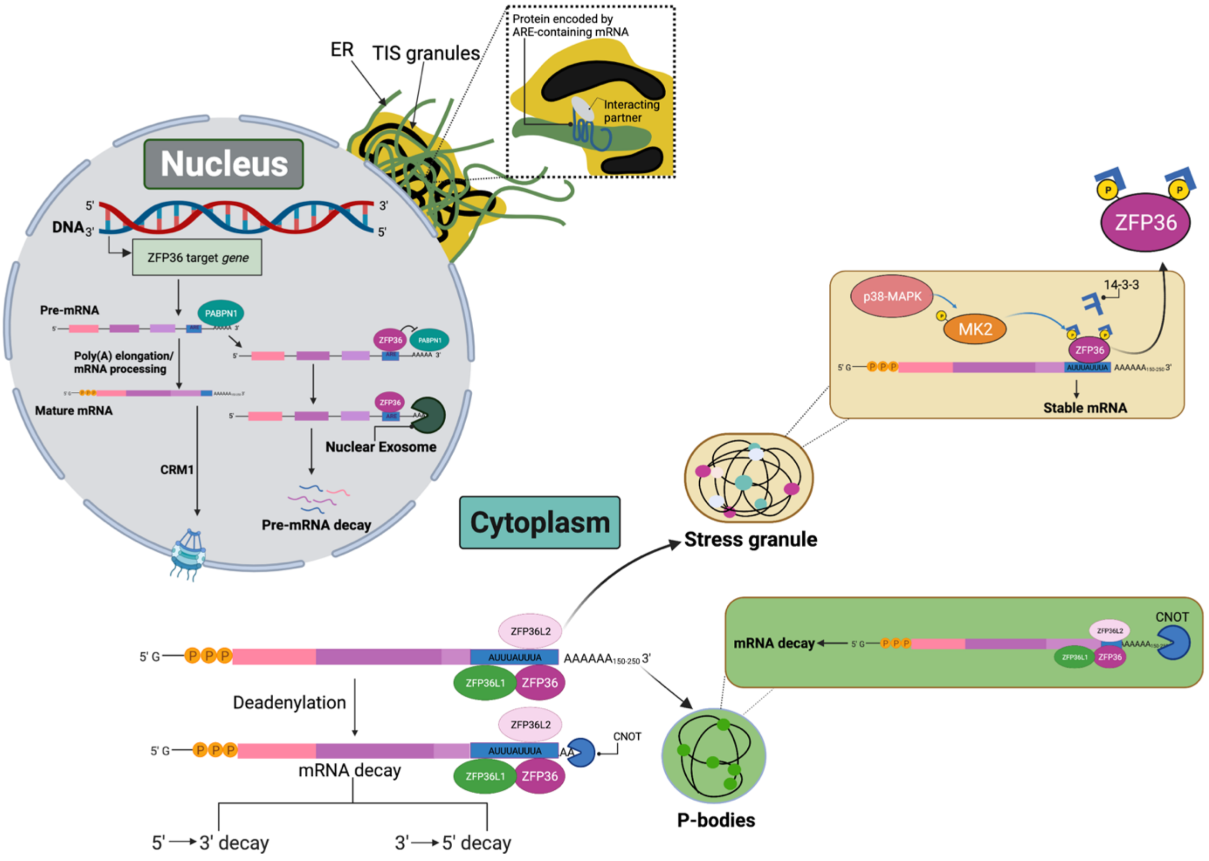
ER
TIS granules
Protein encoded by ARE-containing mRNA
Interacting partner
Nucleus
DNA
5'
3'
3'
5'
ZFP36 target *gene*
Pre-mRNA
PABPN1
ZFP36
PABPN1
ARE
AAAAA 3'
Poly(A) elongation/ mRNA processing
Mature mRNA
ZFP36
Nuclear Exosome
CRM1
Pre-mRNA decay
Cytoplasm
Stress granule
p38-MAPK
MK2
14-3-3
ZFP36
ZFP36
AUUUAUUUA
Stable mRNA
ZFP36L2
5' G
P P P
AUUUAUUUA
AAAAAA150-250 3'
ZFP36L1
ZFP36
Deadenylation
ZFP36L2
CNOT
mRNA decay
5'→3' decay
3'→5' decay
mRNA decay
CNOT
ZFP36L2
ZFP36L1
ZFP36
P-bodies

Figure 1.4 Subcellular localisation of the ZFP36 family.
The ZFP36 family of proteins exhibits diverse roles specific to their subcellular environment. In the nucleus, ZFP36 is involved in pre-mRNA maturation and interaction with PABPN1 results in the degradation of pre-mRNA via the nuclear exosome. ZFP36L1 forms TIS granules associated with the ER reported enriched with ARE-containing mRNAs. In the cytoplasm ZFP36, ZFP36L1 and ZFP36L2 bind ARE-containing mRNA leading to recruitment of the CNOT complex resulting in 5’ to 3’ or 3’ to 5’ mRNA. ZFP36, ZFP36L1 and ZFP36L2 binding to ARE-containing mRNA can also initiate translocation into p-bodies for subsequent processing. Alternatively, ZFP36 is also found to bind to ARE-containing mRNA in stress granules where p38-MAPK/MK2 mediates ZFP36 exclusion from stress granules by the 14-3-4 protein complex (Created with Biorender.com).

1.5 Expression of the ZFP36 family in normal human tissues

Reports depicting ZFP36 family protein levels across various tissue types have not been fully explored, however, some reports elucidate differences in mRNA levels of the ZFP36 family across tissue types. Specifically, elevated mRNA levels for ZFP36, ZFP36L1 and ZFP36L2 have been reported in the adrenal gland, lung, colon, pancreas, and ovaries (Carrick and Blackshear, 2007). Inversely, mRNA expression levels of all the ZFP36 family members were found to be lowest in the heart, stomach, spleen, and liver (Carrick and Blackshear, 2007). It is important to recognise that each of these three family members is not equally expressed within a specific organ. For example, the expression of ZFP36L1 and ZFP36L2 transcripts was demonstrated to be greater in the pancreas than transcripts for ZFP36 (Carrick and Blackshear, 2007). Similarly, ZFP36L1 transcripts expression is highest and more abundant within the lungs than ZFP36L2 and ZFP36 (Carrick and Blackshear, 2007). Although differences in relative expression levels of ZFP36 family transcripts in different organs are apparent, the physiological significance remains unknown. It could be that individual members have a conserved role to play within a tissue type. However, without equivalent studies measuring ZFP36 family protein levels in human tissues, the answer to this question remains unknown. Although there is a shortage of comparative reports on ZFP36 family protein expression across human tissues, databases infer the potential difference in this family of proteins across various tissue types (Figure 1.5).

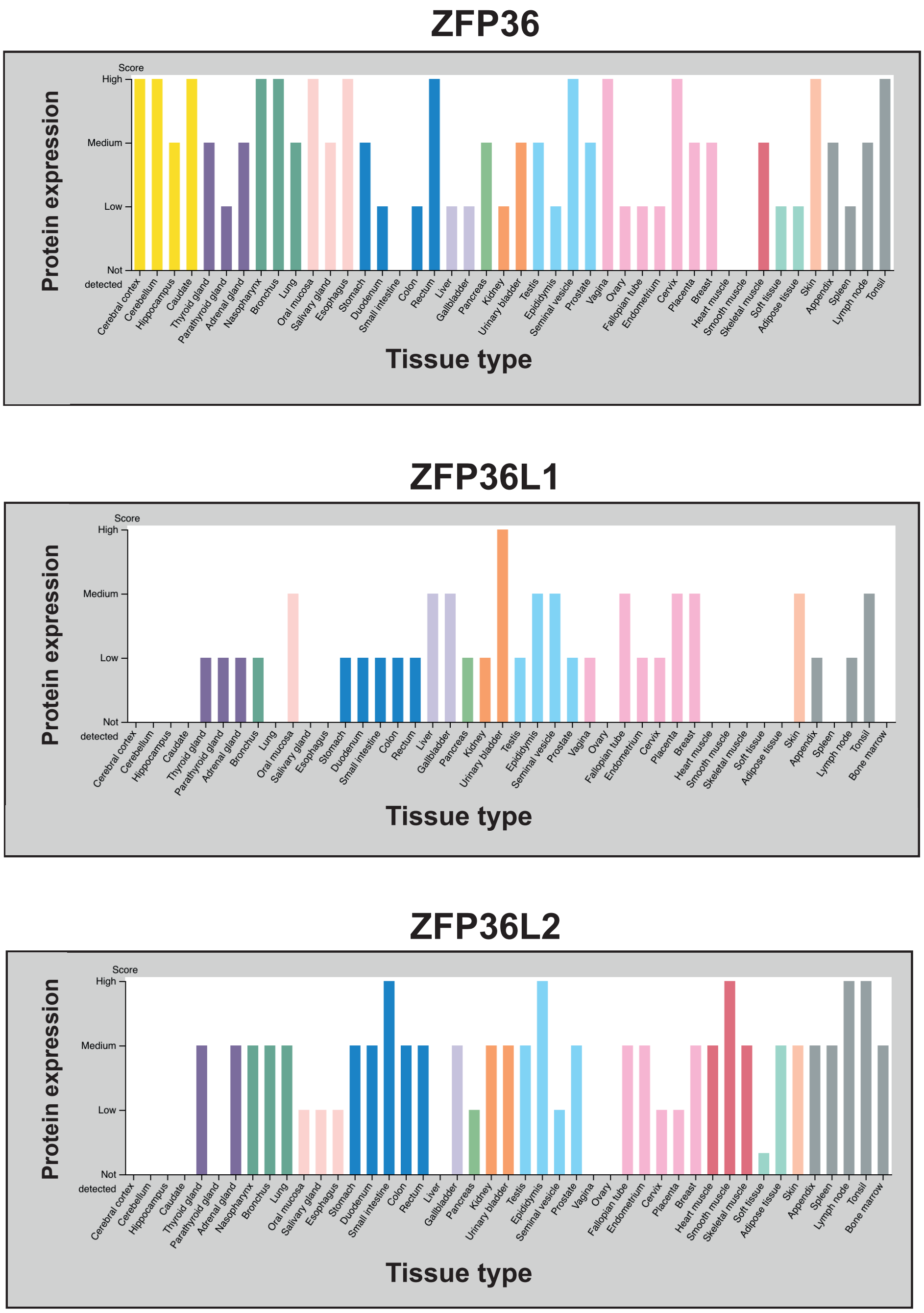

Figure 1.5 Protein expression of ZFP36 family across different human tissue types.

ZFP36, ZFP36L1 and ZFP36L2 protein expression levels across normal human tissues. Expression levels are indicated as no expression (not detected), low, medium, or high relative to a specific tissue type, colour coding corresponds to related tissue groups (Human Protein Atlas; proteinatlas.org).

1.6 ZFP36 family target mRNAs regulate diverse physiological functions

1.6.1 Immune response and immune cell development

The ZFP36 family members are important coordinators of immune responses through post-transcriptional regulation of ARE-containing mRNAs. ZFP36 is known to down-regulate pro-inflammatory cytokine TNF-α protein production by binding to the ARE of *Tnf* mRNA promoting its subsequent decay (Kontoyiannis et al., 1999). Subsequently, ZFP36 expression is also induced by TNF-α signalling pathways (Lai et al., 1999). Thus, suggesting ZFP36 is involved in a negative feedback loop to regulate TNF-α. Per these reports, ZFP36 deficient mouse models develop syndromes reflecting TNF-α overproduction including autoimmunity, inflammatory arthritis, and bone marrow hyperplasia (Taylor et al., 1996; Carballo and Blackshear, 2001). Similarly, ZFP36 post-transcriptionally regulates anti-inflammatory cytokine *IL-10* through ARE binding in the 3'UTR (Stoecklin et al., 2008). Moreover, IL-10 can also induce the expression of ZFP36 through STAT3 (Signal transducer and activator of transcription 3) signalling in macrophages (Gaba et al., 2012). Thus, suggesting once more that ZFP36 is part of a negative feedback loop to suppress anti-inflammatory signalling. Similarly, ZFP36L1 is a key component in the immune response by mediating immune cell development (Newman et al., 2017). Specifically, ZFP36L1 suppresses the expression of transcription factors KLF2 (Kruppel Like Factor 2) and IRF (Interferon Regulatory Factor 8) to regulate marginal-zone B cell compartments (Newman et al., 2017). Moreover, in developing B-cells ZFP36L1 and ZFP36L2 were reported to be essential for maintaining and re-establishing quiescence for the development and expression of precursor B cell receptors (pre-BCR) (Galloway et al., 2016). Importantly, double knock out of *Zfp36l1* and *Zfp36l2* in T-cell lineages results in thymopoiesis resulting in T-cell acute lymphoblastic leukaemia (T-ALL) as a result of defective Notch signalling (Hodson et al., 2010).

1.6.2 Cellular proliferation through cell cycle regulation

The ZFP36 family members have links to the regulation of key cell cycle proteins through ARE binding. For example, important cell cycle regulators c-MYC and cyclin D1 contain ARE in the 3’UTR of their respective mRNAs which are targeted by ZFP36 (Marderosian et al., 2006). Importantly, transcription factor c-MYC exhibits key roles in cellular proliferation, differentiation, and apoptosis whereas Cyclin D1 is important for G1-S progression. Thus, implicating ZFP36 to modulate key events involved in cellular proliferation through cell cycle progression. ZFP36 also modulates E2F transcription factor 1 (E2F1) a key regulator of G1-S phase progression. ZFP36 was reported to influence the stability of *E2F1* mRNA implicating ZFP36 to regulate proliferation post-transcriptionally through *E2F1* mRNA binding (Lee, Lee and Leem, 2014). ZFP36 was also reported to inhibit cellular proliferation albeit in breast tumour cells *in vitro* and breast tumour growth *in vivo* (Saini, Chen and Patial, 2020). Specifically, ZFP36 inhibits c-Jun expression by abrogating NF-κB p65 translocation from the nucleus leading to increased expression of the S-G2 phase progression regulator Wee1, leading to S-phase arrest (Xu et al., 2015). ZFP36L1 was also reported to post-transcriptionally regulate cell cycle genes *E2F1* and *Cyclin D1* mRNA through binding to ARE regions in the 3’UTR. Whereas, ZFP36L1 and ZFP36L2 were shown to inhibit cyclin D expression leading to cell cycle arrest in the G1 phase (Suk et al., 2018). Finally, ZFP36L1 was also suggested to modulate cell cycle progression through binding to the 3’UTR of CDKN1A (Cyclin Dependent Kinase Inhibitor 1A) a key regulator of cell cycle progression in response to DNA damage (Cazzalini et al., 2010; Kaehler et al., 2021). Ablation of ZFP36L1 increased *CDKN1A* mRNA in turn decreasing cellular proliferation suggesting ZFP36L1 can indirectly modulate cellular proliferation through *CDKN1A* mRNA regulation. These studies indicate that the ZFP36 family members have key regulatory roles in cell cycle progression and therefore have the ability to influence cellular proliferation.

1.7 The ZFP36 family and disease: focus on cancer

Post-transcriptional control of gene expression through regulation of mRNA stability and translation leads to prompt alterations in mRNA levels. Therefore, defects to mechanisms that impact mRNA stability and subsequent translation are one of the underlying causes of diseases such as cancer (Reviewed in Audic and Hartley, 2004). Mutations to the ZFP36 family leading to their dysfunctional expression and activity have been implicated in multiple cancer types of the breast, prostate, liver, lung, kidney, and thyroid (Figure 1.7) (Brennan et al., 2009; Loh et al., 2019; Canzoneri et al., 2020). Importantly, alterations to the activity and function of the ZFP36 family are expected to increase the stability of their respective target mRNAs some of which have been linked with various molecular traits of cancer encoded by proto-oncogenes, inflammatory cytokines, and growth factors (Reviewed in Saini, Chen and Patial, 2020).

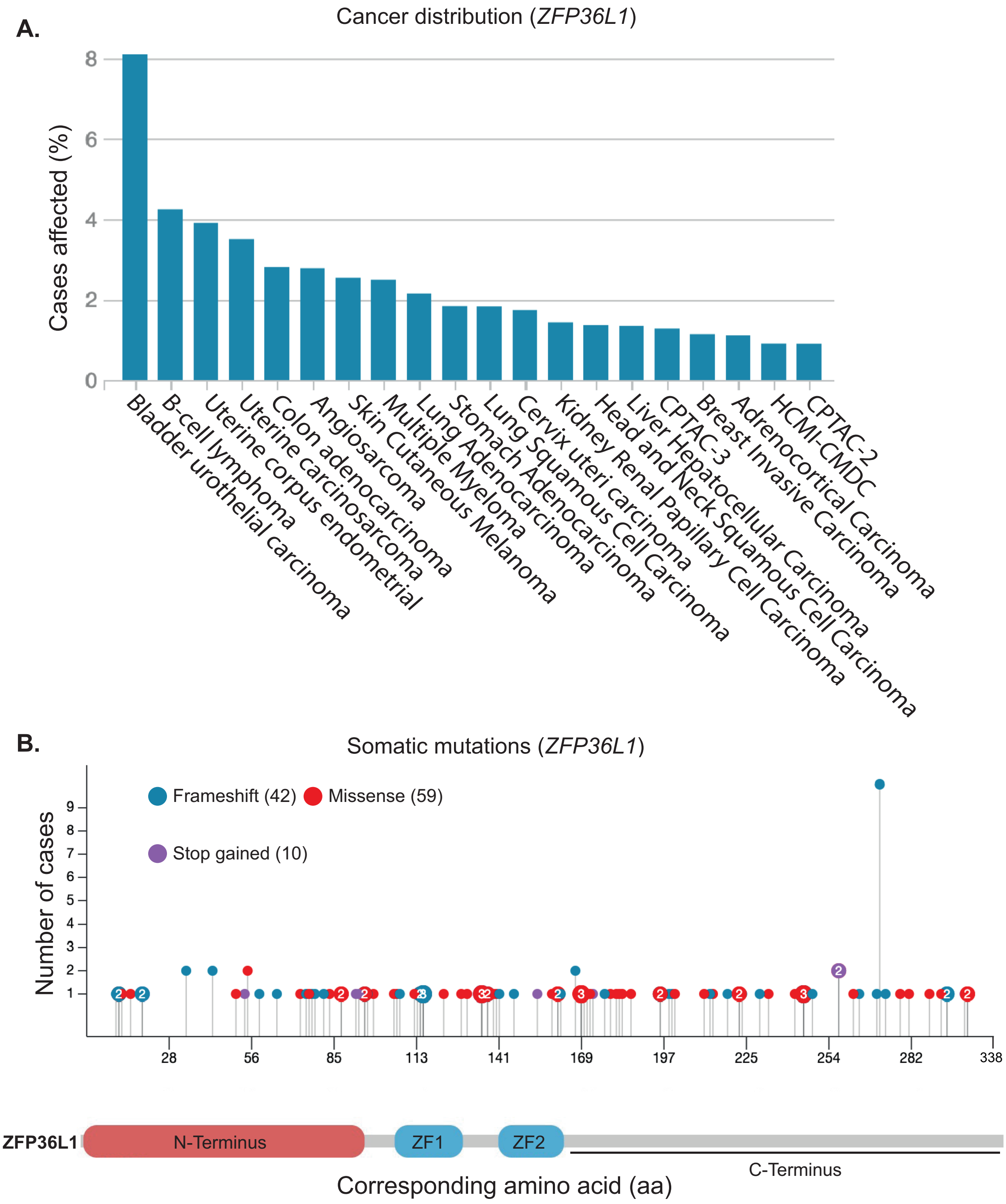

Figure 1.7 Reported ZFP36L1 association with cancers.

(**A**) Number of different cancer cases (194) affected by *ZFP36L1* (Ensembl ID:ENSG00000185650) mutations across 29 projects (Project details for CPTA-2; Breast, Colon, Ovary, CPTA-3; Brain, Head and Neck, Kidney, Lung, Pancreas, Uterus, and HCMI-CMDC; NCI Cancer Model Development for the Human Cancer Model Initiative) (National cancer institute (NCI); The cancer genome atlas (TCGA) (**B**) Number of cancer cases with somatic mutations (frameshift, missense and stop gained) and coordinates corresponding to the location on ZFP36L1 protein, numbers indicate more than one mutation at a specific coordinate (NCI; TCGA).

The ZFP36 family has been described to have tumour suppressor properties linked to their ability to post-transcriptionally regulate oncogenic mRNA. Therefore, it is unsurprising that loss of ZFP36 family regulation over mRNAs is associated with hallmark molecular cancer traits. Specifically, reports have identified that ZFP36 is important for post-transcriptionally regulating levels of the anti-apoptotic protein B-cell lymphoma-2 (BCL-2) in head and neck squamous cell carcinoma (SCCHN) cells (Park et al., 2015). In SCCHN cells ZFP36 destabilises *BCL-2* mRNA, reducing BCL-2 expression and increasing sensitivity to cisplatin treatment (Park et al., 2015). Moreover, inhibition of ZFP36 was demonstrated to decrease sensitivity to cisplatin due to increased BCL-2 expression in SCCHN (Park et al., 2015). Similarly, ZFP36L1 has also been demonstrated to regulate *BCL-2* mRNA in malignant B-cells through ARE binding mediating its pro-apoptotic effects (Zekavati et al., 2014). Unlike ZFP36 and ZFP36L1 a role for ZFP36L2 in regulating apoptosis remains unexplored.

Inflammation is a critical contributor to the tumour microenvironment and progression, as cancers are known to form at sites of chronic inflammation (Reviewed in Coussens and Werb, 2002). The ZFP36 family members have well-established roles in post-transcriptional regulation of pro-inflammatory cytokines and chemokines advocating the ZFP36 family as key modulators of cancer development and progression. ZFP36 was demonstrated to destabilise mRNAs for interleukin 8 (IL-8) and VEGF in malignant glioma cells decreasing cellular proliferation (Suswam et al., 2008). Similarly, a study demonstrated loss of ZFP36L1 upregulates *VEGF* mRNA, increasing translational turnover (Planel et al., 2010). Furthermore, this study indicated that intertumoral injection of ZFP36L1 in nude mice subcutaneously implanted with Lewis Lung Carcinoma (LL/2) cells, exhibited reduced tumour growth due to a decrease in multiple pro-inflammatory and angiogenic cytokines such as VEGF, TNFα, IL-1α, and IL-6 (Planel et al., 2010).

Defects in cell cycle regulatory pathways are major characteristics of cancers (Otto and Sicinski, 2017). The ZFP36 family has been implicated in binding AREs and destabilising key cell cycle regulators. For example, ZFP36 regulates the mRNAs for c-Myc, cyclin D1 and E2F1 that are involved in key physiological roles such as cellular proliferation, differentiation and apoptosis and have been reported to be dysregulated in multiple cancers (Yan et al., 2014; Musgrove et al., 2011; Dang, 2012). ZFP36 overexpression decreased cellular proliferation of PC3 human prostate cancer cells through destabilisation of *E2F1* mRNA a factor that controls cell cycle progression through the G1-S phase (Lee, Lee and Leem, 2014). Contrastingly, knockdown of ZFP36 increased E2F1 expression and cellular proliferation (Lee, Lee and Leem, 2014). Importantly, E2F1 is aberrantly expressed in many cancers and is a poor indicator of prognosis and is associated with high-grade tumours (Liu and Hu, 2020). Therefore, implicating ZFP36 as a potential therapeutic target. Loss of ZFP36L1 and ZFP36L2 mediated post-transcriptional control of *cyclin D* mRNA has been implicated in increased cancer cell proliferation (Suk et al., 2018). Specifically, mutations to the tandem ZFMs of ZFP36L1 and ZFP36L2 were reported to cause defects in their mRNA binding capacity, abolishing post-transcriptional regulation of cyclin D and increasing cellular proliferation of colorectal cancer cell lines HCT116 and SW620 (Suk et al., 2018). On the other hand, overexpression of ZFP36L1 and ZFP36L2 resulted in cell cycle arrest at the G1 phase and decreased cancer cell proliferation through Cyclin D and p53-dependent pathways in these cells, suggesting that defective ZFP36L1 and ZFP36L2 expression can negatively or positively impact cellular proliferation due to aberrant control of cell cycle regulators (Suk et al., 2018).

Defects leading to changes in activity or expression of the ZFP36 family members are associated with a plethora of cancer types (Table 3). Possibly the most convincing evidence for the ZFP36 family's link with tumourigenesis was reported in *Zfp36l1 and Zfp36l2* double knock-out mice which developed T lymphoblastic leukaemia specifically due to loss of the two proteins (Hodson et al., 2010). Multiple studies have also identified that ZFP36 family members are under-expressed in different cancer types implicating their link to tumour suppression (Table 3) (Brennan et al., 2009; Fallahi et al., 2014; Kröhler et al., 2019; Coelho et al., 2017). Specifically, the role of ZFP36L1 in tumourigenesis is further supported by genome-wide screens that have elucidated inactivating mutations in the *ZFP36L1* gene. Intriguingly, ZFP36L1 has been identified as a driver gene in breast cancer (Nik-Zainal et al., 2016), multiple myeloma (Maura et al., 2019) and primary lymphomas of the central nervous system (Radke et al., 2022). Interestingly, evidence also implicates that ZFP36L1 may also exhibit oncogenic functions. Specifically, in acute myeloid leukaemia cells carrying the translocation t(8;21) (q22;q22) that lead to the genesis of Acute Myeloid Leukemia 1-Eight-twenty one (AML-ETO1) fusion proteins, overexpression of ZFP36L1 was found to increase cellular proliferation and inhibit differentiation (Shimada, Ichikawa and Ohki, 2002; Peterson and Zhang, 2004). Furthermore, recent developments demonstrated through CRISPR-Cas9 mediated ablation of ZFP36L1 led to a reduction in the growth rate in chronic myeloid leukaemia cells (Kaehler et al., 2021). Therefore, these reports highlight that ZFP36L1 may exhibit cell-context-specific effects on proliferation and cell growth. The ability for ZFP36L1 to potentially exhibit tumour suppressive or oncogenic roles in a cell-type specific manner has also been demonstrated for family member ZFP36L2 in various cancer types. Specifically, pan-can whole-genome sequencing has identified that ZFP36L2 is significantly mutated in metastatic tumours (Priestley et al., 2019). Contrastingly, in gastric and pancreatic cancer ZFP36L2 exhibits oncogenic potential and increased ZFP36L2 expression promotes cancer aggressiveness (Xing et al., 2019; Yonemori et al., 2017). Based on these reports, studies have adopted cancer therapeutic strategies to induce protein expression of the ZFP36 family (Rounbehler et al., 2012; Planel et al., 2010).

Table 3. The ZFP36 family in multiple cancer types

Cancer type	**ZFP36 family**	**Reported association in cancers**
Bladder	ZFP36	ZFP36 overexpression suppresses proliferation, migration, and invasiveness of bladder cancer cells (Jiang et al., 2020).
	ZFP36L1	Forced expression of ZFP36L1 reduces cellular proliferation, invasiveness and migration in bladder and breast cancer (Loh, Ding and Koeffler, 2017).
	ZFP36L2	ZFP36L2 is identified as a prognostic indicator in invasive bladder cancer (Han et al., 2019)

Breast	ZFP36	ZFP36 is significantly down-regulated in invasive breast cancer cells (Al-Souhibani et al., 2010; Goddio et al., 2012). ZFP36 is downregulated in advanced breast and prostate cancers (Brennan et al., 2009)
	ZFP36L1	*ZFP36L1* is identified as a novel breast cancer drive gene (Nik-Zainal et al., 2016). Forced expression of ZFP36L1 reduces cellular proliferation, invasiveness and migration in bladder and breast cancer (Loh, Ding and Koeffler, 2017).
	ZFP36L2	ZFP36L2 is associated with bone metastasis in breast cancers (Park et al., 2018).

Colorectal	ZFP36L1/ZFP36L2	Overexpression of ZFP36L1 and ZFP36L2 inhibits cellular proliferation of colorectal cancer cell lines (Suk et al., 2018).
	ZFP36L2	*ZFP36L2* is significantly mutated in colorectal cancers (Priestley et al., 2019).
Gastric	ZFP36L2	ZFP36L2 is significantly upregulated in gastric cancer and promotes cell growth (Xing et al., 2019)
Liver	ZFP36	ZFP36 is downregulated in hepatocellular carcinoma patient samples and ZFP36 overexpression inhibits tumour cell growth in xenograft mouse models (Chen et al., 2020)
Leukaemia	ZFP36L1	ZFP36L1 is downregulated in acute myeloid leukaemia (Chen et al., 2015).
	ZFP36L1	Loss of ZFP36L1 reduces cell growth in chronic myeloid leukaemia cells (Kaehler et al., 2021).
	ZFP36L1/ZFP36L2	*Zfp36l1* and *Zfp36l2* disruption in mice causes T lymphoblastic leukaemia (Hodson et al., 2010).
Lung	ZFP36	ZFP36 is downregulated in lung cancers (Fallahi et al., 2014)

Multiple myeloma	ZFP36L1	Whole-genome sequencing (WGS) of 67 Multiple myeloma patient samples identifies *ZFP36L1* as a driver gene (Maura et al., 2019).
Myelofibrosis	ZFP36L1	*ZFP36L1* exhibits tumour suppressor properties in myelofibrosis (Martínez-Calle et al., 2019)
Pancreatic	ZFP36L2	ZFP36L2 overexpression promotes cancer cell aggressiveness (Yonemori et al., 2017).
Pan-cancer	ZFP36L1/ZFP36L2	Genome-wide pan-cancer analysis identifies recurrent mutations to *ZFP36L1* and *ZFP36L2* (Priestley et al., 2019)
Lymphomas	ZFP36L1	Whole-genome sequencing identifies *ZFP36L1* as a driver gene in primary lymphomas of the central nervous system (Radke et al., 2022).
Urinary tract	ZFP36L1	Genome-wide analysis in patient samples identifies recurrent mutations to *ZFP36L1* in urinary tract cancers (Priestley et al., 2019).

1.8 AU-RBPs are key regulators of genome integrity

1.8.1 Regulation of replication and faithful genome duplication

During the DNA synthesis phase (S-phase), cells are constantly engaged in a battle to ensure faithful duplication of their genome. Eukaryotic cells employ a plethora of proteins that act together in complex to replicate DNA to form finely tuned structures known as replication forks to coordinate timely chromosomal replication. Although there are many emerging factors involved in DNA replication (Wessel et al., 2019), a subset of core proteins is essential for DNA replication. Such proteins include a helicase that unwinds duplexed DNA, priming enzymes that synthesise short RNA primers, DNA polymerases that are involved in the extension of primed sites to synthesise two new daughter strands, DNA clamp loading proteins that load DNA clamps and ssDNA binding proteins (Figure 1.8.1) (Reviewed in Zhang and O'Donnell, 2016). Sources that impede DNA synthesis at replication forks or inhibit the progression of DNA replication machinery is termed “replication stress” and can result in chromosomal breaks and deleterious recombination events (Burrell et al., 2013; Wilhelm et al., 2019). Numerous obstacles of endogenous replication stress have been reported and include DNA lesions, aberrant DNA structures, conflicts between replication and transcription machinery, oncogene activation and chromatin inaccessibility (Reviewed in Zeman and Cimprich, 2013). Moreover, replication stress can also be induced by an exogenous source impeding faithful replication fork progression (Table 4). In the event of chronic replication stress or dysfunction to factors involved in key regulatory pathways involved in replication stress resolution, DNA damage or DNA double-strand breaks (DSBs) which are highly deleterious to the genome integirty are generated (Petermann et al., 2010). Therefore, replication stress can promote genome instability, a driver of disease pathogenesis which includes cancer, immunodeficiencies and neurodegenerative disorders (Babbe et al., 2008; Gaillard, García-Muse and Aguilera, 2015; Abugable et al., 2019). Importantly, cells have adopted safeguards namely, DNA damage response (DDR) mechanisms to ensure normal cell function and passing of genetic material to progeny cells. The DDR is essential for monitoring and activation of signalling pathways at cell cycle checkpoints to initiate DNA repair mechanisms. Essential to the DDR are key sensors, mediators and effectors proteins that coordinate the DDR (Zhou and Elledge, 2000). Sensors identify DNA lesions leading to activation of DDR kinases upstream of a signalling cascade (Zhou and Elledge, 2000). While mediators facilitate the phosphorylation of key proteins in the DDR network, effectors are substrates downstream of a signalling cascade and associate with mechanisms integral to genome stability such as DNA replication, repair, and cell-cycle regulation (Zhou and Elledge, 2000).

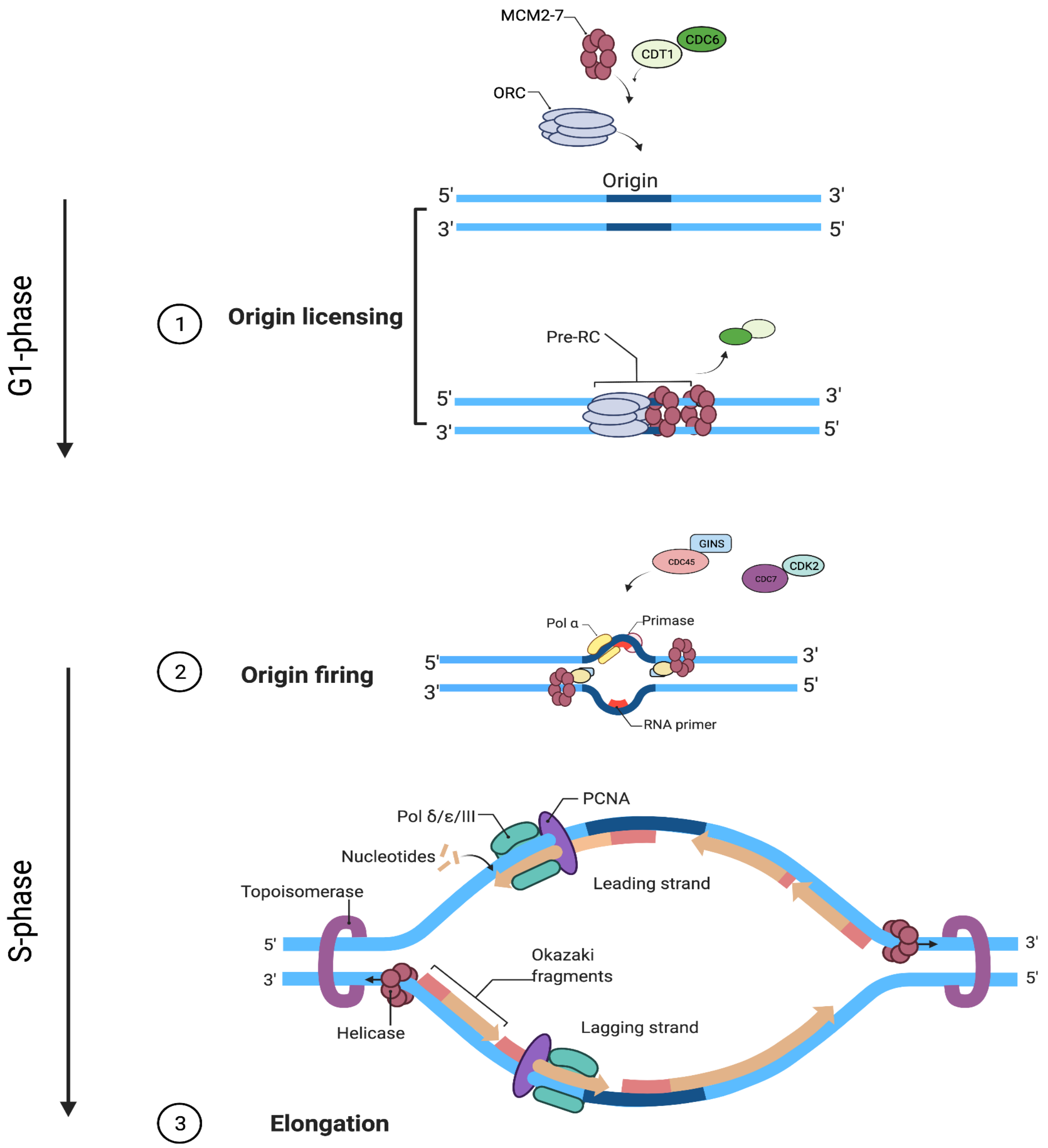
G1-phase
S-phase
MCM2-7
CDT1
CDC6
ORC
Origin
5'
3'
3'
5'
1
Origin licensing
Pre-RC
5'
3'
3'
5'
GINS
CDC45
CDK2
CDC7
Pol α
Primase
2
Origin firing
5'
3'
3'
5'
RNA primer
PCNA
Pol δ/ε/III
Nucleotides
Leading strand
Topoisomerase
5'
3'
Okazaki fragments
3'
5'
Helicase
Lagging strand
3
Elongation

Figure 1.8.1 DNA replication in eukaryotes.

The DNA replication initiation stage is tightly regulated so that the genome is only duplicated once for each cell cycle. To ensure tight regulation of genome duplication, a series of steps are taken and are based on specific proteins that come together to form complexes during the late M phase and throughout the G_1 phase. **(1) Origin licensing**; origins of replication are licensed by the origin recognition complex (ORC), cell division cycle 6 (CDC6) ATPase and the chromatin licensing and DNA replication factor 1 (CDT1) facilitating the docking of the replicative helicase minichromosomal maintenance complex 2-7 (MCM2-7) forming the pre-replication complex (Pre-RC). Before S-phase onset, CDC6 and CDT1 are released and only ORC and MCM2-7 remain bound to DNA. **(2) Origin firing**; as the cell proceeds into the S phase, CDK2 along with DBF4/DRF1-dependent CDC7 kinase leads to recruitment of CDC45 and GINS forming the CDC45-MCM2-7-GINS (CMG) complex enabling DNA unwinding and active replisome formation. Polymerase α (Pol α) and primase cooperate to initiate the DNA synthesis of RNA-DNA primers. **(3) Elongation**; Nucleotides are incorporated throughout the S-phase enabling polymerases ε/δ and III to synthesise the extension of the leading strand in the 5' to 3' direction and lagging strand in the 3' to 5' direction utilising Okazaki fragments. (Created with Biorender.com).

Table 4. Common inhibitors of DNA replication and their effects

Replication Inhibitors	Concentration/ Exposure time	Effect	Cell line (Reference)
Aphidicolin (APH): The tetracyclic diterpenoid antibiotic APH inhibits DNA polymerases α, ε and δ interfering with DNA replication, without disrupting helicase function leading to long stretches of single-stranded DNA.	0.1-0.6µM/24hours	Mild replication stress/ common fragile site expression	U-2OS, Hela, HCT116, NIH3T3 (Durkin et al., 2006; Di Marco et al., 2017; Lafarga et al., 2018)
	0.2µM/ 16-24hours	Induction of anaphase bridges, 53BP1 nuclear bodies and micronuclei	U-2OS, HEK-293 and Hela (Chan, Fugger and West, 2017; Di Marco et al., 2017; Tiwari, Addis Jones and Chan, 2018)
	5–25µM/24 hours	Replication block	Werner syndrome (Basile et al., 2014) Bloom syndrome (Nguyen et al., 2013)
	10µM/15hours	Synchronisation of cells at the G1/S border	Hela and REF-52 (Borel, Lacroix and Margolis, 2002)
	6µM/24hours	Synchronisation of cells at the G0/G1 boundary	DLD-1 (Engstrom and Kmiec, 2008)
Hydroxyurea (HU): Inactivates the enzyme ribonucleotide reductase (RNR) inhibiting the incorporation of	2mM/1 hour	Replication stress	HCC1937 (Yarden et al., 2012)
	2mM/16-24hours	Replication block	MCF-7 and HEK293 (Awate and De Benedetti, 2016)

nucleotides and resulting in the depletion of dNTPs.	4mM/ 2hours	Replication fork stalling	A549 (Lee et al., 2020)
Camptothecin (CPT): CPT is a pentacyclic quinoline alkaloid that inhibits topoisomerase I (TopoI) by covalently linking TopoI to DNA.	25nM/1hour	Checkpoint activation (CHK1 and CHK2)	U-2OS (Ray Chaudhuri et al., 2012)
	1µM/1hour	Checkpoint activation (CHK1 and CHK2)	HCT116 (Regairaz et al., 2011)
	1µM/1hour	Replication inhibition	L1210 (Jayasooriya et al., 2014)
	1µM/1hour	DNA synthesis inhibition	CSB (Bruno, Giaretti and Darzynkiewicz, 1992)
Etoposide (ETP): The derivative of podophyllotoxin, ETP, compromises topoisomerase II (TopoII) function.	2–100µM/1-3hours	Replisome disassembly	Hela, AT1 BR and ATR3 BR (Montecucco et al., 2001)
	100µM	G2/M arrest	HT-29 (Schonn, Hennesen and Dartsch, 2009)
	1.5 µM/18 hours	Apoptosis	MEFs (Jamil et al., 2015)

1.8.2 The Eukaryotic DNA Damage response network

Central to the DDR network are three serine/threonine kinases that belong to the phosphatidylinositol-3-kinase-like kinase family (PIKKs) comprised of ATM and Rad3-related (ATR), Ataxia-telangiectasia mutated (ATM), and DNA-dependent protein kinase (DNA-PK) (Blackford and Jackson, 2017). ATR and ATM are master transducers of DDR signalling pathways involved in activation of their main protein kinase targets checkpoint kinase 1 (CHK1) and checkpoint kinase 2 (CHK2) respectively downstream of a signalling cascade (Smith et al., 2010). DNA-PK targets are much less than targets for ATR and ATM and are mainly involved in DSB repair mechanisms (Blackford and Jackson, 2017). Multiple reports indicate that ATR and ATM’s activation and recruitment correspond to the nature of DNA damage and act in distinct pathways (Marechal and Zou, 2013; Álvarez-Quilón et al., 2014; Haahr et al., 2016). However, their downstream targets and response can also partially overlap based on genotoxic stressor type (Weber and Ryan, 2015).

ATR becomes activated when stretches of single-stranded DNA (ssDNA) are generated due DNA replication stress, double-stranded DNA junctions, and resected DSBs that are coated by a heterotrimeric ssDNA binding protein known as replication protein A (RPA) (Figure 1.8.2A) (Blackford and Jackson, 2017; Kotsantis, Petermann and Boulton, 2018). ATM is primarily activated following the formation of DNA DSBs which are sensed by a multiprotein complex comprised of meiotic recombination 11 homolog 1 (MRE11), RAD50 double strand break repair protein (RAD50), and Nijmegen breakage syndrome protein 1 (NBS1) which constitute the MRN complex (MRE11-RAD50-NBS1 complex). The formation of the MRN complex following DSB detection results in the concomitant recruitment and activation of downstream effectors involved in the ATM pathway (Figure 1.8.2B) (Jackson, 2002; Álvarez-Quilón et al., 2014). Following, ATR mediated activation of CHK1 and ATM mediated activation of CHK2, cyclin-dependent kinase (CDK) activity is inhibited through multiple mechanisms (Reviewed in Bartek and Lukas, 2007; Kastan and Bartek, 2004). Importantly, CDK inhibition enables the slowing of the cell cycle or arrest at G1-S, intra-S and G2-M cell cycle checkpoints (Jackson and Bartek, 2009). Signalling by ATM and ATR following DNA damage leads to upregulated expression of genes involved in DNA repair and subsequent recruitment of DDR proteins at sites of DNA damage. Furthermore, the localisation of proteins to regions of DNA damage are mediated through PTMs including phosphorylation, acetylation or SUMOylation (Huen and Chen, 2007). However, a complete understanding of the significance of multiple ATR/ATM-mediated PTMs specifically phosphorylation events require further work (Jackson and Bartek, 2009; Matsuoka et al., 2007). Ensuring tight regulation of genes associated with the DDR is therefore imperative to for efficient DDR signalling which includes DNA repair mechanisms. Extensive reports focusing on the molecular network of the DDR have implicated dysregulation of these outlined processes to be associated with human diseases such as cancer (Dietlein, Thelen and Reinhardt, 2014).

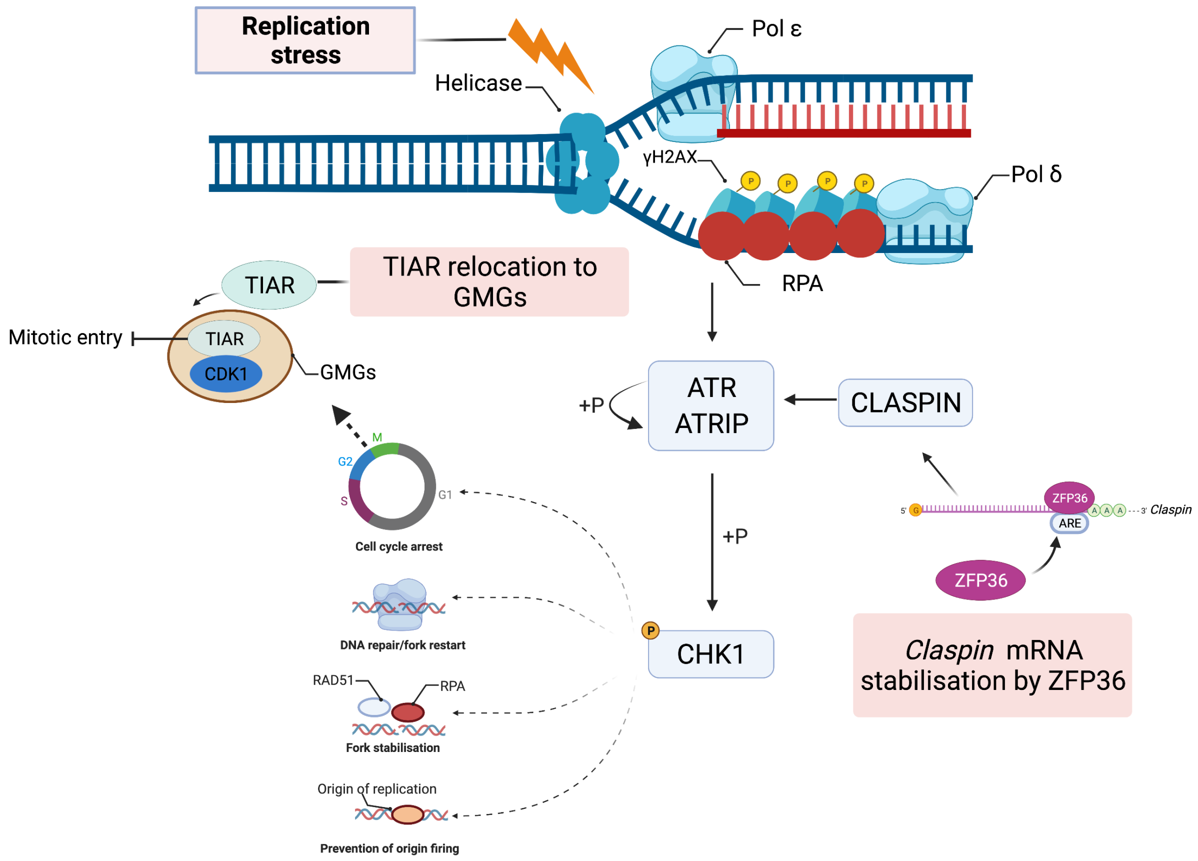
Replication stress
Helicase
Pol ε
γH2AX
P
Pol δ
RPA
TIAR relocation to GMGs
TIAR
Mitotic entry
TIAR
CDK1
GMGs
ATR
ATRIP
+P
CLASPIN
M
G2
S
G1
Cell cycle arrest
ZFP36
ARE
5'
G
A A A
3'
Claspin
ZFP36
+P
DNA repair/fork restart
P
CHK1
Claspin mRNA stabilisation by ZFP36
RAD51
RPA
Fork stabilisation
Origin of replication
Prevention of origin firing

Figure 1.8.2A AU-RBPs coordinate the replication stress response.

Replication stress results in ssDNA formation as the DNA is unwound by the replicate helicase. The exposed ssDNA is protected by RPA initiating the recruitment of ATR kinase coupled to ATR interacting protein (ATRIP) and subsequent ATR autophosphorylation (+P) at Threonine1989. ATR-mediated phosphorylation of master cell-cycle regulator CHK1 is first initiated through ATR-ATRIP interactions with CLASPIN enabling CHK1 phosphorylation at serine residues 317 and 345. H2A histone family member x (H2AX) is phosphorylated by ATR at serine 139 (γH2AX) early in the replication stress response. CHK1 phosphorylation enables replication fork resolution by arresting the cell-cycle, preventing origin firing, stabilisation of replication forks and initiating DNA repair. The AU-RBP ZFP36 has been demonstrated to stabilise *CLASPIN* mRNA increasing CLASPIN protein expression in response to replication stress ensuring faithful activation of CHK1 by ATR. Similarly, replication stress triggers TIAR-mediated arrest at the G2/M border by restricting CDK1 in G2/M transition granules (GMGs) preventing entry into mitosis (discussed below) (Sidali et al 2022).

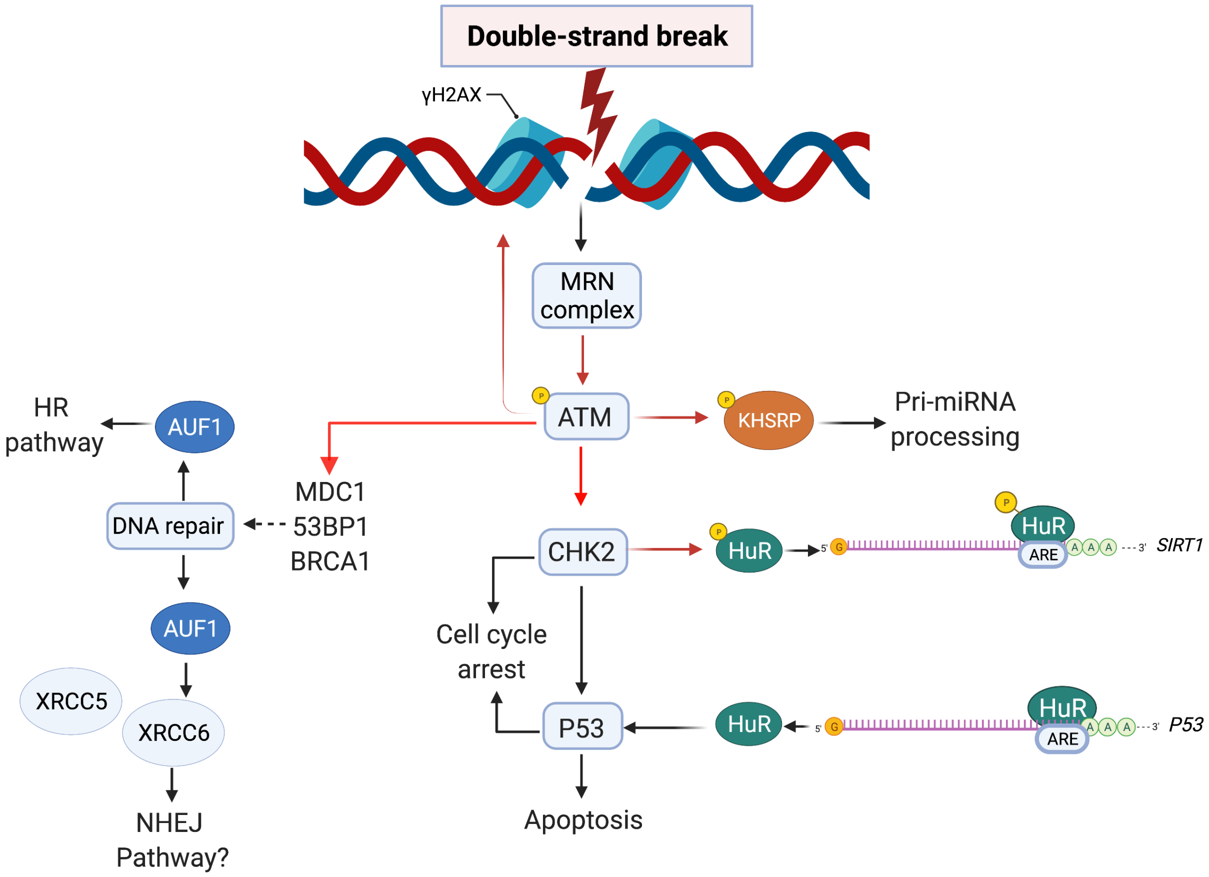
Double-strand break
γH2AX
MRN complex
P
ATM
P
KHSRP
Pri-miRNA processing
HR pathway
AUF1
DNA repair
MDC1
53BP1
BRCA1
AUF1
XRCC5
XRCC6
NHEJ Pathway?
CHK2
P
HuR
5'
G
P
HuR
ARE
A A A
3'
SIRT1
Cell cycle arrest
P53
HuR
5'
G
HuR
ARE
A A A
3'
P53
Apoptosis

Figure 1.8.2B AU-RBPs coordinate the DNA double strand-break response network.

DSBs are sensed by the MRN complex leading to the phosphorylation (red arrow) and activation of ATM. Once activated ATM phosphorylates DSB effector proteins CHK2, p53, BRCA1 and 53BP1. ATM-mediated phosphorylation of these effector proteins results in cell-cycle arrest, apoptosis, and DNA repair through HR or NHEJ pathways. Importantly, ATM mediated activation of γH2AX, leads to the recruitment of MDC1 (Mediator of DNA Damage Checkpoint 1) and γH2AX signalling across large chromatin domains, recruiting DNA repair proteins at sites of DSBs. AU-RBPs form direct interactions with DSB response proteins such as ATM-mediated phosphorylation of KHSRP early in the DSB response pathway promoting pri-miRNA processing by KHSRP. Similarly, CHK2-mediated phosphorylation of HuR promotes HuR's destabilisation action of *SIRT1* mRNA. On the other hand, HuR can also stabilise *p53* mRNA in response to DSB, promoting p53 translation. AU-RBP AUF1 promotes DSB through the HR pathway and has been reported to interact with XRCC5 and XRCC6 which are key factors involved in NHEJ (Discussed below) (Sidali et al 2022).

.

The DDR orchestrates a plethora of processes in response to DNA damage including reducing mRNA stability, transcription inhibition, limiting mRNA 3'-end processing and inhibition of translation factors involved in initiation and elongation (Kleiman and Manley, 2001; Fan et al., 2002; Mirkin et al., 2008, Braunstein et al., 2009; Kruiswijk et al., 2012). Therefore, DNA damage-dependent gene repression can be partially attributed to a reduction in levels of mRNA (Dutertre et al., 2014). Moreover, DNA damage can also lead to a global reduction in protein levels due to translational reprogramming, favouring genes required for the DDR (Powley et al., 2009). Indeed, microarray analysis of polysome-bound mRNAs under DNA damaging conditions demonstrated mRNAs that encode for DDR proteins evade translation repression (Kumaraswamy et al., 2008; Powley et al., 2009; Badura et al., 2012). Importantly, multifaceted *trans*-acting factors namely AU-RBPs have emerged as important modulators of key processes that ensure a faithful DDR. Moreover, AU-RBPs have been implicated in multiple aspects of the DDR from post-transcriptional regulation of key response genes to localising to sites of DNA damage to mediate DNA repair. Here we focus on the ZFP36 family and five other important AU-RBPs and their role key roles in the DDR.

1.8.3 AU-RBPs post-transcriptionally regulate key DDR genes

Key findings have implicated AU-RBPs to post-transcriptionally modulate key DDR genes in response to replication stress and DNA damage (Figure 1.8.3). Recently ZFP36 was found to be associated with the replication stress response pathway by modulating ATR-mediated activation of CHK1 (Lee et al., 2020). Specifically, ZFP36 was reported to bind and stabilise *Claspin* mRNA which is an essential component in mediating ATR-CHK1 interactions in response to replication stress (Lee et al., 2020). ZFP36 mediated stabilisation of *Claspin* mRNA was dependent on 3'UTR binding following induction of replication stress by depleting deoxynucleoside triphosphate pool with hydroxyurea (HU). ZFP36 depleted cells display compromised CLASPIN expression leading to defective ATR-CHK1 activation, slowing of replication forks, DSBs (measured by 53BP1/γH2AX colocalisation), and chromosome aberrations when treated with HU or cisplatin (Lee et al., 2020). Therefore, this report identified that ZFP36's post-transcriptional regulatory mechanisms are important for the maintenance of genome integrity during episodes of replication stress. Similarly, evidence from developing lymphocytes in mice suggests that ZFP36L1 and ZFP36L2 have a role to play in the DDR and genome maintenance. Simultaneous, ablation of both *Zfp36l1 and Zfp36l2* in developing thymic T-cells was shown to increase γH2AX signal and phosphorylation of ATR/ATM substrates CHK1 and the p53 antagonist mouse double minute 2 homolog (MDM2) respectively (Vogel et al., 2016). Furthermore, integration of RNA sequencing (RNA-Seq) expression data with iCLIP to determine the effects on the transcriptome following *Zfp36l1 and Zfp36l2* deletion demonstrated upregulation of DNA damage-related transcripts (Vogel et al., 2016). Therefore, both ZFP36L1 and ZFP36L2 can potentially influence the expression of DDR related proteins post-transcriptionally. Importantly, *in vitro* assays in human cell lines have elucidated that ZFP36L1 and ZFP36L2 are involved in the regulation of cell-cycle progression, achieved through targeted destabilisation of cell cycle-related mRNAs that have known function in the DDR including cyclins and cyclin-dependent kinase inhibitors such as p21 (Al-Haj, Blackshear and Khabar, 2012; Galloway et al., 2016).

Like the ZFP36 family, other AU-RBPs are involved in regulating expression of genes in the DDR. The AU-RBP HuR has been reported to regulate the expression of cell cycle control genes cyclins A2, B1, D1 and E1 and DDR and DNA repair genes such as p53 and BRCA1 (Saunus et al., 2008; Caldon and Musgrove, 2010). Importantly, DNA damage has been reported to influence HuR’s stabilising activity over mRNAs encoding DDR and DNA repair proteins and their subsequent expression (Kim, Abdelmohsen and Gorospe, 2010). Specifically, human colorectal carcinoma cells exposed to short-wavelength UV light (UVC) increase HuR stabilisation of *p53* mRNA thus, increasing P53 expression. Similarly, a recent report suggests that HuR limits radiation-induced DNA damage post-transcriptionally by modulating the expression of AT-rich interactive domain 1A (SWI-like) (ARID1A) which is an important factor in promoting DNA repair through non-homologous end joining (Watanabe et al., 2014; Andrade et al., 2019). Specifically, exposure to ionising radiation induces HuR-mediated stabilisation of ARE containing *ARID1A* mRNA, increasing ARID1A expression and suppressing the formation of DSBs (Andrade et al., 2019). Interestingly, HuR was reported to mediate DNA repair by modulating Poly (ADP-ribose) glycohydrolase (*PARG*) mRNA (Chand et al., 2017), PARG associates with Poly (ADP-ribose) polymerase 1 (PARP-1) to mediate DNA repair (Chand et al., 2017). Exposure to PARP inhibitors promotes *PARG* mRNA stabilisation by HuR, leading to PARG upregulation, and facilitating efficient DNA repair in pancreatic ductal cancer cells (Chand et al., 2017). Whereas knockdown of HuR resulted in DNA damage accumulation (Chand et al., 2017). Thus, collectively, these reports suggest that HuR adopts an important role in facilitating DNA repair through post-transcriptional control of DDR genes in response to genotoxic stress.

Similarly, AU-RBP TIAR has been shown exhibit roles in replication stress response initiation and regulation of the G2/M transition (Lafarga et al., 2018). TIAR was found to attenuate CDK1 activity in stress-induced G2/M transition granules (GMGs) at replication forks which comprise factors involved in DNA replication and repair, transcription, and splicing inducing arrest at the G2/M border (Lafarga et al., 2018). Moreover, the knockdown of TIAR induced the accumulation of DSBs and chromosomal aberrations (Lafarga et al., 2018). Importantly, CDK1 attenuation in GMGs was dependent on TIARs RNA binding domain (Lafarga et al., 2018). However, it is unknown if TIAR exhibits post-transcriptional control over factors involved in the replication stress response. AU-RBP TIA1 was reported to regulate P53 expression in response to genotoxic stress, relocating *P53* mRNA from stress granules to polysomes for swift translation to ensure the generation of a functional B cell receptor (Díaz-Muñoz et al., 2017). AU-RBPs AUF1 and TIAR are reported to post-transcriptionally derepress Growth Arrest and DNA damage-inducible alpha protein (Gadd45α) expression following genotoxic doses of methyl methanesulfonate (MMS) (Lal et al., 2006). Transcripts encoding for *Gadd45α* are typically upregulated in response to stress stimuli. However, in unperturbed conditions AUF1 and TIAR interact with the 3′UTR of *Gadd45α*, destabilising and inhibiting *Gadd45α* translation (Lal et al., 2006). Subsequent treatment with MMS increases the half-life and translation of *Gadd45α* mRNA due to AUF1 and TIAR's dissociation from *Gadd45α* (Lal et al., 2006). Thus, suggesting a DNA damage-dependent role for AUF1 and TIAR dissociation from *Gadd45α* mRNA.

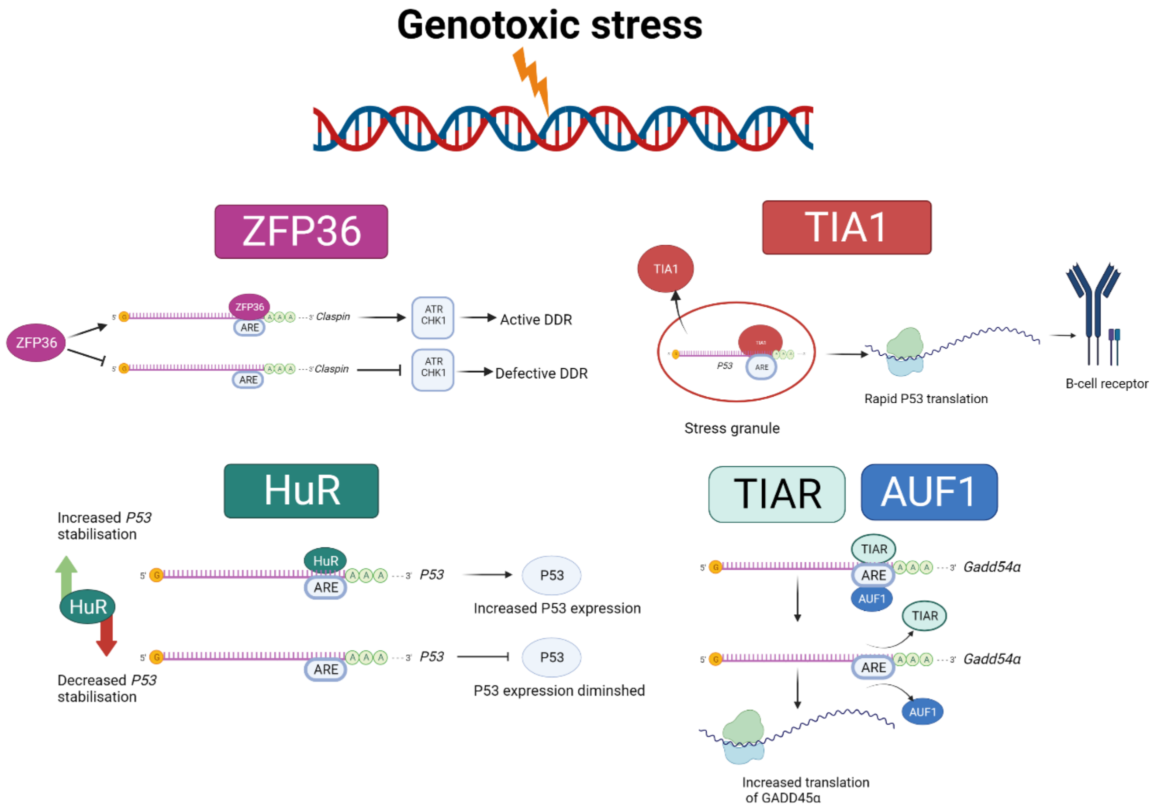
Genotoxic stress
ZFP36
ZFP36
ZFP36
ARE
Claspin
ATR CHK1
Active DDR
ARE
Claspin
ATR CHK1
Defective DDR
TIA1
TIA1
P53
ARE
Stress granule
Rapid P53 translation
B-cell receptor
HuR
Increased P53 stabilisation
HuR
HuR
ARE
P53
P53
Increased P53 expression
ARE
P53
P53
P53 expression diminshed
Decreased P53 stabilisation
TIAR
AUF1
TIAR
ARE
AUF1
Gadd54a
TIAR
ARE
Gadd54a
AUF1
Increased translation of GADD45α

Figure 1.8.3 Genotoxic stress facilitates post-transcriptional gene expression of DDR genes by AU-RBPs.
Genotoxic stress results in *CLASPIN* mRNA stabilisation by ZFP36 leading to an active DDR through the ATR/CHK1 pathway, and ZFP36 inhibition results in a defective DDR. Changes to HuR's protein expression (Green/Red arrow) affect HuR's post-transcriptional stabilisation role over *P53* mRNA thus impacting P53 expression. TIA1 re-localises *P53* mRNA from stress granules for rapid translation to ensure proper B-cell receptor development. TIAR and AUF1 dissociate from *Gadd45α* mRNA leading to increased Gadd45α expression (Sidali et al 2022).

Despite limited information on the molecular mechanisms associated with AU-RBP interactions with intronic AREs. There are, however, reports of intronic AREs present in nuclear pre-mRNAs which pose a potential role for AU-RBP ZFP36 in modulating pre-mRNAs by virtue of intronic binding (Lebedeva et al., 2011; Mukherjee et al., 2011; Mukherjee et al., 2014; Sedlyarov et al., 2016; Bakheet et al., 2018). Moreover, there is evidence to suggest that AU-RBP HuR stabilises nuclear pre-mRNAs through intronic ARE binding (Mukherjee et al., 2011; Bakheet et al., 2018). For example, in HEK-293 cells the knockdown of HuR was demonstrated cause a reduction in the levels of mRNAs for genes containing intronic AREs (Bakheet et al., 2018). Interestingly, DDR and DNA repair genes such as ATR, ATM, CHK1, CHK2 and MRE11 contain intronic AREs and could be potential targets for AU-RBPs (Bakheet, Hitti and Khabar, 2017). More so that these genes experience transcriptional upregulation following genotoxic stress, thus presenting a possibility for AU-RBPs to facilitate their subsequent expression through intronic-ARE binding of pre-mRNAs in the nucleus (Christmann and Kaina, 2013). However, the relevance of intronic AREs to the DDR and maintenance of genomic integrity remains largely unknown.

1.8.4 DNA damage stimulates PTMs of AU-RBPs

PTMs are key for mediating and enduring efficient DDR signalling in conditions of genotoxic stress (Jackson and Bartek, 2009). Studies implementing phosphoproteomic screens have elucidated to the phosphorylation of multiple AU-RBPs by DNA damage sensors, transducers, and downstream kinases in response to DNA damage (Matsuoka et al., 2007; Jungmichel et al., 2013). The AU-RBP HuR is phosphorylated by CHK2 in response to ionising radiation mediating its stabilisation activity on mRNA leading to upregulated expression of multiple proteins, one of which included ZFP36L1 (Mazan-Mamczarz et al., 2011). Thus, this demonstrates that CHK2-dependent phosphorylation of HuR could also potentially promote ZFP36L1's role in the DDR through a feedback loop (Mazan-Mamczarz et al., 2011). Moreover, micro-array analysis in CHK2 proficient and deficient HCT116 cells report that HuR dissociates from its target mRNAs in a CHK2 proficient background and remains bound to mRNAs in the absence of CHK2 following exposure to ionising radiation (Masuda et al., 2011). Therefore, demonstrating a CHK2-dependent mechanism whereby CHK2 modulates HuR's post-transcriptional activity. Similarly, AU-RBP KHSRP is targeted for phosphorylation by ATM in response to DSBs (Moskwa et al., 2011). ATM-mediated phosphorylation of major KHSRP residues S274 and S670 promote KHSRP's role in primary-microRNA (pri-miRNA) biogenesis in response to DSBs, a process that has reported importance in DNA repair (Moskwa et al., 2011; Han et al., 2012).

The AU-RBP TIAR has also been shown to undergo phosphorylation mediated by p38 in response to genotoxic stress, exhibiting its post-transcriptional regulation of *Gadd45α* mRNA, an important factor in blocking entry in mitosis with unrepaired DNA (Dietlein, Thelen and Reinhardt, 2014). Hela cells exposed to DNA damaging agent doxorubicin, followed by RNA-immunoprecipitation (RNA-IP) of TIAR revealed a correlation between p38 activity and TIARs binding to *Gadd45α* mRNA. Disruption of p38 activity increased TIAR's binding to *Gadd45α* mRNA, whereas cells proficient for p38 expression resulted in phosphorylation of TIAR and its dissociation from *Gadd45α* mRNA (Dietlein, Thelen and Reinhardt, 2014). Importantly, p38-mediated phosphorylation of TIAR was also dependent on sequent MK2 (mitogen-activated protein kinase (MAPK)-activated protein kinase-2) phosphorylation of hnRNP A0 (Heterogeneous nuclear ribonucleoprotein A0) and PARN, suggesting TIAR to be involved in a positive feedback loop (Dietlein, Thelen and Reinhardt, 2014). Expression of ZFP36L2 has been reported to be cell cycle related, with increased expression in mitosis and decreased expression in interphase (Noguchi et al., 2018). This apparent reduced ZFP36L2 expression in interphase was shown to be dependent on the ZYG11B-E3 ubiquitin ligase complex mediating ZFP36L2 polyubiquitination and subsequent degradation (Noguchi et al., 2018). Interestingly, cisplatin-treated HCT116 colorectal cancer cells demonstrated increased ZFP36L2 expression, induced S-phase arrest, and increased cell viability (Noguchi et al., 2018). Therefore, implying ubiquitination of ZFP36L2 is inhibited following cisplatin-induced DNA damage, upregulating ZFP36L2 expression to protect cells from DNA damage by controlling S phase transition.

1.8.5 DNA damage orchestrates AU-RBP subcellular localisation

DNA damage can orchestrate AU-RBP subcellular localisation and this apparent change in environment can influence AU-RBP interactions and activities of. Sharing similar characteristics of nucleo-cytoplasmic shuttling activities to the ZFP36 family, other AU-RBPs have been reported to exhibit nuclear to cytoplasmic or cytoplasmic to nuclear translocations in response to genotoxic stress which could partially explain their multi-faceted nature. AU-RBP HuR exhibits changes in cell-cycle-dependent subcellular localisation. HuR was found to be contained in the nucleus in the G1 phase and cytoplasmic in S/G2 regulating mRNA stability and translation (Kim and Gorospe, 2008). Furthermore, UV damage influences the subcellular localisation of HuR in cyclin-dependent kinase 1 (CDK1) dependent manner (Al-Khalaf and Aboussekhra, 2013). ATR phosphorylates CDK1 promoting its dissociation from HuR, resulting in HuR's cytoplasmic translocation from the nucleus where it binds mRNA target *p21/CDKN1A* reducing its turnover (Al-Khalaf and Aboussekhra, 2013). This is further supported by reports demonstrating ATM/p38 signalling promotes cytoplasmic shuttling of HuR from the nucleus in response to ionising radiation, where it stabilises mitochondrial transcription factor A (*TFAM*) mRNA (Zhang and Wang, 2018). TFAM is important for the activation of transcription promoters of mitochondrial DNA (Ngo et al., 2014). Therefore, this suggests that HuR's subcellular localisation can be influenced by both ATR and ATM and possibly responds to various DNA lesions. AU-RBPs TIAR and TIA-1 also exhibit nucleo-cytoplasmic shuttling which is important for their role in alternative splicing of nuclear pre-mRNAs (Förch et al., 2000). Furthermore, TIAR has been demonstrated to exhibit nuclear to cytoplasmic translocation following Fas-mediated apoptotic cell death (Taupin et al., 1995). It is likely, that TIA-1 and TIAR's nuclear-cytoplasmic shuttling plays a role in their cellular function as these two AU-RBPs can bind DNA with high affinity (Suswam, 2005), although TIAR and TIA-1's ability to bind DNA in response to genotoxic stress remains unknown. ZFP36L1 like HuR exhibits nucleo-cytoplasmic shuttling that has also been reported to be cell cycle-dependent remaining mainly nuclear in the G1/S and eliminated in the G2 phase (Matsuura et al., 2020). Importantly, ZFP36L1 and HuR can mediate their post-transcriptional activities on the same mRNAs, albeit through destabilisation or stabilisation mechanisms respectively (Zekavati et al., 2014; Sundvold, 2020). Therefore, it could be possible that ZFP36L1 exhibits similar nucleo-cytoplasmic shuttling in response to DNA damage to modulate the expression of DDR proteins.

1.8.6 Emerging role of AU-RBPs in DNA repair

RBPs have been reported to localise at sites of DNA lesions (Anantha et al., 2013; Ha, Takeda and Dynan, 2011; Polo et al., 2012). Similarly, a selection of AU-RBPs has emerged as key mediators of DNA repair in response to genotoxic stress where they exhibit canonical mRNA interactions or non-canonical interactions at sites of DNA damage mediating efficient DNA repair. Unlike HuR which was shown to mediate DNA repair through stabilisation of *PARG* and *ARID1A* mRNA (Chand et al., 2017; Andrade et al., 2019). AU-RBP AUF1 was reported to mediate efficient DNA repair in an mRNA-independent manner by localising to sites of DNA damage (Alfano et al., 2019). Proteomic screens identified AUF1 to be involved in DNA end resection, a vital process in the HR-mediated DNA repair pathway, providing ssDNA tails to enable the invasion of complementary DNA strands (Huertas, 2010; Alfano et al., 2019).

Specifically, AUF1 was found to bind synthetic protruding nucleotide ends that mimic DNA end-resection intermediates independent of the RPA complex (Alfano et al., 2019). This was further supported through the identification of chromatin-bound AUF1 in Hela cells that demonstrated binding to cellular DNA was independent of AUF1's RRM suggesting AUF1 elicits binding to DNA in an RNA-independent manner (Alfano et al., 2019). Finally, CPT treated Hela cells demonstrated an increased presence of recombinant FLAG-tagged AUF-1 (FLAG-AUF1) at sites of DSBs, knockdown of AUF-1 decreased efficiency of DNA end resection and HR demonstrating its role in HR repair pathway independent of its post-transcriptional regulatory mechanisms (Alfano et al., 2019). Intriguingly, immunoprecipitation of AUF-1 followed by mass spectromtry in oral cancer cell lines SCC4 and MDA1986, identified interactions with NHEJ repair proteins XRCC5 and XRCC6 involved in tethering broken DNA ends (Spagnolo et al., 2006; Kumar et al., 2015).

1.8.7 AU-RBP's association with R-loops

Three stranded nucleic acid structures known as R-loops made up of an RNA: DNA hybrid and a displaced single-stranded non-template DNA strand have been implicated to threaten genome integrity (Gomez-Gonzalez and Aguilera, 2007; Gan et al., 2011; Hamperl et al., 2017; Stirling and Hieter, 2017). The formation of short (8-11bps) RNA-DNA hybrids during transcription or replication of the lagging strand plays important physiological roles in transcription termination, telomere regulation dynamics and immunoglobulin class switching (Santos-Pereira and Aguilera, 2015). However, more stable, and longer co-transcriptional RNA: DNA hybrids occur when transcribed RNA exits from RNA polymerase and re-anneal with a template DNA strand (Stork et al., 2016). These R-loops, if remain unprocessed can prove highly deleterious to genome integrity, leading to mutations of the displaced single-stranded non-template strand by DNA modifying enzymes, obstructing replication progression and increasing replication fork encounters with transcription machinery (transcription-replication conflicts) thus resulting in DNA breaks, chromosome rearrangements and recombination events (Gómez-González and Aguilera, 2007; Gan et al., 2011; Hamperl et al., 2017; Stirling and Hieter, 2017). Therefore, cells must regulate the levels of R-loops to prevent their excessive formation and thus deter genomic instability. Multiple factors involved in distinct pathways have been identified to prevent or resolve R-loop formation (Chakraborty and Grosse, 2011; Wahba et al., 2011; Singh et al., 2018). Importantly, proteins involved in mRNA biogenesis and processing such as RBPs have emerged as important regulators of R-loops and their loss has been associated with increased R-loop accumulation (Huertas and Aguilera, 2003; Wahba et al., 2011; Stirling et al., 2012). The link between R-loops and RBPs can also be expanded to selected AU-RBPs that may prevent or resolve R-loops (Figure 1.8.7). Indeed, pull-down assays followed by mass spectrometry have identified that AU-RBPs TIAR, KSHRP, HuR and AUF1 interact with R-loops in human cells (Cristini et al., 2018; Wang et al., 2018). Furthermore, CRISPR-Cas9 mediated ablation of AUF1 was also found to increase R-loop formation causing defects in DNA repair mechanisms in CPT-treated Hela cells (Alfano et al., 2019). Overexpression of ribonuclease H1 (RNase H1), a ribonuclease that degrades the RNA moiety of the RNA:DNA hybrid leads to a reversal of the phenotype associated with AUF1 ablation (Nguyen et al., 2017, Alfano et al., 2019). Therefore, suggesting that AUF1 exhibits functions to favour R-loop removal to ensure efficient DNA repair and maintain genome integrity similar to other RBPs.

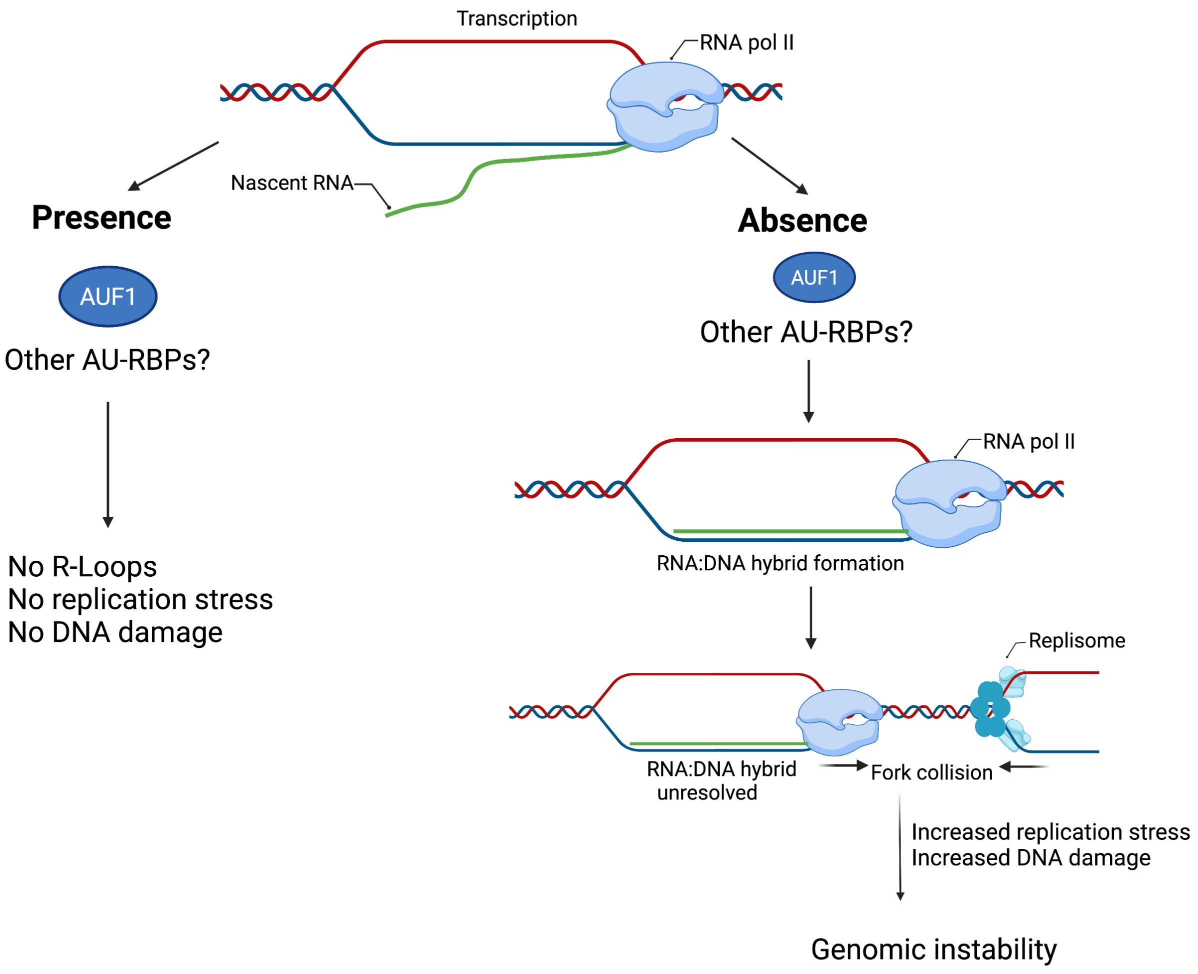
Transcription
RNA pol II
Nascent RNA
Presence
AUF1
Other AU-RBPs?
No R-Loops
No replication stress
No DNA damage
Absence
AUF1
Other AU-RBPs?
RNA pol II
RNA:DNA hybrid formation
Replisome
RNA:DNA hybrid unresolved
Fork collision
Increased replication stress
Increased DNA damage
Genomic instability

Figure 1.8.7 The emergence of AU-RBPs in R-loop prevention for the maintenance of genome integrity

RNA is transcribed by RNA polymerase II (RNA pol II) during transcription. The emerging nascent RNA is prevented from hybridising with the template DNA strand forming an RNA: DNA hybrid (R-loop) by AUF1 and potentially other AU-RBPs known to interact with R-loops. Therefore, In the presence of AUF1 and potentially other RBPs R-loops are suppressed protecting cells from replication stress and DNA damage. In AUF1's absence which may include other AU-RBPs the newly transcribed RNA may hybridise with the template strand causing displacement of the non-template DNA strand into an exposed ssDNA forming a three stranded nucleic acid structure known as an R-loop. When unresolved, R-loops increase the prevalence of transcription and replication fork collisions and compromise genomic integrity due to the increased frequency of replication stress and DNA damage (Sidali et al., 2021).

Substantial evidence has alluded to regions of the genome known as chromosomal fragile sites to be susceptible to forming gaps and breaks (termed ‘expression) under conditions of replication stress, (Tsantoulis et al., 2007). A well-defined category of fragile sites is known as common fragile sites (CFS). *In-vitro* CFS are stable in unperturbed conditions but exhibit breaks (CFS expression) under conditions of mild replication stress by low-doses of the DNA polymerase inhibitor aphidicolin (APH) or *in vivo* due to oncogene activation (Ozeri-Galai, Bester and Kerem, 2012). CFS coincide with large/late replication genes that are adenine thymine (AT)-rich and are often short of dormant origins of replication (Ozeri-Galai, Bester and Kerem, 2012). CFS can be prone to mutations and translocations/deletions due to sister chromatid exchanges and are therefore hotspots for genomic instability (Arlt et al., 2006). Moreover, tumours have been shown to exhibit breakpoints that have been mapped to CFS loci leading to loss of tumour suppressor genes or oncogene amplification (Hellman et al., 2002; Bignell et al., 2010). Separate categories of chromosomal fragile sites known as rare fragile expressed are expressed by folic acid and early replicating fragile sites (ERFSs), located within early replicating actively transcribed genes are expressed under replication arrest with hydroxyurea (Barlow et al., 2013). Importantly, as CFS contain large genes where transcription and replication can occur simultaneously or transcription can be extended beyond one cell cycle this leads to inevitable transcription-replication conflicts (TRC) (Helmrich, Ballarino and Tora, 2011; Hamperl et al., 2017). Thus, the susceptibility to TRC at CFS results in the increased prevalence of R-loop formation that can increase during episodes of replication stress causing further replication fork stalling, DNA breaks and promote genomic instability (Hamperl et al., 2017). Therefore, suggesting that R-loops modulation at CFS is important to maintain genomic integrity. Interestingly, four AU-RBP genes have been mapped to fragile site loci (Kumar et al., 2019). The genes for *ZFP36 and ZFP36L1* are mapped to APH-induced common fragile sites FRA19A and FRA14C respectively (Kumar et al., 2019). Whereas *TIAR* is located at FRA10A *and HuR* at FRA19B which are folate-sensitive rare fragile sites (Kumar et al., 2019). The occurrence of these AU-RBPs at fragile site loci is in relation to R-loops and genomic stability remains unknown. Despite the labile nature of CFS, they remain highly conserved across species and genes spanning these regions have been suggested to act as early sensors of DNA damage, therefore, underlining an interesting area for further research (Georgakilas et al., 2014; Voutsinos, Munk and Oestergaard, 2018).

It has long been assumed that AU-RBPs exhibit important biological activities through established roles in the post-transcriptional regulation of mRNA. Typically, AU-RBPs impact mRNA translation through ARE binding in the 3'UTR of mRNA, resulting in degradation or stabilisation. However, the emerging roles of AU-RBPs presented in this report demonstrate their ability to exhibit functions independent of their mRNA regulatory roles through protein interactions or localising to sites of DNA damage highlighting their multi-faceted nature implicit in the complex mechanisms that constitute the maintenance of genome integrity. Our understanding of the effects post-transcriptional regulation of AU-RBPs has on target mRNA is still evolving as demonstrated by ZFP36 which for the past 20 years has been associated with mRNA destabilisation but has recently been shown to exhibit a stabilising role to maintain genome integrity (Lee et al., 2020). Furthermore, AU-RBPs including the ZFP36 family member ZFP36L1, exhibit key functions in post-transcriptional control of DDR regulators and mediators through canonical mRNA interactions highlighting the importance of post-transcriptional mRNA regulatory mechanisms for the maintenance of genome stability. Alternatively, AU-RBPs also display non-canonical interactions to maintain genome integrity through protein-protein interactions directed for PTMs by DDR components influencing their subsequent activity in response to genotoxic stress. Like ZFP36L1 all AU-RBPs described exhibit nucleo-cytoplasmic shuttling activity most of which are influenced in response to genotoxic stress. Although nucleo-cytoplasmic shuttling is associated with post-transcriptional mRNA regulatory mechanisms, it does hold an intriguing area for further study to identify if AU-RBPs can localise to sites of DNA damage and influence DNA repair mechanisms. Importantly, as we have highlighted in the study, the dysfunction of these AU-RBPs has been implicated in driving the hallmarks of carcinogenesis and genomic instability (Hanahan and Weinberg, 2011). Consistent with these findings is ZFP36L1's ability to adopt tumour suppressive properties, and its loss has been implicated in a plethora of cancers. However, the molecular mechanisms associated with ZFP36L1, and cancer remain unknown. Moreover, the reports highlighted thus far including the emergence of ZFP36 in the replication stress response pose a potential for ZFP36L1 to play a role like other AU-RBPs in suppressing genomic instability.

1.9 Study aim

AU-RBPs including the ZFP36 family members have emerged as pivotal proteins involved in maintaining genomic integrity in response to replication stress and DNA damage. Furthermore, numerous reports highlighting ZFP36L1 to function as a tumour suppressor may suggest an integral role of the protein in the maintenance of genome integrity. However, a potential role for ZFP36L1 and associated mechanisms involved in upholding genome stability, in conditions of replication stress is yet to be determined. Therefore, this study sets out to uncover a link between ZFP36L1 and suppression of replication stress associated genomic instability through the following objectives:

1. Generate a ZFP36L1 CRISPR-Cas9 knock-out (KO) cellular model. For this, we aimed to employ a tetracycline-inducible human osteosarcoma U-2OS (T-REx) cell line as the model system of choice (Chapter 3). U-2OS cells are a widely utilised model to study replication stress (Lukas et al., 2011; Di Marco et al., 2017; Okamoto et al., 2018; Mocanu et al., 2022).
2. Derive a T-REx U-2OS system to study the impact of ZFP36L1 loss in replication stress-associated genomic instability. Specifically, assessing for replication stress-associated defects in mitosis (Chapter 4).
3. Investigate the implications of ZFP36L1 loss through assessment of replication stress-associated DNA damage in interphase cells as the potential origin of mitotic defects and genomic instability (Chapter 5).
4. Generate a stable ZFP36L1 inducible expression system in T-REx U-2OS ZFP36L1 KO background, to verify the specificity of the CRISPR-Cas9 KO system and to demonstrate ZFP36L1's role in suppressing replication stress associated genomic instability (Chapter 6).
5. Utilise the T-REx U-2OS ZFP36L1 KO system for inducible expression of exogenous RNase H1 and a catalytically inactive RNase mutant to explore a potential link between ZFP36L1 and R-loop formation in response to replication stress (Chapter 7).
6. Identify novel ZFP36L1 protein interactions in T-REx U-2OS cells through mass spectrometry to highlight a potential mechanism for ZFP36L1's role in suppressing replication stress-associated genomic instability (Chapter 8).

2. Materials and Methods

2.1 Cell lines and cell culture details

T-REx U-2OS cell lines stably expressing the tetracycline repressor protein (kindly donated by Dr Kanagaraj Radhakrishnan, The Francis Crick Institute) were cultured in complete Dulbecco Modified Eagle's Medium (DMEM; Gibco # 11965092) containing tetracycline free fetal bovine serum (FBS; Biowest #S181T-500), 20mM L-Glutamine (Gibco, # 25030081), 100 U/mL penicillin-streptomycin (Gibco #15140122) and 50 µg/ml hygromycin B (Gibco #10687010) at 37°C in a humified incubator set at 5% CO_2. HCT-116 and Hela cells were purchased from American Type Culture Collection (ATCC; HTB-96, CCL-247 and CCL-2) and were cultured in complete DMEM containing with 10% FBS (Sigma-Aldrich, # F7524) and 100 U/mL penicillin-streptomycin (Gibco #15140122) at 37°C in a humified incubator set at 5% CO_2. At 80% confluence cells were washed with phosphate buffer saline (PBS, Gibco #11593377) and dissociated with trypsin-EDTA (Gibco, #25300054). Trypsin action was neutralised with a complete medium. Cell viability was examined regularly with 0.4% trypan blue (Gibco, #15250061) using a haemocytometer under a Leitz Wilovert inverted microscope and subcultured into new culture vessels. Cells were passaged for a maximum number of 12-15 passages. All cell lines utilised in this study contain wild-type protein 53 ($p53^{wt}$) (Bamford et al., 2004; Berglind et al., 2008; Ottaviano et al., 2010).

2.2 ZFP36L1 sgRNA plasmid construction

2.2.1 ZFP36L1 guide RNA design

ZFP36L1 is located on the antisense strand of the q arm of chromosome 14 at genomic location 14q24.1 (Ensemble transcript ID: ENST00000439696.2). Two single guide RNAs (sgRNA) 20 nucleotides in length with the highest on-target specificity to protospacer adjacent motif (PAM) were designed *in silico* from Feng Zhang's database (crispr.mit.edu now known as benchling.com) targeting the first 250 bp of *ZFP36L1* exon 2. It should be noted that exon 1 codes for 15aa are not related to any functional domain of the protein.

The following sgRNAs were selected:

sgRNA1: 5'- TGTCTCGCGAGCTCAGAGCG -3'

sgRNA2: 5'- GTCTCGCGAGCTCAGAGCGG -3'

Modifications were made to sgRNAs to clone into the all-in-one CRISPR plasmid pSpCas9(BB)-2A-Puro V2.0 (PX459) (Addgene, #62988). sgRNA modifications included 5' and 3' BbsI overhangs (green) for ligation in the BbsI restriction sites on the plasmid and a guanine (G) nucleotide (red) required to initiate transcription by the U6 promoter. The following modified forward and complementary sgRNAs were synthesized by Eurofins to enable the construction of a DNA oligo duplex:

sgRNA1-F: 5'- CACCGTGTCTCGCGAGCTCAGAGCG -3'

sgRNA1-R: 5'-AAACCGCTCTGAGCTCGCGAGACAC-3'

sgRNA2-F: 5'- CACCGGTCTCGCGAGCTCAGAGCGG -3'

sgRNA2-R: 5'-AAACCCGCTCTGAGCTCGCGAGACC -3'

2.2.2 Construction of sgRNA oligo duplex and ligation into PX459

Single-stranded oligos corresponding to the guides were synthesized from Eurofins. DNA oligo duplexes were prepared by phosphorylating and annealing 100µM forward and reverse oligos in a 10µl reaction using 10 units of T4 polynucleotide kinase for 5' phosphorylation (New England Biolabs (NEB), #M0201S), 1µl of 10X T4 ligase buffer (NEB, #B0202S) and nuclease-free water (Invitrogen, #AM9939). The reaction mixture was incubated on a heating block (techne) at 95°C for 5 minutes and remained at room temperature (RT) until reaching 25°C.

Before ligation, a 50µl restriction digestion reaction of PX459 was prepared, which included 3µg of PX459,10 units of BbsI restriction enzyme (NEB# R0539), 5µl 10X buffer 2.1 (NEB#B7202S) and remaining volume made up with nuclease-free water. The restriction digestion reaction was incubated for 30 minutes at 37°C. The BbsI digested PX459 plasmid was then treated with shrimp alkaline phosphatase (rSAP) (NEB Cat# M0371S) for dephosphorylation of 5' ends for 30 minutes at 37°C. The digested and dephosphorylated PX459 plasmid was run on a 0.8% agarose gel excised and purified using a Qiagen gel extraction kit (cat# 28706) following the manufacturer's instructions. For ligation of annealed oligos into the PX459 backbone, the oligo duplex was diluted at a 1:100 ratio (1µl of annealed oligo: 99µl nuclease-free water). Subsequently, 60ng of diluted annealed oligo was ligated into 25ng of digested PX459 at an insert to vector molar ratio of 6:1 respectively, using 1 unit of T4 DNA ligase (NEB# M0202) and incubated overnight in a water bath at 16°C. The overnight ligation reaction was then heat-inactivated at 65°C for 10 minutes. Next, the ligation reaction was transformed in One Shot® TOP10 Chemically Competent *E. coli*

(Invitrogen # C404010) following the manufacturer's instructions and incubated at 37^{o}C for 1 hour at 180rpm on a shaker incubator. The transformation mixture was then plated on pre-warmed Luria broth agar (Lennox L agar) (Invitrogen, #22700025) plates containing 100µg/ml ampicillin and incubated at 37^{o}C overnight. Individual bacterial colonies were isolated and inoculated into 5ml LB medium (Miller's LB Broth Base) (Invitrogen# 12795027) containing 100µg/ml ampicillin and incubated at 37^{o}C overnight with constant agitation at 200rpm. Subsequently, bacterial pellets were harvested by centrifugation at 5000rpm for 10 minutes at 4^{o}C, and plasmid DNA was isolated and purified utilising the QIAprep Spin Miniprep Kit (Qiagen #27104) according to the manufacturer's protocol. Purified plasmid DNA samples were sequenced by Sanger sequencing to assess for correctly orientated gRNA inserts employing a U6 polymerase III forward primer (5'-GAGGGCCTATTTCCCATGATTCC-3') provided by GENEWIZ, UK. Upon confirmation of successful gRNA cloning into PX459, plasmids containing the gRNA insert were purified utilising the QIAGEN plasmid Midi Kit (cat. #12143).

2.3 CRISPR-Cas9 targeting of *ZFP36L1*

T-REx U-2OS cells were seeded in 6-well culture plates containing complete DMEM without penicillin at a density of 0.35x10^{6} and 0.25x10^{6} cells respectively and grown to 70% confluency for 24 hours. After 24 hours cells were transfected with two PX459 plasmids containing either sgRNA1 (PX459-sgRNA1) or sgRNA2 (PX459-sgRNA2) targeting *ZFP36L1* utilising Lipofectamine 3000 reagent (Invitrogen# L3000001). For each plasmid 5µg of PX459-sgRNA1 or PX459-sgRNA2 was diluted in 250µL of reduced serum media (Opti-MEM, Gibco# 31985062) and 10µL of p3000 buffer reagent. Next 5µL of lipofectamine 3000 transfection reagent was diluted in 125µL of reduced serum media. 125µl of diluted plasmid DNA was then mixed with 125µL of the diluted transfection reagent, incubated at room temperature for 15 minutes and added to cells. Cells were also individually transfected with PX459 lacking a sgRNA insert (empty vector) following the same conditions to be used as a control for downstream experiments. The following day, cells were released from transfection complexes for a period of 7h and selected with 2µg/ml of puromycin dihydrochloride (Gibco #A1113803) for 24 hours. Post-24hour selection, puromycin-containing media was substituted with a complete medium and incubated until 70% confluent at 37°C in a humified incubator containing 5% CO_2. Single cells were isolated through limiting dilution as previously described with few adjustments (Waldmann and Lefkovits, 1984). Specifically, cells were harvested using standard cell culture techniques described and sub-cultured in 96-well cell culture plates at a seeding density of 0.9 cells per 100µL of supplemented medium and incubated at 37°C in a humified incubator containing 5% CO_2 until 70% confluent. Monoclonal cell populations were expanded into 12-well culture vessels and expanded into 6-well culture plates and T25 flasks for further screening.

2.4 Screening and validation of *ZFP36L1* mutants

2.4.1 *ZFP36L1* Indel screening by agarose gel electrophoresis

To assess for insertion/deletions (indel) at the CRISPR-Cas9 *ZFP36L1* target site. Genomic DNA was extracted from the monoclonal cell population utilising the QIAamp DNA mini kit (Qiagen #51304), following the manufacturer's instructions. Extracted genomic DNA was used to amplify a 449bp (40-489 *ZFP36L1)* CRISPR-Cas9 *ZFP36L1* target site by PCR amplification utilising the following primers:

ZFP36L1 40F: 5’ACCCCTGCTGGTGGGGGC’3 (Eurofins)

ZFP36L1 489R: 5’GTACTTGGGGTGGCGGGTC’3 (Eurofins)

50µl Taq DNA polymerase reaction was prepared as follows 5µl of 10X standard (final concentration: 1X), 1µl of 10mM dNTPs (final concentration 200 µM) (NEB #M0273), 1µl of 10µM forward and reverse primers (final concentration 0.2µM), 500ng genomic DNA and 0.5µl Taq DNA polymerase (2.5units) (NEB #M0273), the final volume was made up with nuclease-free water. The reaction mix was subjected to polymerase chain reaction (PCR) amplification (95°C for 5 minutes, then 25 cycles of 95°C for 30 seconds, 55°C for 30 seconds, 72°C for 45 seconds and final extension for 72°C for 5 minutes) carried out in a Bio-Rad T100 thermal cycler. Finally, PCR amplification products were loaded onto 1% agarose gels and electrophoresis was performed for 1 hour at 100V to verify visual changes to the DNA amplicon size. A DNA size marker was used (1kb DNA ladder, Invitrogen# 10787018).

2.4.2 Analysis of ZFP36L1 protein expression in monoclones

Cells were trypsinised and washed with PBS before being lysed with RIPA buffer (25 mM Tris-HCl pH 7.6, 150 mM NaCl, 5 mM EDTA, 1% Triton X-100, 1% sodium deoxycholate, 0.1% SDS, supplemented with protease inhibitor (Roche # 1836153001)). Lysed samples were incubated on ice for 30 minutes and sonicated for 10 seconds at 20 kHz with a Diagenode sonicator. Cellular debris was separated by centrifugation at 14,000 x g for 20 minutes at 4°C. The supernatant was collected, and protein concentration was quantified through a standard Bradford method (Biorad, # 5000002). Total protein extracts were denatured at 95°C for 5 minutes in 4X SDS sample loading buffer (0.2 M Tris-HCl, 0.4M DTT, 277 mM SDS, 6 mM Bromophenol blue 4.3 M Glycerol) and separated (along with a pre-stained protein marker (Thermofisher scientific #26619) on NuPAGE 10% Bis-Tris protein gels (Invitrogen, #NP0301) in MOPS SDS running buffer (Invitrogen# NP0001) using the XCell Sure Lock Mini-Cell System at 150V for 1hour. Separated proteins were transferred onto Immobilon®-P PVDF Membrane (Millipore, # IPVH00010) in a wet transfer apparatus (Biorad Mini Trans-Blot® Cell) containing ice-cold Towbin buffer (25 mM Tris, 192 mM glycine (pH 8.3) and 20% Methanol (v/v)) at 100V for 90minutes at 4^{o}C. The quality of transferred proteins was assessed by staining the PDVF membrane with Ponceau S solution (1.3mM Ponceau S and 0.874 M glacial acetic acid) with constant agitation for 5 minutes. PVDF membrane was then destained with TRIS-buffered saline containing 0.1% tween (TBS-T; 20 mM Tris-HCl, 150 mM NaCl (pH 7.4) and 0.1% Tween-20) wash buffer. PVDF membrane was then blocked in 5% non-fat dry milk in TBST to prevent non-specific binding of the primary antibody for 1 hour with constant agitation at room temperature. After blocking, the membrane was washed once with TBST and incubated with respective primary antibodies in 5% bovine serum albumin (BSA) or non-fat dry milk in TBST with constant agitation at 4^{o}C overnight (Table 5). Following the primary antibody incubation membranes were washed four times in TBST and incubated with corresponding horseradish peroxidase (HRP)-conjugated secondary antibody at room temperature for 1hour (Table 5). Protein bands were detected with SuperSignal™ West Femto Maximum Sensitivity enhanced chemiluminescent (ECL) substrate (Thermofisher scientific #34094) in a UVP bioimaging system.

Table 5. Antibodies utilised for ZFP36L1 mutant screen by immunoblotting

Primary antibody	Dilution	Supplier; #Catalogue
BRF1/BRF2 (ZFP36L1/ZFP36L2) Rabbit polyclonal	1:1000 in 5%BSA/TBST	Cell Signalling #2119
Loading control: Minichromosome Maintenance Complex Component 7 (MCM-7) Mouse monoclonal.	1:1000 in 5% non-fat milk/TBST	Santa Cruz #9966
Secondary antibody		
Anti-rabbit-HRP conjugated	1:5000 in 5% non-fat milk/TBST	ThermoFisher Scientific #31460
Anti-mouse-HRP conjugated	1:5000 in 5% non-fat milk/TBST	Cell Signalling #7076

2.4.3 Indel verification of ZFP36L1 KO cells by amplicon sequencing

Genomic DNA was extracted from potential ZFP36L1 knock-out (KO) T-REx U-2OS clones and the CRISPR-Cas9 *ZFP36L1* target site was PCR amplified as described in Section 2.3.1. Subsequently, PCR amplification products from T-REx U-2OS ZFP36L1 KO, T-REx U-2OS Wild-type (WT) and empty vector controls were analysed through Next-Generation sequencing (NGS) based amplicon sequencing (GENEWIZ, UK). Paired-end reads generated from NGS amplicon sequencing were analysed with

CRISPResso2 (Clement et al., 2019) to assess genome editing outcomes. Amplicon sequencing data were deposited in the national centre for biotechnology information (NCBI) sequence read archive (SRA). SRA accession number: PRJNA715499.

2.5 Growth curve analysis

T-REx U-2OS WT and T-REx U-2OS ZFP36L1 KO (ΔL1-T-REx) cells were seeded at a density of 5 x 10^4 in 60mm cell culture plates in triplicates. Cells were harvested every 24 hours for five days and counted using a haemocytometer. The average number of cells was recorded. The experiment was repeated a total of three times independently.

2.6 Micronuclei, anaphase bridges and lagging chromosomes

Cells were seeded at a density of 3.5x10^4 into 12-well plates containing Poly-D-Lysine-coated coverslips (Corning, #354086) and incubated for 24 hours at 37^{o}C in a humified incubator containing 5% CO_2. Cells were then untreated or treated with 0.2μM APH (Sigma-Aldrich #A0781) for 24 hours to induce mild replication stress. The cell culture medium was supplemented with 2 mg/ml of Cytochalasin B (Sigma-Aldrich, #C6762) (Inhibitor of micro-filament formation) for the final 16hours of APH treatment to block cells in cytokinesis. Cells were then fixed in PTEMF (20 mM PIPES (pH 6.8), 10 mM EGTA, 0.2% Triton X-100, 1mM MgCl2 and 4% Formaldehyde) buffer for 10 minutes at RT, washed with PBS four times and stained/mounted on glass slides with Prolong Gold Antifade Mounting medium containing DAPI (ThermoFisher Scientific, #P36935). Micronuclei formation was assessed as the percentage of DAPI-stained binucleated cells with micronuclei from 300 binucleated cells in each experiment. Only distinct micronuclei near a DAPI-stained binucleated cell were included in quantification. For chromosome mis-segregation detection, 50 anaphase cells were assessed for DAPI-stained bulky bridges and lagging chromosomes in each experiment with a fluorescent microscope at 100X magnification (Olympus BX41 microscope coupled to the Elite Micropix digital camera). Images were captured using Cytocam software V2.09 (Micropix). The experiment was repeated three times independently.

2.7 Immunofluorescence assays

Cells were seeded at a density of $9x10^4$ into 6-well plates containing glass coverslips and incubated for 24 hours at 37°C in a humified incubator containing 5% CO_2. Next, cells were either untreated or treated with 0.2μM APH for 24 hours. After 24 hours cells were simultaneously crosslinked and permeabilised using PTEMF for 10 minutes at RT. Next, the cells were washed with PBS four times and permeabilised once more with 0.2% Triton X-100/PBS (PBS supplemented with 0.2% Triton X-100) for 5 minutes at RT. Cells were blocked in 5%BSA/ PBS with Glycine (20mM) (Glycine binds free aldehyde groups stopping non-specific antibody binding) for 15 minutes at RT, and subsequently washed four times with PBS. Cells were blocked once more with 5%BSA/PBS for 15 minutes and incubated with appropriate primary antibodies diluted in 5%BSA/PBS at 4°C overnight (Table 6). Coverslips were then washed four times with PBS and incubated with respective secondary antibodies for 1 hour at 37°C in the dark (Table 6). Finally, coverslips were washed four times with PBS and stained/mounted with Prolong Gold Antifade Mounting medium containing DAPI. Slides were analysed with a fluorescent microscope at 63X and 100X magnification (Olympus BX41 microscope couple to the Elite Micropix digital camera). Images were captured using Cytocam software V2.09 (Micropix).

Table 6. List of antibodies used for immunofluorescence assays

Primary antibody	**Dilution (5%BSA/PBS)**	**Supplier; #Catalogue**
53BP1 mouse monoclonal	1:500	Sigma-Aldrich #MAB3802
Cyclin A rabbit monoclonal	1:500	Gift from JG laboratory
RPA32/RPA2 mouse monoclonal	1:150	Abcam #ab2175
Phospho-Histone H2A.X (Ser139) (γH2AX) rabbit monoclonal	1:400	Cell signalling #2577
Phospho-Histone H2A.X (Ser139) (γH2AX) mouse monoclonal	1:50	Sigma-Aldrich #05-636-I
Secondary antibody		
Alexa Fluor 488 Goat Anti-Rabbit IgG	1:500	ThermoFisher Scientific #A-11034
Alexa Fluor 568 Donkey Anti-Mouse IgG	1:500	ThermoFisher Scientific #A-10037

Ultra-fine bridge detection was carried out as previously described with changes (Bizard, Nielsen and Hickson, 2017). Specifically, cells were seeded at a density of 1.1×10^5 in 6-well plates containing glass coverslips and incubated for 24 hours at 37°C in a humified incubator containing 5% CO_2. Next, cells were either untreated or treated with 0.2μM APH for 24 hours, the medium was then removed and 1ml of PBS was added to each well. Cells were pre-extracted by adding 1ml of pre-extraction buffer A (0.2% Triton-X 100, 20mM PIPES pH 6.8, 1mM $MgCl_2$, and 10mM EGTA) to wells containing PBS and incubated for 90 seconds. Next, cells were simultaneously pre-extracted and fixed with 2ml pre-extraction buffer B (0.1% Triton X-100, 20mM PIPES pH 6.8, 1mM $MgCl_2$, and 10mM EGTA, 8% paraformaldehyde) for 15minutes at RT with no movement. Coverslips were then washed with PBS four times for 5 minutes and further permeabilized and blocked overnight at 4°C in PBSAT (3% BSA, 0.5% Triton X-100 in PBS). The next day, cells were incubated with primary antibodies for FANCD2 mouse monoclonal (Santa Cruz #sc-20022; 1:500 dilution) and PICH rabbit monoclonal (Cell signalling#8886; 1:50 dilution) diluted in PBSAT at 4°C overnight. After primary antibody incubation, coverslips were washed with PBSAT three times for 10 minutes then incubated with respective secondary antibodies (Table 6) diluted in PBSAT for 2 hours at RT protected from light. Next, coverslips were washed four times for 15 minutes with PBSAT and once more with PBS for 10 minutes. Coverslips were then stained and mounted with Prolong Gold Antifade Mounting medium containing DAPI. 50 anaphase cells were assessed for PICH stained UFBs with twin FANCD2 foci in each experiment with a fluorescent microscope at 100X magnification (Olympus BX41 microscope coupled to the Elite Micropix digital camera). Images were captured using Cytocam software V2.09 (Micropix). The experiment was repeated three times independently.

2.8 Metaphase spread preparation

Cells were seeded in 10cm culture dishes at a seeding density of 9.5×10^5 and incubated at 37^oC in a 5% CO_2 incubator overnight. Cells were then untreated or treated with 0.2µM APH for 24 hours. The medium was then supplemented with 0.2 µg/ml of Colcemid (ThermoFisher Scientific, #15212012) (Mitotic spindle inhibitor) to block cells in metaphase for the final 90minutes of APH treatment. Medium-containing mitotic cells were collected in 15mL centrifuge tubes using the mitotic shake-off method. The remaining adherent cells were detached using trypsin-EDTA and collected in the same 15mL centrifuge tube and centrifuged for 5 minutes at 1500rpm at 4^oC. The supernatant was removed and washed with PBS. Next, 8ml of hypotonic solution (75mM KCl; Gibco #10575090) pre-warmed at 37^oC, was added to the cells and incubated at 37°C for 15 minutes. Cells in hypotonic solution were then fixed with 5mL of freshly made Carnoy's buffer (75% methanol, 25% glacial acetic acid) added dropwise with gently mixing and incubated for 15 minutes at RT. Cell pellets were isolated from the supernatant by centrifugation at 1500 RPM for 10 minutes. The fixation step was repeated three times with 8mL of freshly made Carnoy's buffer for each repetition. The cell pellet was then resuspended in 500µL Carnoy's and spread dropwise from approximately 8 inches, on pre-wet glass slides angled at 45^o and dried overnight at RT. The next day, slides were stained with Giemsa staining solution (7% Giemsa (Gibco #10092013), 500mM PIPES (Sigma-Aldrich #P6757)) and mounted with coverslips using DPX mounting medium (Fisher Scientific, #D/5319/05). Metaphase spreads were analysed with a Zeiss Axioskop 2 microscope at 100X magnification coupled with an Elite Micropix digital camera. Images were captured using Cytocam software V2.09 (Micropix) and visible gaps/breaks and constrictions were quantified for each experiment and replicate (three independent experiments).

2.9 Flow cytometry

2.9.1 Cell cycle analysis

To perform cell cycle analysis, 7.4 x 10^5 cells were seeded in 10cm cell culture dishes incubated at 37°C at 5%CO_2 overnight. The following day, cells were either untreated or treated with 0.1, 0.2 or 0.4µM APH for 24 hours. Next cells were harvested and washed twice with PBS and resuspended to a concentration of 1x10^6. Cell pellets were isolated by centrifugation at 1500rpm for 5 minutes at 4°C and supernatant was decanted. Cells were then fixed with 5mL ice-cold 70% ethanol added dropwise with gentle vortexing and stored overnight at -20°C. Next, the fixative was removed from the cells and washed once with PBS. Cells were then stained with propidium iodide (PI) using FxCycle PI/RNase staining solution (Invitrogen, #F10797) following the manufacturer's instruction. Briefly, cells were resuspended and incubated in 500 µL of FxCycle PI/RNase staining solution for 30 minutes at RT protected from light. Cells were then analysed with the BD LSRFortessa X-20 flow cytometer (BD Biosciences) by 488nm excitation and data was analysed using FCS expression V7 flow cytometry software (De Novo Software, Pasadena, CA). The experiment was repeated three times independently.

2.9.2 Apoptosis assay

7.4 x 10^5 cells were seeded in 10cm cell culture dishes and incubating them at 37°C at 5%CO_2 overnight. Next, cells were either untreated or treated with 0.1, 0.2 or 0.4µM APH for 24 hours. After 24 hours media was removed, and cells were washed twice with PBS before harvesting. Apoptotic cells were then detected by Annexin V-FITC/PI double staining using the Annexin V-FITC apoptosis staining Kit (Abcam# ab14085). Specifically, after the PBS wash, cells were resuspended to a concentration of 5x10^5 in a 500µL binding buffer, and then 5µL of Annexin V-FITC was added to the cells followed by 5µL of PI and incubated for 10 minutes at RT protected from light. Apoptosis in each condition was detected by flow cytometry using the BD LSRFortessa X-20 flow cytometer (BD Biosciences) by 488nm (Detection filter 530/30 and 695/40 for Annexin V-FITC and PI respectively). The frequency of apoptotic cells was quantified using BD FACSDiva v9.0 software (BD Bioscience). The experiment was repeated three times independently.

2.10 Generation of a ZFP36L1 tetracycline-inducible cell line

2.10.1 Plasmid construction

The open reading frame of *ZFP36L1* was first PCR amplified from a donor plasmid (PCDNA6-His-ZFP36L1 kindly donated by Dr John Murphy, University of Westminster) employing a high-fidelity Q5 DNA polymerase to limit the incorporation of incorrect nucleotides and create a blunt-ended PCR product. For this purpose, we utilised the following primers to PCR amplify full-length *ZFP36L1* (1017 bps):

ZFP36L1 Forward primer: 5’ ATGACCACCACCCTCGT 3’ (Eurofins)
ZFP36L1 Reverse primer 5’ TTAGTCATCTGAGATGGAAAGTCT 3’ (Eurofins)

Next, full-length *ZFP36L1* was PCR amplified by first utilising the following 50 µL Q5 High-Fidelity DNA polymerase PCR reaction: 10 µL 5X Q5 reaction buffer (final concentration 1X), 1 µL 10mM dNTPs (NEB, #M0273) (final concentration 200µM), 2.5µL 10 µM forward and reverse primers (final concentration 0.5 µM), 100ng donor plasmid, 0.5µL Q5 High-Fidelity DNA Polymerase (0.02 U/µl) and remaining volume made up with nuclease-free water. The reaction mixture was then subjected to PCR amplification (98^{o}C for 1 minute, then 30 cycles of 98^{o}C for 30 seconds, 63^{o}C for 30 seconds, 72°C for 45 seconds and final extension for 72°C for 5 minutes) in a Bio-Rad T100 thermal cycler.

Post verification of the amplicon size by agarose gel electrophoresis, the blunt-ended PCR product was cloned into a pCR-Blunt-II-TOPO plasmid (Appendix C; Figure 1) using the Zero Blunt TOPO PCR Cloning Kit (Invitrogen, #450245) following manufacturer's protocol. Briefly, 4 µL of fresh PCR product was incubated with 1 µL pCR-Blunt-II-TOPO and 1 µL salt solution (1.2 M NaCl; 0.06 M MgCl2) for 7 minutes at RT. Next, the reaction was transformed into One Shot® TOP10 Chemically Competent *E. coli* as described in Section 2.1.2. The transformation mix was then spread onto LB agar containing 50mg/mL kanamycin and incubated at 37°C overnight. Utilising the same primers and PCR conditions, bacterial colonies were then screened for the *ZFP36L1* insert by colony PCR (Appendix C; Figure 2B). Following, confirmation of the *ZFP36L1* insert bacterial colonies were inoculated in LB broth containing 50mg/mL kanamycin and incubated overnight at 180rpm at 37°C in a shaker incubator. Plasmid DNA was then extracted and purified as described in Section 2.1.2. Next, the *ZFP36L1* insert was released from pCR-Blunt-II-TOPO through a restriction digestion reaction with EcoRI (NEB #R3101) and insert size was assessed by agarose gel electrophoresis (Appendix C; Figure 2C), The remaining reaction mix was loaded onto a 0.8% agarose gel and the *ZFP36L1* insert was excised and purified as described in Section 2.1.2 for subcloning into the inducible express plasmid PCDNA4/TO-FLAG-Strep II (Appendix C; Figure 3) (Donated by Dr Kanagaraj, Francis Crick Institute).

To clone the *ZFP36L1* insert into PCDNA4/TO-FLAG-Strep II, PCDNA4/TO-FLAG-Strep II was first linearised downstream of the Strep II tag with EcoRI and dephosphorylated with rSAP, simultaneously the 5' ends of the *ZFP36L1* insert were phosphorylated with T4 polynucleotide kinase. Next, the *ZFP36L1* insert was ligated into PCDNA4/TO-FLAG-Strep II with T4 ligase and incubated overnight at 16°C. The following day the ligation reaction was transformed in One Shot® TOP10 Chemically Competent *E. coli*, inoculated in LB broth (100mg/mL ampicillin) and spread on LB agar (100mg/mL ampicillin) as described in Section 2.1.2. Bacterial colonies were then screened for the *ZFP36L1* insert as previously described with the following primers to PCR amplify the first 550bps of *ZFP36L1*:

ZFP36L1 Forward primer: 5' ATGACCACCACCCTCGT 3' (Eurofins)
ZFP36L1 Reverse primer: 5' CAAAAGCCGATGGTGTGGAA 3' (Eurofins)

Q5 High-Fidelity DNA polymerase reaction mix was prepared as previously described and PCR amplified (98°C for 30 seconds, then 25 cycles of 98°C for 30 seconds, 67°C for 30 seconds, 72°C for 30 seconds and final extension for 72°C for 5 minutes) in a Bio-Rad T100 thermal cycler with the following cycling conditions:

Following confirmation of the *ZFP36L1* insert (Appendix C; Figure 4), bacterial cells were inoculated in LB broth (100mg/mL ampicillin) overnight at 180rpm at 37°C in a shaker incubator. Plasmid DNA was then extracted and purified as described in Section 2.1.2. Plasmid DNA was analysed by Sanger sequencing to assess for orientation and nucleotide composition of the *ZFP36L1* insert employing a human CMV immediate early promoter forward primer (5'-GAGGGCCTATTTCCCATGATTCC-3') provided by GENEWIZ, UK (Appendix C; Figure 4B). Following confirmation of the correct sequence and orientation of the

ZFP36L1 insert in PCDNA4/TO-FLAG-Strep II (PCDNA4/TO-FLAG-Strep II-ZFP36L1) plasmid yield was increased for further use as described in Section 2.1.2.

2.10.2 Generation of a stable cell line

T-REx U-2OS ZFP36L1 KO cells (ΔL1-T-REx) were seeded in 60mm cell culture dishes at a density of $4x10^5$ cells to reach 70% confluency overnight. Cells were then transfected with 1µg of PCDNA4/TO-FLAG-Strep II-ZFP36L1 or empty vector (PCDNA4/TO-FLAG-Strep II with no insert) using effectene transfection reagent (Qiagen, # 301425) following manufacturer’s instructions. 24hours post-transfection cells were selected in the presence of 450µg/mL zeocin (Gibco, #R25001) and cultured for 10-14 days. Cell culture media containing zeocin was changed every 2-3 days. Monoclones were isolated by limiting dilution procedure and expanded as described in Section 2.2.1. Positive clones were identified by first supplementing cell culture media with 0.4µg/ml tetracycline (Gibco, # A39246) for 24 hours and testing for ZFP36L1 expression by western blotting using anti-ZFP36L1/ZFP36L2 antibody Appendix C; Figure 5) described in Section 2.3.2.

2.10.3 ZFP36L1 KO phenotype rescue

For assessment of 53BP1 NBs and micronuclei formation, stable cells and respective controls were seeded at a density of $9x10^4$ into 6-well plates containing glass coverslips and incubated for 24 hours at 37°C in a humified incubator containing 5% CO_2. The cell culture medium was supplemented with or without 0.4µg/ml tetracycline for 24 hours. Next, cells were treated with or without 0.2µM APH for a further 24 hours and assessed for 53BP1 NB formation by immunofluorescence Section 2.5. For micronuclei assay, 2 mg/ml of Cytochalasin B was added to the cell culture medium for the final 16hours of APH treatment, fixed and stained with DAPI as described in Section 2.6. Slides were analysed with a fluorescent microscope at 100X magnification (Olympus BX41 microscope coupled to the Elite Micropix digital camera). Images were captured using Cytocam software V2.09 (Micropix). 300 G1 cells and 300 binucleated cells were analysed for 53BP1 NB and micronuclei respectively. The experiment was repeated three times independently.

2.11 R-loop assays

2.11.1 Plasmids

Inducible expression plasmids encoding the M27 variant of human RNase H1 and a catalytically inactive mutant RNase H1(RNase H1 D210N) (generated by a point mutation in the catalytic site (GAC to AAC)) absent of a mitochondrial localisation signal were used to study R-loops (kind gifts by Dr Kanagaraj Radhakrishnan, The Francis Crick Institute). The tetracycline-inducible expression plasmid pAIO containing GFP-tagged wild-type RNase H1 (pAIO-RNase H1-GFP) or catalytically inactive RNase H1 mutant (D210N) (pAIO-RNaseD210N-GFP) were used to detect R-loops. For assessment of R-loop impact on 53BP1 NB formation, pAIO encoding wild-type RNase H1 (pAIO-RNase H1) or RNase H1 D210N (pAIO-RNase H1D210N) only were utilised.

2.11.2 Western blot detection of inducible RNase H1 expression

T-REx U-2OS ZFP36L1 KO cells were seeded in 60mm cell culture plates at a density of 7.4×10^5 to reach 80% confluency overnight. Cells were then transfected with 1µg of respective plasmid DNA using effectene transfection reagent as described in Section 2.8.2. The cell culture medium was then supplemented with 1µg/mL tetracycline for 24 hours. Cells were then harvested and lysed in RIPA buffer to test for expression of respective proteins as described in Section 2.3.2. To test for protein expression of RNase H1 in cells transfected with pAIO-RNase H1-GFP and pAIO-RNaseD210N-

GFP, an anti-GFP rabbit polyclonal antibody (Cell Signalling, #2555) was used. Anti-RNase H1 rabbit polyclonal antibody (ab229078) was used to detect protein expression from pAIO-RNase H1 and pAIO-RNaseD210N transfected cells.

2.11.3 Detection of R-Loops

T-REx U-2OS ZFP36L1 KO cells were seeded in 6-well culture plates containing glass coverslips at a density of $4x10^5$ to reach 70% confluency overnight. Cells were then transfected with 0.4µg of pAIO-RNase H1-GFP or pAIO-RNase H1D210N-GFP using effectene transfection reagent described in Section 2.8.2. Next, culture media was supplemented with 1 µg/mL to induce expression of RNase H1 WT or RNase H1 D210N for 24 hours. 8 hours after tetracycline addition, cells were then treated with or without 0.2µM APH for the remainder of the 24 hours (16hours total APH treatment). Next, cells were washed with PBS and pre-extracted on ice for 10 minutes with CSK buffer (25 mM HEPES, 50 mM NaCl, 300 mM sucrose, 1 mM EDTA, 3 mM MgCl2, and 0.5% Triton X-100) followed by fixations with 4% formaldehyde to preserve chromatin-bound proteins. Cells were then stained and mounted with Prolong Gold Antifade Mounting medium containing DAPI. 300 cells were analysed for GFP foci in three independent experiments.

2.11.4 Impact of R-loops on 53BP1 NB formation in ZFP36L1 KO cells

To determine R-loop involvement in 53BP1 NB formation in G1. T-REx U-2OS ZFP36L1 KO cells were seeded in 6-well culture plates containing glass coverslips at a density of $4x10^5$ to reach 70% confluency overnight. Cells were then transfected with 0.4µg of pAIO-RNase H1 or pAIO-RNaseD210N. Next, culture media was supplemented with 1 µg/mL to induce expression of RNase H1 WT or RNase H1 D210N for 24 hours. 8 hours after tetracycline induction, cells were then treated with or without 0.2μM APH for the remainder of the 24 hours. Cells were fixed and subjected to immunofluorescent staining using respective antibodies for 53BP1, and cyclin A as described in Section 2.5. Slides were analysed with a fluorescent microscope at 100X magnification (Olympus BX41 microscope coupled to the Elite Micropix digital camera). Images were captured using Cytocam software V2.09 (Micropix).

2.12 Isolation of chromatin and soluble proteins

U-2OS, HCT-116 and Hela cells were seeded at a density of 1.1×10^6 in 10cm cell culture plates for 24 hours at 37°C in 5% CO_2. Cells were then harvested and collected in low-salt isotonic buffer A (100mM pipes (pH 6.8), 300mM sucrose, 100mM NaCl, 1mM EGTA, 0.2% Triton-X 100, supplemented with protease inhibitors (Roche, # 11836153001)) for 10minutes on ice. Subsequently, samples were centrifuged for 10 minutes at 14,000rpm to separate the soluble cytoplasmic supernatant fraction (S) from the chromatin fraction (C) For chromatin extraction, a high-salt buffer B (50mM Tris-HCl (pH 8.5), 400mM NaCl, 5mM EDTA, 1% Triton-X 100 supplemented with protease inhibitor) was added to the remaining cell pellet and vigorously agitated back and forth on a linear shaker at 4°C for 15minutes. Next, samples were sonicated at 20 kHz for 30 seconds set at 3 cycles for a total of two times. Following SDS-PAGE, ZFP36L1 expression was detected from soluble and chromatin fractions by western blotting using the anti-ZFP36L1/ZFP36L2 antibody as previously described in Section 2.3.2. Histone H3 rabbit polyclonal antibody was used as a marker of chromatin fractions (Abcam# ab18521). For detection of ZFP36L1 in chromatin and soluble fractions from cells untreated or treated with 0.1, 0.2 and 0.4μM APH for 24 hours. All purification procedures were conducted with incubation with 0.3mg/ml RNase A (Qiagen, # 19101) for 30 minutes on ice.

2.13 Mapping the ZFP36L1 interactome

2.13.1 Constructing a tetracycline-inducible expression plasmid encoding FLAG-StrepII in frame with ZFP36L1

We utilised the previously constructed vector (PCDNA4-TO-FLAG-StrepII-ZFP36L1) encoding wild-type *ZFP36L1* described in Section 2.10.1 as a template to generate ZFP*36L1* with an in-frame N-terminal FLAG-StrepII tag. To generate the in-frame N-terminal FLAG-StrepII tag, a single bp (underlined) was introduced into PCDNA4-TO-FLAG-StrepII-ZFP36L1 by site-directed mutagenesis utilising the following primers:

FP: 5'GGTCCCGAATTCGCCCTTATCAATGACCACCACCCTCGTGTCT '3

RP:5' AGACACGAGGGTGGTGGTCATTGATAAGGGCGAATTCGGGACC'3

The template (200ng) was incubated in the presence of these primers (100 µM) in 1X Phusion high fidelity (HF) buffer, 1 unit of Phusion HF DNA polymerase (NEB #, 10mM dNTPs and subjected to PCR amplification (98^{o}C for 30 seconds, then 25 cycles of 98^{o}C for 30seconds, 55^{o}C for 30 seconds, 72^{o}C for 2.5 minutes and final extension for 72^{o}C for 10 minutes). Next, the PCR product was then digested with 40-Units of DpnI (NEB# R0176) for 1 hour at 37^{o}C. The plasmid was then transformed into One Shot® TOP10 Chemically Competent *E. coli* and plasmid DNA was isolated as described in Section 2.2.2. Plasmid DNA was analysed by Sanger sequencing to assess for successful incorporation of the desired nucleotide.

Following Sanger sequence confirmation plasmids were transfected into ΔL1-T-REx cells using effectene transfection reagent (Qiagen, # 301425) and media was supplemented with 1ng/ml tetracycline for 24 hours as described in Section 2.10.2. Cells were lysed using Pierce IP lysis buffer (Thermo Scientific #87787) supplemented protease inhibitor following the manufacturer's instructions and harvested with a cell scraper on ice. Cell lysates were separated by SDS-PAGE followed by western blotting as described in Section 2.3.2 and recombinant FLAG-StrepII-ZFP36L1 protein was detected utilising an anti-ZFP36L1/ZFP36L2 antibody and rabbit anti-DYKDDDDK (FLAG) antibody (Cell signalling #14793) diluted 1:1000 in 5%BSA/TBST.

2.13.1 Immunoprecipitation of FLAG-StrepII-ZFP36L1 for proteomic analysis

T-REx U-2OS ZFP36L1 KO cells were seeded into ten 150mm cell culture plates at a seeding density of $3x10^6$ and incubated at 37°C at 5%CO_2 overnight. The following day cells were transfected with PCDNA4-TO-FLAG-StrepII-ZFP36L1 or PCDNA-TO-FLAG-Strep II empty vector (EV) using effectene transfection reagent and media was supplemented with 1µg/ml tetracycline for 24hours as described in Section 2.10.2. Next, transfected cells were washed twice with ice-cold PBS after removal of growth media, lysed using Pierce IP lysis buffer (Thermo Scientific #87787) supplemented protease inhibitor following the manufacturer's instructions and harvested with a cell scraper on ice as described in Section 2.13.1. Total cell lysates ($1.5x10^7$) were incubated with anti-FLAG magnetic agarose beads (Thermo Scientific #A36797) following the manufacturer's instructions with minor changes. Briefly, total lysates were incubated with 200 µL of anti-FLAG magnetic agarose beads overnight at 4°C with constant mixing. The next day magnetic beads were separated from the supernatant with a magnetic rack (Invitrogen #12321D) and washed with 2 mL PBS (Thermo Scientific #28372) and 2mL Milli-Q H_2O. To determine successful IP, bound proteins were eluted in acidic conditions with 400µL Pierce IgG Elution Buffer, pH 2.8 (Thermo Scientific #21004) and neutralised with 60 µL of 1 M Tris; pH 8.5, elution step was repeated once more to maximise protein recovery. 20µg of cell lysate was then separated by SDS-PAGE with a non-reducing sample buffer followed by western blotting to detect ZFP36L1 or FLAG expression as described in Section 2.13.1.

2.13.2 Mass spectrometry detection of proteins

Proteomics experiments were carried out as previously described (Casado et al., 2013; Rajeeve et al., 2014). Briefly, IP protein complex magnetic beads were digested into peptides using trypsin. Peptides were then desalted and eluted using C18+carbon top tips (Glygen corporation, #TT2MC18.96) and 70% acetonitrile (ACN) with 0.1% formic acid respectively. 0.1% trifluoroacetic acid (TFA) was subsequently used to dissolved peptides which were then analysed by nanoflow ultimate 3000 RSL nano instrument connected online to a Q Exactive plus mass spectrometer (Thermo Fisher Scientific). Gradient elution was from 3% to 28% buffer B (0.1% formic acid in ACN) in 90min at a flow rate of 250nL/min with buffer A (0.1% formic acid in water) being used to balance the mobile phase. Xcalibur software (version 4.0) was used to control the mass spectrometer and operated in the positive mode. The spray voltage and the capillary temperature were set to 1.95 kV and 255 ºC respectively. Q-Exactive plus was controlled in data-dependent mode with a single survey MS scan followed by 15 MS/MS scans. Mass analyser was set at 375- 1500m/z with a resolution of 70,000 to acquire full scans, and a resolution of 17,500 was used to obtain tandem mass spectrometry (MS/MS) scans. Raw data obtain from MS was used to search for proteins against the Uni Prot database for human entries using Mascot search engine with the following parameters: false discovery rate (FDR) of ~1%, mass tolerance of 10 ppm for parent mass to charge value and peptide tolerance of 25 mmu, variable oxidation of methionine, pyro-glu and serine, threonine, and tyrosine phosphorylation.

2.13.3 Classification of ZFP36L1 protein interactions

To elucidate ZFP36L1 protein interactors, all lysates were analysed twice by MS for each condition and the average number of peptides were determined from two independent experiments (N=2). ZFP36L1 interacting proteins were classified from a list of 1418 proteins identified through MS with a corresponding peptide count and mascot protein score. Non-specific protein interactions were eliminated to generate a final list of 153 proteins. To remove non-specific ZFP36L1 interactions, proteins identified in the FLAG-Strep II-ZFP36L1 IP were only retained if the equivalent protein in the FLAG-Strep II EV control IP contained a peptide count <1. To classify ZFP36L1 interacting proteins DAVID (Database for Annotation, Visualization and Integrated Discovery) was used to classify the ZFP36L1 interactome based on gene ontology run with medium classification stringency and threshold p-value of <0.005 (Sherman et al., 2022).

2.14 Statistical analysis

Statistical analysis was carried out through Graphpad prism version 9 (Graphpad). Statistical significance between samples was assessed using a student *t*-test. Statistical details of experiments with corresponding replicates and standard error of the mean are described in figures and figure legends. Statistical significances are reported as P values designated (*) not significant $p>0.05$ (ns); $p \leq 0.05$(*); $p \leq 0.01$ (**); $p \leq 0.001$ (***), $p \leq 0.0001$(****).

2.15 Analysis of Immunofluorescence assays

Immunofluorescent assays were captured with a Zeiss Axioskop 2 microscope at 100X or 60X magnification coupled with an Elite Micropix digital camera using Cytocam software V2.09 (Micropix) and scored manually as previously described (Di

Marco et al., 2017; Lukas et al., 2011) (total number of Nuclei scored for each experiment are indicated in their respective figure legends). For colocalisation of 53BP1 and yH2AX foci experiments, 200 nuclei were captured and analysed using Fiji (Schindelin et al., 2012). A blinded scoring approach was not used for analysis of IF assays. To reduce potential biases IF microscopic slides scored in this study were randomly quantified and cross referenced against results generated in this study by an independent expert (Dr Kanagaraj Rajikrishnan, The Francis Crick Institute). To further validate IF experiments RPA and 53BP1 experiments were further independently carried out utilising siRNA against ZFP36L1 (Dr Kanagaraj Rajikrishnan, The Francis Crick Institute; data not shown). Results from Micronuclei experiments were further validated utilising artificial intelligence (AI) (Surendranath et al., 2022).

3. Generation of a tetracycline-inducible (T-REx) ZFP36L1 knock-out model utilising CRISPR-Cas9 technology

3.1 Introduction

The human genome is composed of billions of base pairs. The ability to manipulate these DNA bases has enabled researchers to understand the impact of genetic alterations in disease pathogenesis and holds potential future applications in precision medicine to treat different diseases (Reviewed in Das et al., 2022). Earlier breakthroughs enabled genome manipulation to study gene function through random homologous recombination (HR), which integrates exogenous repair templates that share sequence homology to donor sites (Reviewed in Capecchi, 1989). However, HR-mediated genome manipulation is limited by the low efficiency of desired recombination events (1 in 10^6–10^9 cells) and lack of control over the insertion sites at genomic loci (Reviewed in Capecchi, 1998). Alternatively, RNA inference (RNAi) has been utilised to provide inhibition or knockdown of gene expression through mRNA targeting to study loss-of-function mutations (Fire et al., 1998). Although vastly different from gene inactivation through homologous recombination, RNAi technology suffers from limitations such as incomplete knockdown of gene expression, unpredictable off-target effects and provides only time-limited knockdown of gene expression. Therefore, the use of RNAi technology limits the ability to conduct experiments over long periods to directly link genotype to phenotype (Boettcher and McManus, 2015).

This decade, new, more sophisticated approaches have been adopted, enabling researchers to overcome the limitations presented by the previous techniques mentioned thus far and have allowed for the targeted disruption of genomic regions in most cell types and organisms (Gaj, Gersbach and Barbas, 2013). At the centre of these approaches, now commonly known as ‘genome editing’, are engineered (chimeric) nucleases containing sequence-specific DNA-binding domains that are fused to DNA cleavage modules (Gaj, Gersbach and Barbas, 2013). Early stages of precise genome editing utilised zinc finger nucleases (ZFNs) or meganucleases which are synthetic proteins composed of complementary DNA-binding domains modified from zinc finger transcription factors and non-specific DNA cleavage domains of the bacterial type IIS restriction enzyme, FokI (Urnov et al., 2010). Building on the discovery of ZFNs as a platform for genome manipulation, a new class of FokI endonucleases known as transcription activator-like effectors (TALENs) were introduced with the ability to target and cleave any DNA sequence with moderate frequency (Sung et al., 2013). However, the requirement of complex molecular cloning for each target, low efficiency, and large size of the complexes (~3kb) impose difficulties when applying TALENs based technologies for basic and clinical research. The limitations of these genetic manipulation techniques led to the discovery of a more improved and robust gene-editing method known as clustered regularly interspaced short palindromic repeats-CRISPR-associated protein Cas9 (CRISPR-Cas9). CRISPR-Cas9 is the adaptive immune system of bacteria comprised of an RNA-guided nuclease mechanism that bacteria utilise to cleave foreign genetic components (Ran et al, 2013). Specifically, Cas9 endonucleases create DNA double-strand breaks (DSBs) at target sites that are repaired through the error-prone nonhomologous end-joining (NHEJ) or homology-directed repair (HDR) pathways. Thus, CRISPR-Cas9 enables for exploitation of repair pathways for gene knockout studies and integration of exogenous genes through NHEJ and HDR respectively (Ryu, Hur and Kim, 2019; Cho et al., 2013; Cong et al., 2013; Jinek et al., 2013)

The native type II CRISPR-Cas system consists of a Cas9 endonuclease, CRISPR RNA (crRNA), and the auxiliary trans-activating crRNA (tracrRNA). The crRNA units are comprised of a 20 nucleotide (nt) guide sequence that directs the Cas9 proteins to a 20-base pair (bp) target through Watson-Crick base pairing and fractional direct repeats (Ran et al., 2013). These native CRISPR components can be engineered into non-viral and viral plasmids encoding a chimeric single-guide RNA (sgRNA) following the fusion of the crRNA-tracrRNA duplex and a Cas9 binding cassette enabling a convenient process of genome engineering (Hille and Charpentier, 2016). sgRNAs consists of a sequence (typically 20nt) complementary to the target site and a scaffold sequence. The sgRNA can be designed *in silico* to target any DNA sequence *in vivo* and *in vitro* if two specific requirements are met. Firstly, the target sequence must be unique compared to the rest of the genome. Secondly, the target sequence must immediately proceed a 5’-NGG-3' (N can be any nucleotide) which is referred to as the canonical protospacer adjacent motif (PAM), immediately downstream of the targeted loci for *Streptococcus pyogenes* derived Cas9 (spCas9) activity. PAM requirements are determined by the CRISPR variant utilised (Kim et al., 2015). SgRNA binds to target sequences through Watson-crick base pairing, guiding the Cas9 protein to subsequently generate site-specific cleavage on the target DNA strand using the two distinct nuclease domains RuvC and HNH initiating a double-strand break (DSB) ~3 bps 5′ of the PAM sequence. DSBs can be repaired and processed via two mechanisms such as the error-prone non-homologous end joining (NHEJ) and homologous-directed repair (HDR) initiating small indels or point mutations for loss of function studies and precise knock-in mutations for loss or gain of function and additions of genes reporters respectively (Figure 3.1).

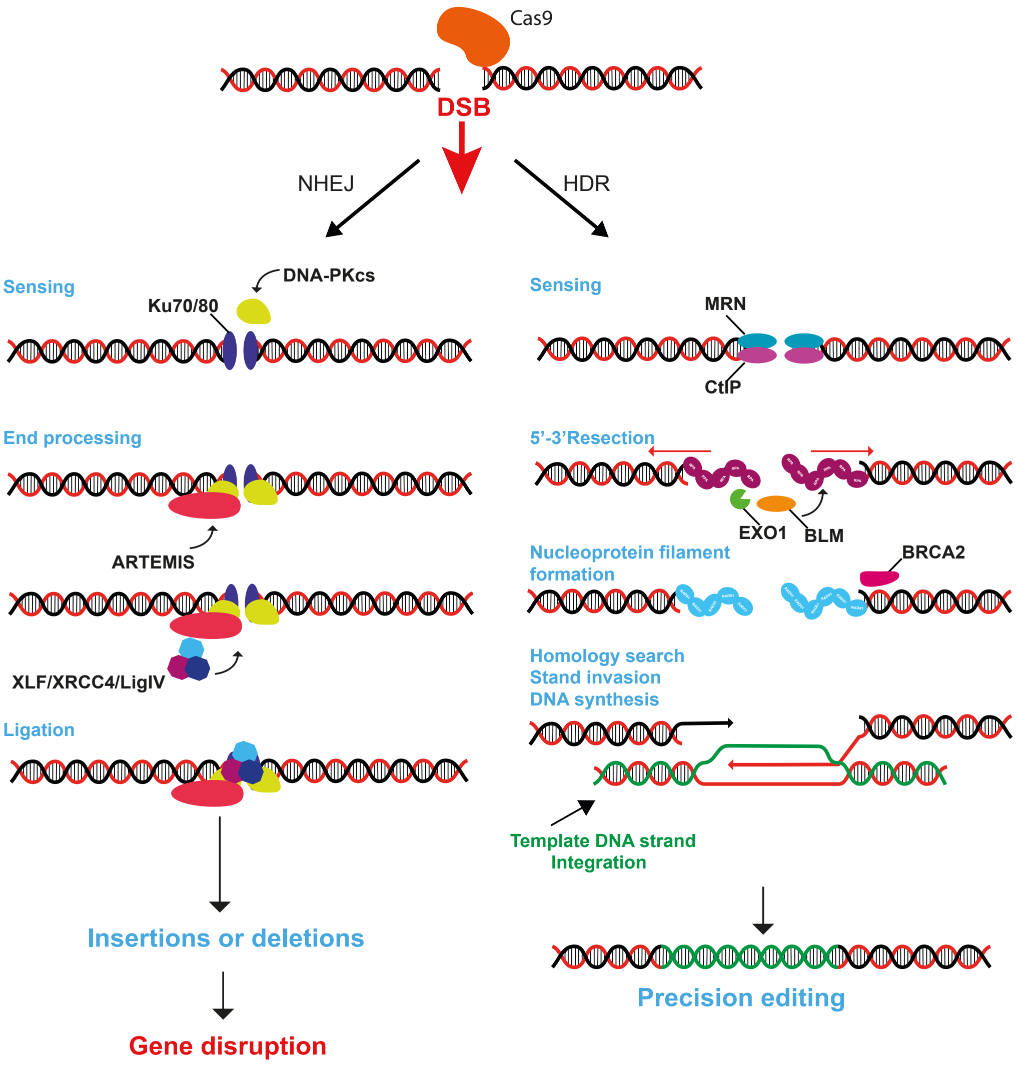
Cas9
DSB
NHEJ
HDR
Sensing
DNA-PKcs
Ku70/80
Sensing
MRN
CtIP
End processing
5'-3'Resection
ARTEMIS
EXO1
BLM
Nucleoprotein filament formation
BRCA2
XLF/XRCC4/LigIV
Homology search
Stand invasion
DNA synthesis
Ligation
Template DNA strand Integration
Insertions or deletions
Precision editing
Gene disruption

Figure 3.1 Mechanisms of NHEJ and HDR following CRISPR-Cas9-mediated introduction of DNA double-strand breaks at the target site.

NHEJ and HDR represent the major DNA DSB repair pathways. In the error-prone NHEJ pathway, broken DNA ends are sensed and bound by the KU70/KU80 heterodimer, and other repair factors. One of which is ARTEMIS which is thought to process broken DNA ends before ligation. The ligase complex consisting of XRCC4, XLF and LIG4 subsequently join broken DNA ends (ligation) leading to insertions or deletions and potential gene disruption (Yang et al., 2020). In contrast to NHEJ, HDR is error-free this pathway involves the MRE11-RAD50-NBN (MRN) complex that recruits factors involved in end resection such as exonuclease 1 (EXO1) and the bloom syndrome (BLM). DNA ends are coated and protected by RPA which is replaced by DNA repair protein RAD51 homolog 1 (RAD51) assisted by BRCA2 forming nucleoprotein filaments mediating homology search of a homologous DNA template, at this stage if a template DNA strand was introduced it can integrate into the parental DNA strand so is therefore known as precise editing (Yang et al., 2020).

3.2 Construction of an all-in-one CRISPR-Cas9/sgRNA expression plasmid targeting *ZFP36L1*

To explore *ZFP36L1's* role in maintaining genome integrity in response to replication stress, we set out to abolish ZFP36L1 activity in human osteosarcoma cells. To accomplish this, we utilised CRISPR-Cas9 technology to target *ZFP36L1* in T-REx-U-2OS cells. Specifically, we aimed to abolish ZFP36L1 expression in a tetracycline-inducible system that could enable the controlled expression of exogenous gene products (Chapters 6, 7 and 8). Here, we provide a methodological approach adapted from Ran A et al., 2013 to abolish ZFP36L1 expression in T-REx-U-2OS cells. The gene *ZFP36L1* is located on *chromosome: 14.q24.1* and is composed of 3017 base pairs (bp) (Ensembl transcript ID: ENST00000439696.3). *ZFP36L1* contains two exons (exon 1 and exon 2) that encode open reading frames (ORF) for the 338 amino acids (aa) of ZFP36L1. Exon 2 contains an ORF of 960 bps in length that encodes the vast majority (316aa) of the 338aa that form the final ZFP36L1 protein structure. We, therefore, decided to target exon 2 to increase the likelihood of ZFP36L1 protein ablation. Firstly, a list of single guide RNAs (sgRNA) was generated targeting the first 300bps of exon 2 *in silico* utilising a CRISPR guide design software (http://crispr.mit.edu/; (now known as Benchling; https://benchling.com). The list of sgRNAs was listed based on the specificity of PAM target sites, the sgRNA with the highest specificity was selected to increase on-target efficiency. From the potential list s, two were selected targeting the anti-sense strand of *ZFP36L1* (Figure 3.2).

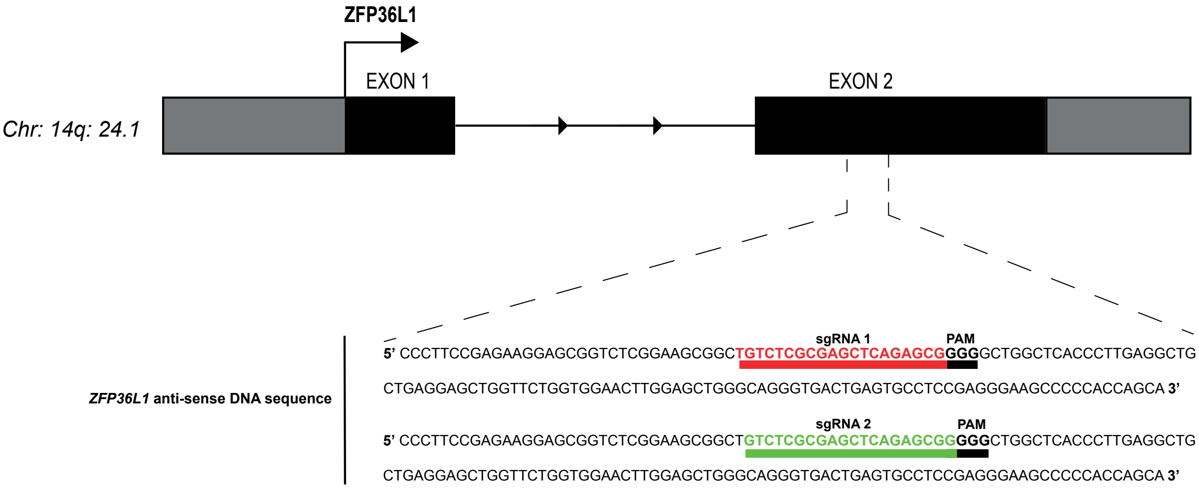
ZFP36L1
EXON 1
EXON 2
Chr: 14q: 24.1
ZFP36L1 anti-sense DNA sequence
sgRNA 1
PAM
5' CCCTTCCGAGAAGGAGCGGTCTCGGAAGCGGCTTGTCTCGCGAGCTCAGAGCGGGGGCTGGCTCACCCTTGAGGCTG
CTGAGGAGCTGGTTCTGGTGGAACTTGGAGCTGGGCAGGGTGACTGAGTGCCTCCGAGGGAAGCCCCCACCAGCA 3'
sgRNA 2
PAM
5' CCCTTCCGAGAAGGAGCGGTCTCGGAAGCGGCTGTCTCGCGAGCTCAGAGCGGGGGCTGGCTCACCCTTGAGGCTG
CTGAGGAGCTGGTTCTGGTGGAACTTGGAGCTGGGCAGGGTGACTGAGTGCCTCCGAGGGAAGCCCCCACCAGCA 3'

Figure 3.2 Scheme for targeted disruption of human *ZFP36L1* located on Chromosome 14: q24.11 using CRISPR-Cas9.

Exon architecture of the Chromosome *14: q24.1* corresponding to human *ZFP36L1* comprised of exon 1, intronic regions (double arrowhead) and exon 2. The ORF encoding for ZFP36L1 protein begins in exon 1 (Curved arrow) and ends in exon 2 (Black boxes). Exon 2 encoding the majority of *ZFP36L1's* ORF was selected for CRISPR-Cas9 mediated disruption utilising two sgRNAs that targeted the anti-sense DNA sequence of *ZFP36L1*: sgRNA1 (red line) and sgRNA 2 (green line) preceding a PAM sequence (NGG).

To achieve CRISPR-Cas9 mediated targeting of *ZFP36L1,* we utilised the all-in-one Cas9 expression plasmid pSpCas9(BB)-2A-Puro (PX459) composed of the complementary DNA (cDNA) that encodes human optimised *Streptococcus pyogenes* Cas9 (hSpCas9), and the chimeric CRISPR RNA- auxiliary trans-activating crRNA (cRNA-tracrRNA). Furthermore, pSpCas9(BB)-2A-Puro contains a gRNA scaffold that enables the cloning of sgRNAs within *Bbs*I restriction sites which guide Cas9 to the target region. The two selected sgRNAs were separately cloned into the pSpCas9(BB)-2A-Puro plasmid within the *Bbs*I restriction sites (Figure 3.2.1A**)** Successful cloning of the sgRNAs was sequence verified by Sanger sequencing (Figure 3.2.1B).

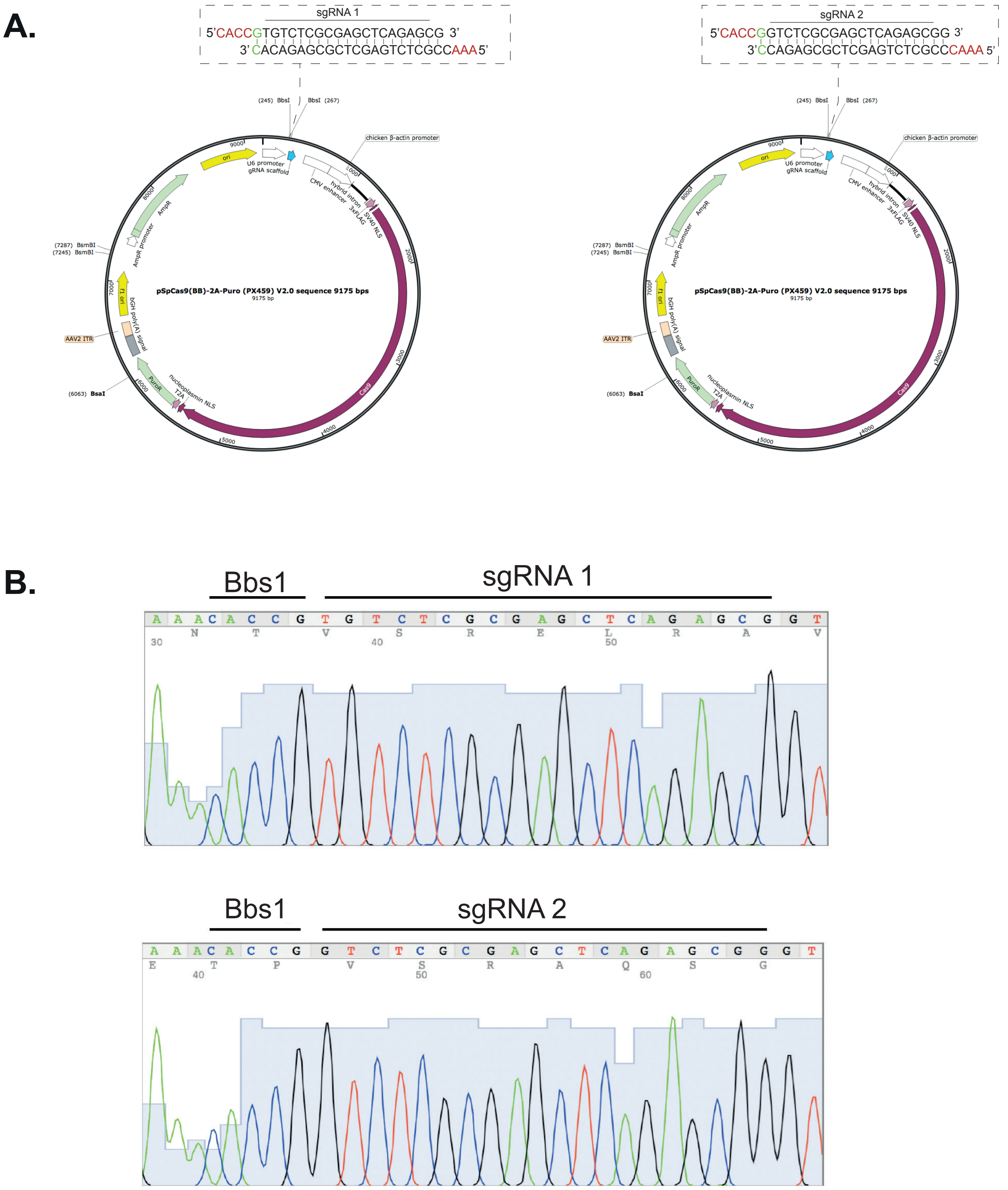
A.
sgRNA 1
5'CACCGTGTCTCGCGAGCTCAGAGCG 3'
3' CACAGAGCGCTCGAGTCTCGCCAAA 5'
sgRNA 2
5'CACCGGTCTCGCGAGCTCAGAGCGG 3'
3'CCAGAGCGCTCGAGTCTCGCCCAAA 5'
(245) BbsI
BbsI (267)
chicken β-actin promoter
U6 promoter
gRNA scaffold
ori
AmpR
AmpR promoter
(7287) BsmBI
(7245) BsmBI
f1 ori
bGH poly(A) signal
AAV2 ITR
PuroR
T2A
nucleoplasmin NLS
(6063) BsaI
Cas9
CMV enhancer
hybrid intron
3xFLAG
SV40 NLS
pSpCas9(BB)-2A-Puro (PX459) V2.0 sequence 9175 bps
9175 bp
B.
Bbs1
sgRNA 1
A A A C A C C G T G T C T C G C G A G C T C A G A G C G G T
N T V S R E L R A V
30 40 50
Bbs1
sgRNA 2
A A A C A C C G G T C T C G C G A G C T C A G A G C G G G T
E T P V S R A Q S G
40 50 60

Figure 3.2.1 Construction of an all-in-one CRISPR-Cas9/sgRNA expression plasmid targeting *ZFP36L1*.

A. Representation of cloning of individual sgRNAs into pSpCas9(BB)-2A-Puro in *Bbs*I sites. **B**. Chromatograms obtained from Sanger sequencing of cloned constructs demonstrating successful cloning of sgRNA 1 and sgRNA 2 positioned downstream of the Bbs1 restriction site in pSpCas9(BB)-2A-Puro.

.

3.3 CRISPR-Cas9/*ZFP36L1* sgRNA expression plasmid delivery into T-REx U-2OS cells

To achieve CRISPR-Cas9 mediated ablation of ZFP36L1, we introduced the sequence verified CRISPR expression plasmid containing the sgRNAs targeting *ZFP36L1* in T-REx U-2OS cells via cationic lipid-mediated transfection. Furthermore, a pSpCas9(BB)-2A-Puro (empty vector) was used as a negative control and non-transfected T-REx U-2OS cells were utilised as an antibiotic selection control. pSpCas9(BB)-2A-Puro encodes the puromycin resistance gene enabling isolation of successfully transfected cells by treatment with puromycin dihydrochloride. Therefore, we utilised a concentration of 2 μg/ml of puromycin to enrich plasmid-containing cells that gained resistance to puromycin. The nature, availability, stages of cell division and efficiency of DNA repair across cell types in the event of successful CRISPR-Cas9 cleavage of the *ZFP36L1* target site would result in various genome editing outcomes. Moreover, some cells would remain unedited due to highly efficient HDR mechanisms resulting in a heterogeneous, polyclonal population. Therefore, we isolated single cells through limiting dilution to generate a monoclonal cell population that would ensure a homogeneous single (*ZFP36L1)* edited background (Figure 3.3).

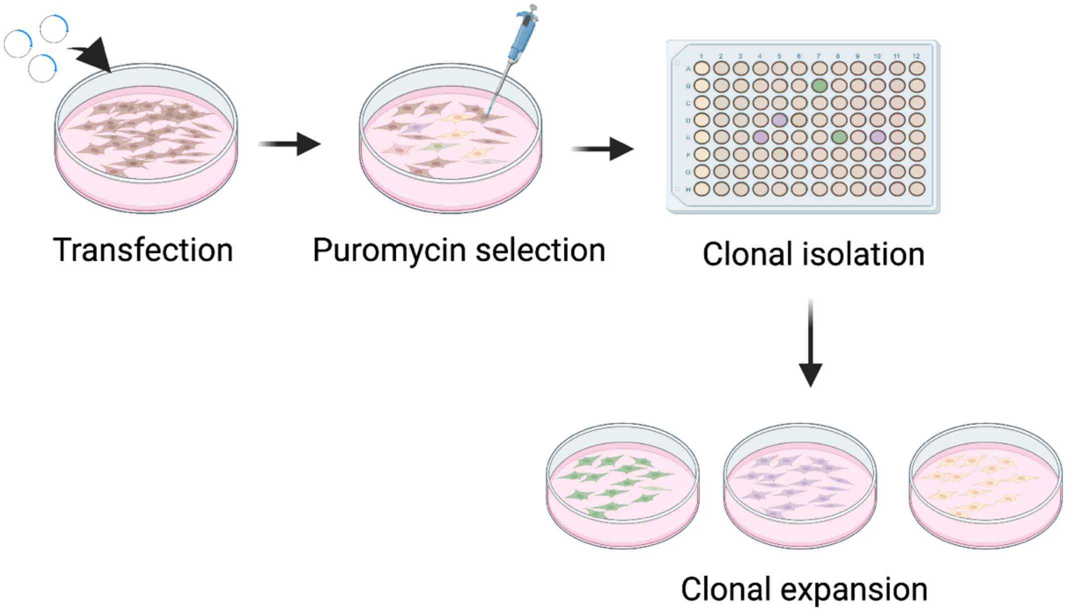

Figure 3.3 Experimental workflow from transfection to clonal expansion.
T-REx U2OS cells were first transfected with specific sgRNAs containing pSpCas9(BB)-2A-Puro. Transfected T-REx-U-2OS cells were then selected with 2 µg/ml of puromycin and clonally isolated by limiting dilution in 96 well plates followed by expansion into larger cell culture vessels where they were subsequently screened for insertions or deletions (Indel) at the target site**.**

3.4 Testing editing efficiency at the CRISPR-Cas9 *ZFP36L1* target site by genomic PCR amplification screens

To determine if we had successfully introduced mutations to the *ZFP36L1* target site, we first set out to determine the editing outcomes through genomic PCR followed by analysis by agarose gel electrophoreses. Specifically, we extracted genomic DNA from 15 monoclones and utilised primers flanking a region of 449bps that encompassed the *ZFP36L1* sgRNA target region and performed PCR amplification. ‘’ T-REX U-2OS cells containing WT *ZFP36L1* were used as a negative control and genomic DNA extracted from U-2OS cells expressing a truncated form of ZFP36L1 was utilised as a positive control (PC). We also utilised genomic DNA from an empty vector (EV) transfected T-REx U-2OS monoclone to determine the specificity of the sgRNA plasmids created. We suspected that monoclones exhibiting no changes to the targeted region will result in a fragment size similar to that of WT *ZFP36L1* at approximately 450bps, whereas deletions or insertions to the *ZFP36L1* target site would result in DNA fragments larger or smaller than the expected 450bps. Observations from the PCR amplified *ZFP36L1* DNA fragments demonstrated noticeable changes that indicated the presence of possible homozygous and heterozygous indels in 13 out of the 15 monoclones (Figure 3.4). No noticeable changes to DNA fragment size were observed from EV transfected cells (Figure 3.4). In the event of homozygous mutations, we expected to observe a single overlapping band (C8), whereas possible heterozygous mutations can result in multiple bands due to various indel patterns (C14). Furthermore, we did not exclude the possibility of indels for DNA fragments of similar size to WT bands (C6), as smaller indels are increasingly difficult to differentiate through agarose gel electrophoresis. Therefore, we set out further to characterise the clones through analysis of ZFP36L1 protein expression through western blotting.

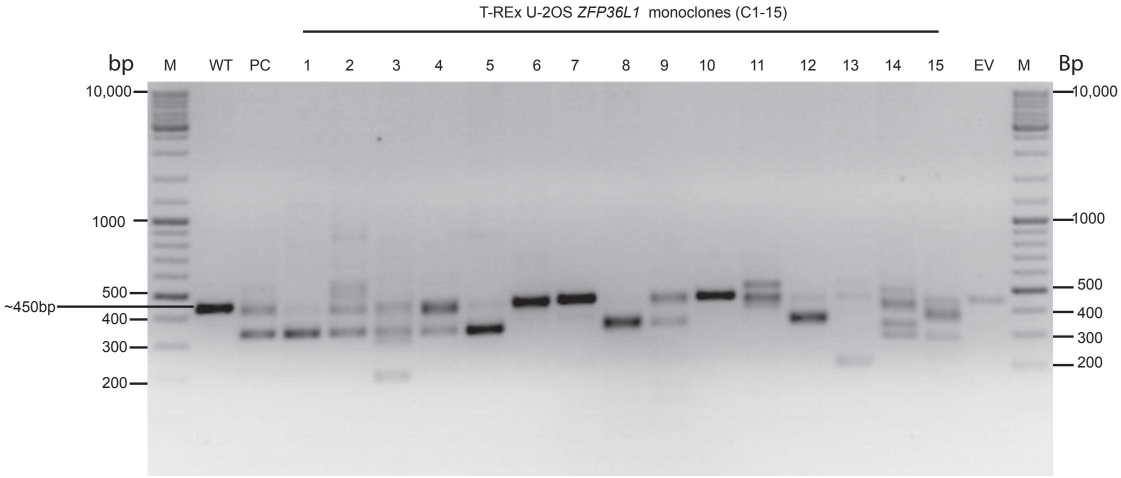

Figure 3.4 PCR amplification of target site of *ZFP36L1* gene in T-REx U-2OS cells.
1% agarose gel image from PCR amplification of 449 bp encompassing the CRISPR-Cas9 *ZFP36L1* target region in T-REx U-2OS cells. DNA fragments for wild-type (WT) corresponded to a size of approximately (≈) 450bp. DNA fragment from the positive

control (PC) exhibits two DNA bands demonstrating a heterozygous mutation, T-REx U-2OS monoclones (C1-15) demonstrate variations in their DNA fragment size corresponding to different editing outcomes, empty vector (EV) transfected monoclone exhibited similar DNA fragment size to that of WT. Maker (M) corresponds to a 10,000 bp DNA ladder.

3.5 Protein expression analysis of ZFP36L1 mutants

To determine if the observed indels resulted in changes to ZFP36L1 protein, total cell extracts were prepared to probe for ZFP36L1 utilising polyclonal antibodies against ZFP36L1 and ZFP36L2 and analysed by western blotting. Observations from western blot s corroborated with PCR analysis of the *ZFP36L1* target region. Clonally isolated cells that exhibited clear changes in DNA fragment size in comparison to the WT *ZFP36L1,* also demonstrate changes in expression of ZFP36L1 protein in comparison to WT (Figure 3.5). In contrast, monoclone 6 (referred to as C6 from here on in) lacked ZFP36L1 expression. It is worth noting that previously C6 PCR amplicon did not show mobility changes in DNA fragment sizes. Taken together, there was no detectable ZFP36L1 expression from C6 resulting in the generation of the ZFP36L1 KO system in U-2OS-T-REx cells. To further verify this result, we set out to assess for genomic alterations induced by CRISPR-Cas9 cleavage that led to ZFP36L1 protein ablation by next-generation sequence (NGS) amplicon sequencing of the target region.

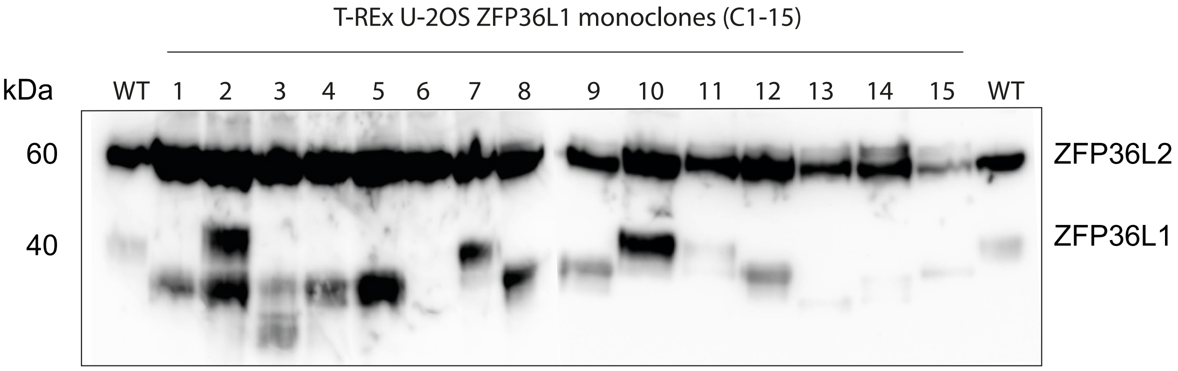

Figure 3.5 Western blot screen for ZFP36L1 mutants.

Western blot analysis for protein expression of ZFP36L1 (40 kDa) and ZFP36L2 (60 KDa) in U-2OS-T-REx cells from WT and the monoclonal population of cells (C1-15). Observations demonstrate changes in levels of ZFP36L1 expression and alterations in protein size following CRISPR-Cas9 targeting.

3.6 NGS analysis of ZFP36L1 KO T-REx U-2OS cellular model

To confirm the loss of ZFP36L1 expression in T-REx U-2OS cells was a result of indels at the target site we employed targeted amplicon deep sequencing (NGS) to determine the indel profile at the *ZFP36L1* target region. We PCR amplified a region surrounding the *ZFP36L1* target locus from genomic DNA isolated from WT, C6 and EV cells and subsequently assessed for changes by amplicon deep sequencing (Genewiz). Generated amplicon reads were aligned to a *ZFP36L1* reference sequence (Ensembl Id: ENST00000555997.1) encompassing the same target region and were subsequently analysed through an automatic bioinformatic analysis software (Clement et al., 2019). A total of 243,818 reads encompassing the target region were generated by amplicon deep sequencing for C6 (Figure 3.6A). Analysis of the reads demonstrated that 99.53% (242,681) of reads contained modifications whereas 0.47% (1137) were found to be unmodified (Figure 3.6A). Furthermore, analysis of indel size distributions in C6 revealed that modified reads were comprised of various deletions contributing to the total read output. Specifically, we found reads contained the following deletion size and percentage, (deletion= percentage of reads): 41bp deletion = 31.20%; 17bp deletion= 24.36%; 7bp deletion= 22.72%; 10bp deletion=5.30%; 3bp deletion=4.92%; 2bp deletion= 4.49%) (Figure 3.6B). Moreover, analysis of indel patterns in the *ZFP36L1* target region amplified from both WT and EV demonstrated no significant modifications. Specifically, WT contained 99.46% (303,668) unmodified and 0.54% (1645) modified reads maintaining 94.82% alignment to the reference sequence (Figure 3.6C). Similarly, EV reads contained unmodified 99.49% (293,559) and 0.51% (1516) with 95.1% alignment to the reference sequence (Appendix B:

Figure 1). Therefore, these results suggest that CRISPR-Cas9 mediated cleavage of the target region of *ZFP36L1* resulted in different repair outcomes at multiple alleles leading to heterozygous deletions. Furthermore, the deletions specified correlate to an out-of-frame alteration in the coding sequence that would result in an early termination abolishing the expression of ZFP36L1 protein. Following, the analysis of indel patterns in C6 we reconfirmed the absence of ZFP36L1 protein expression through the western blot analysis. Western blot analysis demonstrated no detectable ZFP36L1 expression in C6 cells in comparison to WT cells (Figure 3.6E). Importantly, ZFP36L1 expression in EV transfected cells remained unchanged (Figure 3.6F). Overall, these results demonstrated successful CRISPR/Cas9 mediated targeting of *ZFP36L1* in T-REx U-2OS cells resulting in total ZFP36L1 protein ablation and the successful creation of knock out cellular model of ZFP36L1 in T-REx U-2OS cells.

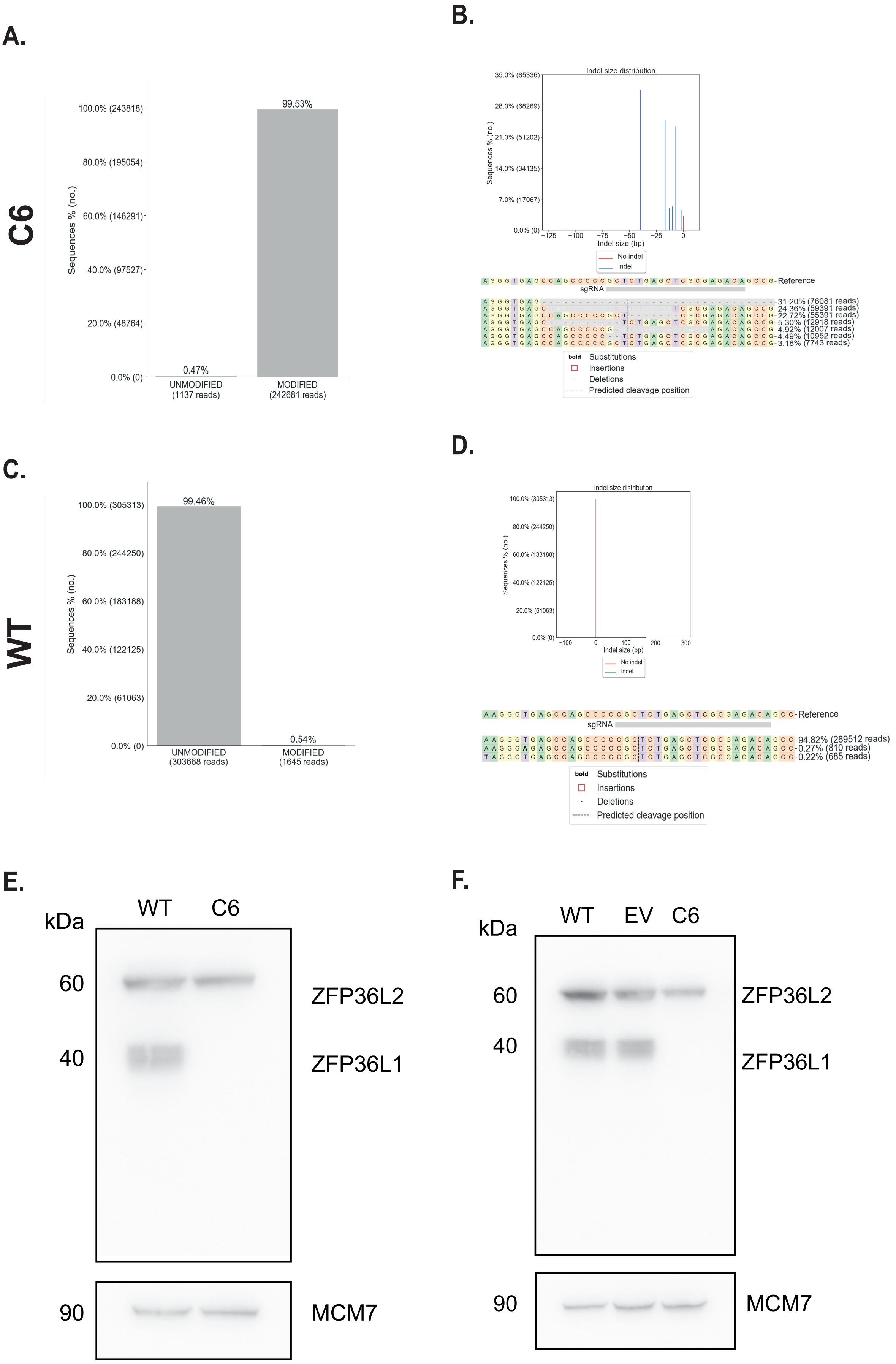
A.
C6
Sequences % (no.)
100.0% (243818)
80.0% (195054)
60.0% (146291)
40.0% (97527)
20.0% (48764)
0.0% (0)
0.47%
99.53%
UNMODIFIED
(1137 reads)
MODIFIED
(242681 reads)
B.
Indel size distribution
35.0% (85336)
28.0% (68269)
21.0% (51202)
14.0% (34135)
7.0% (17067)
0.0% (0)
−125
−100
−75
−50
−25
0
Indel size (bp)
No indel
Indel
AGGGTGAGCCAGCCCCCGCTCTGAGCTCGCGAGACAGCCG-Reference
sgRNA
AGGGTGAG--------------------------------31.20% (76081 reads)
AGGGTGAGC-----------------TCGCGAGACAGCCG-24.36% (59391 reads)
AGGGTGAGCCAGCCCCCGCT-------CGCGAGACAGCCG-22.72% (55391 reads)
AGGGTGAGC----------TCTGAGCTCGCGAGACAGCCG-5.30% (12918 reads)
AGGGTGAGCCAGCCCCCG-------------AGACAGCCG-4.92% (12007 reads)
AGGGTGAGCCAGCCCCC--TCTGAGCTCGCGAGACAGCCG-4.49% (10952 reads)
AGGGTGAGCCAGCCCCCGCTCTGAGCTCGCGAGACAGCCG-3.18% (7743 reads)
bold Substitutions
Insertions
Deletions
Predicted cleavage position
C.
WT
Sequences % (no.)
100.0% (305313)
80.0% (244250)
60.0% (183188)
40.0% (122125)
20.0% (61063)
0.0% (0)
99.46%
0.54%
UNMODIFIED
(303668 reads)
MODIFIED
(1645 reads)
D.
Indel size distributon
100.0% (305313)
80.0% (244250)
60.0% (183188)
40.0% (122125)
20.0% (61063)
0.0% (0)
−100
0
100
200
300
Indel size (bp)
No indel
Indel
AAGGGTGAGCCAGCCCCCGCTCTGAGCTCGCGAGACAGCC-Reference
sgRNA
AAGGGTGAGCCAGCCCCCGCTCTGAGCTCGCGAGACAGCC-94.82% (289512 reads)
AAGGGAGAGCCAGCCCCCGCTCTGAGCTCGCGAGACAGCC-0.27% (810 reads)
TAGGGTGAGCCAGCCCCCGCTCTGAGCTCGCGAGACAGCC-0.22% (685 reads)
bold Substitutions
Insertions
Deletions
Predicted cleavage position
E.
kDa
WT
C6
60
40
90
ZFP36L2
ZFP36L1
MCM7
F.
kDa
WT
EV
C6
60
40
90
ZFP36L2
ZFP36L1
MCM7

Figure 3.6 NGS analysis of the ZFP36L1 KO T-REx U-2OS cellular model
A and **C** CRISPresso2 allele alignment table and editing frequency in sequence read as determined by the percentage and number of sequence reads with unmodified and modified alleles in T-REx U-2OS cell from Clone 6 (C6) (**A**) and wild type (WT) (**C**). **B and D.** Indel distribution and visualisation of identified alleles around sgRNA cleave site from C6 (**B**) and WT (**D**). Nucleotides are colour coded (A = green; C = red; G = yellow; T = purple). Substitutions are shown in bold font. Red rectangles indicate insertions, Horizontal dashed lines correspond to deletions. The vertical dashed line highlights the predicted CRISPR-Cas9 cleavage site (Clement et al., 2019)**.** **E** and **F** Western blot confirmation of ZFP36L1 KO in T-REx U-2OS cells. Protein expression of ZFP36L1 (40 kDa) and ZFP36L2 (60 kDa) from WT and C6 (**E**) and WT, EV and C6 (**F**). MCM7 (90KDa) was used as a loading control.

3.7 CRISPR-Cas9 mediated ablation of ZFP36L1 reduces growth rate in T-REx U-2OS cells

There have been contrasting reports that demonstrate loss or depletion of ZFP36L1 to have a negative or positive effect on cell proliferation. Specifically, CRISPR-Cas9 mediated ablation of ZFP36L1 in chronic myeloid leukaemia cells (K-562) was shown to decrease cellular proliferation (Kaehler et al., 2021). Contrastingly, shRNA knockdown of ZFP36L1 in human colorectal cancer cells (HCT116) was reported to increase cell proliferation (Suk et al., 2018). Therefore, we set out to investigate the impact of the CRISPR-Cas9 mediated knockout of ZFP36L1 in the T-REx U-2OS osteosarcoma system. To do this we assessed cellular growth by growth curve analysis on ΔL1-T-REx and T-REx U-2OS WT cells (WT) over 5-days. We found that cells with ablated ZFP36L1 exhibited a growth rate slower than that of WT cells (Figure 3.7). The maximum cell count for ΔL1-T-REx cells on day 5 was less than that of WT at 0.8×10^6 and 1.3×10^6 respectively. Furthermore, the cell count for ΔL1-T-Rex cells at each time point (day) during the 5 days was found to be significantly less than WT cells, suggesting that loss of ZFP36L1 negatively affects the growth rate of T-REx U-2OS cells.

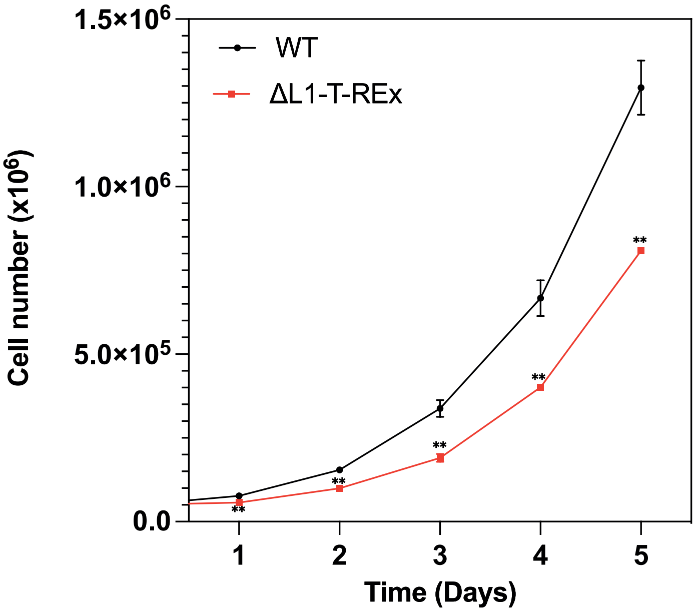

Figure 3.7 CRISPR-Cas9 ablation of ZFP36L1 in T-REx U-2OS cells exhibits a reduced growth rate.

Growth curve of WT and ΔL1-T-REx cells with recorded changes in cell number over 5 days. Data are means of triplicate values obtained from three independent experiments. Error bars represent S.E.M. *p* values were calculated using an unpaired two-tailed t-test.; not significant p>0.05 (ns); p ≤ 0.05(*); p ≤0.01 (**); p ≤0.001 (***), p≤0.0001(****).

3.8 Discussion

The development of novel techniques and technologies is indispensable for continued scientific advancements. Among these technologies, CRISPR-Cas9 gene editing has moved to the forefront of scientific research empowering both basic and clinical researchers to better understand genetic variations that underly human health and disease. CRISPR-Cas9 is composed of an RNA-guided nuclease that can be utilised for precision genome engineering in eukaryotic cells by specifying a 20bp target sequence generating a DSB in the target DNA. Due to its simplicity and high specificity compared to traditional genome editing techniques CRISPR-Cas9 has moved to the forefront of genome engineering (Reviewed in Barman, Deb and Chakraborty, 2019). Here we demonstrate an optimised plasmid-based CRISPR-Cas9 approach to target and abolish ZFP36L1 in T-REx U-2OS cells. We successfully adapted a methodology from Ran et al., (2013) and abolished ZFP36L1 expression in T-REx U-2OS cells through the following steps: **1.** Identification of a *ZFP36L1* target site and *in silico ZFP36L1* sgRNA design from a CRISPR database, **2.** Cloning of the *ZFP36L1* sgRNA into the all-in-one CRISPR plasmid pSpCas9(BB)-2A-Puro and transfection, **3**. Antibiotic selection with puromycin dihydrochloride, **4**. Isolation of single cells from a heterogenous *ZFP36L1* edited population, **5**. PCR amplification of the *ZFP36L1* target region and analysis of editing outcomes, **6**. Observation and validation of ZFP36L1 expression in total cell protein extracts **7**. And successful assessment of indel frequencies by NGS.

The first key phase required the identification of an appropriate *ZFP36L1* target site for *in silico* gRNA design to increase the likelihood of introducing indels that would subsequently result in ZFP36L1 ablation. Therefore, we targeted an early ORF region of *ZFP36L1* in exon 2 in anticipation that alterations in this region would result in premature termination of ZFP36L1 abolishing its activity. This method is supported by reports that indicate frameshift mutations that occur within early exons trigger the degradation of mRNA through the nonsense-mediated decay (NMD) pathway (Nickless, Bailis and You, 2017). Furthermore, as our main aim was to abolish ZFP36L1 activity in T-REx U-2OS the target region needed to be constitutively expressed in *ZFP36L1* transcripts that encode primary mRNA isoforms for *ZFP36L1*. Therefore, our target region was chosen within the ORF of primary *ZFP36L1* transcripts maintaining 100% identity across multiple genome databases.

CRISPR-Cas9 requires complementary binding of sgRNAs to target genes. However, often sgRNAs can bind to other regions of the genome that share similar sequence homology and exhibit off-target binding resulting in the misinterpretation of phenotypic alterations (Anderson et al., 2018). Therefore, with apprehensions over the off-target effects of CRISPR-Cas9, sgRNAs designed for targeting *ZFP36L1* were selected based on a scoring system that accounted for sgRNA specificity and off-target activity. Taken together sgRNAs utilised in this project had the highest specificity to the *ZFP36L1* target region and were less likely to bind to any other region in the genome reducing the possibility of off-target activity. Although the *s*gRNA design database considers both specificity and off-targeting, many sgRNA design databases cannot account for all factors that affect sgRNA specificity (reviewed in Wu, Kriz and Sharp, 2014). Therefore, this highlights the importance of improved algorithms for generating sgRNAs. Overall, we adopted an approach to maximise the target specificity of the sgRNA utilised in this project. Importantly, we address the specificity of the *ZFP36L1* ablation in later chapters.

Evidence for potential CRISPR/Cas9 mediated editing of the *ZFP36L1* was demonstrated through PCR amplification of the *ZFP36L1* target region from clonally isolated cells followed by agarose gel electrophoresis. Results demonstrated potential changes to the *ZFP36L1* target region as observed by changes in DNA fragment size in 13 clonally isolated populations (Figure 3.4). Although we were able to demonstrate potential *ZFP36L1* targeting, editing outcomes cannot be definitively determined through this method alone despite apparent changes in DNA fragment sizes in comparison to the *ZFP36L1 WT* target region (Figure 3.4). Moreover, DNA fragments that do not exhibit clear changes in mobility, were not eliminated for further analysis as smaller indels are difficult to distinguish through agarose gel electrophoresis. Thus we, further assessed clonally isolated cells for ZFP36L1 protein expression and sequence composition by western blotting and NGS amplicon deep sequencing respectively. Western blot analysis demonstrated that the observed changes in DNA fragment sizes corresponded to alterations in ZFP36L1 protein expression from 15 monoclones (Figure 3.5). Importantly, we did not detect ZFP36L1 expression for monoclone 6 (C6) a clone that did not elicit notable changes in DNA fragment size in PCR screens, highlighting the importance of further analysis (Figure 3.4 and Figure 3.5). To determine if loss of ZFP36L1 expression from C6 was a consequence of successful CRISPR-Cas9 target cleavage, we assessed for changes at the CRISPR-Cas9 *ZFP36L1* target site through NGS amplicon deep sequencing. Analysis of reads generated from NGS amplicon sequencing demonstrated that CRISPR-Cas9 targeting of *ZFP36L1* in C6 cells induced heterozygous deletions (bp deletions= 41, 17, 7, 10,3, and 2), a majority of generated reads contained deletions of 41, 17 and 7bps corresponding to 31.20%, 24.36% and 22.72% of total reads respectively. Smaller deletions of 10, 3 and 2bps made up a smaller percentage of reads (5.30%; 4.92% and 4.49% respectively) (Figure 3.6 A and B). Importantly, the observed deletions corresponded to out-of-frame mutations that would result in premature protein termination, thus abolishing ZFP36L1 protein expression. Sequence reads from WT cells demonstrated no noticeable changes in the ZFP36L1 target site (Figure 3.6 C and D). We once again confirmed that C6 lacked ZFP36L1 expression through comparison with WT cells (Figure 3.6 E). Moreover, we demonstrated that the amplified *ZFP36L1* target region from EV transfected T-REx U-2OS cells shared similar sequence reads to WT cells and presented no changes in ZFP36L1 protein expression (Appendix A: Figure 1) (Figure 3.6H). Thus, the findings demonstrated that

ZFP36L1 targeting and ablation were achieved through sgRNA-guided Cas9 activity in T-REx U-2OS cells. Overall, our results demonstrate the first recorded approach to target and abolish ZFP36L1 expression utilising CRISPR-Cas9 in T-REx U-2OS cells. Finally, we assessed the impact of ZFP36L1 loss in relation to the cell growth of T-REx U2OS cells. Our observations demonstrated that loss of ZFP36L1 significantly reduced cell growth in comparison to ZFP36L1 proficient WT cells (Figure 3.7). Recent evidence supporting our findings reports that CRISPR-Cas9 mediated ablation of ZFP36L1 in K-562 chronic myelogenous leukaemia cells reduces cell growth (Kaehler et al., 2021). On the other hand, contrasting evidence has implicated the downregulation of ZFP36L1 activity to increase cancer cell proliferation. Specifically, knockdown of ZFP36L1 utilising short hairpin RNA (shRNA) in HCT116 colorectal cancer cells was shown to increase cell proliferation (Suk et al., 2018). Thus, taken together our results and indicated reports suggest that ZFP36L1 may exhibit a cell type-specific role concerning cell growth and proliferation.

4. Loss of ZFP36L1 contributes to chromosomal segregation impairments and genomic instability in response to replication stress

4.1 Introduction

The timely progression of replication machinery is frequently impaired by obstacles such as unrepaired DNA lesions or DNA secondary structures. The slowing down of DNA synthesis or arrest of replication fork progression is termed replication stress and is a primary contributor to genomic instability observed in the early stages of cancer development (Bartkova et al., 2005; Gorgoulis et al., 2005; Kotsantis, Petermann and Boulton, 2018). Replication stress can lead to structural and numerical chromosomal aberrations that drive a form of genomic instability known as chromosomal instability (CIN) (Thompson, Bakhoum and Compton, 2010). Structural chromosomal aberrations drive structural CIN (s-CIN) defined as chromosome parts that are lost or become attached to another chromosome (Wilhelm, Said and Naim, 2020). Chromosome parts that remain under-replicated or dicentric chromosomes can lead to DNA bridges connecting two DNA masses that are prone to chromosomal breakages (Reviewed in Mankouri, Huttner and Hickson, 2013). On the other hand, numerical aberrations that drive numerical CIN (n-CIN) arise from errors in mitosis frequently caused by lagging chromosomes in anaphase cells (Potapova and Gorbsky, 2017). These scenarios that occur in mitosis itself are invariably pathological, the main source of chromosomal aberrations and segregation defects is associated with replication stress-associated DNA structures or lesions that arise during S-phase and persist into mitosis (Mankouri, Huttner and Hickson, 2013). Significantly, genomic loci known as fragile sites are regions of the genome with intrinsic replication and segregation difficulties and experience a plethora of obstacles in the form of lesions or DNA structures that challenge the progression of replication forks (Groh et al., 2014; Thys et al., 2015). It is thought that these obstacles further contribute to replication stress or exacerbate the already intrinsically labile nature of these genomic loci leading to defects in mitosis (Reviewed in Maffia, Ranise and Sabbioneda, 2020). Importantly, fragile sites are known hot stops for chromosomal instability and are considered preferential targets for genomic instability from the onset of pre-cancerous lesions (Reviewed in Li and Wu, 2020).

Cytogenetic markers of replication stress-associated DNA lesions that remain unresolved in mitosis, manifest as structural chromosome aberrations characterised by gaps, breaks and constrictions on metaphase chromosomes (Durkin and Glover, 2007) (Figure 4.1). Furthermore, in anaphase, unresolved DNA structures in mitosis such as bulky DNA bridges and lagging chromosomes can form from chromosomal aberrations or deficiencies in mitotic machinery (Figure 4.1). These structures can lead to daughter cells that contain an atypical number of chromosomes (aneuploidy) (Jo, Kusano and Hirota, 2021). A more frequent type of anaphase bridge known as an ultra-fine bridge (UFB) acts as a physical link between segregating sister chromatids during anaphase and form due to unresolved lesions (Chan, North and Hickson, 2007). However, unlike anaphase bulky bridges or lagging chromosomes, UFBs lack histones and cannot be visualised in cells with conventional DNA intercalating dyes such as DAPI (Bizard, Nielsen and Hickson, 2017). Instead, immunofluorescent staining with UFB interacting proteins can be used to visualise UFBs by fluorescent microscopy. Proteins that can be detected on UFBs are the SNF2-family of DNA translocases Plk1-interacting checkpoint helicase (PICH) and the RecQ DNA helicase

BLM. PICH recognises DNA under tension to mediate the resolution of UFBs through the recruitment of other UFB-associated factors such as BLM (Biebricher et al., 2013). Several subclasses of UFBs have been characterised and originate from centromeres, ribosomal-DNA, telomeres and common fragile sites (CFS) (Reviewed in Sarlós et al., 2017). The most common UFBs arise in centromeric regions (C-UFBs) and are prevalent across anaphase in undamaged cells (Chan and West, 2018). Given the frequency and origin of UFBs, their formation can be influenced by various factors. UFBs can arise at intrinsically unstable regions of the genome such as common fragile sites (CFS) which have been identified to be genome instability hotspots in cancers, and form under conditions of replication stress, particularly under mild replication stress with the DNA polymerase α/δ/ϵ inhibitor APH (Li and Wu, 2020). Exposure to APH is thought to exacerbate the intrinsic labile nature of these loci. Unlike C-UFBs CFS associated UFBs (CFS-UFBs) are marked by Fanconi Anaemia pathway protein complexes FANCD2-FANCI at the terminus of the UFB (Lukas et al., 2011). The association of FANCD2-FANCI with CFS is thought to be due to the protection of stalled replication forks subsequently aiding in its resolution (Fernández-Casañas and Chan, 2018).

Upon exit of mitosis, unresolved errors in chromosome segregation may fail to integrate into descendant cell nuclei forming extra-nuclear bodies known as micronuclei. Micronuclei containing whole or chromosome fragments can have detrimental pathological consequences leading to s-CIN or n-CIN a common characteristic in cancer cells (Wilhelm, Said and Naim, 2020). Alternatively, unresolved DNA bridging lesions become transmitted into the subsequent G1 daughters where they are protected in large nuclear bodies (NB) comprised of 53BP1, a factor involved in NHEJ (Harrigan et al., 2011; Lukas et al., 2011). 53BP1 NBs are thought to protect inherited damaged DNA in the G1-phase to facilitate repair in the S-phase (Moreno et al., 2016). Following the emergence of AU-RBPs as key factors in maintaining genome integrity including ZFP36's association with suppressing the formation of chromosome aberrations in response to replication stress (Lee et al., 2020). We set out to investigate if ZFP36L1 is involved in ensuring faithful chromosomal segregation to limit genome instability in response to replication stress utilising low dose APH in ZFP36L1 KO T-REx U-2OS cells (ΔL1-T-REx). Here, we provide several lines of evidence that suggests loss of ZFP36L1 increases replication stress-associated chromosome segregation errors and genomic instability.

.

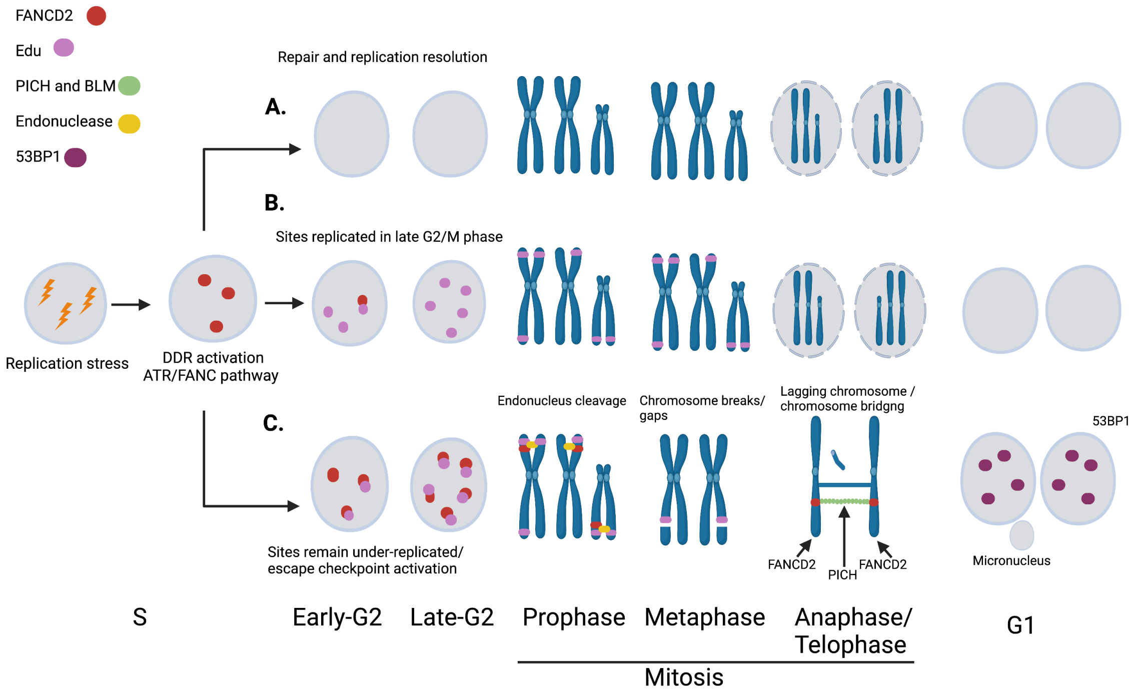
FANCD2
Edu
PICH and BLM
Endonuclease
53BP1
Repair and replication resolution
A.
B.
Sites replicated in late G2/M phase
Replication stress
DDR activation
ATR/FANC pathway
Endonucleus cleavage
Chromosome breaks/
gaps
Lagging chromosome /
chromosome bridgng
53BP1
C.
Sites remain under-replicated/
escape checkpoint activation
FANCD2
PICH
FANCD2
Micronucleus
S
Early-G2
Late-G2
Prophase
Metaphase
Anaphase/
Telophase
G1
Mitosis

Figure 4.1 Characteristics of replication stress-induced chromosomal segregation defects and genomic instability in human cells.

A. In response to mild replication stress, cells initiate a DNA damage response, recruiting factors involved in the ATR and FANC pathways. These activations can lead to the resolution of replication stress before entry into the G2 phase, enabling cells to divide effectively. B. At the end of the S-phase, if chromosomal regions remain under replication, DNA synthesis can be extended throughout the G2 phase and early M-phase, enabling proper duplication of chromosomes. This late DNA synthesis mechanism can be visualised by immunofluorescent staining depicting the incorporation of the nucleoside analogue Edu (pink dot) in prophase and metaphase chromosomes. C. By late G2 if cells fail to completely replicate their DNA, FANCD2 foci and Edu co-localisation can be visualised through fluorescent microscopy. In prophase and metaphase, endonucleases are recruited along with FANCD2 to cleave intertwined under-replicated DNA, inducing chromosome breaks/gaps. Unresolved DNA lesions in anaphase can give rise to lagging chromosomes, chromatin bridges, and nucleosome-free bridges known as ultra-fine bridges (UFB) marked by Plk1-interacting checkpoint helicase (PICH) and twin FANCD2 foci at the terminus of the bridge to mediate UFB resolution. In the subsequent G1 phase, these regions are protected by 53BP1 (purple dot). Unresolved DNA lesions and chromosome breaks can also give rise to micronuclei when exiting mitosis (Created with Biorender.com).

4.2 Loss of ZFP36L1 results in aberrations on metaphase chromosomes

Unresolved DNA lesions that impair replication fork progression can result in structural chromosome aberrations characterised by gaps, breaks and constrictions on metaphase chromosomes (Durkin and Glover, 2007). We examined Giemsa-stained metaphase chromosome spreads to determine if the loss of ZFP36L1 leads to aberrations on metaphase chromosomes (Figure 4.2A). Specifically, we assessed for aberrations in the form of chromatid breaks/gaps, chromosome breaks/gaps and constrictions markers of replication stress-induced mitotic defects (Figure 4.2B). Analysis of metaphase chromosome spreads demonstrated that the loss of ZFP36L1 resulted in increased chromosome aberrations in the presence and absence of APH (Figure 4.2C). In 0.2 μM APH treatment conditions the frequency of metaphase spreads with aberrations was significantly higher in ΔL1-T-REx cells in comparison to WT cells ($p<0.0001$). Specifically, ΔL1-T-REx cells contained approximately 2 aberrations per metaphase spread in comparison to WT cells that exhibited approximately 1 aberration, representing a more than two-fold increase in aberrations observed in ΔL1-T-REx cells relative to WT when treated with 0.2 μM APH (Figure 4.2C). Similarly, the loss of ZFP36L1 also resulted in a significant increase in chromosome aberrations even in the absence of APH in comparison to WT cells ($p \leq 0.05$; $p=0.0241$) (Figure 4.2C). We found that ΔL1-T-REx cells contained approximately 1 aberration in contrast to WT cells that exhibited <1 aberration per metaphase spread representing a 2-fold increase in ΔL1-T-REx cells displaying chromosome aberrations per metaphase spread relative to WT cells in the absence of APH (Figure 4.2C). Taken together, these results demonstrate that ZFP36L1 is required to suppress the formation of chromosomal aberrations in response to mild replication stress.

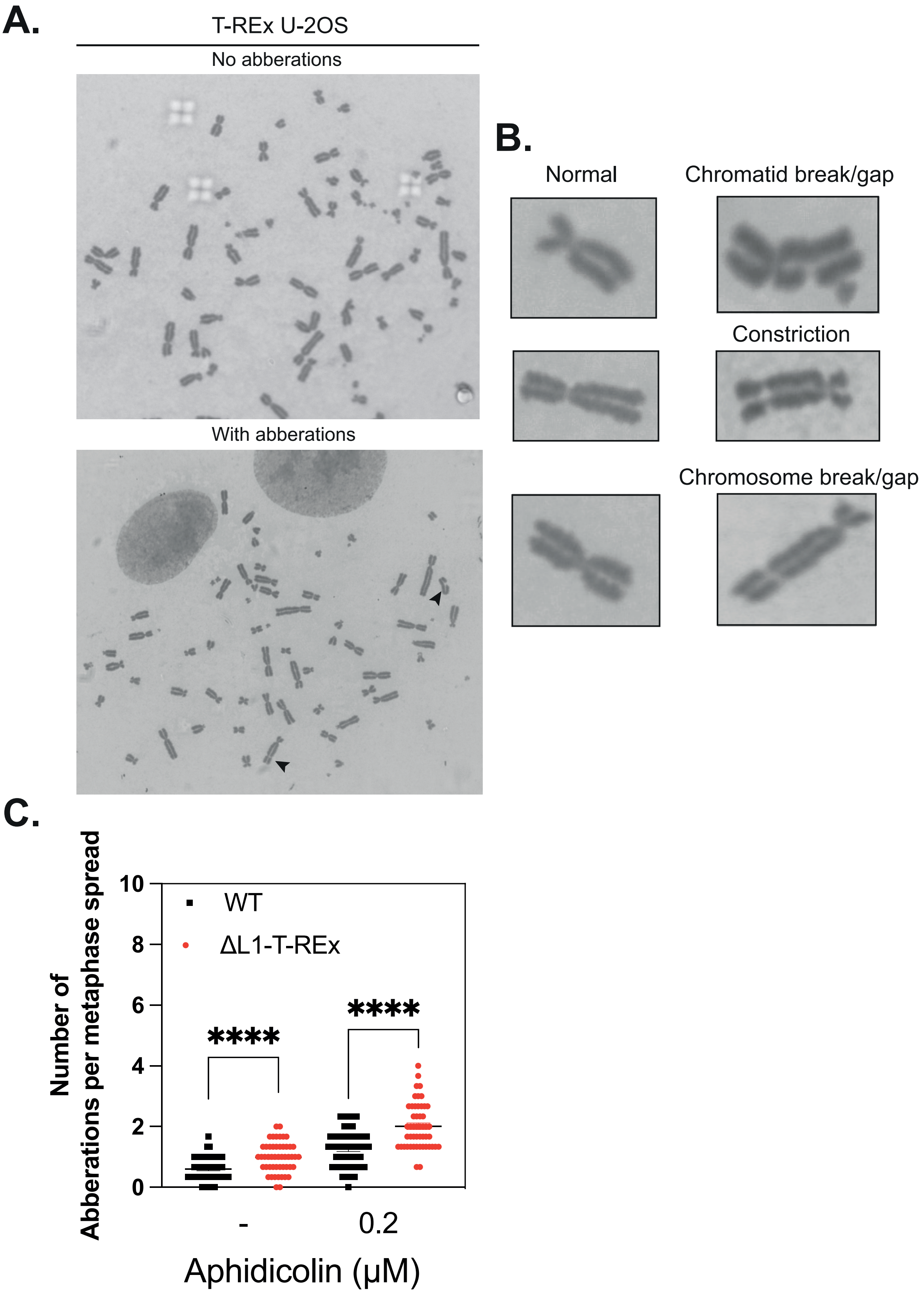
A.
T-REx U-2OS
No abberations
With abberations
B.
Normal
Chromatid break/gap
Constriction
Chromosome break/gap
C.
Number of
Abberations per metaphase spread
10
8
6
4
2
0
WT
ΔL1-T-REx
****
****
-
0.2
Aphidicolin (μM)

Figure 4.2 Loss of ZFP36L1 results in chromosome aberrations.
A. Metaphase Spreads without chromosomal aberrations (top) and with chromosomal aberrations (bottom) in T-REx U-2OS cells. Black arrowheads indicate chromosomal aberrations. **B**. Scored chromosomal aberrations examples: chromatid breaks/gap, chromosome breaks/gaps, and constrictions. **C**. Results of the number of chromosomal aberrations per metaphase spread in untreated and 0.2 µM APH treated WT and ΔL1-T-REx cells. Data generated are of three independent replicates from a total of 50 metaphase spreads analysed in each condition and replicate. Error bars represent S.E.M. *p* values were calculated using an unpaired two-tailed t-test.; not significant p>0.05 (ns); p ≤ 0.05(*); p ≤0.01 (**); p ≤0.001 (***), p≤0.0001(****).

4.3 Loss of ZFP36L1 results in chromosome segregation defects during conditions of replication stress

Chromosome segregation defects are widely associated with replication stress-associated genomic instability and are frequently observed in many cancers (Wilhelm et al., 2019). Generally, chromosomal segregation errors can be characterised by the appearance of incorrectly separated chromosomes that appear as bulky DNA bridges or chromatin lagging in between daughter nuclei during anaphase (reviewed in Fernández-Casañas and Chan, 2018). Bulky anaphase bridges represent histone-bound physical links between two incompletely separated sister chromatids and can be detected with classical DNA binding dyes such as 4′,6-diamidino-2-phenylindole (DAPI). In the study described, we utilised ZFP36L1 KO T-REx U-2OS cells (ΔL1-T-REx) and T-REx U-2OS Wild-Type (WT) cells to investigate whether the loss of ZFP36L1 resulted in chromosome segregation defects in response to replication stress following a 24-hour exposure to the DNA polymerase inhibitor APH. We found that loss of ZFP36L1 increased the frequency of anaphase cells containing bulky bridges (Figure 4.3A and B). Quantification of bulky-anaphase bridges demonstrated that in comparison to WT cells, ZFP36L1 ablation resulted in a significant increase in bulky anaphase bridges when treated with 0.2 µM APH (p ≤0.01; *p* =0.0021) (Figure 4.3B). Specifically, 33% of ΔL1-T-REx anaphase cells contained bulky-anaphase bridges in contrast to 19% in WT when treated with 0.2 μM APH representing a 1.5-fold increase of anaphase cells encompassing bulky anaphase bridges in ΔL1-T-REx relative to WT cells (Figure 4.3B). Strikingly, untreated cells also demonstrated a two-fold increase in bulky-anaphase bridges in ΔL1-T-REx relative to WT ($p \leq 0.01$; $p = 0.0029$). Similarly, we observed a significant increase in anaphase cells with lagging chromosomes in ZFP36L1 KO cells as compared to WT in the presence and absence of APH (Figure 4.3B and D). Quantification of data demonstrated that approximately 39% of ΔL1-T-REx cells were marked by the presence of lagging chromosomes in comparison to 21% in WT representing a 2-fold increase when treated with 0.2 μM APH ($p \leq 0.01$; $p = 0.0038$) (Figure 4.3D). Moreover, in the absence of APH, loss of ZFP36L1 also significantly increased the frequency of lagging chromosomes ($p \leq 0.001$; $p = 0.0005$) (Figure 4.3D), supporting similar findings of increased bulky-anaphase bridges in ΔL1-T-REx cells under unperturbed conditions. Specifically, 13% of WT and 26% of ΔL1-T-REx anaphase cells exhibited lagging chromosomes representing a two-fold increase in untreated conditions (Figure 4.3D). Together, these results suggest that the loss of ZFP36L1 increases the occurrence of both bulky anaphase bridges and lagging chromosomes known markers of defects in chromosome segregation. Furthermore, these pathological structures are further exacerbated in the event of mild replication stress. Therefore, implying that ZFP36L1 is required to limit replication stress-associated chromosome segregation defects in mitosis.

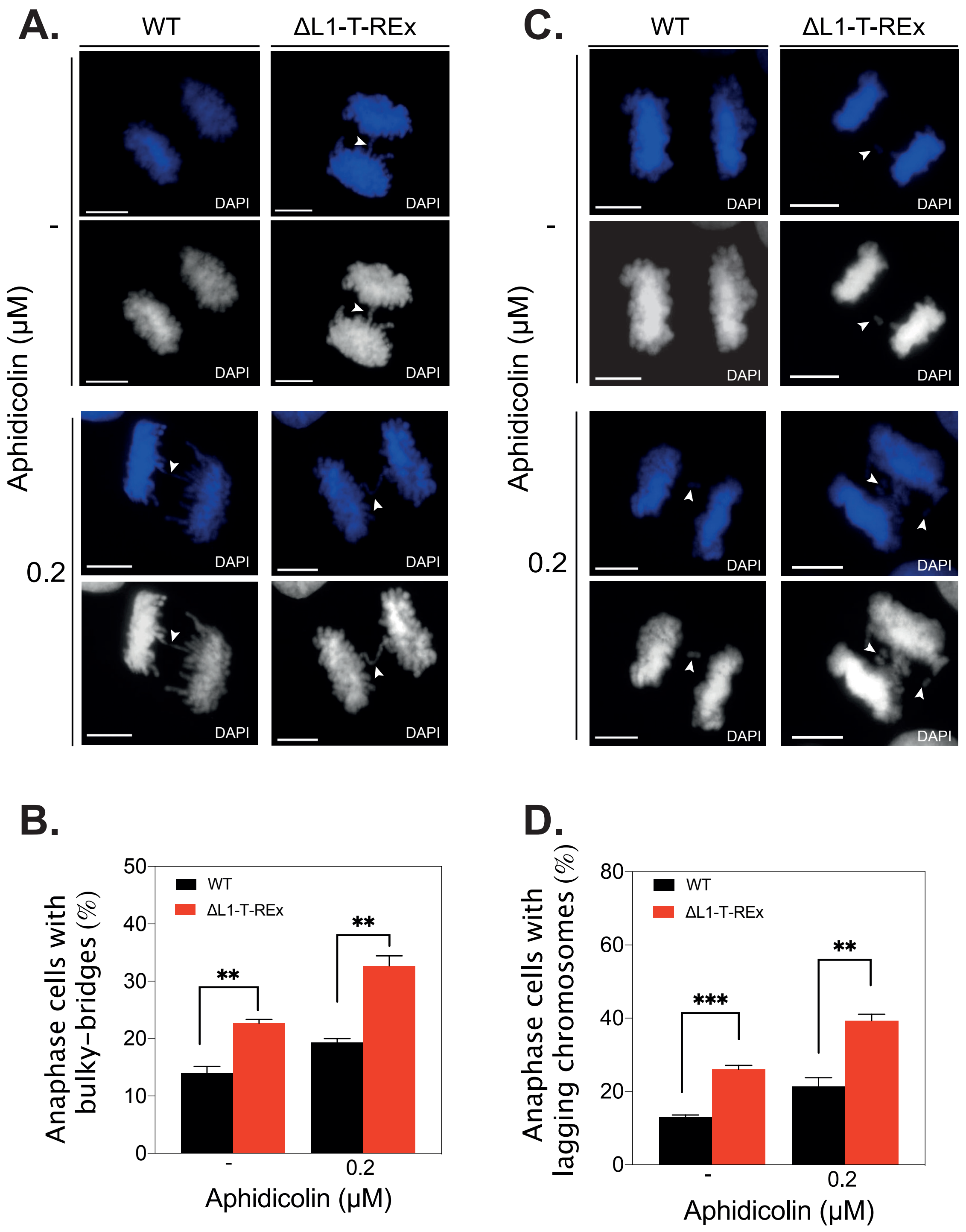

Figure 4.3 Loss of ZFP36L1 results in chromosome segregation defects in response to replication stress.

A. Images representing bulky-anaphase bridges recorded in T-REx U-2OS WT (WT) and ZFP36L1 Knockout (ΔL1-T-REx) T-REx U-2OS cells, white arrows indicate bulky-anaphase bridge. Scale bar, 10 μm. **B**. Quantifications of the percentage of anaphase cells with bulky-bridges in untreated and 0.2 μM APH treated WT and ΔL1-T-REX cells. **C**. Images representing lagging chromosomes recorded in WT and ΔL1-T-REx cells. White arrows indicate lagging chromosomes. Scale bar, 10 μm. (**D**) Quantification of the percentage of anaphase cells with lagging chromosomes in untreated and 0.2 μM

APH treated WT and ΔL1-T-REx cells. White arrows indicate lagging chromosomes. Scale bar, 10 μm. Data generated are of three independent replicates from a total of 50 anaphase cells analysed in each experiment. Error bars represent S.E.M. *p* values were calculated using an unpaired two-tailed t-test.; not significant p>0.05 (ns); p ≤ 0.05(*); p ≤0.01 (**); p ≤0.001 (***), p≤0.0001(****).

4.4 Loss of ZFP36L1 results in CFS-specific chromatid non-disjunction

Treatments with low doses of APH induce mild replication stress resulting in DNA entanglements known as anaphase ultrafine bridges (UFBs) that preferentially arise at intrinsically unstable loci such as common fragile sites (CFS) (Chan et al., 2009). Furthermore, it is thought that UFBs at CFS increase when lesions that perturb DNA replication are unresolved due to deficiencies in processing or repair factors, resulting in mitotic defects such as chromosomal aberrations and chromosome segregation errors (Di Marco et al., 2017; Naim & Rosselli, 2009). Our results thus far demonstrated that mild replication stress results in chromosomal aberrations and segregation errors in ZFP36L1 ablated cells. Importantly, these aberrations in mitosis have been demonstrated to be accompanied by FANCD2-associated UFBs in the presence of unresolved lesions or DNA structures (Lukas et al., 2011; Di Marco et al., 2017). It is noteworthy that CFSs show increased instability in precancerous lesions playing a direct role in cancer development (Glover, Wilson and Arlt, 2017). We, therefore evaluated the effect of ZFP36L1 ablation through immunofluorescence staining for FANCD2 and PICH to assess for CFS-UFBs. Only anaphase cells with PICH UFBs marked by twin FANCD2 (FANCD2 positive UFBs) at their terminus are associated with segregation defects arising from intrinsically unstable loci i.e., CFS (Figure 4.4A). Inversely, PICH-stained UFBs devoid of twin FANCD2 foci (FAND2-negative) at their extremities primarily originate from centromeric regions (Figure 4.4C). Results from our observations demonstrated deletion of ZFP36L1 increased anaphase cells exhibiting FANCD2-associated UFBs both in the presence and absence of APH (Figure 4.4B). Specifically, in APH-induced replication stress conditions, ΔL1-T-REx anaphase cells exhibiting FANCD2 positive UFBs significantly increased in comparison to WT cells ($p \leq 0.05$; *p* =0.0283). We found that 24% of ΔL1-T-REx anaphase cells were marked by the presence of FANCD2 positive UFBs when exposed to 0.2 µM APH in contrast to 11% in WT cells representing an increase of over two-fold in ΔL1-T-REx relative to WT cells. Moreover, a significant increase in FANCD2 positive UFBs was also observed in untreated ΔL1-T-REx cells in comparison to WT ($p \leq 0.05$; *p* =0.0389). We found that only 4% of WT contained FANCD2 positive UFBs in comparison to 15% in ΔL1-T-REx cells, signifying an increase of over 3-fold even in unperturbed conditions. Moreover, loss of ZFP36L1 and APH treatment did not affect the frequency of FAND2-negative that preferentially arise from centromeres (Figure 4.4B and C). Thus, taken together, these results implicate loss of ZFP36L1 in the increased prevalence of UFBs that arise at CFS loci marked by FANCD2 in mild replication stress conditions.

A.

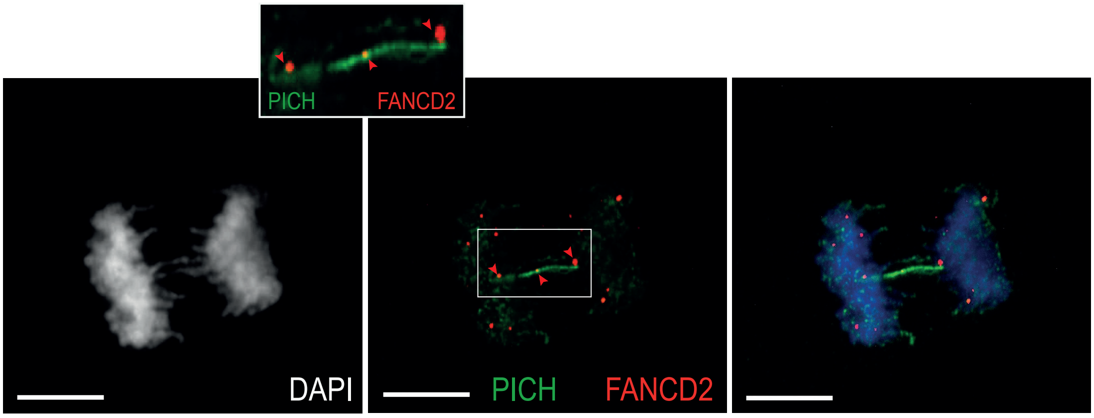
PICH
FANCD2
DAPI
PICH
FANCD2

B.

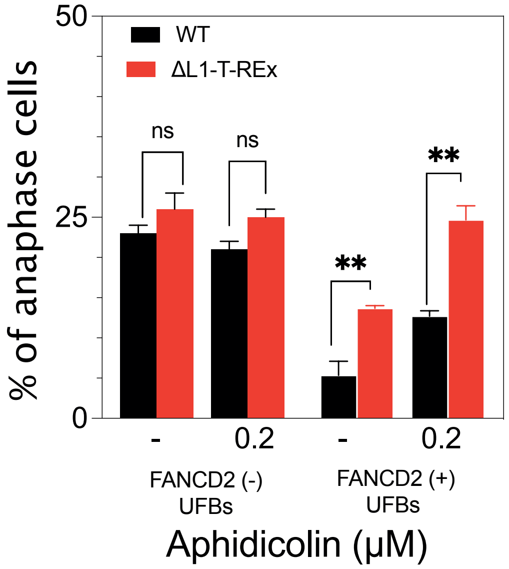
50
25
0
% of anaphase cells
WT
ΔL1-T-REx
ns
ns
**
**
-
0.2
-
0.2
FANCD2 (-)
UFBs
FANCD2 (+)
UFBs
Aphidicolin (μM)

C.

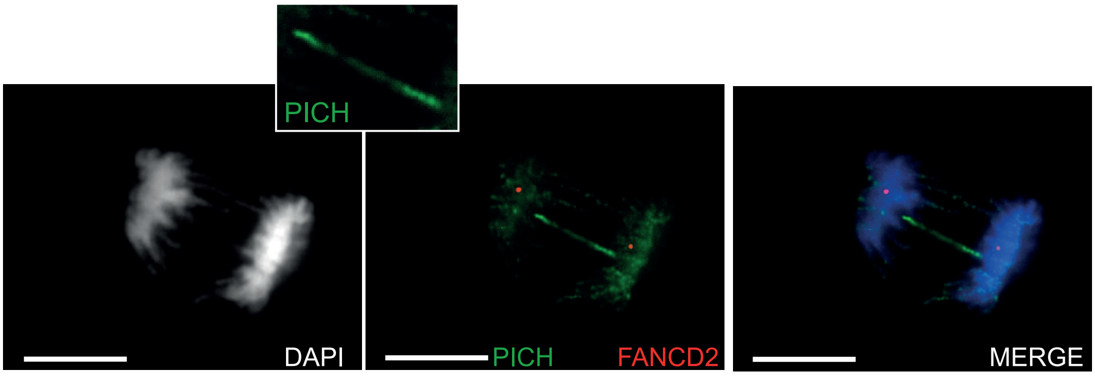
PICH
DAPI
PICH
FANCD2
MERGE

Figure 4.4 Loss of ZFP36L1 results in CFS-specific chromatid non-disjunction. **A**. Image representing FANCD2 (red) positive PICH green) UFBs scored in T-REx U-2OS WT (WT) and ZFP36L1 knockout (ΔL1-T-REX) U-2OS-T-REx cells, red arrows indicate FANCD2 foci at the termini of PICH positive UFBs. Scale bar, 10 μm. **B**. Quantifications of the percentage of anaphase cells with FANCD2 negative (-) and FANCD2 positive (+) UFBs in untreated and 0.2 μM APH-treated WT and ΔL1-T-REX cells. (**C**) Image representing a PICH stained FANCD2 negative UFB. Data generated are of three independent replicates from a total of 50 anaphase cells analysed in each condition and replicate. Error bars represent S.E.M. *p* values were calculated using an unpaired two-tailed t-test.; not significant p>0.05 (ns); p ≤ 0.05(*); p ≤0.01 (**); p ≤0.001 (***), p≤0.0001(****).

4.5 Loss of ZFP36L1 increases micronuclei formation

Micronuclei are extra-nuclear bodies that can be comprised of damaged chromosome fragments or whole chromosomes that are not incorporated into daughter nuclei and are markers of CIN and genomic instability (Wilhelm et al., 2019). In response to replication stress, micronuclei can form due to defective chromosome segregation leading to chromosome mis-segregation (Wilhelm et al., 2019). We demonstrated that ZFP36L1 loss resulted in chromosomal segregation errors, we further investigated the implications of the observed mitotic defects in the context of replication stress-induced chromosome mis-segregation. To accomplish this, we blocked cell cytokinesis utilising cytochalasin B for analysis of micronuclei in binucleated cells (Figure 4.5A) (Fenech et al., 2011). We assessed the frequency of binucleated cells with micronuclei in T-REx U-2OS WT and U-2OS ΔL1-T-REx cells untreated or treated with APH. We found that the ablation of ZFP36L1 significantly increased the frequency of binucleated cells harbouring micronuclei both in the presence and absence of low-dose APH (Figure 4.5 A and B). When treated with 0.2 μM APH, ΔL1-T-REx exhibited a higher frequency of binucleated cells with micronuclei compared to WT cells (p ≤0.001; *p* =0.0002). Approximately 29% of binucleated ΔL1-T-REx and 17% of WT cells were found to contain micronuclei representing a consistent two-fold increase in the absence of

ZFP36L1 under conditions of APH-induced replication stress. Similarly, loss of ZFP36L1 alone also significantly increased the percentage of binucleated cells with micronuclei relative to WT (p ≤0.01; *p*=0.0025). Specifically, approximately 14% of ΔL1-T-REx and 9% of WT binucleated cells exhibited micronuclei formation corresponding to a 1.5-fold increase in ΔL1-T-REx compared to WT in untreated conditions. Taken together our results demonstrated that the loss of ZFP36L1 increases chromosome mis-segregation and genomic instability as demonstrated by the increased prevalence of micronuclei in unperturbed and APH-induced replication stress conditions. Therefore, supporting a role for ZFP36L1 in maintaining genome integrity by limiting chromosome mis-segregation in response to replication stress.

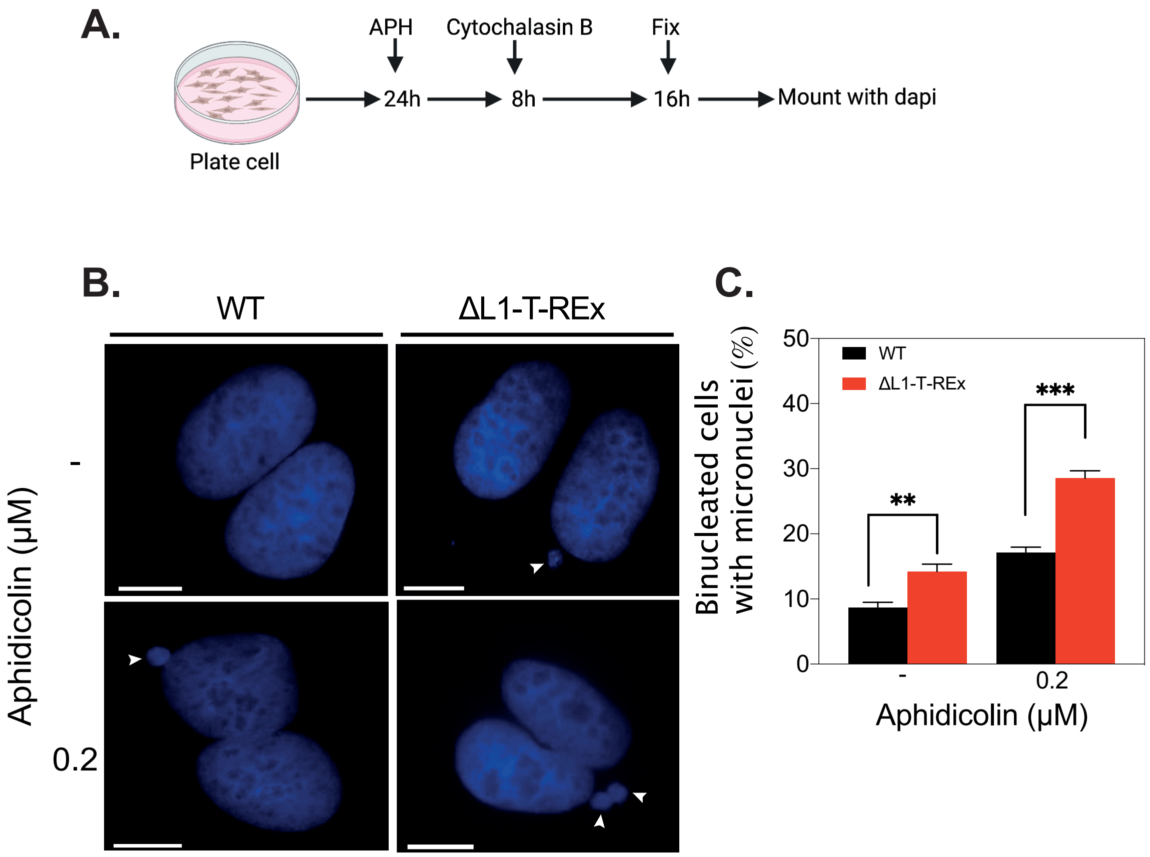

Figure 4.5 Loss of ZFP36L1 results in the formation of micronuclei.
A. Experimental workflow for micronuclei analysis. **B**. Images representing binucleated cells with micronuclei scored in T-REx U-2OS WT (WT) and ZFP36L1 Knockout (ΔL1-T-REX) T-REx U-2OS cells, white arrows indicate micronuclei. Scale bar, 10 µm. (**C**) Quantifications of the percentage of binucleated cells with micronuclei in untreated and 0.2 µM APH treated conditions in WT and ΔL1-T-REx cells. Data generated are of three independent replicates from a total of 300 binucleated cells analysed in each condition and experiment. Error bars represent S.E.M. *p* values were calculated using an unpaired two-tailed t-test.; not significant p>0.05 (ns); p ≤ 0.05(*); p ≤0.01 (**); p ≤0.001 (***), p≤0.0001(****).

4.6 Loss of ZFP36L1 results in DNA lesions sequestered by 53BP1 nuclear bodies in G1 cells

In the event of replication stress, lesions that remain unprocessed in mitotic chromosomes can lead to the transmission of DNA damage to daughter cells in the G1 phase that exhibit persistent 53BP1 nuclear bodies (NBs) (Harrigan et al., 2011). Moreover, these lesions that are marked by 53BP1 NBs have been shown to also originate from unprocessed CFS-UFBs in mitosis where they are marked by 53BP1 NBs in G1 and repaired in S-phase (Lukas et al., 2011). As our results thus far indicate that the loss of ZFP36L1 increases replication stress associated mitotic defects and genomic instability. We next assessed for 53BP1 NBs in cyclin A negative cells as a marker for WT and ΔL1-T-REx cells in the G1 phase by immunofluorescence staining (cyclin A antibodies stain for cells in the S/G2 phase). Our results demonstrated that ZFP36L1 ablation increased the percentage of G1 cells exhibiting >3 53BP1 NBs in untreated and APH treated conditions (Figure 4.6A and B). We observed a significant increase of G1 cells with >3 53BP1 NBs in ΔL1-T-REx when treated with 0.2µM APH relative to WT (p ≤0.01; p=0.0013) (Figure 4.6B). Specifically, we found that 7% of WT G1 cells exhibited >3 53BP1 NBs in contrast to 29% in ΔL1-T-REx representing a 4-fold increase in the absence of ZFP36L1 in conditions of APH-induced replication stress (Figure 2.5B). We also detected a significant increase in G1 cells with >3 53BP1 NBs in untreated conditions (p ≤ 0.05; *p*=0.0214) (Figure 4.6B). Specifically, 12% of

ΔL1-T-REx G1 cells were marked by the presence of >3 53bp1 in contrast to only 1% in WT G1 cells correlating to a 12-fold increase in the absence of ZFP36L1 relative to ZFP36L1 proficient cells in untreated conditions (Figure 4.6B). These results indicate that loss of ZFP36L1 increases the prevalence of 53BP1 NBs in G1 cells which are further exacerbated in response to APH-induced replication stress. Overall, our results suggest that in the absence of ZFP36L1, lesions or DNA structures remain unresolved in mitosis and are passed on to the subsequent cell cycle where they can manifest as micronuclei or shielded by 53BP1 NBs in the G1 cells.

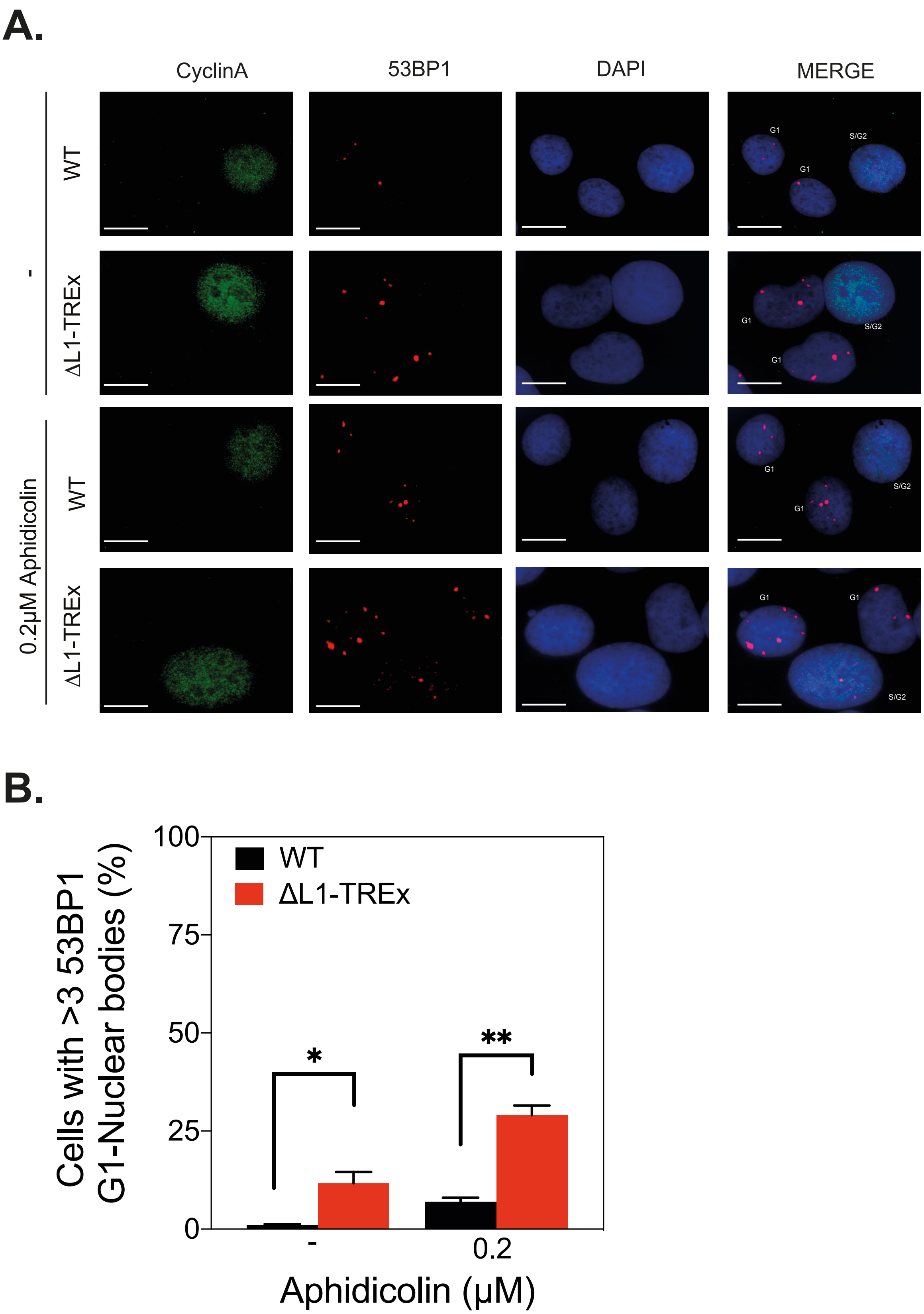
A.
CyclinA
53BP1
DAPI
MERGE
-
WT
ΔL1-TREx
0.2μM Aphidicolin
WT
ΔL1-TREx
G1
S/G2
G1
G1
S/G2
G1
G1
S/G2
G1
G1
G1
S/G2
B.
Cells with >3 53BP1 G1-Nuclear bodies (%)
100
75
50
25
0
WT
ΔL1-TREx
*
**
-
0.2
Aphidicolin (μM)

Figure 4.6 Loss of ZFP36L1 results in DNA lesions sequestered by 53BP1 nuclear bodies in the G1 phase.

A. Images representing cyclin A (green), 53BP1 (red), DAPI and Merge with indicated 53BP1 NBs scored only in G1 cells in WT and ΔL1-T-REx cells. Scale bar, 10 μm. **B.** Quantifications of the percentage of G1 cells with >3 53BP1 NBs in untreated and 0.2 μM APH treated conditions in WT and ΔL1-T-REx cells. Data generated are of three independent replicates from a total of 200 G1 cells analysed in each experiment. Error bars represent S.E.M. *p* values were calculated using an unpaired two-tailed t-test.; not significant p>0.05 (ns); p ≤ 0.05(*); p ≤0.01 (**); p ≤0.001 (***), p≤0.0001(****).

4.7 Discussion

Replication stress induces the formation of lesions that enter mitosis unresolved leading to chromosomal segregation errors and genomic instability (Fragkos and Naim, 2017). These defects manifest as structural chromosome aberrations and anaphase bridging or lagging chromosome fragments that are passed down to daughter cells as DNA lesions marked by G1-specific 53BP1 NBs or form extranuclear bodies such as micronuclei, a potent marker of CIN (Mankouri, Huttner and Hickson, 2013). The formation of micronuclei can be detrimental to genome integrity as they a prone to fragmentation and can become re-arranged thus driving hyper-mutation exhibited in cancers (Roberts and Gordenin, 2014; Zhang et al., 2015; Fenech et al., 2020). Evidence suggests that RBPs including AU-RBPs such as ZFP36, AUF1 and TIAR are involved in the maintenance of genome integrity in response to replication stress and DNA damage. Importantly, the loss of these AU-RBPs has been demonstrated to lead to chromosomal aberrations (Pont et al., 2012; Lafarga et al., 2018; Alfano et al., 2019; Lee et al., 2020). In line with this emerging role for RBPs and AU-RBPs, we have provided evidence that the loss of ZFP36L1 leads to chromosome aberrations, chromosomal segregation errors and genomic instability biomarkers. Importantly, we demonstrate segregation errors arising at CFS in response to mild replication could be attributed to unresolved lesions or DNA structures.

Specifically, we demonstrated that loss of ZFP36L1 induces the formation of chromosome aberrations in the form of chromatid gaps/breaks, chromosomal breaks and constrictions which were further exacerbated in response to mild replication stress (Figure 4.2). Chromosome aberrations are known to be induced on metaphase chromosomes due to failure to complete DNA replication in late S-phase and G2-phase or breaks that are carried over into mitosis at intrinsically unstable loci due to mild replication stress. Furthermore, the appearance of gaps and breaks on metaphase chromosomes in response to mild replication stress has been reported to form because of CFS instability (Di Marco et al., 2017; Ying et al., 2013). Moreover, gaps or breaks in metaphase chromosomes in response to low dose APH have been shown to be mediated by the structure-specific endonucleases that cleave DNA structures at CFS loci to promote faithful chromosome segregation (Di Marco et al., 2017; Ying et al., 2013). Suggesting that the loss of ZFP36L1 may increase the prevalence of DNA structures that require resolution in early mitosis.

Mild replication stress-induced chromosomal aberrations precede segregation defects in anaphase cells. Our results demonstrated that loss of ZFP36L1 induces the formation of anaphase bulky bridges and lagging chromosomes (Figure 4.3). Furthermore, our results shed light on an unexpected association with segregation defects that arise at CFS loci in the form of FANCD2 positive UFBs (Figure 4.4). We found that loss of ZFP36L1 increases the prevalence of FANCD2 positive UFBs in mild replication stress conditions corroborating our findings of aberrations on metaphase chromosomes. Importantly, FANCD2-associated UFBs are thought to stem from unresolved DNA lesions or secondary structures that persist into mitosis, inevitably leading to the formation of UFBs resulting in chromosome segregation errors (Chan et al., 2009). On the other hand, in response to replication stress, FANCD2 has also been shown to accumulate at large transcribed genes that often overlap with CFS loci in dependent on unresolved DNA structures (Okamoto et al., 2018). Therefore, this could pose a potential mechanistic association of ZFP36L1 with increased segregation errors in mitosis.

The persistence of FANCD2-associated UFBs carrying unresolved DNA lesions can undergo breakages transitioning into 53BP1 NBs as shielded DNA lesions in the subsequent G1 phase (Lukas et al., 2011). Here, we have also demonstrated that the loss of ZFP36L1 increases the occurrence of 53BP1 NBs that are present within G1 phase cells and increases when exposed to mild replication stress, suggesting DNA lesions that potentially arise at these sites remain unresolved and become shielded in the next cell cycle (Figure 4.6). Interestingly, the loss of family member ZFP36 was reported to result in the accumulation of 53BP1 foci in response to hydroxyurea-mediated replication stress (Lee et al., 2020). However, this study focused on 53BP1 foci across interphase cells as a surrogate marker of DSBs and not inherited segregation errors marked in G1 cells. Moreover, 53BP1 NBs are distinct from smaller 53BP1 foci and appear mainly in G1 cells (Harrigan et al., 2011). Importantly, when lagging chromosome and anaphase bridges are not resolved on time or if they occur in excess, they can be detrimental to genome stability resulting in the formation of micronuclei (Soto et al., 2018). Indeed, our findings elucidated that the loss of ZFP36L1 induces micronuclei formation with is further exacerbated in response to mild replication stress (Figure 4.5). Overall, these results demonstrate that ZFP36L1 suppresses replication stress-associated chromosome segregation deficiencies that lead to genome instability.

5. Loss of ZFP36L1 leads to recruitment of DNA damage response and repair proteins under replication stress conditions

5.1 Introduction

DNA replication is vulnerable to impediments originating from both endogenous and exogenous sources such as DNA-damaging agents and inherent properties of DNA sequences that are prone to form secondary structures (Zeman and Cimprich, 2013). Specifically, replication fork progression can be hindered by intrinsic factors that include non-B DNA structures such as R-loops, cruciform, hairpins, trinucleotide repeats and conflicts with transcription machinery leading to replication stress (Zhao et al., 2009). DNA replication typically occurs with the S-phase, however, during episodes of replication stress, DNA replication can be delayed and extend into the G2 phase (Maya-Mendoza et al., 2018). Replication stress leading to replication fork stalling is sensed by key DNA damage response and repair proteins that work in concert to resolve and restore replication fork progression (Reviewed in Zeman and Cimprich, 2013). Stalled replication forks lead to the formation of ssDNA as the DNA helicase continues to unwind DNA leading to the recruitment of Replication Protein A (RPA) (Rinaldi et al., 2021). Furthermore, due to the protective role of RPA on exposed ssDNA, it is also recruited to sites of DNA repair (Dueva and Iliakis, 2020). Therefore, the accumulation of RPA in replication stress conditions is a potent marker of stalled replication forks. Excess ssDNA is prone to DNA damage under prolonged replication fork stalling conditions (Zeman and Cimprich, 2013). In response to DNA damage H2A histone family member X (H2AX) is phosphorylated at serine residue 139 recruiting DNA repair and signalling proteins at sites of DNA damage (Gagou, Zuazua-Villar and Meuth, 2010). Furthermore, replication stress-induced γH2AX has been shown to represent sites of persistent replication fork damage and appear as discrete nuclear foci (Gagou, Zuazua-Villar and Meuth, 2010). H2AX phosphorylation spreads from stalled forks over large chromatin domains and has been demonstrated to precede fork collapse and ultimately double-strand break (DSB) formation (Sirbu et al., 2011). Moreover, replication fork collapse is reported to arise due to unresolved DNA structures that impede replication fork progression leading to collisions with transcription machinery (Hamperl et al., 2017). Upon DSB formation, γH2AX signalling recruits repair factors such as 53BP1 that localise to sites of DSBs. Importantly, reports have reported 53BP1 nuclear foci to colocalise with γH2AX (Holcomb et al., 2008). The replication stress-mediated DNA damage repair process is initiated by activation of CHK1 by ATR through phosphorylation at serine residues 317 and 345. Subsequently, CHK1 coordinates cell cycle delay to mediate DNA repair and protects cells from undergoing apoptosis (Ward and Chen, 2001 Chanoux et al., 2009; Myers et al., 2009) (Figure 5.1). Moreover, unrepaired lesions induced by mild replication stress have been shown to bypass CHK1 signalling and continue into mitosis leading to mitotic defects and genomic instability (Ward and Chen, 2001; Chan et al., 2009; Lukas et al., 2011; Eykelenboom et al., 2013; Liu et al., 2014; Minocherhomji and Hickson, 2014). We, therefore, set out to investigate if the observed mitotic defects and genomic instability could be due to unprocessed replication stress-associated DNA damage.

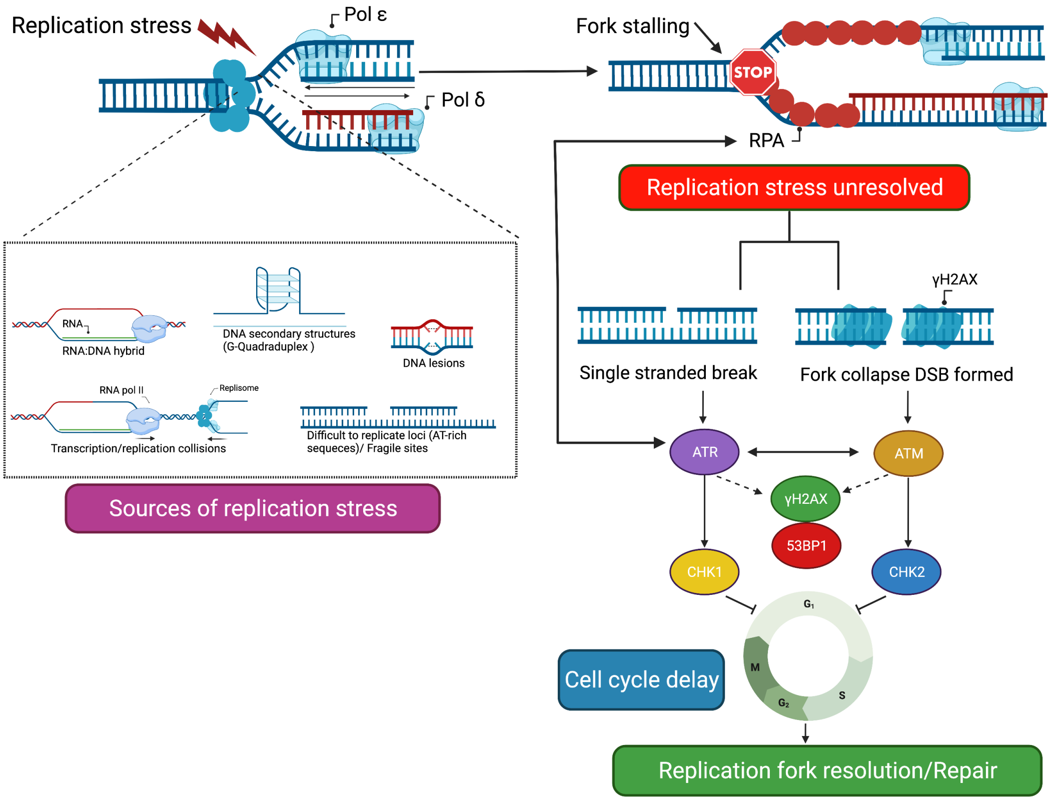
Replication stress
Pol ε
Pol δ
RNA
RNA:DNA hybrid
DNA secondary structures
(G-Quadraduplex)
DNA lesions
RNA pol II
Replisome
Transcription/replication collisions
Difficult to replicate loci (AT-rich
sequeces)/ Fragile sites
Sources of replication stress
Fork stalling
STOP
RPA
Replication stress unresolved
γH2AX
Single stranded break
Fork collapse DSB formed
ATR
ATM
γH2AX
53BP1
CHK1
CHK2
G₁
S
G₂
M
Cell cycle delay
Replication fork resolution/Repair

Figure 5.1 Causes and consequences of replication stress.
Replication stress originating from different sources can lead to replication fork stalling (STOP) generating stretches of ssDNA protected by RPA and activation of ATR. If the source of replication stress is unresolved this can lead to single-stranded breaks or fork collapse generating DSBs. Following DNA damage γH2AX signalling can lead to the activation and recruitment of both ATR and ATM leading to recruitment of repair factors such as 53BP1 and activation of CHK1 and CHK2 respectively. CHK1 and CHK2 activation lead to cell cycle delay to mediate replication fork resolution and repair (Created with Biorender.com).

Here we assessed for key replication stress associated damage response and repair proteins RPA and γH2AX foci in cyclin A positive cells as a marker of cells in S/G2 through immunofluorescence. We demonstrated that loss of ZFP36L1 increases RPA and γH2AX foci formation, markers of replication stress-associated DNA damage during integral stages of DNA replication in S/G2 cells. Furthermore, we show that this increased DNA damage in the absence of ZFP36L1 could be due to DSB formation through observations of colocalisation of 53BP1 and γH2AX foci. We also shed light on the cell cycle dynamics following mild replication stress in ZFP36L1 abolished cells and demonstrate increasing S-phase cell population, potentially implicating mild S-phase delay. Furthermore, we demonstrate that APH-induced replication stress results in CHK1 phosphorylation however loss of ZFP36L1 resulted only in slight differences. Importantly, this activation of CHK1 potentially limits cell death as we demonstrate loss of ZFP36L1 does not result in apoptosis in response to low dose APH. Finally, we identify ZFP36L1 in chromatin fractions presenting a potential role for ZFP36L1 to maintain genome integrity through interactions with chromatin-associated proteins and/or structures.

5.2 Loss of ZFP36L1 induces RPA accumulation in S/G2 cells

We first assessed the frequency of RPA foci as a biomarker of ssDNA and DNA repair in cyclin A positive cells by immunofluorescence staining in T-REx U-2OS wild-type (WT) and T-REx U-2OS ZFP36L1 KO cells (ΔL1-T-REx). Our results demonstrated that ZFP36L1 ablation increased the percentage of cyclin A positive cells exhibiting >9 RPA foci in the presence and absence of APH in ΔL1-T-REx compared to WT cells (Figure 5.2A and B). A significant increase in the frequency of cells with >9 RPA foci between ΔL1-T-REx and WT was observed in APH-treated conditions ($p \leq 0.01$; $p=0.0031$) (Figure 5.2B). Specifically, we found that 22% of WT cyclin A positive cells exhibited >9 RPA foci in contrast to 39% in ΔL1-T-REx representing a 1.75-fold increase (Figure 5.2B). Astonishingly, the percentage of cyclin A positive cells exhibiting >9 RPA foci in untreated conditions was also deemed significant ($p \leq 0.01$; $p=0.0093$) (Figure 5.2B). Specifically, in unperturbed conditions 24% of ΔL1-T-REx cyclin A positive cells exhibited >9 RPA foci in contrast to 7% in WT cells, corresponding to an increase of approximately 3-fold of ΔL1-T-REx cells with >9 RPA foci relative to WT cells (Figure 5.2B). Overall, these results indicate that loss of ZFP36L1 significantly increases the frequency of replication stress-induced ssDNA bound by RPA foci in S/G2 cells which is a fundamental component of the replication stress response and DNA repair machinery.

A.

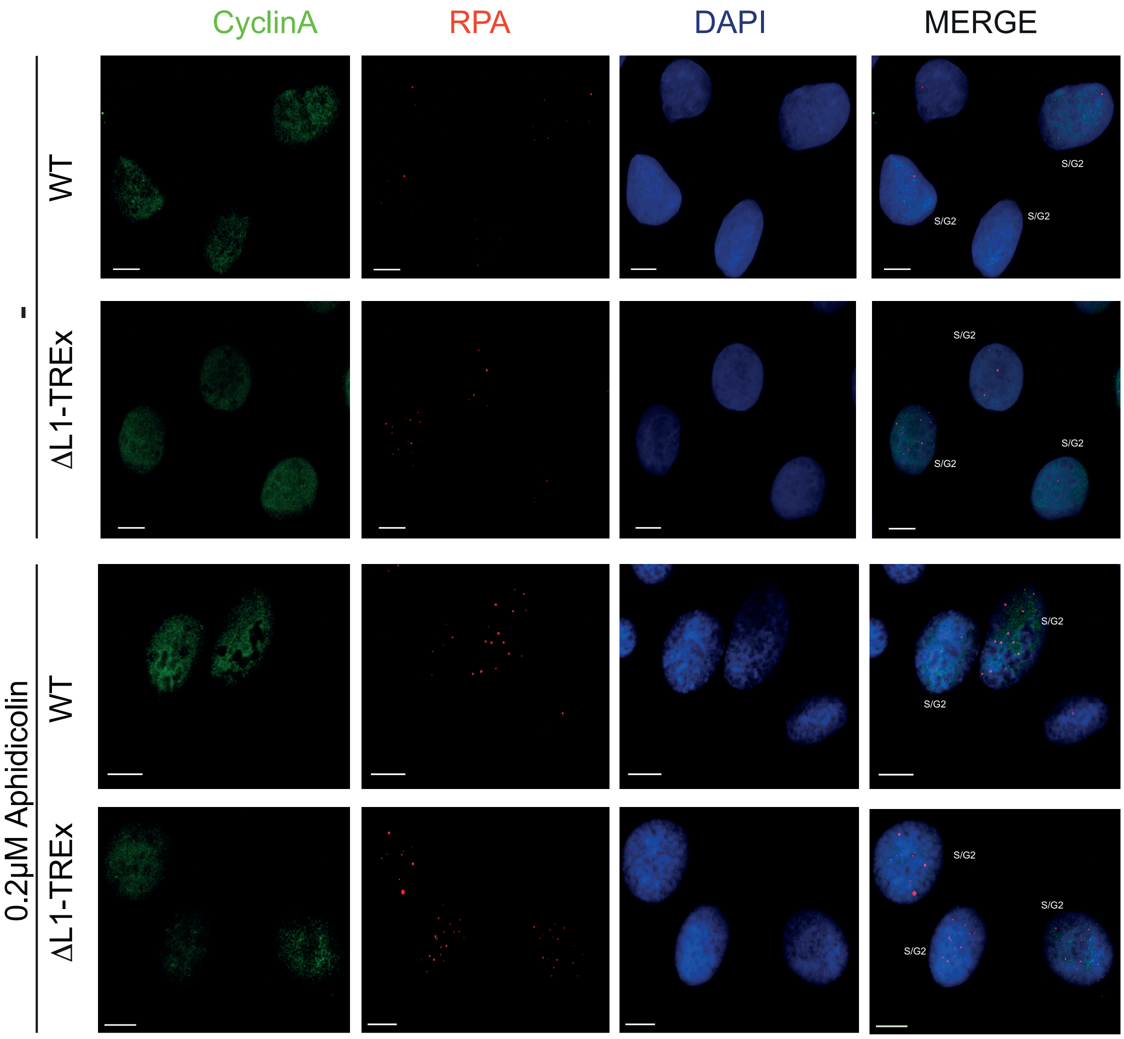
CyclinA
RPA
DAPI
MERGE
-
WT
ΔL1-TREx
0.2μM Aphidicolin
WT
ΔL1-TREx
S/G2
S/G2
S/G2
S/G2
S/G2
S/G2
S/G2
S/G2
S/G2
S/G2
S/G2
S/G2

B.

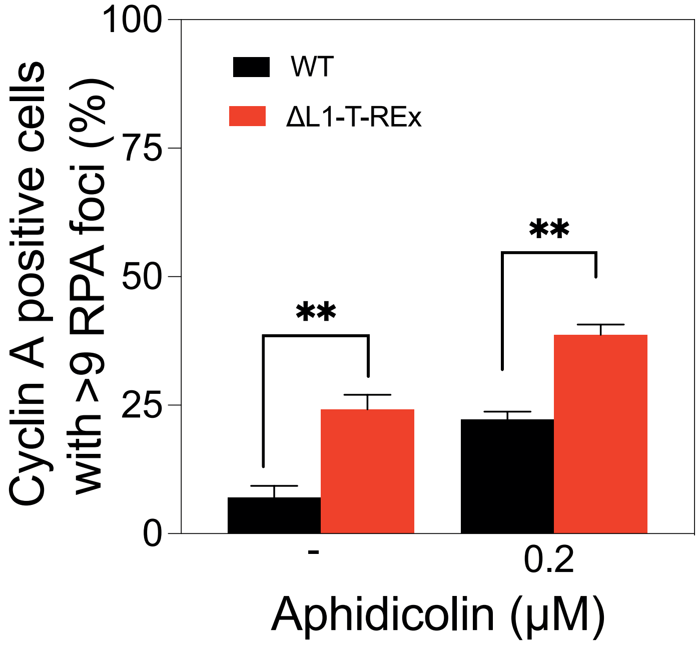
Cyclin A positive cells with >9 RPA foci (%)
100
75
50
25
0
WT
ΔL1-T-REx
**
**
-
0.2
Aphidicolin (μM)

Figure 5.2 Loss of ZFP36L1 increases RPA accumulation in S/G2 cells.
A. Images representing cyclin A (green), RPA (red), DAPI and Merge with indicated RPA foci scored only in S/G2 cells in T-REx U-2OS WT (WT) and ZFP36L1 Knockout T-REx U-2OS (ΔL1-T-REX). Scale bar, 10 μm. **B.** Quantifications of the percentage of cyclin A positive cells with >9 RPA foci in untreated and 0.2 μM APH-treated WT and ΔL1-T-REX cells. Data generated are of three independent replicates from a total of 200 S/G2 cells analysed in each experiment. Error bars represent S.E.M. *p* values were calculated using an unpaired two-tailed t-test.; not significant p>0.05 (ns); p ≤ 0.05(*); p ≤0.01 (**); p ≤0.001 (***), p≤0.0001(****).

5.3 Loss of ZFP36L1 increases γH2AX foci in S/G2 phase cells

Unresolved DNA-associated structures can result in chronic replication stress leading to replication fork arrest and DNA breaks (Fragkos and Naim, 2017). Replication stress response results in phosphorylation of histone H2A variant X (H2AX) at Serine -139 (γH2AX) initiating signalling mechanisms for subsequent DNA repair (Chanoux et al., 2009). Following our observations that indicated the loss of ZFP36L1 increased RPA accumulation in S/G2 cells in response to replication stress, we suspected that accumulation of ssDNA could result in increased susceptibility to DNA damage. Therefore, we examined ZFP36L1 KO cells for γH2AX, a marker of replication stress-induced DNA damage, and cyclin A, a marker of cells in S/G2. Our results demonstrated that the loss of ZFP36L1 increased the frequency of γH2AX in cyclin A positive cells both in the presence and absence of APH (Figure 5.3 A and B). In APH-induced replication stress conditions, we observed a significant increase in average γH2AX foci present in cyclin A positive ΔL1-T-REx cells relative to WT cells (p ≤ 0.0001; *p*,0.0001). Specifically, we observed an average of approximately 15 γH2AX foci in ΔL1-T-REx cells compared to 9 in WT cells in the presence of 0.2 μM APH, representing a 60% increase in γH2AX foci in ΔL1-T-REx cells relative to WT (Figure 2.6.2 A and B). Similarly, we also observed an increase in γH2AX foci in untreated conditions in ΔL1-T-REx cells relative to WT (p ≤0.001; *p*=0.0006) (Figure 5.3 A and

B). In untreated conditions, we observed an average of 8 γH2AX foci in ΔL1-T-REx Cyclin A positive cells compared to 4 in WT corresponding to a 50% increase in ΔL1-T-REx cells relative to WT. Overall, these results indicate loss of ZFP36L1 increases the susceptibility of replication stress-associated DNA damage through observations of γH2AX foci in S/G2 cells.

.

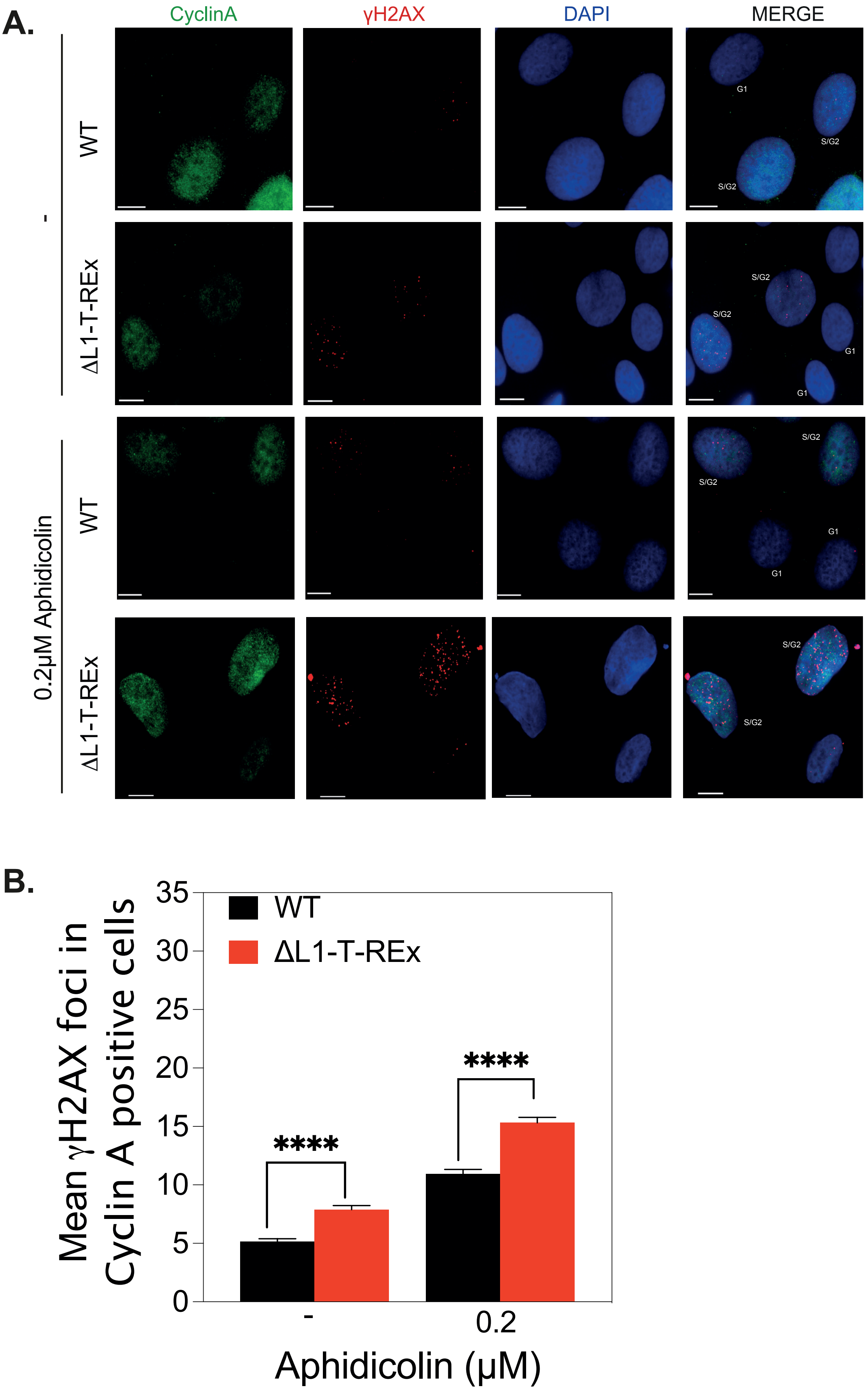
A.
CyclinA
γH2AX
DAPI
MERGE
-
WT
ΔL1-T-REx
0.2μM Aphidicolin
WT
ΔL1-T-REx
G1
S/G2
S/G2
S/G2
S/G2
G1
G1
S/G2
S/G2
G1
G1
S/G2
S/G2
B.
Mean γH2AX foci in Cyclin A positive cells
0
5
10
15
20
25
30
35
WT
ΔL1-T-REx
****
****
-
0.2
Aphidicolin (μM)

Figure 5.3. Loss of ZFP36L1 increases γH2AX foci in S/G2 phase cells.
A. Images representing cyclin A (green), γH2AX (red), DAPI and Merge with indicated γH2AX foci scored only in S/G2 cells in T-REx U-2OS WT (WT) and ZFP36L1 knockout (ΔL1-T-REX) U-2OS-T-REx. Scale bar, 10 μm. **B.** Quantifications of the percentage of S/G2 cells with >12 γH2AX foci in untreated and 0.2 μM APH-treated WT and ΔL1-T-REX cells. Data generated are of three independent replicates from a total of 200 S/G2 cells analysed in each condition and replicate. Error bars represent S.E.M. *p* values were calculated using an unpaired two-tailed *t*-test.; not significant p>0.05 (ns); p ≤ 0.05(*); p ≤0.01 (**); p ≤0.001 (***), p≤0.0001(****).

5.3 ZFP36L1 is required to limit replication stress-induced DSBs

When DNA replication is perturbed and cannot be effectively resolved, stalled replications forks are generated and become susceptible to fork collapse resulting in DNA double-strand breaks (DSB) (Schoonen, Guerrero Llobet and van Vugt, 2019). 53BP1 has been demonstrated to colocalise with γH2AX at sites of DSBs and mediate subsequent repair. Therefore, we set out to undertake simultaneous analysis of γH2AX and 53BP1 through immunofluorescence microscopy by measuring the frequency of colocalised γH2AX and 53BP1 in T-REx WT and ΔL1-T-REx cells. Our results demonstrated that the loss of ZFP36L1 increased the frequency of 53BP1 NBs co-localising with γH2AX cells in the presence and absence of APH (Figure 5.4A). When treated with 0.2 μM APH, we observed that the frequency of colocalised 53BP1 NBs and γH2AX significantly increased in ΔL1-T-REx cells in comparison to WT cells (p ≤0.01; *p*=0.0031) (Figure 5.4B). Specifically, we found that in the presence of 0.2 μM APH 18.1% of ΔL1-T-REx cells exhibited 53BP1 and γH2AX co-localisation in contrast to approximately 7.6% in WT correlating to a two-fold increase in ΔL1-T-REx cells with colocalised 53BP1 and γH2AX as compared to WT cells. To our surprise, even in the absence of APH, loss of ZFP36L1 significantly increased the frequency of 53BP1 and γH2AX co-localisation (p ≤0.01; *p*=0.0002) (Figure 5.4B). Moreover, we found that 53BP1 and γH2AX co-localisation increased 3-fold in the absence of

ZFP36L1 correlating to 10.1% in ΔL1-T-REx and 3% in WT cells. Based on these findings, we propose that ZFP36L1 is required to protect cells against replication stress-induced DNA DSBs that pose a threat to genome integrity.

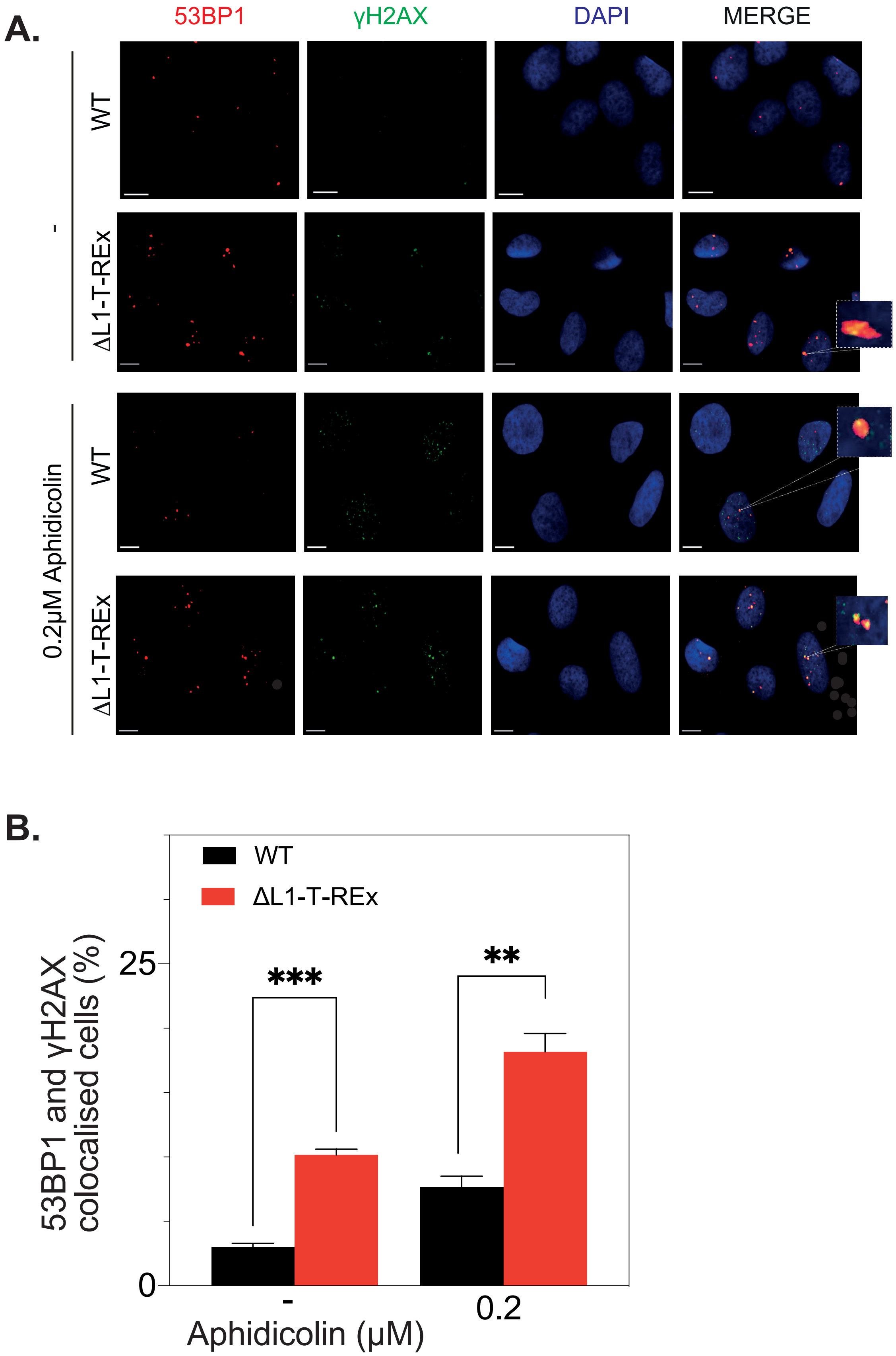
A.
53BP1
γH2AX
DAPI
MERGE
-
WT
ΔL1-T-REx
0.2µM Aphidicolin
WT
ΔL1-T-REx
B.
WT
ΔL1-T-REx
53BP1 and γH2AX colocalised cells (%)
25
0
***
**
-
0.2
Aphidicolin (µM)

Figure 5.4 ZFP36L1 is required to limit replication stress-induced double-stranded DNA breaks (DSB).
A. Images representing 53BP1 NBs (Red), γH2AX (Green), DAPI and Merge. 53BP1 and γH2AX co-localisation (orange foci) visualised in T-REx U-2OS WT (WT) and ZFP36L1 knockout (ΔL1-T-REX) U-2OS-T-REx. Scale bar, 10 μm. **B.** Quantifications of the percentage of cells with colocalised 53BP1 and γH2AX in untreated and 0.2 μM APH-treated WT and ΔL1-T-REX cells. Data generated are of three independent replicates from a total of 200 cells analysed in each condition and replicate. Error bars represent S.E.M. *p* values were calculated using an unpaired two-tailed t-test.; not significant p>0.05 (ns); p ≤ 0.05(*); p ≤0.01 (**); p ≤0.001 (***), p≤0.0001(****).

5.5 Ablation of ZFP36L1 increases S-phase cells and CHK1 phosphorylation in response to low dose APH

Mild replication stress induced by low doses of APH is associated with mild delays in interphase specifically in the S-phase (Zeman and Cimprich, 2013). Since our results thus far have demonstrated that the loss of ZFP36L1 results in increased replication stress-associated DNA damage and repair biomarkers, we next sought to investigate if loss of ZFP36L1 could lead to changes in the cell cycle in response to APH-induced replication stress. To measure the potential impact on the cell cycle as a result of the loss of ZFP36L1 during episodes of mild replication stress, we treated T-REx U-2OS WT(WT) and ZFP36L1 KO (ΔL1-T-REx) cells with low doses of APH (0.1, 0.2 and 0.4μM) for 24hours and examined cell cycle profiles by flow cytometry utilising propidium iodide (PI) staining. Indeed, treatments with 0.2μM and 0.4μM APH demonstrated a significant increase (*p*=0.0420 and *p*=0.0441) in the population of cells within the S-phase in the absence of ZFP36L1 in comparison to WT cells (Figure 5.5A and B). Specifically, treatment with 0.2μM APH increased the S-phase population from 54.3% in WT cells to 61.17% in ΔL1-T-REx cells suggesting potential S-phase delay in response to mild replication stress (Figure 5.5A and B). Indeed, we also found that APH concentrations of 0.4μM significantly increased ΔL1-T-REx cells in the S-phase compared to WT cells, corresponding to 57.3% and 62.13% in WT and ΔL1-T-REx cells respectively (Figure 5.5A and B). Importantly, we detected fewer ΔL1-T-REx cells in the G2 phase compared to WT in 0.2 and 0.4μM treated conditions (Figure 5.5A and B). However, this was deemed to be statistically non-significant between WT and ΔL1-T-REx cells suggesting loss of ZFP36L1 induces mild cell cycle delay without inducing cell cycle arrest. Furthermore, ΔL1-T-REx cells treated with 0.1μM did not cause significant changes in the S-phase population when compared to WT cells in. Specifically, we found a slight increase in the S-phase cell population in ΔL1-T-REx cells compared to WT at 58.67% and 56.67% respectively (Figure 5.5A and B). Similarly, in untreated conditions, ZFP36L1 ablation alone did not lead to any significant changes in the S-phase population (Figure 5.5A and B). These results suggest the observed cell cycle-related changes of increased cell population in the S-phase are triggered by a combination of ZFP36L1 ablation and low dose concentrations of APH of 0.2μM and 0.4μM. Overall, cell cycle analysis demonstrated an expected increase in the percentage of cells in the S-phase in both WT and ΔL1-T-REx following treatment of low doses of APH. Interestingly, loss of ZFP36L1 exacerbates the number of cells in the S-phase with 0.2μM and 0.4μM compared to WT cells indicating a potential slowing of DNA replication or intra-S phase checkpoint signalling pathways due to obstructions or lesions reported thus far.

Increased S-phase population in replication stress conditions can be attributed to intra-S phase checkpoint activation (Wilhelm et al., 2019). Furthermore, the non-significant decrease in the G2 cell population could indicate S-phase delay without affecting G2 progression. We, therefore, suspected that the increase in the S-phase population could be attributed to increased replication stress leading to the activation of the DDR. Specifically, during episodes of replication stress, the main effector is the ATR/CHK1 axis (Wilhelm et al., 2019). Since replication stress induces S-phase delay through the

ATR/CHK1 pathway and low doses of APH have been shown to induce CHK1 phosphorylation at serine 345 (S345) (Basile et al., 2014; Durkin et al., 2006). We utilised a phospho-specific antibody targeted against CHK1 pS345 to determine the impact of low-dose APH on CHK1 phosphorylation in ZFP36L1 abolished cells. WT and ΔL1-T-REx Cells were either untreated (-) or treated with low dose concentrations of APH (0.1, 0.2 and 0.4μM) for 24 hours and total cell protein extracts were utilised to assess CHK1 phosphorylation status in each condition. Western blotting for CHK1 pS345 demonstrated slight increases in CHK1 phosphorylation specifically, with APH concentrations of 0.2μM and 0.4μM relative to untreated conditions (Figure 5.5C). Whereas treatment with 0.1μM APH did not demonstrate a notable increase in CHK1 phosphorylation relative to the untreated conditions (Figure 5.5C). Likewise, WT cells treated with 0.2μM and 0.4μM also demonstrated slight increases in CHK1 phosphorylation relative to untreated conditions. On the other hand, 0.1μM APH treatment conditions did not elicit a distinct increase in CHK1 phosphorylation. Together western blot analysis demonstrated that we were able to detect a slight increase in CHK1 phosphorylation at low doses concentrations of APH at 0.2μM and 0.4μM in both WT and ΔL1-T-REx cells indicative of a functional replication stress response.

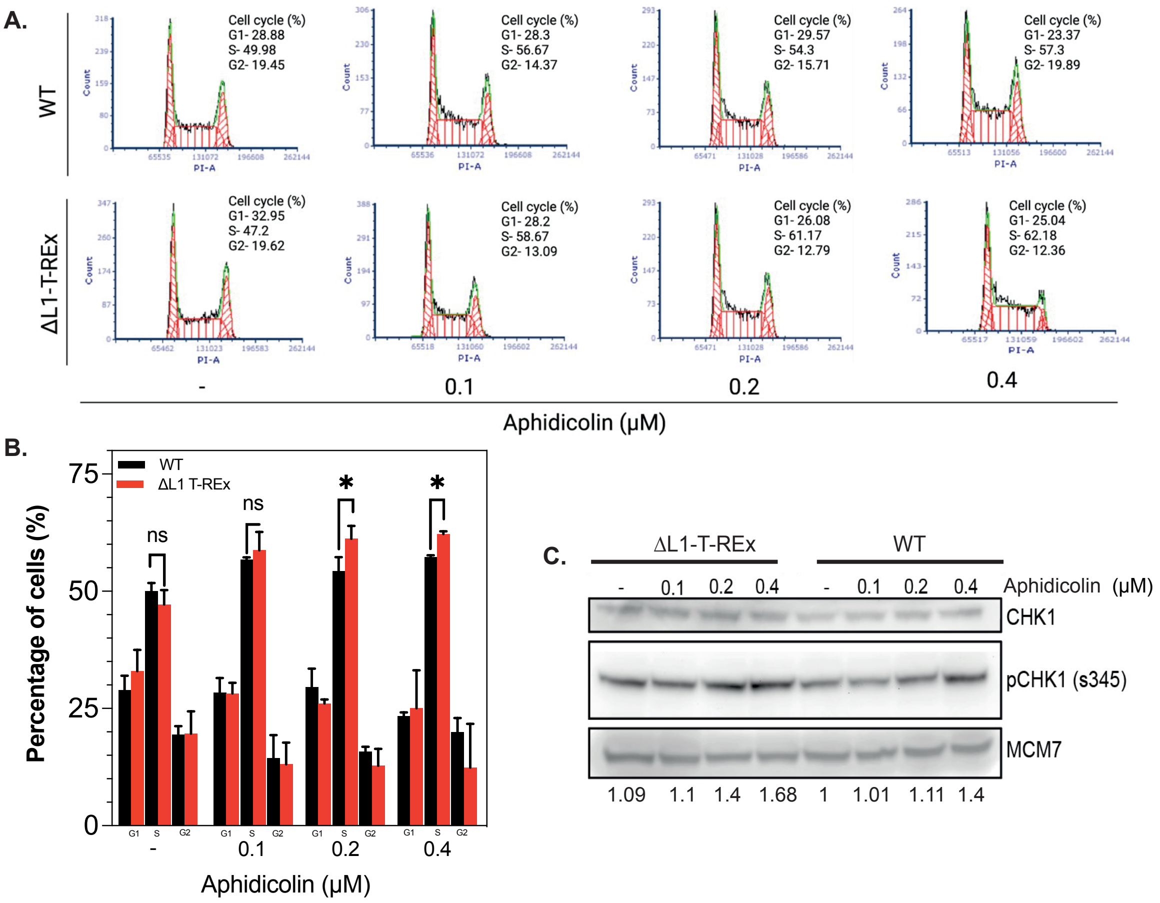

Figure 5.5 Ablation of ZFP36L1 increases S-phase population and induces low CHK1 phosphorylation in response to low dose APH.

A. Flow cytometric analysis of cell cycle distribution in U-2OS WT and ZFP36L1 KO cells (ΔL1-T-REx) cells in response to mild replication stress treated without (-) or with 0.1, 0.2 and 0.4μM APH for 24hours. Cells were harvested and their cell cycle profiles were assessed by flow cytometry utilising propidium iodide staining (PI). **B.** Cell cycle distribution data indicating the percentage of cells in G1, S and G2 in each condition were quantified from three independent replicates. (**C**) Western blot analysis of total protein extracts from ΔL1-T-REx and WT cells untreated (-) or treated with 0.1, 0.2 and 0.4μM APH for 24 hours probed for CHK1 phosphorylated (pCHK1) at Serine 345 (s345) CHK1 and MCM7 was utilised as total protein and loading controls Error bars represent S.E.M. *p* values were calculated using an unpaired two-tailed t-test.; not significant p>0.05 (ns); p ≤ 0.05(*); p ≤0.01 (**); p ≤0.001 (***), p≤0.0001(****).

5.6 Loss of ZFP36L1 does not induce apoptosis in APH -induced replication stress conditions

To determine if checkpoint activation and the increased S phase cell population induce cell death, exponentially growing WT and ΔL1-T-REx cells were either untreated or treated with low doses of APH (0.1, 0.2 and 0.4μM) for 24 hours, stained for Annexin V and propidium iodide then analysed by flow cytometry. Flow cytometry analysis in WT and ΔL1-T-REx cultures demonstrated a slight dose-dependent increase in the number of Annexin V-positive cells in the early stages of apoptosis (lower right quadrant) and late stages of apoptosis (top right quadrant) (Figure 5.6 A and B). Specifically, WT and ΔL1-T-REx cells treated with APH concentrations (0.1, 0.2 and 0.4μM) did not affect cells in the early stages of apoptosis relative to untreated cells (Figure 5.6 A and B). Although, we observed a greater dose-dependent increase of WT and ΔL1-T-REx cells in the late apoptotic stages the overall difference between the two cell types was statistically non-significant (Figure 5.6 A and B). Importantly, the analysis demonstrated that treatments with 0.1, 0.2 and 0.4μM APH in WT and ΔL1-T-REx cells only slightly impacted cell viability (lower left quadrant) (Figure 5.6 A and B). Specifically, WT and ΔL1-T-REx cells treated with 0.1μM APH demonstrated that viability was only slightly affected. Analysis revealed that 93.5% of WT and 92% in ΔL1-T-REx were viable representing a 0.2% and 2.4% decrease relative to untreated cells for WT and ΔL1-T-REx cells respectively. Similarly, in the presence of 0.2μM APH, a 2.9% decrease in cell viability was observed in ΔL1-T-REx cells treated decreasing from 94.4% in untreated conditions to 91.5% in the presence of 0.2μM APH. Whereas there were no noticeable changes to the viability of WT cells in 0.2μM conditions. Likewise, 0.4μM APH treatment conditions elicited the highest overall decrease in viability of 4.1% in WT and 3.7% ΔL1-T-REx from 93.7% and 94.4% respectively in comparison to untreated WT and ΔL1-T-REx cells. Unsurprisingly, the changes in cell viability between WT and ΔL1-T-REx cells were deemed to be non-significant. Overall, these results suggest that loss of ZFP36L1 does not impact cell viability and leads to apoptosis in APH-induced replication stress conditions.

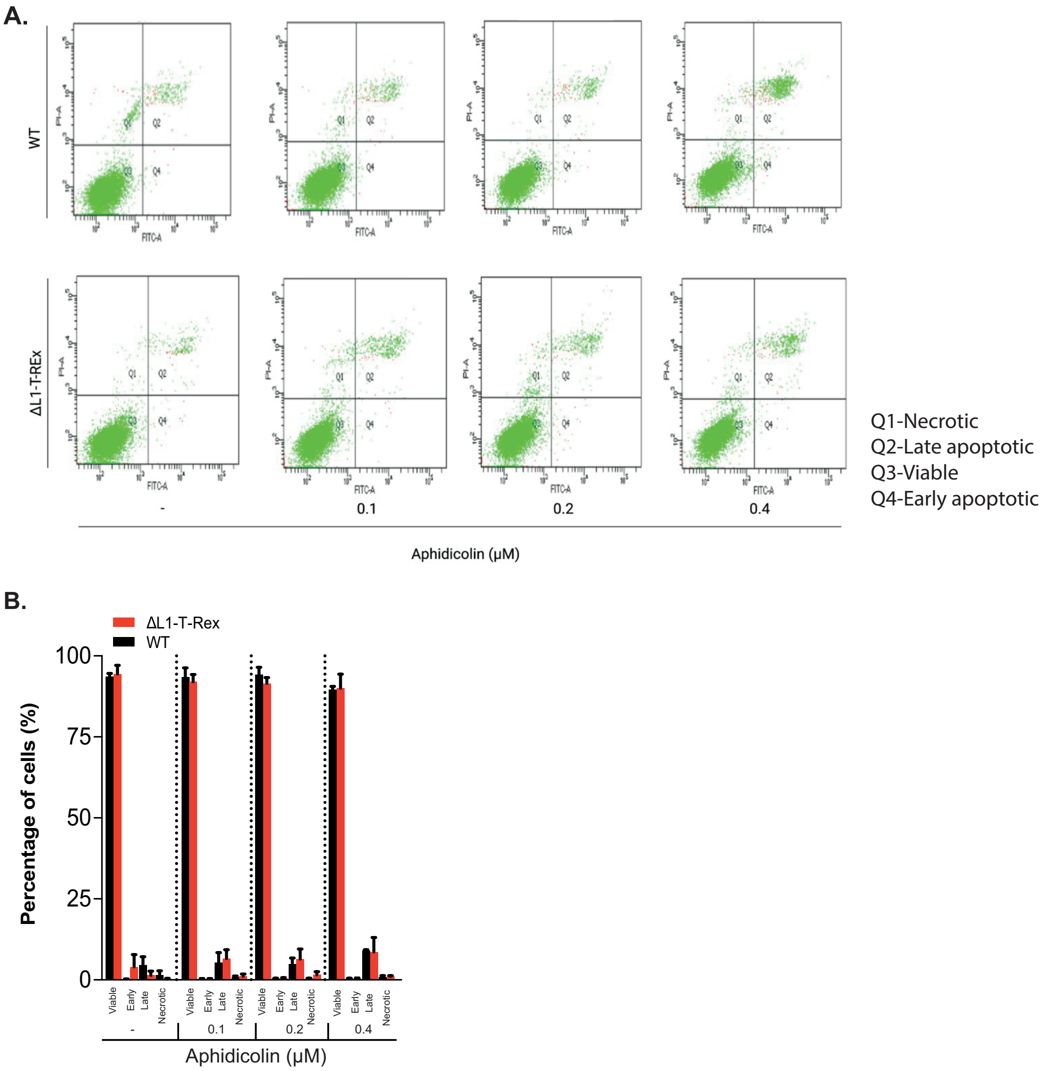

Figure 5.6 Loss of ZFP36L1 does not induce apoptosis in response to low-dose APH.

A. Flow cytometry analysis of WT and ΔL1-T-REx either untreated or treated with low doses of APH (0.1, 0.2 and 0.4µM) for 24 hours and stained with Annexin V and PI. Viable cells indicated negative for both Annexin V and PI (Q3), cells in early stages of apoptosis (Q4) are Annexin V positive and PI negative or late apoptotic (Q2) Annexin V positive and PI positive. Necrotic cells (Q1) are indicated as Annexin V negative and PI positive. **B**. Quantification of the number of cells (%) that appear in each respective quadrant; viable, early/late apoptosis and necrotic either untreated or treated with low doses of APH (0.1, 0.2 and 0.4µM) for 24 hours. Data generated are of three independent replicates analysed in each condition and replicate. Error bars represent

S.E.M. p values were calculated using an unpaired two-tailed t-test.; not significant $p>0.05$ (ns); $p \leq 0.05$(*); $p \leq 0.01$ (**); $p \leq 0.001$ (***), $p \leq 0.0001$(****).

5.7 ZFP36L1 exhibits chromatin binding in human cells

Recent reports have begun to uncover the non-canonical roles of RBPs and AU-RBPs in their ability to maintain genome stability (Dutertre et al., 2014; Alfano et al., 2019). Furthermore, the ability of these AU-RBPs and RBPs to exhibit such roles has been attributed to their association with chromatin which has uncovered novel protein interactions or highlighted non-canonical DNA binding capabilities (Azzalin and Lingner, 2006; Alfano et al., 2019). We, therefore, sought to determine if ZFP36L1 could potentially exhibit similar roles. To this end, we first examined if ZFP36L1 could bind chromatin by extracting chromatin fractions from three cell lines U-2OS, HCT116 and Hela cells followed by western blotting to probe for ZFP36L1 expression (Figure 5.7A and B). To our surprise, for the first time, we detected ZFP36L1 expression in chromatin-containing fractions (C) from U-2OS, HCT116 and Hela, therefore, suggesting that ZFP36L1 is bound to chromatin in human cells (Figure 5.7A). ZFP36L1 expression levels in the chromatin fractions seemed to be cell type-specific, U-2OS cells showed the highest levels of ZFP36L1 expression in comparison to HCT116 cells with the least ZFP36L1 expression (Figure 5.7 4A). We also detected ZFP36L1 expression in cytoplasmic containing soluble (S) fractions in all cell types (Figure 5.7 4A). These findings suggest novel chromatin interactions for ZFP36L1 while studies have previously demonstrated ZFP36L1 to be mainly localised within the cytoplasm (Matsuura et al., 2020).

To further understand the association of ZFP36L1 in chromatin fractions we performed chromatin purification in the presence of RNase A to remove potential interference from RNA substrates. This was carried out in U-2OS cells either untreated (-) or treated with low doses of APH (0.1, 0.2 and 0.4μM). Indeed, we found that in RNase A treated chromatin (C) fractions ZFP36L1 maintains its ability to bind cellular chromatin (Figure 5.7C). Furthermore, treatments with APH did not inhibit ZFP36L1's expression in chromatin fractions. Instead, we observed that APH concentrations of 0.2μM potentially increased the expression of ZFP36L1 in chromatin fractions (Figure 5.7C). Moreover, we observed decreased ZFP36L1 in soluble (S) fractions in the presence of all low-dose APH concentrations relative to untreated conditions. Thus, these results suggest that the replication stress could potentially influence ZFP36L1's translocation from the cytoplasm to the nucleus promoting the nuclear role of this protein in association with chromatin.

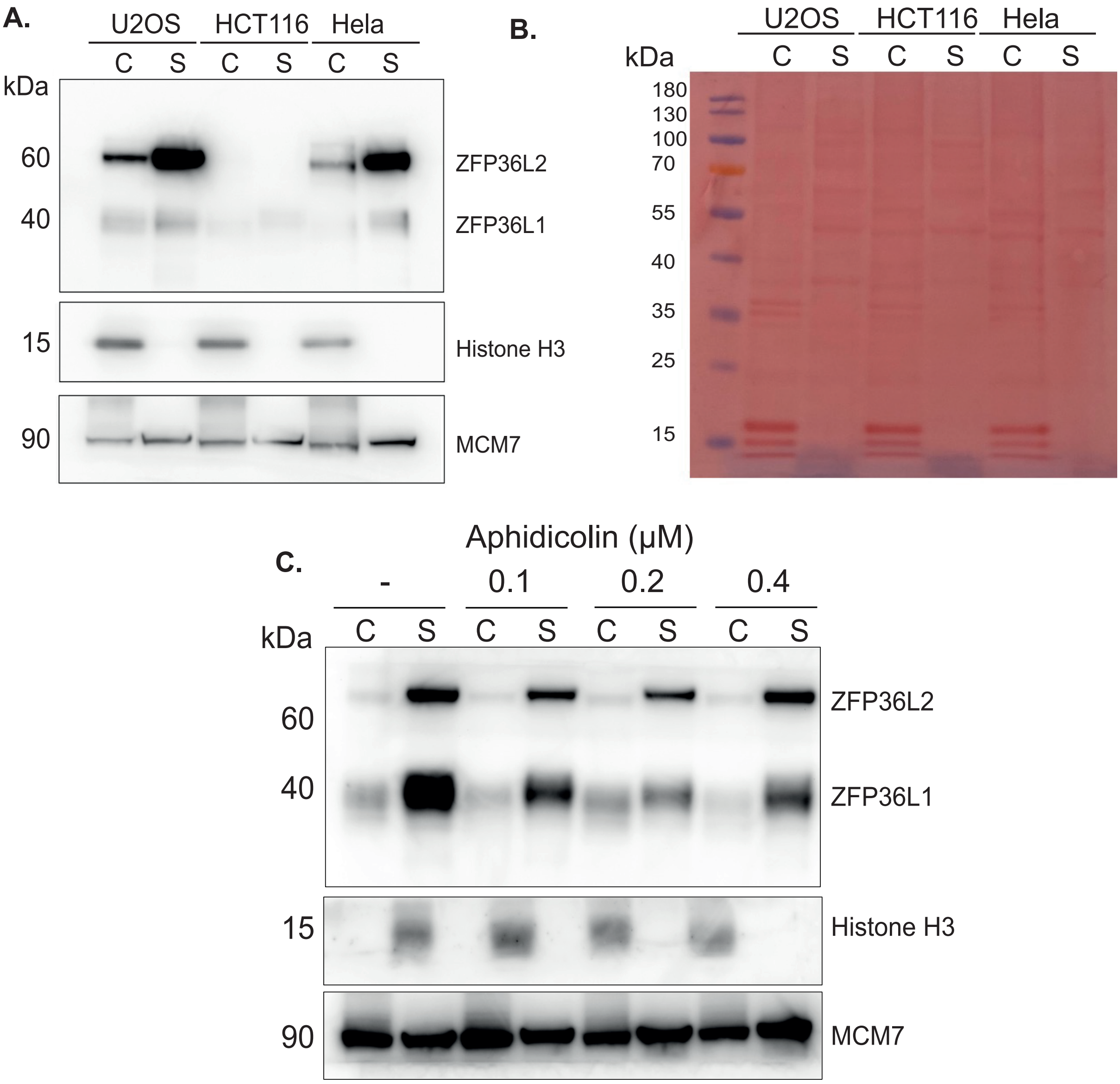
A.
U2OS
HCT116
Hela
C
S
C
S
C
S
kDa
60
40
15
90
ZFP36L2
ZFP36L1
Histone H3
MCM7
B.
U2OS
HCT116
Hela
kDa
C
S
C
S
C
S
180
130
100
70
55
40
35
25
15
C.
Aphidicolin (μM)
-
0.1
0.2
0.4
kDa
C
S
C
S
C
S
C
S
60
40
15
90
ZFP36L2
ZFP36L1
Histone H3
MCM7

Figure 5.7 ZFP36L1 expression in chromatin fractions is influenced during episodes of mild replication stress.

A. Chromatin (C) and soluble (S) extracts were isolated from U-2OS, HCT116 and Hela cells followed by western blot analysis to probe for ZFP36L1 utilising a polyclonal ZFP36L1/ZFP36L2 antibody, Histone H3 and MCM7 were utilised as chromatin fraction and loading controls respectively. **B**. Ponceau S stain of Chromatin (C) and soluble (S) extracts from U-2OS, HCT116 and Hela cells demonstrating histone enrichment in chromatin fractions at approximately 15kDa. (**C**) Chromatin (C) and soluble (S) extracts were isolated from U-2OS cells untreated (-) or treated with 0.1, 0.2 and 0.4μM for 24 hours followed by western blot analysis to probe for ZFP36L1 utilising a polyclonal ZFP36L1/ZFP36L2 antibody, purification was performed following a 30minute incubation with 0.3 mg/ml RNase A on ice, Histone H3 and MCM7 were utilised as chromatin fraction and loading controls respectively.

5.8 Discussion

In this chapter, we provide evidence to suggest that ZFP36L1 limits replication stress-induced DNA DSBs that could be associated with chromosomal segregation defects and genomic instability. Emerging studies, associate the loss of AU-RBPs with increased susceptibility to DNA damage. However, little is known with respect to AU-RBPs suppressing DNA damage during DNA replication and during events that perturb replication fork progression. Here, we demonstrate loss of ZFP36L1 increases the presence of RPA (Figure 5.1) and γH2AX (Figure 5.2) foci in S/G2 in the absence and presence of low-dose APH. These results suggest that loss of ZFP36L1 potentially increases the risk of DNA damage when replication fork progression is perturbed or that loss of ZFP36L1 increases the presence of unresolved structures leading to chronic fork stalling and subsequent collapse. Importantly, RPA is a multi-faceted protein exhibiting functions in DNA replication, repair and DDR signalling through binding to ssDNA (Maréchal and Zou, 2014). Therefore, RPA accumulation alone can signify intrinsic dysfunctions to multiple aspects that constitute the maintenance of genome integrity. However, during S/G2 RPA is known to shield ssDNA as well as protect replication and repair intermediates during replication stress conditions (Lezaja et al., 2021). As our results indicated increased RPA in S/G2 cells in ZFP36L1 ablated cells, we further tested if this accumulation could lead to increased susceptibility to DNA damage as a result of chronic replication fork arrest by assessing for γH2AX focus formation as a marker of replication stress-associated DNA damage in S/G2 cells (Gagou et al., 2010). Indeed, we found that loss of ZFP36L1 increased γH2AX foci formation in S/G2 cells during low-dose APH conditions (Figure 5.2). Importantly, these results are supported by reports of increased γH2AX signalling in mouse thymocytes depleted of *Zfp36l1* and *Zfp36l2* (Vogel et al., 2016). However, the increase in γH2AX signalling in relation to replication stress in S/G2 cells remained unknown. Unresolved lesions or DNA structures can lead to replication fork collapse forming DSBs. We speculated that loss of ZFP36L1 could increase susceptibility to DSB formation. Importantly, γH2AX foci form around sites of DSBs signalling for the recruitment of DNA repair factors such as 53BP1. Specifically, nuclear colocalisation of 53BP1 and γH2AX foci are indicators of DSBs (Schultz et al., 2000). For the first time, we elucidate that the source of the increased occurrence of DNA damage may be attributed to DSB formation as presented with an increased colocalisation of 53BP1 and γH2AX foci in ZFP36L1 KO cells (Figure 5.4). Strikingly, supporting evidence in ZFP36 deficient cells treated with hydroxyurea or cisplatin has been reported to result in increased 53BP1 and γH2AX colocalisation, highlighting an increased susceptibility to DSB formation in ZFP36 deficient cells (Lee et al.,2020). (Lee et al.,2020). Thus, overall, these results show that ZFP36L1 is required to limit the formation of DSBs in response to replication stress.

Replication stress occurs primarily during the S-phase. When replication fork progression is perturbed due to the presence of lesions this results in an extended S-phase (Mocanu et al., 2022). Moreover, the progression of the S-phase has been correlated to the severity of DNA damage (Chao et al., 2017). We examined the extent of ZFP36L1 loss on cells in different stages of the cell cycle in response to low dose concentrations of APH. Unsurprisingly, we observed a mild increase in cell population within the S-phase in response to mild replication stress. Specifically, we observed an increase in S-phase cells treated with low dose APH concentrations of 0.2μM and 0.4μM (Figure 5.5A and B). The effect on cells in S-phase was exacerbated in the absence of ZFP36L1, possibly due to the increased replication stress-associated DNA damage reported thus far. Moreover, we determined that loss of ZFP36L1 results in decreased G2 cell population in response to 0.2μM and 0.4μM APH although we determined this was statistically non-significant (Figure 5.5A and B). Thus, these results suggest that loss of ZFP36L1 induces potential S-phase delay without significantly impacting progression into the G2 phase. Intriguingly, relevant studies demonstrate ablation of ZFP36L1 and ZFP36L2 in pro-B cells in mice increases the proportion of pro-B cells in the S-phase (Galloway et al., 2016). Furthermore, knockdown of ZFP36 family member ZFP36L2 was also shown to impact cells in S-phase in response to cisplatin-induced replication stress (Noguchi et al., 2018). Thus, overall, these results suggest that ZFP36L1 is an important regulator of cells in the S-phase under replication stress conditions. Our findings are further supported through observations of low levels of CHK1 phosphorylation in response to low doses of APH (Figure 5.5C). CHK1 is phosphorylated in response to replication stress through intra-S checkpoint signalling pathways, mediating DNA repair by slowing replication fork progression (Liu et al., 2006). Recently reports utilising U-2OS cells have suggested that low doses of APH increase the S-phase cell population and induce low levels of CHK1 phosphorylation on Serine 345 but do not induce cell cycle arrest (Courtot et al., 2021). Therefore, it could be that the lesions caused by loss of ZFP36L1 slow down replication fork progression but continue through the cell cycle. Furthermore, low doses of APH are known to compromise replication fork progression but do not block G2 progression leading to chromosome aberrations and segregation defects (Mocanu et al., 2022). However, if the increased population of S-phase cells is due to the slowing of replication fork progression is unclear due to the use of PI staining which is unable to distinguish cells in G1 or G2 from cells in early or late S-phase and G2 from M (Cecchini, Amiri and Dick, 2012). We could better understand S-phase progression by measuring DNA synthesis utilising proliferative markers such as

Bromodeoxyuridine (BrdU) that is able to distinguish cells in G1 from early S-phase and late S phase from G2/M (Cecchini, Amiri and Dick, 2012). This would demonstrate if loss of ZFP36L1 under replication stress conditions induces a slower rate of DNA synthesis and not cell cycle arrest. Finally, we reveal that loss of ZFP36L1 does not significantly affect cell viability or induce apoptosis in response to mild replication stress (Figure 5.6 A and B). This demonstrated that APH- induced replication stress in ZFP36L1 abolished cells does not lead to cell death. Moreover, CHK1 has been reported to inhibit apoptosis through ATM/ATR-caspase2 and RPA-caspase3 pathways (Myers et al., 2009; Sidi et al., 2008). Studies demonstrating the loss of ZFP36L1 impact alone on apoptosis are lacking. However, relevant reports from early developing mouse thymocytes deficient in ZFP36L1 and ZFP36L2 demonstrated no changes in apoptosis (Vogel et al., 2016).

RBPs and AU-RBPs have been identified to exhibit non-canonical interactions through DNA binding or forming protein complexes to maintain genome integrity (Polo et al., 2012; Anantha et al., 2013; Alfano et al., 2019). Here we have also identified that ZFP36L1 binds chromatin in U-2OS, HCT116 and Hela cells a prerogative for proteins involved in the DDR (Figure 5.7A) (Polo and Jackson, 2011). Interestingly, the removal of interfering free RNA demonstrated that ZFP36L1 maintained expression in chromatin fractions (Figure 5.7C). Furthermore, low dose concentrations of APH did not inhibit ZFP36L1 expression in chromatin fractions but potentially reduced expression in cytoplasmic containing soluble fractions suggesting ZFP36L1 could exhibit nucleo-cytoplasmic shuttling in response to replication stress (Figure 5.7C). This is further supported by a recent report indicating cell cycle-dependent nuclear accumulation of ZFP36L1 (Matsuura et al., 2020). Our results identifying ZFP36L1 to bind chromatin may present a novel role for ZFP36L1 in the nucleus increasing the potential for forming interactions separate from interactions reported in the cytoplasm. The significance of ZFP36L1's ability to bind cellular chromatin is currently unknown, however, this does pose an avenue to explore potential ZFP36L1 interactions with DNA or DNA structures to maintain genome integrity in response to replication stress. Supporting evidence suggests that proteins containing zinc finger domains can bind DNA (Li et al., 2022), although ZFP36L1's DNA binding ability requires further investigation.

The mechanisms underlying the increased susceptibility to mild replication stress in the absence of ZFP36L1 remain to be explored. It is a possibility that deficiencies in DNA damage response pathways predispose cells to DNA damage in the event of replication stress. Recently, ZFP36 has been described to regulate DNA damage repair through mRNA regulatory pathways (Lee, et al 2020). Knockdown of ZFP36 resulted in abrogated CHK1 activation leading to genomic instability in the presence of HU or Cisplatin (Lee, et al 2020). However, it is unlikely ZFP36L1 functions similarly as we have been able to show clear CHK1 phosphorylation in response to low-dose APH. Several AU-RBPs have been associated with the RNA:DNA (R-loops) hybrid-interactome (Cristini et al., 2018). Moreover, depletion of AU-RBP AUF1 sensitised cells to DSB formation leading to the formation of R-loops that inhibit DNA repair mechanisms in human Hela cells (Alfano et al., 2019). Interestingly, AUF1 was reported to be expressed in chromatin fractions which were dependent on DNA binding to ensure efficient R-loop removal (Alfano et al., 2019). Therefore, loss of ZFP36L1 could also result in the formation of these deleterious R-loops that lead to replication stress and genomic instability. It has become apparent that transcriptionally active regions of the genome are susceptible to the formation of R-loops that impede replication fork progression (Helmrich, Ballarino and Tora, 2011; Groh et al., 2014). Importantly, these regions coincide with large genes in CFS, that inevitably cause transcription and replication collisions, inducing R-loop formation which results in DSB formation (Helmrich, Ballarino and Tora, 2011). In later chapters, we demonstrate that the defective replication stress-associated phenotype in the absence of ZFP36L1 could be attributed to the increased formation of RNA: DNA hybrids (Chapter 7).

6. Genetic complementation reverses phenotypic abnormalities associated with loss of ZFP36L1 in T-REx U-2OS cells

6.1 Introduction

The CRISPR-Cas9 system has been utilised to successfully edit eukaryotic genomes leading to a revolution in molecular medicine against cancer and genetic disease (Zhu et al., 2020; Hsu et al., 2014). Significantly, CRISPR-Cas9 technology has contributed to the understanding of the functional organisation of the genome and has helped establish causal links between genetic variations and biological phenotype (Smith et al., 2015). However, there remain concerns due to unwanted off-target mutations that occur at frequencies much greater than the intended target mutations, which could lead to genomic instability. Therefore, the potential of off-target mutations is still one of the significant concerns when utilising CRISPR-Cas9 technology for biomedical and clinical applications (Cho et al., 2013; Fu et al., 2013; Hsu et al., 2013). Genetic complementation/rescue experiments are utilised to reintroduce a functional copy of a mutated gene typically cloned within mammalian expression plasmids to ensure the specificity of an observed phenotype. Therefore, successful complementation studies rule out potential off-target mutations in other genes rather than the intended target. However, complementation methods can also lead to non-specific effects when a gene is located within an autonomous, multicopy plasmid resulting in overexpression of the gene product (Van Alstyne et al., 2021). Therefore, it becomes essential to regulate gene expression in complementation assays for genes that can cause undesirable effects when overexpressed (Pucci et al., 2000). Furthermore, overexpression of the ZFP36 family has been reported to induce cell death in different cellular models such as osteosarcoma cell lines U-2OS, SAOS2 and B-lymphocyte cell line Ramos (Johnson, Geha and Blackwell, 2000; Baou et al., 2008). ZFP36L1 exhibits post-transcriptional control over multiple cell cycle regulators such as cyclin D, cyclin E and cyclin A, and p21 and overexpression of ZFP36L1 has been reported to result in cell cycle arrest decreasing cell proliferation and viability (Suk et al., 2018).

Many regulatory mechanisms have been adapted and developed to enable quantitative and temporal control over the expression of gene products in mammalian cells utilising exogenous effector molecules (Reviewed in Fussenegger, 2001). Regulation of gene expression is based on the binding of transactivators to their cognate promoter. This interaction is modulated by exogenous effector molecules such as antibiotics or hormones that induce the expression of a gene of interest (GOI) when the transactivation domain encounters a minimal promotor. Operator systems that utilise the antibiotic tetracycline (Tet) as an exogenous effector are the most common for gene regulation in mammalian cells (Matsunaga and Yamashita, 2014). In this system, treatment with tetracycline enables the regulation of exogenous gene expression within a genetically targeted cell population (Reviewed in Kallunki et al., 2019). The tetracycline repressor (TetR) protein and tetracycline operon (tetO) components of Tn10-encoded tet operon from *E.coli* are essential elements that constitute tetracycline-regulated systems (Gossen et al 1995). Yao., et al. (1998) demonstrated that potent gene regulation could be achieved with TetR alone without fusions with a viral transactivation domain or hybrid regulatory molecules producing an inducible expression system that is now commercially known as T-REx. This enables powerful gene regulation modulated by TetR interactions with tetO located within a promoter region of a gene expression plasmid. In this system, the addition of tetracycline represses TetR interactions with tetO enabling controlled expression of a GOI (Appendix C: Figure 1)

In this report, we utilised U-2OS cells stably expressing TetR (T-REx U-2OS) under the control of the human CMV promotor to generate a tetracycline-inducible expression system enabling the genetic rescue of *ZFP36L1* in ZFP36L1 KO cells. Firstly, we report here for the first time, a workflow for generating a stable inducible ZFP36L1 expression system. Most importantly, we demonstrate genetic rescue of a WT phenotype through the inducible expression of ZFP36L1 in ZFP36L1 KO cells. Specifically, we show inducible ZFP36L1 expression represses both micronuclei and 53BP1 NB in the presence and absence of APH-induced replication stress. Further supporting a role for ZFP36L1 in preserving genome integrity in response to replication stress.

6.2 Generation of stable inducible expression system of ZFP36L1

An essential component of the T-REx system is an inducible expression plasmid containing a gene of interest (GOI) controlled by a strong cytomegalovirus immediate-early (CMV) promoter and a Tet operator. For this purpose, we utilised the plasmid PCDNA4/TO-FLAG-Strep II cloned with full-length *ZFP36L1* (PCDNA4/TO-FLAG-Strep II-ZFP36L1) for genetic complementation/rescue in ΔL1-T-REx cells (Appendix C: Figure 3). We first tested for tetracycline-inducible expression of exogenous ZFP36L1 in ΔL1-T-REx cells transiently transfected with PCDNA4-TO-ZFP36L1 treated with tetracycline (0.4, 0.6 and 0.8µg) for 24hours. Next, total protein was extracted to assess for ZFP36L1 expression, simultaneously, total protein extracts were also harvested from T-REx U-2OS WT and ΔL1-T-REx cells as positive and negative controls for ZFP36L1 expression respectively. Successful expression of exogenous ZFP36L1 was verified in all tetracycline treatment conditions by western blotting (Figure 6.2A). Furthermore, tetracycline-induced ZFP36L1 in PCDNA4-TO-ZFP36L1 transfected ΔL1-T-REx cells exhibited a similar molecular weight (MW) of approximately 40kDa to that of endogenous ZFP36L1 from WT cells (Figure 6.2A). Importantly, no detectable ZFP36L1 expression was observed in the absence of tetracycline (Figure 6.2A).

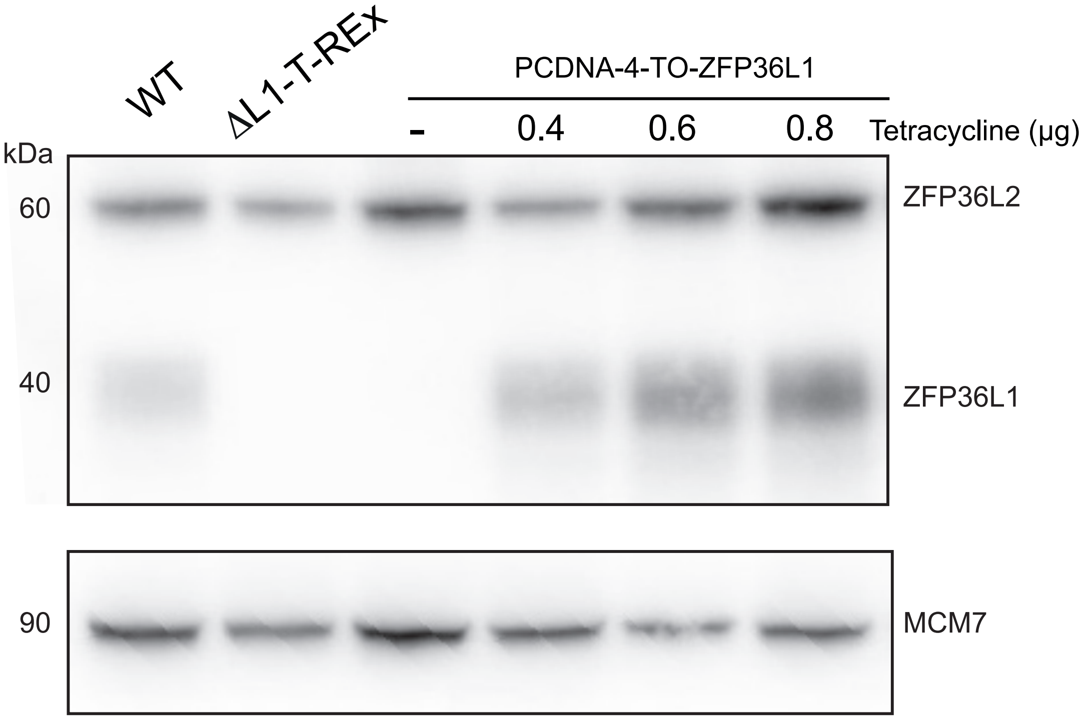

Figure 6.2A Inducible expression of exogenous ZFP36L1 in ZFP36L1 KO cells.

Western blot analysis of ZFP36L1 (40 kDa) and ZFP36L2 (60 KDa) from WT, ΔL1-T-REx and PCDNA4-TO-ZFP36L1 transiently transfected ΔL1-T-REx cells. Results indicate the inducible expression of ZFP36L1 (40kDa) in the presence of 0.4-0.8 μg tetracycline. PCDNA4-TO-ZFP36L1 transfected ΔL1-T-REx cells in the absence of tetracycline (-) have no detectable ZFP36L1 band comparable to ΔL1-T-REx cells. MCM7 (90 KDa) was used as a loading control.

Transient expression systems are limited by transfection efficiencies that do not guarantee 100% incorporation of PCDNA4-TO-ZFP36L1 resulting in a heterogenous population of cells. Transiently transfected cells also lose their ability to maintain exogenous DNA in comparison to stable expression systems, that enable DNA integration within the host cells' genome. Stable integration of PCDNA4-TO-ZFP36L1 in ΔL1-T-REx cells would mean the expansion of a single cell that maintains the ability to induce ZFP36L1 expression even after cell division. Therefore, generating a homogenous population of cells that can be induced to express exogenous ZFP36L1 in ΔL1-T-REx cells eliminates the need for continuous transfection steps, reducing cellular toxicity. Therefore, we generated ΔL1-T-REx stably expressing PCDNA4-TO-ZFP36L1 or PCDNA4-TO-empty vector (PCDNA4-TO-EV) as a control for downstream complementation assays (Appendix C: Figure 6) (ΔL1-T-REx stably expressing PCDNA4-TO-ZFP36L1 or PCDNA4-TO-EV will now be indicated as ΔL1-T-REx-TO-ZFP36L1 or ΔL1-T-REx-TO-EV respectively).

Utilising ΔL1-T-REx-TO-ZFP36L1 cells we questioned if ZFP36L1 expression could be sustained for more than 24 hours following tetracycline induction. To this end, ΔL1-T-REx-TO-ZFP36L1 cells were either treated with (+Tet) or without (-Tet) 0.4µg/mL tetracycline to induce exogenous ZFP36L1 expression for 48hours. Total cell extracts were harvested from tetracycline treated and untreated ΔL1-T-REx-TO-ZFP36L1 cells at identical time points. Western blot results demonstrated expression of exogenous ZFP36L1 at 24 hours and 48 hours in ΔL1-T-REx-TO-ZFP36L1 cells in the presence of 0.4 µg/mL tetracycline (Figure 6.2B). Like our previous observation, tetracycline-induced ZFP36L1 exhibited the expected MW of 40kDa, comparable to that of WT ZFP36L1. Importantly, no detectable expression of ZFP36L1 was observed in tetracycline untreated ΔL1-T-REx-TO-ZFP36L1 cells, indicating repression of exogenous ZFP36L1 (Figure 6.2B). Overall, our results demonstrate a tightly regulated inducible system expression system that could be utilised to further investigate the role of ZFP36L1 in suppressing replication stress-associated genomic instability.

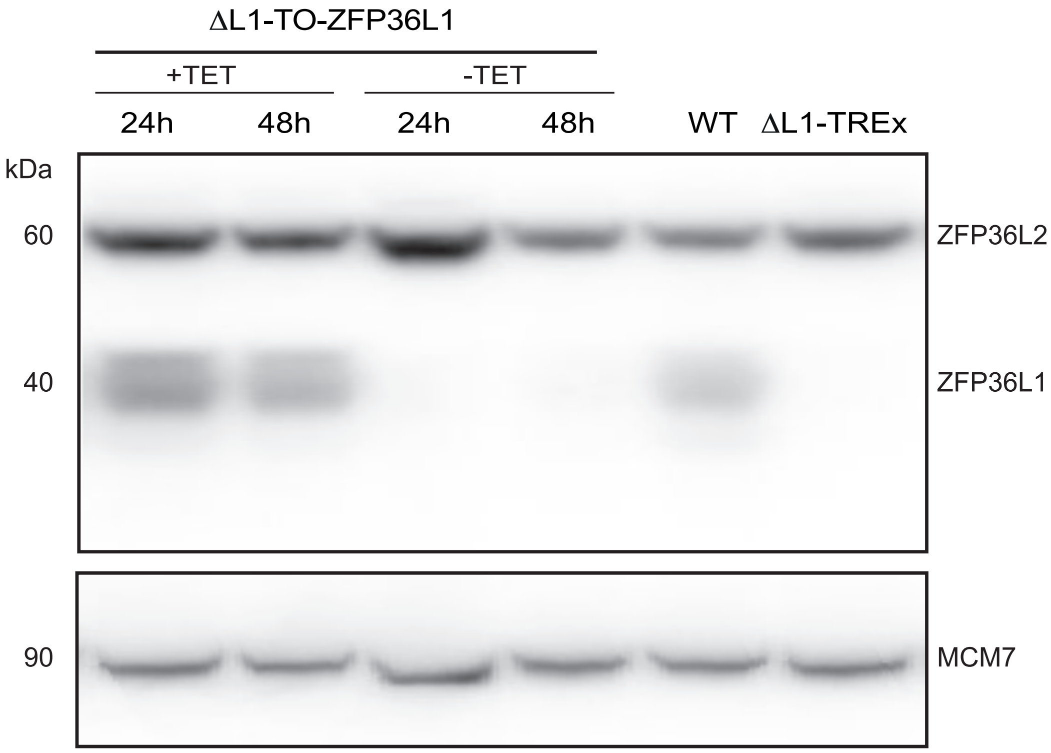
ΔL1-TO-ZFP36L1
+TET
-TET
24h
48h
24h
48h
WT
ΔL1-TREx
kDa
60
40
90
ZFP36L2
ZFP36L1
MCM7

Figure 6.2B Stable inducible expression of ZFP36L1 in ZFP36L1 KO cells.

Western blot analysis of ZFP36L1 (40 kDa) and ZFP36L2 (60 kDa) from WT, ΔL1-T-REx and ΔL1-T-REx stably expressing inducible ZFP36L1 (ΔL1-TO-ZFP36L1). Results indicated tetracycline-induced (+Tet) expression of ZFP36L1 in ΔL1-TO-ZFP36L1 for 48 hours with no detectable ZFP36L1 expression in the absence of tetracycline (-Tet). MCM7 (90Kda) was used as a loading control.

6.3 Tetracycline-induced expression of ZFP36L1 limits micronuclei formation in ZFP36L1 KO cells

Our results thus far demonstrate the generation of a stable tetracycline-inducible ZFP36L1 system in ΔL1-T-REx cells (ΔL1-T-REx-TO-ZFP36L1). We set out to demonstrate the specificity of the ZFP36L1 KO system and reinforce the role of ZFP36L1 in the maintenance of genome integrity in response to replication stress. We examined if the inducible expression of exogenous ZFP36L1 could rescue the abnormal phenotype associated with the loss of ZFP36L1. To this end, we employed the ΔL1-T-REx-TO-ZFP36L1 system to examine if the induced expression of ZFP36L1 could repress the formation of micronuclei. Moreover, if the inducible expression of ZFP36L1 in ZFP36L1 KO cells could suppress the occurrence of micronuclei to a level comparable to WT cells, this would demonstrate the specificity of our CRISPR-Cas9 KO system and provide further evidence for ZFP36L1's role in suppressing replication stress-induced genomic instability.

Firstly, we set out to investigate the occurrence of micronuclei formation in the presence and absence of low-dose APH. We quantified the frequency of micronuclei in ΔL1-T-REx-TO-ZFP36L1 cells when ZFP36L1 expression was repressed (-TET) or induced (+TET) as a measure of ZFP36L1's ability to limit the formation of micronuclei. Furthermore, we compared the prevalence of micronuclei formation with WT and ΔL1-T-REx cells to determine if the induced expression of ZFP36L1 in ΔL1-T-REx-TO-ZFP36L1 demonstrated differences between cells with WT or depleted ZFP36L1. We suspected similarities in the frequency of micronuclei between WT and ΔL1-T-REx-TO-ZFP36L1 induced to expression ZFP36L1 would demonstrate that exogenous ZFP36L1 was indeed functional. Likewise, we utilised ΔL1-T-REx-TO-EV as a control to account for any effects the vector had on micronuclei formation. To account for the potential adverse effects of tetracycline, we also measured micronuclei formation with and without tetracycline in all conditions.

Remarkably, results demonstrated that tetracycline-induced expression of ZFP36L1 in ΔL1-T-REx-TO-ZFP36L1 cells reduced the occurrence of binucleated cells with micronuclei, both in the presence and absence of low dose APH compared -Tet controls (Figure 6.3A and B). In untreated conditions, we found that when ZFP36L1 expression was repressed in ΔL1-T-REx-TO-ZFP36L1 cells 11.8% of binucleated cells exhibiting micronuclei (Figure 6.3B), upon induced expression of ZFP36L1 in ΔL1-T-REx-TO-ZFP36L1, binucleated cells marked by the presence of micronuclei was significantly reduced to 7.6% ($p \leq 0.01$, $p=0.0028$) (Figure 6.3B) corresponding to a 4.2% decrease in the frequency of binucleated cells exhibiting micronuclei upon induced ZFP36L1 expression. Moreover, in untreated conditions the frequency of micronuclei in tetracycline induced ΔL1-T-REx-TO-ZFP36L1 cells was similar to WT cells (7.6 and 7.8% respectively) as opposed to a higher frequency of micronuclei in ΔL1-T-REx and ΔL1-T-REx-TO-EV cells (13.3% and 12.85% respectively) which were comparable to -Tet controls (Figure 6.3B). Importantly, our results also demonstrated that the addition of tetracycline had no significant impact on micronuclei formation as demonstrated through WT and ΔL1-T-REx cells ($p>0.05$, $p= 0.5522$; $p>0.05$, $p= 0.5125$) (Figure 6.3B).

Supporting evidence that inducible expression of exogenous ZFP36L1 in ΔL1-T-REx-TO-ZFP36L1 limits micronuclei formation was also observed in APH treated conditions (Figure 6.3A and B). Specifically, treatment with 0.2μM APH in tetracycline induced ΔL1-T-REx-TO-ZFP36L1 cells significantly reduced the frequency of binucleated cells exhibiting micronuclei by 6.1%, compared to -Tet control ($p \leq 0.05$, p=0.0039) representing 19.1% and 13% of ΔL1-T-REx-TO-ZFP36L1 cells exhibiting micronuclei when ZFP36L1 expression was repressed or induced respectively (Figure 6.3B). Observations in tetracycline induced ΔL1-T-REx-TO-ZFP36L1 cells demonstrated a non-significant 1.5% increase in micronuclei (13%) compared to WT cells (11.5%) (P>0.05, P=0.4603) (Figure 6.3B). Furthermore, micronuclei formation in ZFP36L1 induced ΔL1-T-REx-TO-ZFP36L1 cells was significantly less than ΔL1-T-REx and ΔL1-T-REx-TO-EV cells in 0.2μM APH treatment conditions (18.9%, p ≤ 0.05;18.8%; p ≤ 0.05) (Figure 6.3B). Reproducibly tetracycline had no significant impact in APH treated WT and ΔL1-T-REx cells (p>0.05, p= 0.7225; p>0.05, p= 0.3790). Taken together our results demonstrate a functional inducible genetic complementation system in ZFP36L1 KO cells that can suppress the formation of micronuclei in the presence and absence of APH.

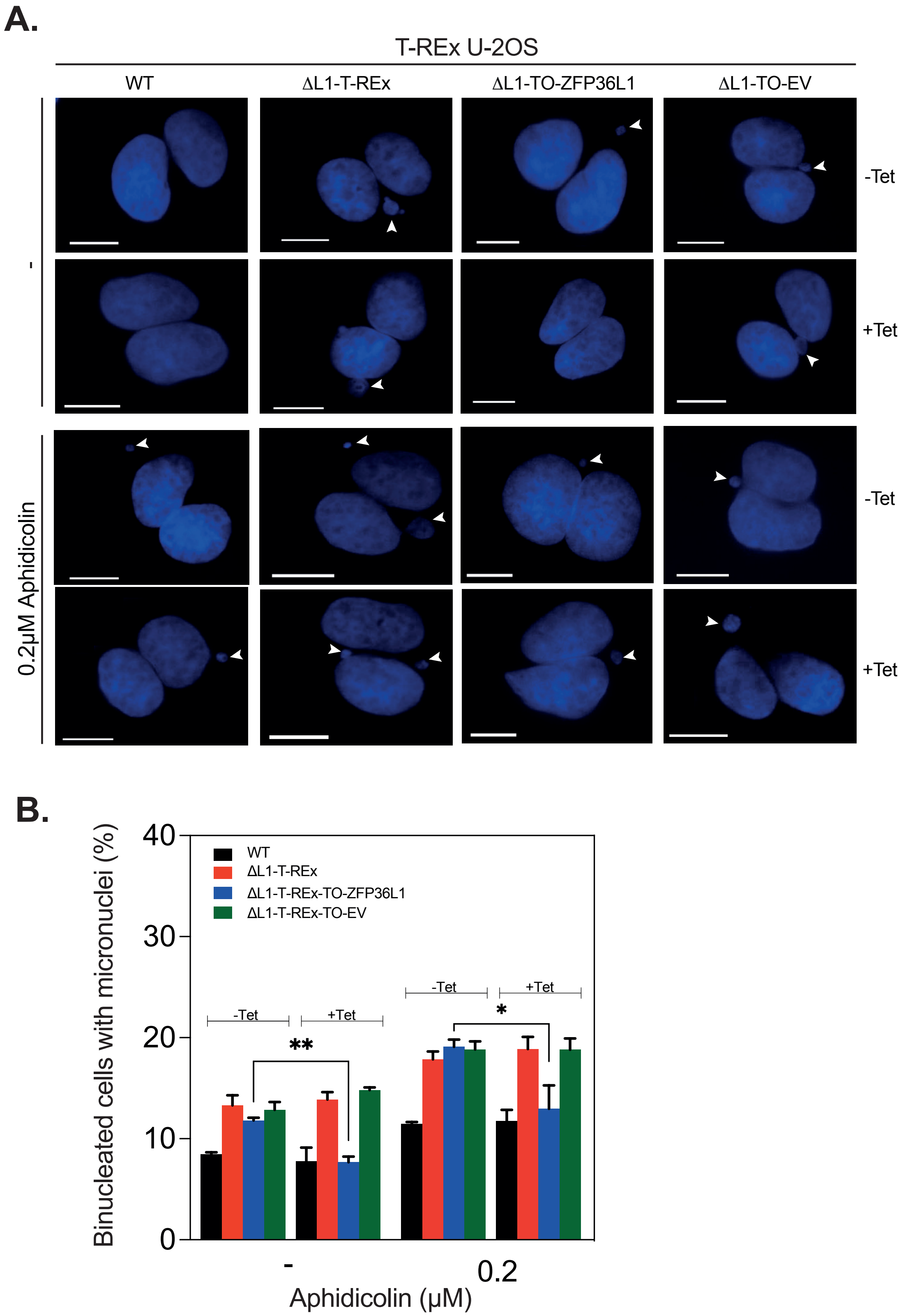

Figure 6.3 Tetracycline-induced expression of ZFP36L1 suppresses micronuclei formation.

A. Representative images of binucleated cells with micronuclei scored in wild-type T-REx U-2OS (WT), ZFP36L1 KO (ΔL1-T-REx), tetracycline-inducible ZFP36L1 ΔL1-T-

REx (ΔL1-T-REx-TO-ZFP36L1) and ΔL1-T-REx containing tetracycline-inducible empty vector (ΔL1-T-REx-TO-EV) cells. **B.** Quantification of the percentage of binucleated cells with micronuclei in WT, ΔL1-T-REx, ΔL1-T-REx-TO-ZFP36L1 and ΔL1-T-REx-TO-EV cells untreated and treated with 0.2μM APH in the absence (-Tet) and presence (+Tet) of tetracycline. Data generated are of three independent replicates from a total of 300 binucleated cells analysed in each condition in each replicate. Error bars represent S.E.M. p values were calculated using an unpaired two-tailed t-test.; not significant p>0.05 (ns); p ≤ 0.05(*); p ≤0.01 (**); p ≤0.001 (***), p≤0.0001(****).

6.4 Tetracycline-induced expression of ZFP36L1 suppresses 53BP1 NB formation in ZFP36L1 KO cells

To further validate the ZFP36L1 inducible expression system, we set out to assess for 53BP1 NBs in G1 cells. We found that expression of ZFP36L1 in ΔL1-T-REx-TO-ZFP36L1 significantly reduced the prevalence of 53BP1 NBs in G1 cells in both untreated and APH-treated conditions (Figure 6.4A and B). Specifically, in untreated conditions, we observed that inducible expression of ZFP36L1 in ΔL1-T-REx-TO-ZFP36L1 cells significantly reduced the frequency of G1 cells exhibiting >3 53BP1 NBs by more than half relative to when ZFP36L1 expression was repressed (Figure 6.4A and B). This decrease corresponded to 12.6% in ZFP36L1 repressed ΔL1-T-REx-TO-ZFP36L1 cells and 5% following induced expression of ZFP36L1 (p ≤ 0.05; p=0.0332). Importantly, the frequency of G1 cells exhibiting >3 53BP1 NBs following expression of ZFP36L1 was comparable to WT and less than ΔL1-T-REx cells (Figure 6.4A and B). Inversely, we found that ΔL1-T-REx-TO-ZFP36L1 cells expressing ZFP36L1 exhibited significantly fewer cells with >3 G1 53BP1 NBs in comparison to ΔL1-T-REx cells (>10%; p≤0.05, p=0.0387). Similarly, tetracycline-induced expression of ZFP36L1 in ΔL1-T-REx-TO-ZFP36L1 cells treated with 0.2μM APH exhibited significantly fewer cells with >3 G1 53BP1 NBs relative to when ZFP36L1 expression was repressed (p≤0.05, p=0.0308). This corresponded to a 2-fold decrease in cells exhibiting >3 G1 53BP1 NBs from 25% to 12% in ΔL1-T-REx-TO-ZFP36L1 cells upon tetracycline-induced expression of ZFP36L1. Importantly, the frequency of ΔL1-T-REx-TO-ZFP36L1 cells with >3 G1 53BP1 NBs following expression of ZFP36L1 was significantly less than ΔL1-T-REx cells in response to mild replication stress (>18%; $p \leq 0.05$, p=0.0145). In contrast, we did not observe a significant difference between ΔL1-T-REx-TO-ZFP36L1 cells expressing ZFP36L1 and WT cells (>1%; $p > 0.05$, p=0.7786), demonstrating that inducible expression of ZFP36L1 in ΔL1-T-REx cells reverses the formation of 53BP1 NBs to frequencies similar to WT cells. Overall, our results have demonstrated that inducible expression of exogenous ZFP36L1 in ZFP36L1 KO T-REx U-2OS cells reduces the frequency of both micronuclei and 53BP1 NBs in G1 cells. Furthermore, these results have indicated rescue of a defective phenotype associated with loss of ZFP36L1 comparable to WT cells supporting our findings of ZFP36L1's role in limiting replication stress-induced genomic instability.

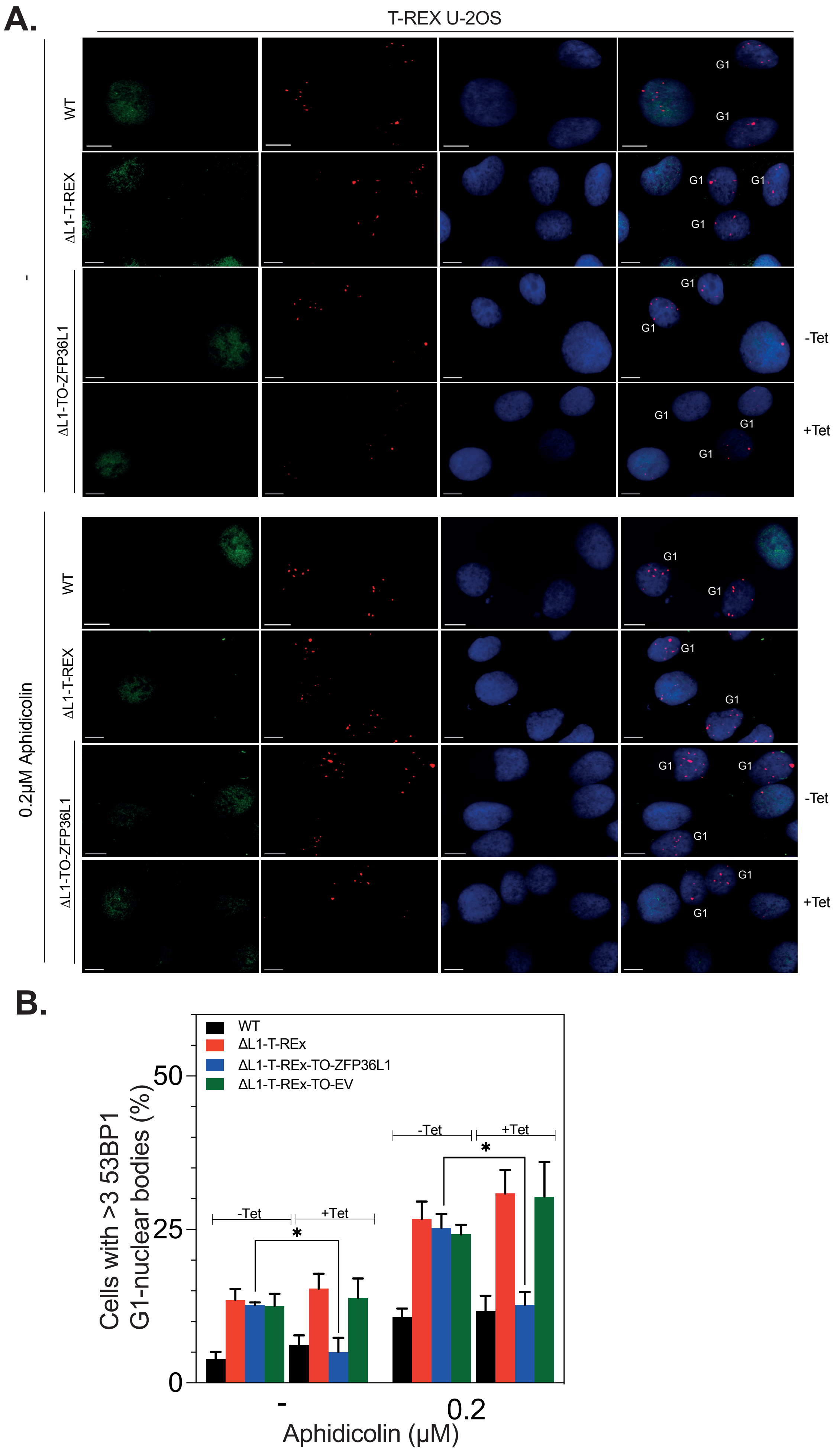
A.
T-REX U-2OS
-
WT
ΔL1-T-REX
ΔL1-TO-ZFP36L1
G1
-Tet
+Tet
0.2µM Aphidicolin
B.
WT
ΔL1-T-REx
ΔL1-T-REx-TO-ZFP36L1
ΔL1-T-REx-TO-EV
Cells with >3 53BP1 G1-nuclear bodies (%)
0
25
50
-Tet
+Tet
*
-
0.2
Aphidicolin (µM)

Figure 6.4 Tetracycline-induced expression of ZFP36L1 suppresses 53BP1 NB formation.
A. Images representing Cyclin A (green), 53BP1 (red), DAPI and Merge with indicated 53BP1 NBs scored in G1 wild-type T-REx U-2OS (WT), ZFP36L1 KO (ΔL1-T-REx) and tetracycline-inducible ZFP36L1 ΔL1-T-REx cells (ΔL1-T-REx-TO-ZFP36L1). **B.** Quantification of the percentage of cells with > 53BP1 G1 NBs in WT, ΔL1-T-REx, ΔL1-T-REx-TO-ZFP36L1 and ΔL1-T-REx-TO-EV cells untreated and treated with 0.2μM APH in the absence (-Tet) and presence (+Tet) of tetracycline. Data generated are of three independent replicates from a total of 200 G1 cells analysed in each condition and replicate. Error bars represent S.E.M. p values were calculated using an unpaired two-tailed t-test.; not significant p>0.05 (ns); p ≤ 0.05(*); p ≤0.01 (**); p ≤0.001 (***), p≤0.0001(****).

6.5 Discussion

Our study utilises CRISPR-Cas9 technology to disrupt *ZFP36L1* gene expression in T-REx U-2OS cells to study its role in limiting replication stress-associated genomic instability. We could not be completely certain that the reported changes in phenotype were completely due to the loss of ZFP36L1, due to the caveats of CRISPR-Cas9 technology such as unintended disruption of non-targeted genes (Alkan et al., 2018). To address this issue, we employed a genetic complementation strategy to develop a system for re-expressing ZFP36L1 in CRISPR-Cas9 mediated ZFP36L1 KO cells Specifically, in this study we demonstrate an optimised approach to enable tetracycline-regulated expression of exogenous ZFP36L1 in ZFP36L1 KO U-2OS-T-REx cells, enabling the reversal of major biomarkers of replication stress associated genomic instability, micronuclei and 53BP1 NBs. Firstly, we verified that treatments with various tetracycline concentrations (0.4, 0.6 and 0.8μg) in ΔL1-T-REx transiently expressing PCDNA4-TO-ZFP36L1 plasmid could induce the expression of exogenous ZFP36L1 (Figure 6.2A). Furthermore, observations from western blots demonstrated no detectable exogenous ZFP36L1 expression in absence of tetracycline indicating exogenous ZFP36L1 expression could be kept repressed (Figure 6.2A). Importantly, the lowest concentration (0.4μg) of tetracycline utilised was sufficient to induce ZFP36L1 expression comparable to WT cells, thus limiting potential non-specific effects of ZFP36L1 overexpression. Next, we generated ΔL1-T-REx cells stably expressing stable PCDNA4-TO-ZFP36L1 (Figure 6.2B) to ensure a homogenous population of cells that could be induced to express exogenous ZFP36L1. Moreover, we demonstrated that inducible expression of ZFP36L1 could be detected after 48hours with 0.4 μg tetracycline, although ZFP36L1 expression was slightly reduced (Figure 6.2B). The concentration of tetracycline utilised was an important consideration in this study as reports have suggested that some concentrations of tetracycline >0.5 μg can be toxic and genotoxic to cells, increasing micronuclei frequency in human blood lymphocytes (Cullot et al., 2019).

Most importantly, we demonstrated that inducible expression of ZFP36L1 in ΔL1-T-REx cells could repress both micronuclei and 53BP1 NB formation in untreated and APH treated conditions indicating a functional inducible ZFP36L1 expression system (Figure 6.3 and 6.4). Furthermore, our experiments exemplified that when ZFP36L1 was repressed due to the absence of tetracycline no significant difference in both the frequency of micronuclei or 53BP1 NBs in G1 cells was observed in comparison to ΔL1-T-REx cells (Figure 6.3 and 6.4). Importantly, we show that tetracycline addition had no significant impact on both micronuclei or 53BP1 NB formation (Figures 6.3 and 6.4). Most importantly, by inducing the expression of exogenous ZFP36L1, we were able to rescue a defective ZFP36L1 KO phenotype that exhibited increased micronuclei and 53BP1 NBs to a frequency similar to WT cells in untreated and APH-induced replication stress conditions. Thus collectively, these findings strongly support the specificity of CRISPR-Cas9 mediated KO of ZFP36L1 in T-REx U-2OS cells and the role of ZFP36L1 in limiting replication stress-associated genomic instability. We demonstrated convincingly that inducible expression of exogenous ZFP36L1 in ZFP36L1 KO cells represses micronuclei and 53BP1 NB formation, biomarkers of replication stress associated segregation errors and genomic instability.

Finally, by rescuing a WT phenotype through genetic complementation in ZFP36L1 KO cells, we were confident that the observed replication stress-associated genomic instability phenotypes were due to CRISPR-Cas9 mediated KO of ZFP36L1. The importance of genetic complementation is highlighted by a plethora of studies that have employed this approach to demonstrate CRISPR-Cas9 on-target specificity and rescue phenotypic abnormalities (Matsunaga and Yamashita, 2014; Chen et al., 2017; Voloshanenko et al., 2017; Ma et al., 2020). Importantly, our system demonstrated tight control over the inducible expression of exogenous ZFP36L1 in ZFP36L1 KO cells enabling comparative analysis before and after ZFP36L1 expression was induced. However, this method alone cannot conclusively demonstrate the absence of off-targeting. Specifically, whole-genome sequencing would provide a more sensitive measure of off-target mutagenesis to identify genes that have been unintendedly mutated when utilising CRISPR-Cas9 to target *ZFP36L1* (Reviewed in Zhang et al., 2015). Moreover, combining genetic complementation with whole-genome sequencing could be utilised in future studies to provide more conclusive proof of target-specific CRISPR-Cas9 editing.

7. Loss of ZFP36L1 induces replication stress associated R-loop formation

7.1 Introduction

Progression of replication forks becomes impaired in the presence of DNA synthesis inhibitors; this can be attributed to the slowing of DNA polymerase or the presence of obstructions that prevent polymerase progression (Reviewed in Aguilera and García-Muse, 2012). Three stranded nucleic acid structures known as R-loops made up of an RNA: DNA hybrid and a displaced single-stranded nontemplate DNA strand have been implicated to obstruct the progression of replication forks. Unresolved R-loops can be deleterious to genome integrity leading to increased replication stress and DNA damage, increasing the occurrence of replication fork collisions with the transcription machinery (transcription-replication conflicts) (Hamperl et al., 2017). Once formed, R-loops can be removed by nucleases such as RNase H1 which degrades the RNA moiety hybridised to the DNA strand (Cerritelli and Crouch, 2009). Moreover. R-loops can be removed by helicases such as Senataxin (SETX), Aquarius (AQR) and DHX9 (Skourti-Stathaki, Proudfoot and Gromak, 2011; Sollier et al., 2014; (Cristini et al., 2018) (Figure 7.1). Factors involved in RNA biogenesis such as the messenger ribonucleoprotein particle (mRNP) biogenesis factor THO complex and SRSF1 have been proposed to prevent hybridisation of the nascent RNA thus preventing the formation of R-loops (Huertas and Aguilera, 2003; Olazabal-Herrero et al., 2020). Interestingly, RNA processing factors including RBPs and AU-RBPs have also emerged as key components in deterring the formation of R-loops through direct processing of hybridised RNA or protein interactions to resolve R-loops (Alfano et al., 2019; reviewed in Klaric, Wüst and Panier, 2021).

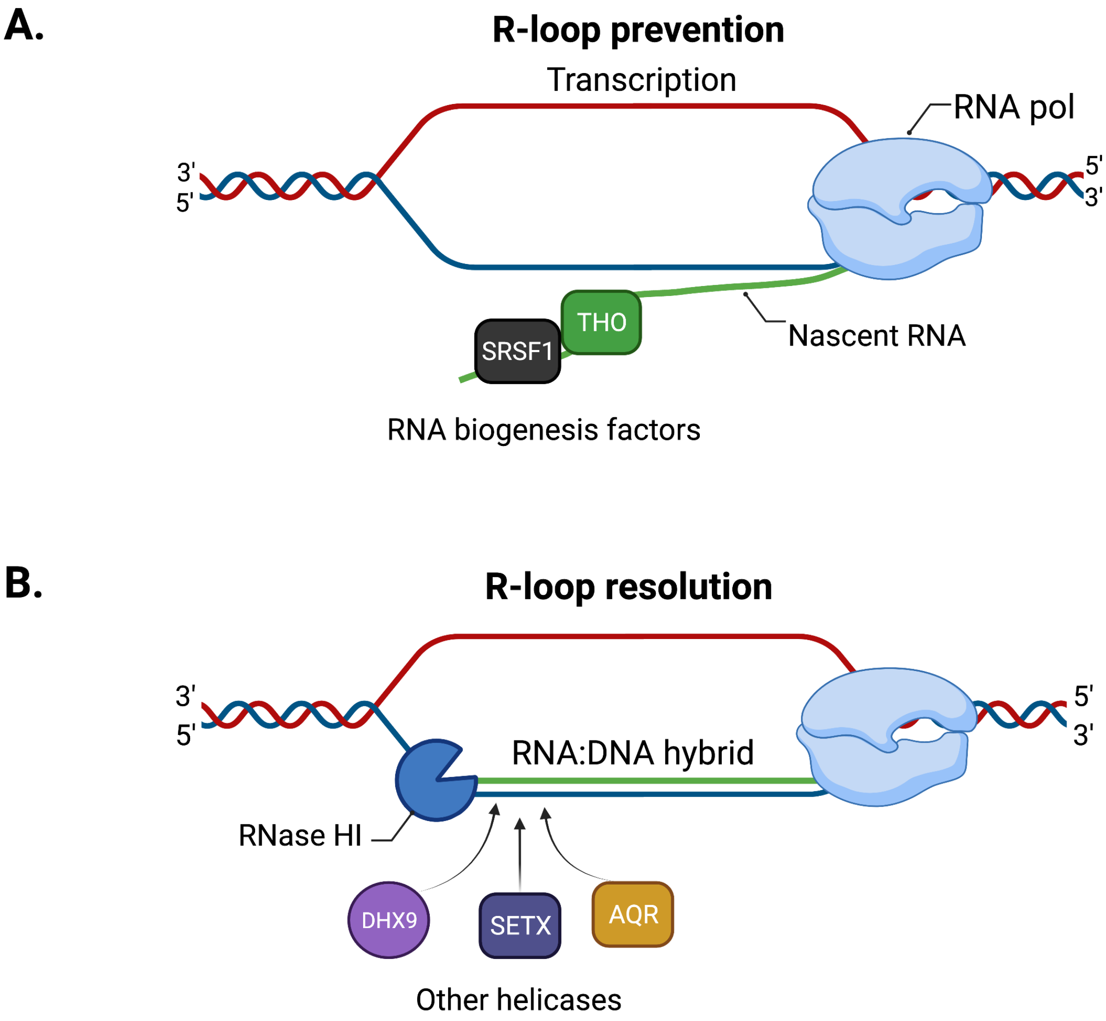
A.
R-loop prevention
Transcription
RNA pol
3'
5'
5'
3'
THO
SRSF1
Nascent RNA
RNA biogenesis factors
B.
R-loop resolution
3'
5'
5'
3'
RNA:DNA hybrid
RNase HI
DHX9
SETX
AQR
Other helicases

Figure 7.1 Proteins involved in suppressing R-loop accumulation.
A. During transcription, R-loop formation is prevented by RNA binding proteins involved in RNA biogenesis such as THO and SRF1 that bind the nascent mRNA inhibiting its hybridisation with the template DNA strand. **B**. R-loop removal can be achieved by degradation of the RNA moiety of RNA: DNA hybrid by nuclease RNase H1 or by DNA: RNA helicases such as DHX9, SETX and AQR that unwind the hybrid (Created with Biorender.com).

7.2 Loss of ZFP36L1 increases replication stress-associated R-loop formation

To investigate if ZFP36L1 plays a role in deterring R-loops that could be contributing to the replication stress associated genomic instability, we utilised T-REx U-2OS WT (WT) and U-2OS ΔL1-T-REx (ΔL1-T-REx) cells to express a catalytically inactivate RNase H1 mutant (D210N) fused with green fluorescence protein (GFP) (RNH1(D210N)-GFP) (Figure 7.2A). Utilising the RNase H1 mutant would enable efficient binding to R-loops without degrading, thus enabling the detection of R-loop formation and comparative analysis in ZFP36L1 abolished cells by fluorescent microscopy. As a control, an RNase H1 wild-type (WT) tagged with GFP (RNase H1(WT)-GFP) that maintains its ability to degrade R-loops upon induction with tetracycline was used (Figure 7.2B). To detect differences in R-loop formation WT and ΔL1-T-REx cells were induced to express mutant RNase H1 and WT RNase H1 with 1µg/ml tetracycline for 24 hours and either untreated or treated with 0.2µM APH for 16hours. To ensure only chromatin-bound RNH1(D210N)-GFP foci were analysed, cells were pre-extracted to remove chromatin unbound proteins (Figure 7.2C). We observed that ΔL1-T-REx cells contained significantly more R-loops in both untreated (-) and 0.2µM APH treatment conditions relative to WT cells. Specifically, in untreated conditions WT cells exhibited an average of 11 RNH1(D210N)-GFP foci compared to an average of 18 RNH1(D210N)-GFP foci in ΔL1-T-REx cells representing a significant increase of more than 1.5-fold relative to WT cells (*p*=0.0055, P≤0.001) (Figure 7.2D and E). Furthermore, in APH-induced replication stress conditions, we observed significantly more R-loops in the absence of ZFP36L1 compared to WT cells. Specifically, we found that WT cells contained an average of 15 RNH1(D210N)-GFP foci compared to 27 in ΔL1-T-REx cells representing a near 2-fold significant increase relative to WT cells (p<0.001) (Figure 7.2D and E). Unsurprisingly, both WT and ΔL1-T-REx expressing RNH1(WT)-GFP, exhibited a low number of GFP foci in both untreated and 0.2μM APH treatment conditions (Figure 7.2D and E). Overall, these results demonstrated that RNH1(D210N)-GFP bound to R-loops without resolving them and loss of ZFP36L1 increases the formation of R-loops in both untreated and APH treated conditions.

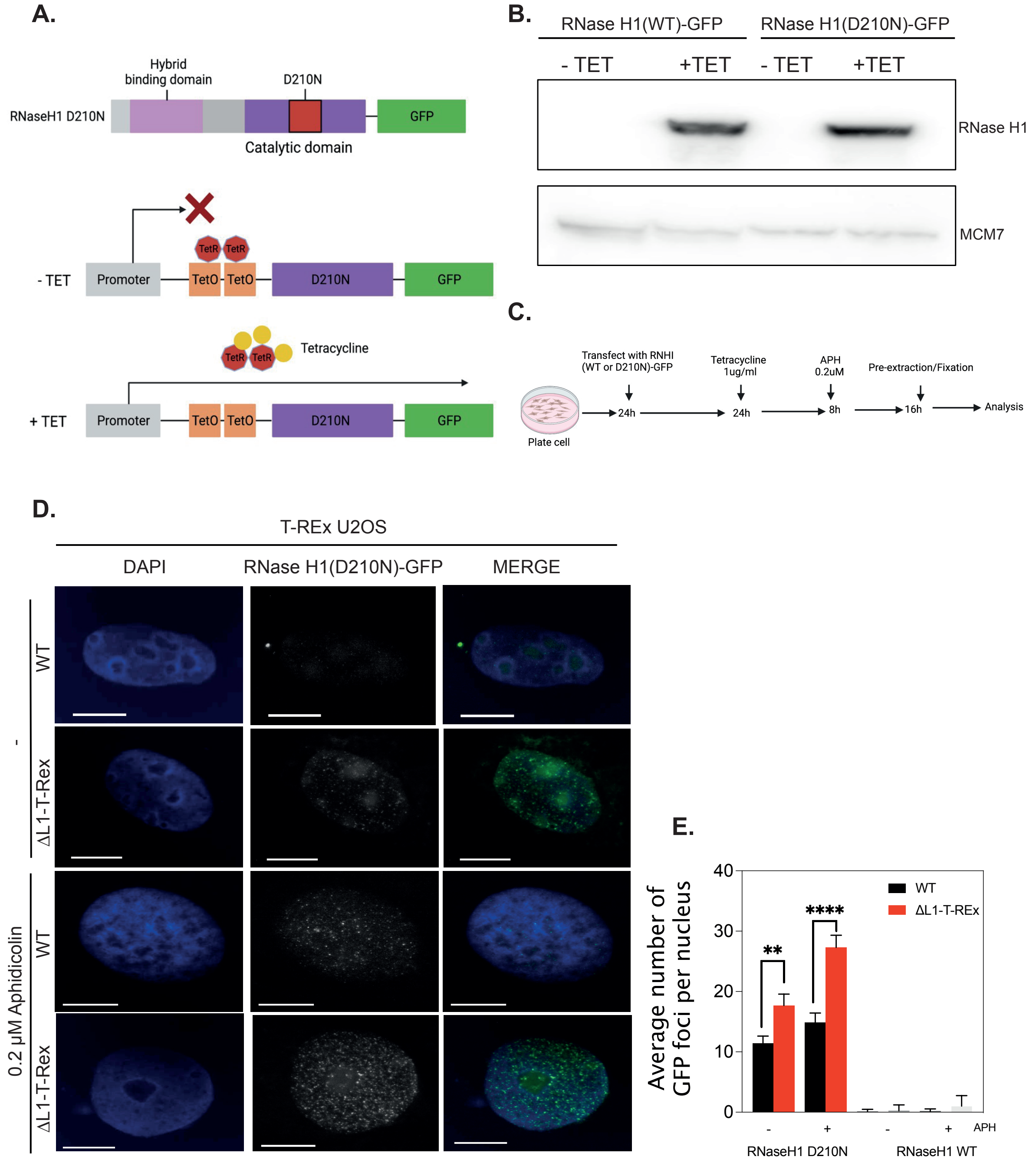

Figure 7.2 Loss of ZFP36L1 increases replication stress-associated R-loop formation.

A. Schematic of RNase H1-green fluorescence protein fusion (GFP) with D210N substitution (red box) located within the catalytic domain of RNase H1. Schematic of inducible expression of RNase H1(D210N)-GFP in T-REx U-2OS cells. In the absence of tetracycline, the constitutively expressed Tet repressor binds to the Tet operator (TetO2) and inhibits the expression of RNase H1(D210N)-GFP. In the presence of tetracycline, the Tet repressor is relieved from the TetO2 and binds to tetracycline enabling the expression of RNase H1(D210N)-GFP. **B**. Western blot analysis of RNase H1(D210N)-GFP and RNase H1(WT)-GFP following induction with 1µg/ml tetracycline for 24 hours utilising a GFP antibody, MCM-7 was utilised as a loading control. **C**. Workflow of analysis of R-loop formation in T-REx U-2OS. T-REx U-2OS were transfected with either RNase H1(D210N)-GFP or RNase H1(WT)-GFP for 24 hours, then induced with 1µg/ml tetracycline for 8 hours and treated with 0.2µM APH for 16hours, followed by pre-extraction, formaldehyde fixation and analysis. **D**. Representative images of WT and ΔL1-T-REx cells nuclei (DAPI) induced to express RNase H1(D210N)-GFP either untreated or treated with 0.2µM APH. **E**. Quantification of the average number of GFP foci per nucleus following induction of RNase H1(D210N)-GFP and RNase H1(WT)-GFP in the absence or presence of 0.2µM APH. Scale bar, 10 µm. Data generated are of two independent replicates from a total of 300 cells analysed in each condition and replicate. Error bars represent S.E.M. p values were calculated using an unpaired two-tailed t-test.; not significant $p>0.05$ (ns); $p \leq 0.05$(*); $p \leq 0.01$ (**); $p \leq 0.001$ (***), $p \leq 0.0001$(****).

7.3 R-loops contribute to replication stress associated 53BP1 NBs in ZFP36L1 abolished cells

Thus far, we have elucidated that ZFP36L1 plays a role in maintaining genome integrity in response to replication stress. Specifically, throughout the study, we have demonstrated that in response to mild replication stress loss of ZFP36L1 results in unprocessed DNA lesions that enter mitosis leading to characteristic chromosomal abnormalities, that can then appear as micronuclei or sequestered in 53BP1 NBs in the subsequent G1 phase. Importantly, R-loops that remain unresolved can prove detrimental to genome integrity (Gan et al., 2011; Hamperl and Cimprich, 2014; Costantino and Koshland, 2018). Having implicated a possible link between loss of ZFP36L1 and an increase in R-loop formation upon replication stress conditions, we explored if R-loops could lead to the defective phenotype observed in ZFP36L1 abolished cells by firstly assessing 53BP1 NB formation as a read-out for unresolved replication stress associated mitotic defects. We induced expression of WT RNase H1 (Figure 7.3) and catalytically inactivate RNase H1 (D210N) (Figure 7.3) in WT and ΔL1-T-REx cells either untreated (-) or treated with 0.2µM APH and assessed for the frequency of 53BP1 NBs in G1 cells.

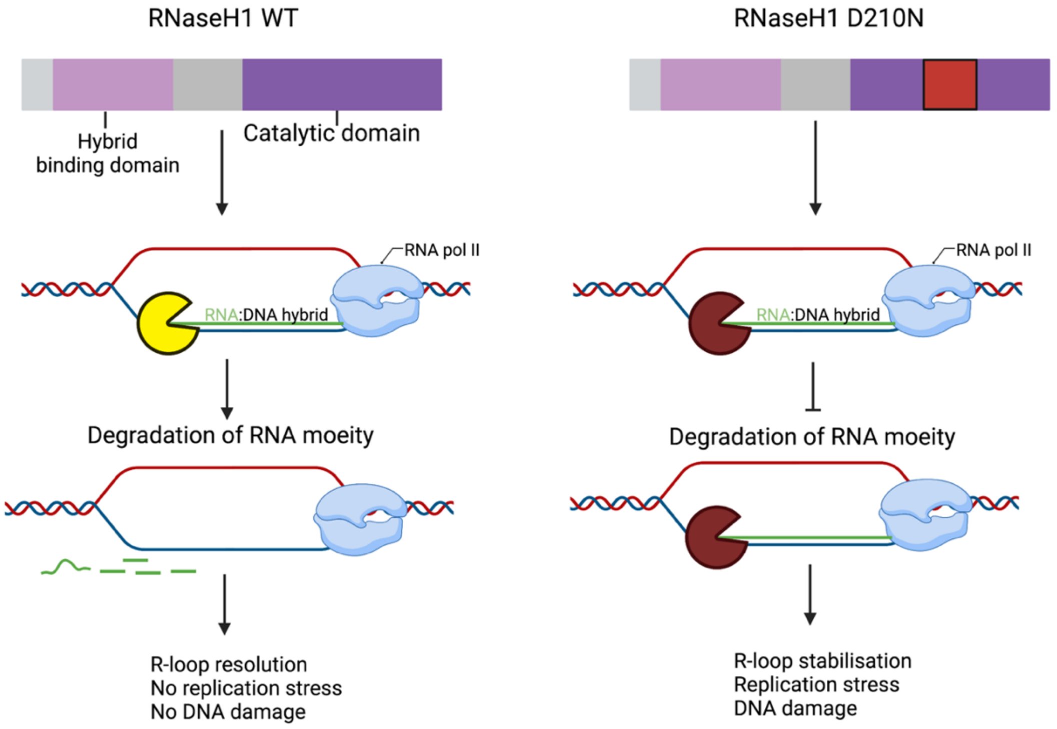
RNaseH1 WT
Hybrid binding domain
Catalytic domain
RNA pol II
RNA:DNA hybrid
Degradation of RNA moeity
R-loop resolution
No replication stress
No DNA damage
RNaseH1 D210N
RNA pol II
RNA:DNA hybrid
Degradation of RNA moeity
R-loop stabilisation
Replication stress
DNA damage

Figure 7.3 Schematic representation of RNase H1 WT and mutant RNase H1 D210N and their action on RNA: DNA hybrids.
RNase H1 WT can bind RNA: DNA hybrids with its hybrid binding domain, degrading the RNA moiety utilising its catalytic domain leading to the resolution of R-loops, limiting replication stress and DNA damage. Mutant RNase H1 D210N binds but is unable to degrade the RNA moiety due to disruption in its catalytic domain (red box), further stabilising R-loops and leading to replication stress and DNA damage (Created with Biorender.com).

Resolution of R-loops through the expression of WT RNase H1 significantly reduced the frequency of G1-associated 53BP1 NBs in ΔL1-T-REx cells to levels comparable to WT cells in untreated and APH treated conditions (7.3.1A-C). In untreated conditions expression of WT RNase H1 (+TET) in ΔL1-T-REx cells demonstrated a significant reduction in cells >3 G1 53BP1 NBs by approximately 1.5-fold from 17.5% to 11% relative to when WT RNase H1 was repressed (-TET) ($p<0.05$; $p=0.0464$) (7.3.1C). Furthermore, the difference between cells with >3 G1 53BP1 in WT and ΔL1-T-REx when WT RNase H1 was induced was non-significant, demonstrating that the resolution of R-loops in ΔL1-T-REx cells could reduce the prevalence of 53BP1 NBs to WT frequency (7.3.1C). Similarly, ΔL1-T-REx cells treated with 0.2μM APH decreased from 36.75% to 13.25% corresponding to a >2.5-fold reduction of cells with >3 G1 53BP1 before and after WT RNase H1 expression ($p<0.05$; $p=0.0135$) (7.3.1C). Moreover, there was no significant difference between WT and ΔL1-T-REx exhibiting >3 G1 53BP1 NBs in 0.2μM APH treatment conditions following R-loop resolution, thus suggesting R-loops contribute to the formation of 53BP1 NBs in APH-induced replication stress conditions (7.3.1C). The reduction in 53BP1 NBs was not observed upon expression of catalytically inactive RNase H1(D210N) (7.3.1D-F). Specifically, we did not observe a reduction in G1 53BP1 NBs, in both untreated and 0.2μM APH treatment conditions (Figure 7.3.1F). Therefore, these results suggest that R-loops contribute to the increased prevalence of 53BP1 NBs in the absence of ZFP36L1.

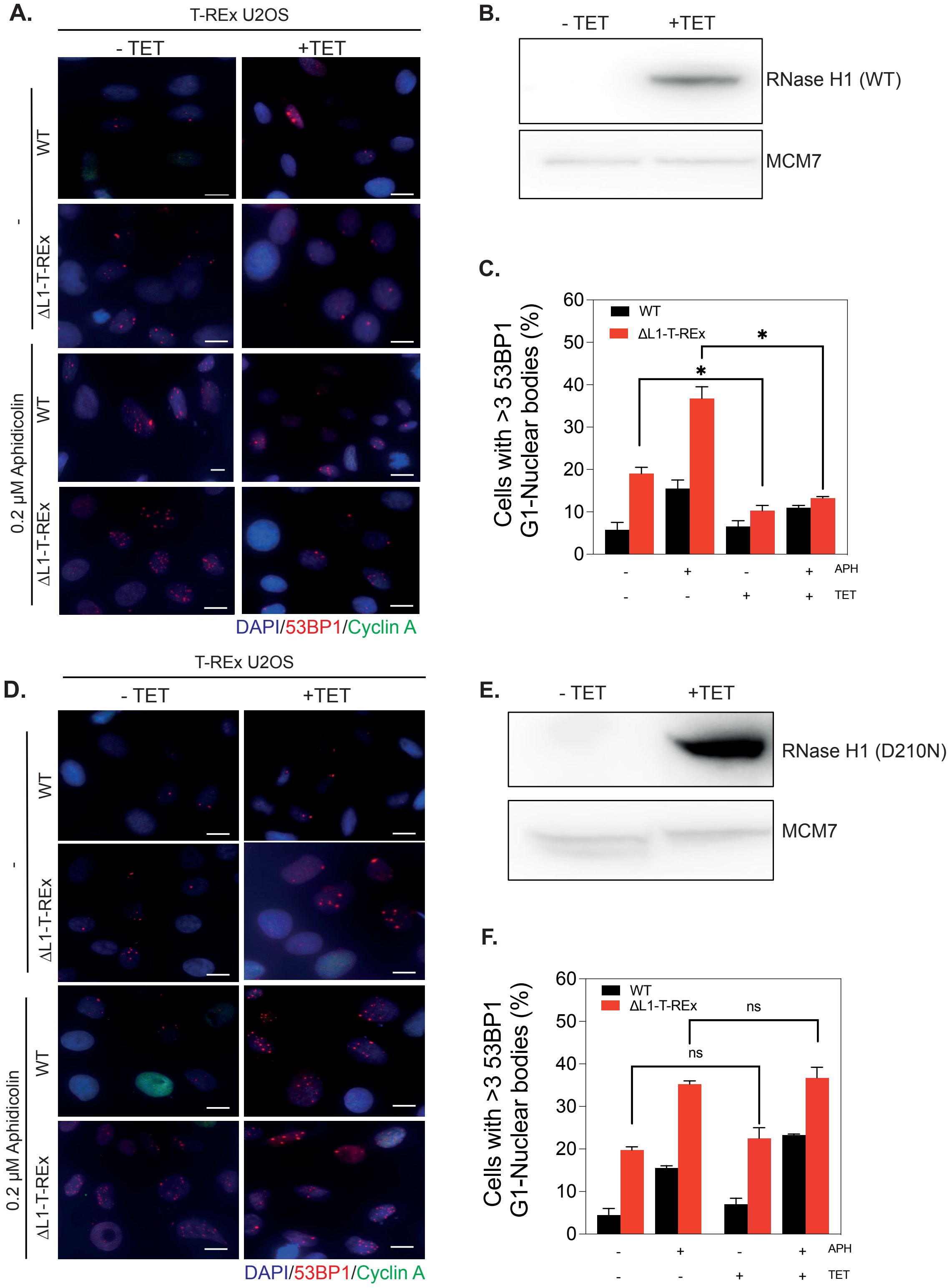

Figure 7.3.1 R-loops contribute to replication stress-associated 53BP1 NBs in ZFP36L1 abolished cells.

A. Representative image of cyclin A (green) and 53BP1 NBs (red) in DAPI (purple) stained nuclei from T-REx U-2OS WT (WT) and ZFP36L1 Knockout (ΔL1-T-REx) cells either induced to express RNase H1 WT with 1μg/ml tetracycline (+Tet) or not (-Tet) in the absence (-) and presence of 0.2 μM APH. **B**. Western blot analysis of extracts from ΔL1-T-REx cells expressing WT RNase H1 upon induction with 1μg/ml tetracycline for 24 hours **C**. Quantification of cells with >3 53BP1 G1-nuclear bodies treated with tetracycline (+ Tet) to express RNase H1 WT or not (-Tet) in the absence (-APH) or presence (+APH) of 0.2μM APH. **D**. Representative image from WT and ΔL1-T-REx cells either treated to express mutant RNase H1 D210N with 1μg/ml tetracycline or not in the absence and presence of 0.2 μM APH. **E**. Western blot analysis of extracts from ΔL1-T-REx cells expressing RNase H1 D210N upon induction with 1μg/ml tetracycline for 24 hours. **F**. Quantification of WT and ΔL1-T-REx cells with >3 53BP1 G1-nuclear bodies induced with tetracycline (+Tet) to express mutant RNase H1 (D210N) or not (-Tet) in the absence (- APH) or presence (+APH) of 0.2μM APH. Scale bar, 10 μm. Data generated are of two independent replicates from a total of 300 G1 cells analysed in each condition and replicate. Error bars represent S.E.M. p values were calculated using an unpaired two-tailed t-test.; not significant p>0.05 (ns); p ≤ 0.05(*); p ≤0.01 (**); p ≤0.001 (***), p≤0.0001(****).

7.4 R-loop resolution suppresses RPA accumulation in S/G2 cells in ZFP36L1 abolished cells

Having observed that R-loops increase G1-associated 53BP1 NBs upon replication stress conditions, we further examined the implications of an increase in R-loop formation in ZFP36L1 abolished cells by assessing for RPA foci in S/G2 cells. Importantly, RPA has been reported to associate with R-loops in human cells in addition to its key roles in DNA damage and replication stress (Nguyen et al., 2017). Therefore, we sought to determine if resolving R-loops in ZFP36L1 KO cells utilising RNase H1 would impact the prevalence of RPA foci in S/G2 cells. To determine the impact of potential R-loops on RPA foci in S/G2 cells we expressed WT RNase H1 and catalytically inactivate RNase H1 D210N in WT and ΔL1-T-REx cells either untreated (-) or treated with 0.2μM APH. Upon induction of RNase H1 WT in ΔL1-T-REx cells, we found that the prevalence of RPA foci in S/G2 decreased in untreated and APH-induced replication conditions (Figure 7.4A-C). Specifically, induction of WT RNase H1 (+TET) in ΔL1-T-REx cells reduced the frequency of Cyclin A positive cells with >RPA foci from 21.5% to 12% in untreated conditions, representing a significant

>1.5-fold decrease relative to when RNase H1 was repressed (-TET) ($p<0.05$; $p=0.0101$) (Figure 7.4 A-C). Similarly, cyclin A positive cells exhibiting >9 RPA foci was also recorded in the presence of 0.2µM APH. We found that expression of RNase H1 WT in ΔL1-T-REx cells reduced the accumulation of cyclin A positive cells with >9 RPA foci by approximately 1.5-fold ($p<0.05$; $p=0.0342$) (Figure 7.4 A-C). Importantly, we did not detect a significant difference between WT and ΔL1-T-REx cyclin A positive cells following R-loop resolution in both untreated and 0.2µM APH treatment conditions ($p>0.05$) (Figure 7.4 A-C). Interestingly, expression of RNase H1 D210N in ΔL1-T-REx cells increased the frequency of cyclin A positive cells with >9 RPA foci in untreated conditions from 18% to 24% and 36% to 48% in the presence of 0.2µM APH (Figure 7.4 D-F). However, the observed increase in RPA foci in ΔL1-T-REx cells expressing RNase H1 D210N was deemed to be statistically non-significant ($p>0.05$) (Figure 7.4 D-F). Taken together our results suggest that the significant increase in RPA foci in ZFP36L1 KO cells could be attributed to replication stress-associated R-loop formation.

A.

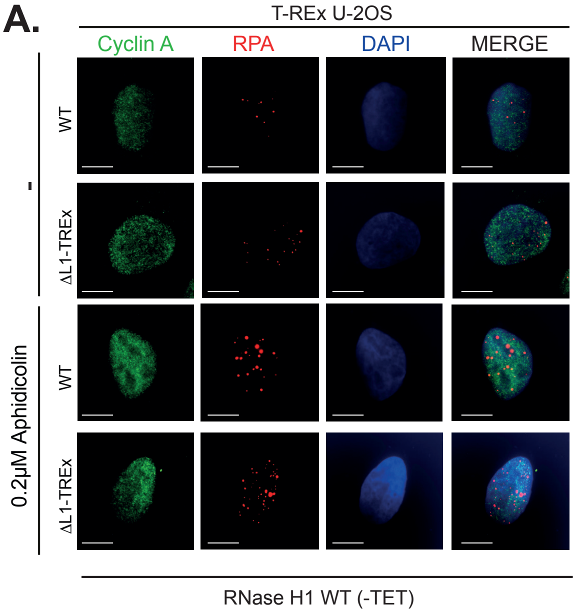
T-REx U-2OS
Cyclin A
RPA
DAPI
MERGE
-
WT
ΔL1-TREx
0.2µM Aphidicolin
WT
ΔL1-TREx
RNase H1 WT (-TET)

B.

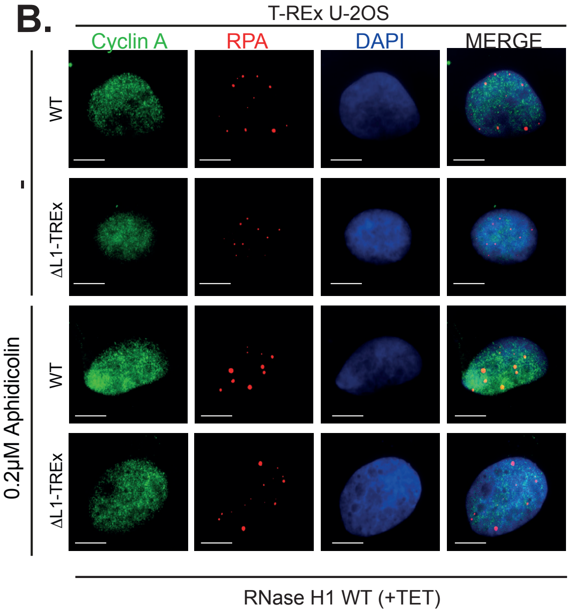
T-REx U-2OS
Cyclin A
RPA
DAPI
MERGE
-
WT
ΔL1-TREx
0.2µM Aphidicolin
WT
ΔL1-TREx
RNase H1 WT (+TET)

C.

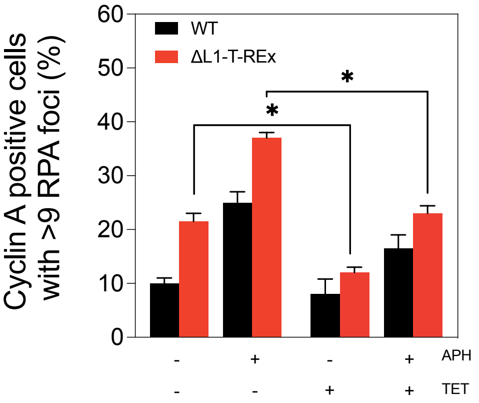
Cyclin A positive cells
with >9 RPA foci (%)
60
50
40
30
20
10
0
WT
ΔL1-T-REx
*
*
-
+
-
+
APH
-
-
+
+
TET

D.

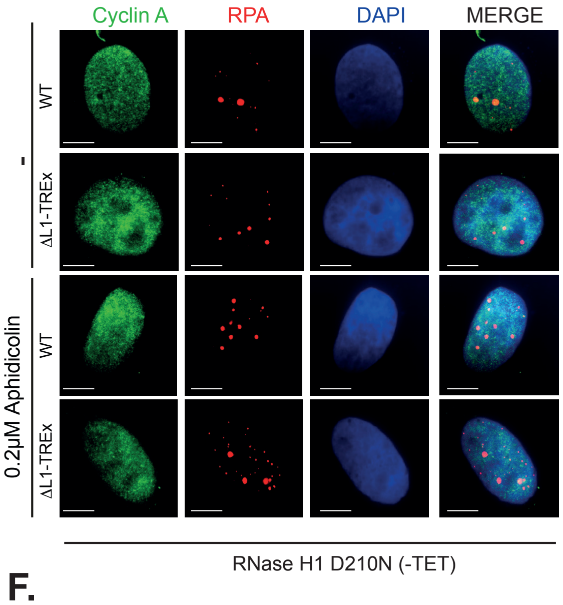
T-REx U-2OS
Cyclin A
RPA
DAPI
MERGE
-
WT
ΔL1-TREx
0.2µM Aphidicolin
WT
ΔL1-TREx
RNase H1 D210N (-TET)

E.

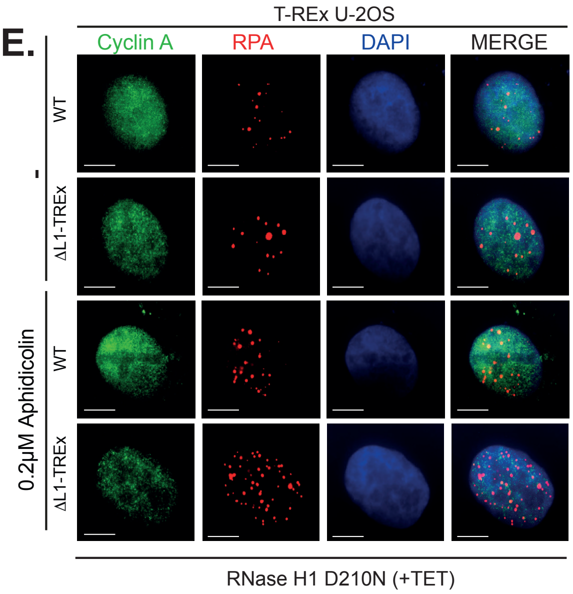
T-REx U-2OS
Cyclin A
RPA
DAPI
MERGE
-
WT
ΔL1-TREx
0.2µM Aphidicolin
WT
ΔL1-TREx
RNase H1 D210N (+TET)

F.

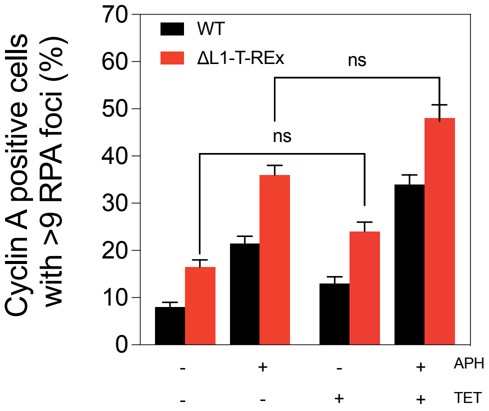
Cyclin A positive cells
with >9 RPA foci (%)
70
60
50
40
30
20
10
0
WT
ΔL1-T-REx
ns
ns
-
+
-
+
APH
-
-
+
+
TET

Figure 7.4. R-loop resolution suppresses RPA accumulation in S/G2 cells in ZFP36L1 abolished cells.
A and **B**. Representative image of cyclin A (green) and RPA (red) in DAPI (purple) stained nuclei from T-REx U-2OS WT (WT) and ZFP36L1 Knockout (ΔL1-T-REx) cells not induced (-TET) or induced (+TET) to express RNase H1 WT with 1µg/ml tetracycline (+Tet) or not (-Tet) in the absence (-) and presence of 0.2 µM APH. **C.** Quantification of cyclin A cells >9 RPA foci induced with tetracycline (+ TET) to express RNase H1 WT or not (-TET) in the absence (- APH) or presence of 0.2µM APH (+APH). **D** and **E** Representative images of WT and ΔL1-T-REX cells non-induced (-TET) or tetracycline induced (+TET) to express mutant RNase H1 D210N with 1µg/ml tetracycline in the absence (-) and presence of 0.2 µM APH. **F**. Quantification of cyclin A cells >9 RPA induced with tetracycline (+ TET) to express RNase H1 D210N or not (-TET) in the absence (- APH) or presence of 0.2µM APH(+APH). Scale bar, 10 µm. Data generated are of two independent replicates from a total of 200 cyclin A positive cells analysed in each condition and replicate. Error bars represent S.E.M. p values were calculated using an unpaired two-tailed t-test.; not significant p>0.05 (ns); p ≤ 0.05(*); p ≤0.01 (**); p ≤0.001 (***), p≤0.0001(****).

7.5 Discussion

R-loops play an integral role in transcription termination, mitochondrial DNA replication, chromatin modifications and telomere regulation dynamics (Reviewed in Allison and Wang, 2019; Reviewed in Uruci et al., 2021). However, the formation of unscheduled R-loops that remain unprocessed can prove deleterious to genome integrity. Studies have demonstrated that R-loops may form in cells due to abnormalities in mRNA processing factors and become stabilised, blocking replication fork progression (Crossley, Bocek and Cimprich, 2019). Unprocessed R-loops can result in somatic hypermutagensis when the displaced ssDNA is targeted by DNA altering enzymes such as activation-induced cytidine deaminase (AID) or result in DNA breaks because of collisions between replication and transcription machinery (transcription-replication conflicts) (Santos-Pereira et al., 2013; Hamperl et al., 2017).

Utilising a catalytically inactive form of RNase H1 tagged with GFP that binds R-loops we found that loss of ZFP36L1 results in an increase in replication stress-associated R-loop formation (Wu, Lima and Crooke, 2001; Nguyen et al., 2017; Crossley et al., 2021; Nascakova et al., 2021) These findings were characterised by an increase in chromatin-bound RNase H1(D210N)-GFP foci in unperturbed conditions and increased under APH-induced replication stress conditions (Figure 7.2A-C). Moreover, the resolution of R-loops in cells expressing catalytically active RNase H1(WT)-GFP exhibited little to no chromatin-bound GFP foci (Figure 7.2D-F). Therefore, these results indicated increased replication stress-associated R-loop formation in the absence of ZFP36L1. Although we are confident that our observations point to an increase in R-loop formation, our results could be further verified by utilising the monoclonal antibody S9.6 which is also able to recognise RNA:DNA hybrids in human cells (Wan et al., 2015). However, recent reports have suggested fluorescently tagged catalytically inactive RNase H1(D210N) to be a more specific marker of RNA: DNA hybrids than the monoclonal antibody S9.6 (Crossley et al., 2021).

Our study thus far has elucidated that loss of ZFP36L1 results in replication stress-associated DNA damage biomarkers that result in genomic instability. We speculated due to the emerging roles of RBPs and AU-RBPs in R-loop processing, that the detection of DNA damage and chromosome segregation defects could be due to persistent unresolved R-loops. Analysis of 53BP1 NBs in G1 cells expressing RNase H1 WT significantly decreased the prevalence of G1-associated 53BP1 NBs in ZFP36L1 KO cells (Figure 7.3.1A-C). Furthermore, the expression of catalytically inactive RNase H1 did not have any effect on the formation of G1-associated 53BP1 NBs i (Figure 7.3.1D-F). Therefore, these results demonstrated unprocessed R-loops to be an important factor contributing to the increase in G1-associated 53BP1 NBs in the absence of ZFP36L1. Here our results also demonstrate R-loops as a potential cause for the increased prevalence of RPA foci in S/G2 cells in the absence of ZFP36L1 (Figure 7.4A-F). We demonstrate that R-loop resolution was able to significantly decrease the levels of RPA foci in S/G2 cells in the presence and absence of APH-induced replication stress (Figure 7.4A-C). The decrease in RPA foci formation following R-loop resolution suggests that R-loops pose a potential block to replication fork progression leading to increased ssDNA that is bound by RPA. Importantly, reports have also demonstrated that R-loops can increase the accumulation of RPA foci potentially because of increased binding to the displaced ssDNA that forms the R-loop structure, thus increased RPA could also indicate unresolved R-loop in ZFP36L1 ablated cells (Nguyen et al., 2017). Furthermore, the expression of RNase H1 D210N that can bind R-loops without resolving them may increase the local concentration of RPA foci due to its ability to colocalise with RNase H1 (Nguyen et al., 2017). Therefore, this may also explain the increased levels of RPA foci following expression of the mutant RNase H1 D210N, although this increase was deemed to be statistically non-significant (Figure 7.4 E-F). Thus, taken together we implicate R-loops as a potential source of the replication stress-associated genomic instability observed in ZFP36L1 KO cells and that ZFP36L1 may play a role in deterring R-loops like other RBPs. The mechanisms underlying ZFP36L1's role in maintaining genome integrity in response to replication stress potentially through the resolution of unscheduled R-loop formation are currently unknown. In an attempt to fill in the gaps in our understanding of the molecular networks of ZFP36L1, we have mapped the interactome of ZFP36L1 for the first time in literature, through proteomic screens of immune-enriched FLAG-tagged ZFP36L1 (Chapter 8) We believe that the data presented in chapter 8 may help elucidate the potential mechanisms associated with ZFP36L1's role in maintaining genomic integrity in response to replication and suppressing R-loop formation.

8. Mapping the ZFP36L1 interactome

8.1 Introduction

Proteins rarely exhibit key regulatory roles in isolation; rather they are organised into complex molecular machines that enable them to carry out their biological roles. Quantitative mass spectrometry (MS) based proteomic studies are utilised to detect protein complexes on a global scale from cell lysates. A commonly used method to identify and study protein complexes is through immunoprecipitation (IP) assays followed by MS (IP-MS) and is a powerful tool to identify novel protein-protein interactions (van Andel et al., 2022). Typical IP-MS experiments employ a solid support with antibodies directed against a "bait" protein that is utilised for precipitation of protein complexes. Captured proteins are then digested into peptides and analysed by MS (van Andel et al., 2022). To shed light on mechanisms that enable ZFP36L1 to limit replication stress associated genomic instability, we conducted IP-MS to identify protein interactors for ZFP36L1 in a tightly regulated tetracycline-inducible system. In this short chapter we report for the first time, multiple novel protein interactions that are important for the maintenance of genomic integrity and other yet-to-be-discovered physiological roles of ZFP36L1.

8.2 IP-MS identifies multiple novel ZFP36L1 interactors

The protein interactions that ZFP36L1 undertakes in human cells have focused mainly on ZFP36L1's primary role in post-transcriptional regulation over mRNA (Lykke-Andersen and Wagner, 2005; Otsuka et al., 2020). The primary focus of this study was to identify novel interacting partners for ZFP36L1 to explain ZFP36L1's role in suppressing replication stress-associated genomic instability. Therefore, we performed FLAG-IP of ZFP36L1 containing an N-terminal FLAG-Strep II tag followed by MS to identify peptides associated with the protein. To avoid competition for interacting protein partners, cell lines lacking the endogenous protein are preferred (Cannavo et al., 2007). For this reason, we utilised ZFP36L1 KO T-REx U-2OS cells transfected with PCDNA-4-TO- FLAG-Strep II-ZFP36L1 or PCDNA-4-TO-FLAG-Strep II-empty vector (EV) as a control for potential proteins that bind to FLAG-Strep II alone. Transfected cells were either induced (+TET) or not (-TET) to express recombinant FLAG-Strep II-ZFP36L1 expression with 1ng/µL tetracycline for 24 hours. Recombinant FLAG-Strep II-ZFP36L1 was detected through western blotting exhibiting an expected molecular weight of approximately 57 kDa (Figure 8.2A). Similarly, FLAG expression was also confirmed following tetracycline-induced expression of recombinant FLAG-Strep II-ZFP36L1 in ΔL1-T-REx cells (Figure 8.2A). Thus, confirming that we had generated a system that could be utilised to induce recombinant FLAG-Strep II-ZFP36L1 for FLAG IP. For IP of FLAG-Strep II- ZFP36L1, ΔL1-T-REx cells were transfected with PCDNA-4-TO- FLAG-Strep II-ZFP36L1 or PCDNA-4-TO-FLAG-Strep II-empty vector (EV) and induced (+TET) with 1µg/µL tetracycline for 24hours. FLAG-IP was then performed to enrich for recombinant FLAG-Strep II- ZFP36L1 and subjected to SDS-page followed by western blot to detect ZFP36L1 and FLAG expression. Results from western blot demonstrated expression of ZFP36L1 and FLAG in the FLAG-IP elution from ΔL1-T-REx cells transfected with PCDNA-4-TO- FLAG-Strep II-ZFP36L1 (Figure 8.2A). For proteomic experiments, IP FLAG-Strep II-ZFP36L1 and FLAG-Strep II-EV protein complex beads were digested into peptides and subjected to MS as described before (Casado et al., 2013; Rajeeve et al., 2014) (Figure 8.2C).

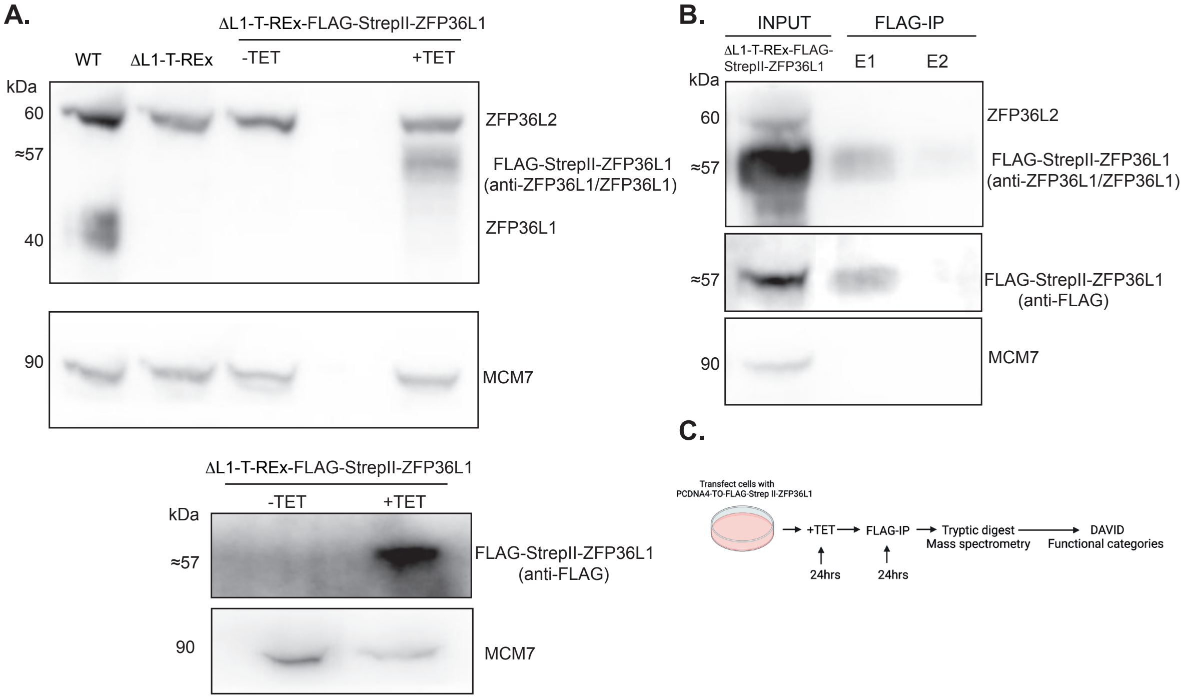
A.
ΔL1-T-REx-FLAG-StrepII-ZFP36L1
WT
ΔL1-T-REx
-TET
+TET
kDa
60
≈57
40
ZFP36L2
FLAG-StrepII-ZFP36L1
(anti-ZFP36L1/ZFP36L1)
ZFP36L1
90
MCM7
ΔL1-T-REx-FLAG-StrepII-ZFP36L1
-TET
+TET
kDa
≈57
FLAG-StrepII-ZFP36L1
(anti-FLAG)
90
MCM7
B.
INPUT
FLAG-IP
ΔL1-T-REx-FLAG-StrepII-ZFP36L1
E1
E2
kDa
60
≈57
ZFP36L2
FLAG-StrepII-ZFP36L1
(anti-ZFP36L1/ZFP36L1)
≈57
FLAG-StrepII-ZFP36L1
(anti-FLAG)
90
MCM7
C.
Transfect cells with
PCDNA4-TO-FLAG-Strep II-ZFP36L1
+TET
FLAG-IP
Tryptic digest
Mass spectrometry
DAVID
Functional categories
24hrs
24hrs

Figure 8.2 Confirmation and enrichment of ZFP36L1 with anti-flag magnetic beads for proteomic analysis.
A. Western blot image of ZFP36L1 (anti-ZFP36L1/ZFP36L2) and FLAG (anti-FLAG) expression from ΔL1-T-REx cells transfected with PCDNA4-TO-FLAG-StrepII-ZFP36L1. **B.** FLAG IP followed by western blot analysis testing ZFP36L1 expression from ΔL1-T-REx expressing FLAG-StrepII-ZFP36L1. Following FLAG-IP, eluted FLAG-StrepII-ZFP36L1 samples (E1 and E2) were probed with anti-ZFP36L1/ZFP36L2 and anti-FLAG antibodies to confirm enrichment of ZFP36L1 and FLAG expression respective to INPUT samples. **C**. Workflow for mapping the interactome of ZFP36L1.

Proteins detected by MS in FLAG-StrepII-ZFP36L1 were only retained if peptide counts were <1 in the corresponding FLAG-EV control generating a list of ZFP36L1 specific interactions (N=153) (Appendix D; Table 1). ZFP36L1 specific interactors were then classified into several groups based on biological and molecular function (Table 7) and demonstrated functional interactions as demonstrated by different protein clusters (Appendix D; Figure 1). One of the most prominent groups belonged to proteins involved in RNA degradation including CNOT1 which is the core subunit of CCR4-NOT poly (A) deadenylase complex important for initiating mRNA decay through poly (A) tail removal and was identified with a very high mascot (Table 7). We also identified other subunits of the CCR4-NOT poly (A) deadenylase complex (CNOT3 and CNOT10) and 5’ to 3’ RNA exonuclease XRN1 which has also been previously reported to interact with ZFP36L1 (Lykke-Andersen and Wagner, 2005), consistent with ZFP36L1’s primary role in mRNA degradation (Table 7). We also identified potential novel ZFP36L1 interactions including several proteins classified as RNA helicases including DEAD-box (DDX), DEAH-box (DHX) family members, and zinc finger-containing helicases (Table 7). Interestingly, results from MS identified RECQ1 belonging to the RecQ family of DNA helicases which is involved in unwinding DNA and/or DNA structures and has been reported to be integral for the maintenance of genome integrity in response to replication stress (Debnath and Sharma, 2020). Other proteins identified to potentially interact with ZFP36L1 included proteins involved in RNA splicing and of particular interest is the identification of THO complex subunit THOC1 a protein involved in the prevention of R-loops (Domínguez-Sánchez et al., 2011; Salas-Armenteros et al., 2017; Luna et al., 2019). Surprisingly, we found proteins involved in mismatch repair (MMR) pathways including MutL homologue 1 (MLH1) in FLAG-Strep II-ZFP36L1 eluates suggesting potential nuclear roles for ZFP36L1. Finally, other detected potential interactors of ZFP36L1 belonged to groups involved in translation, ribosome biogenesis and transcription. Overall, our results demonstrate potential novel protein interactors for ZFP36L1, some of which may elucidate potential mechanisms involved in maintaining genome integrity through the resolution of R-loops. Significant interactions that are relevant to the aims of the presented work have been listed in table 7 however, an extensive list reporting novel networks of ZFP36L1 can be found in Appendix D; Table 1.

Table 7. Table listing proteins present in FLAG-StrepII-ZFP36L1 eluates with a peptide score <1 in FLAG-EV control.

Function/Protein	Uni-Prot accession	Protein mass (Da)	Score^a	Matching peptides	Matching peptides (Flag-EV)
RNA degradation					
XRN1	Q8IZH2	195524	92	2	0
CNOT1	A5YKK6	269105	537	11	0
CNOT3	O75175	82049	128	3	0
CNOT10	Q9H9A5	83397	136	2	0
PAP1M	Q5JQF8	22955	122	3	0
PABP3	Q9H361	70214	536	16	0
LSM1	O15116	15170	100	3	0
RNA helicases					
DHX37	Q8IY37	130546	80	2	0
DDX18	Q9NVP1	75701	112	2	0
HELZ2	Q9BYK8	298285	152	3	0
ZNFX1	Q9P2E3	225102	195	3	0
DDX24	Q9GZR7	96898	71	2	0
HELZ	P42694	220600	376	11	0
DHX8	Q14562	140081	117	3	0
DNA helicases					
RECQ1	P46063	74436	210	3	0
SMCA4	P51532	185100	122	3	0
Mismatch repair					
MLH1	P40692	85175	137	3	0
RFC3 38 kDa subunit	P40938	41328	72	3	0
RNA splicing					

DHX8	Q14562	140081	117	3	0
SYF2	O95926	28761	86	2	0
THOC1	Q96FV9	76359	75	2	0
NCBP1	Q09161	92863	110	2	0
PPIL1	Q9Y3C6	18339	123	2	0
RU2B	P08579	25470	143	3	0
ZMAT2	Q96NC0	23768	100	2	0
Translation					
RM49	Q13405	19242	84	2	0
RL7L	Q6DKI1	29821	113	2	0
SYYM	Q9Y2Z4	53393	142	6	0
RT21	P82921	10909	123	2	0
RT10	P82664	23099	74	2	0
RM22	Q9NWU5	23796	136	2	0
RLA2	P05387	11657	403	9	0
RT05	P82675	48489	137	3	0
EI2BE	Q13144	81070	72	2	0
RM02	Q5T653	33564	174	2	0
AGO2	Q9UKV8	98400	167	5	0
RT18B	Q9Y676	29719	152	3	0
Ribosome biogenesis					
	Q8IZH2	195524	92	2	0
XRN1	Q13823	83831	76	2	0
NOG2	Q9NVN8	62467	155	3	0
GNL3	Q9BVJ6	88095	78	2	0
UT14A	Q969X6	77525	135	3	0
UTP4	Q9NRR4	160810	119	2	0
RNC					
Transcription					
RPB1					
RPB2	P24928	218407	127	4	0
RPAC1	P30876	135236	125	3	0
	O15160	39453	97	2	0

---

[a]Mascot protein score >70 was considered significant ($p < 0.05$) results are from two independent experiments (N=2).

8.3 Discussion

The literature surrounding protein interactors for ZFP36L1 has largely focused on its interactions with proteins involved in mRNA decay (Otsuka et al., 2020). Here we demonstrate for the first time, a framework that could be further extended to identify ZFP36L1's role in maintaining genome integrity and other important biological processes through novel protein interactions. Our results demonstrated successful expression of recombinant FLAG-Strep II-ZFP36L1 (Figure 8.2A) and enrichment following FLAG-IP in T-REx U-2OS ZFP36L1 KO cells (Figure 8.2B) enabling proteomic investigation through MS analysis. A total of 153 significant protein interactions with ZFP36L1 were identified through MS (Appendix D; Table 1). The interactome consisted of proteins belonging to different functional categories including RNA degradation, RNA and DNA helicases, MMR, RNA splicing, translation, ribosome biogenesis and transcription (Table 7). ZFP36L1 contains a CNOT1 binding domain that interacts directly with the CNOT1 core central subunit of CCR4-NOT poly (A) deadenylase, initiating deadenylation of mRNA and subsequent decay (Otsuka et al., 2020; Makita, Takatori and Nakajima, 2021). We show in this report that MS analysis of FLAG-Strep II-ZFP36L1 eluates contained subunits of the CCR4-NOT poly (A) complex (CNOT1, CNOT3 and CNOT10) and identified CNOT1 with the highest mascot score compared to other subunits (Table 7). Importantly, the identification of XRN1, which is involved in 5' to 3' mRNA decay and is also a well-known interactor of ZFP36L1 further validates the experimental approach (Lykke-Andersen and Wagner, 2005). We also identified a plethora of novel ZFP36L1 protein interactions some of which are important for the maintenance of genome integrity. Specifically, we identified peptides for THOC1, a key subunit of the THO complex that promotes RNP assembly and has been shown to inhibit unscheduled R-loop formation in order to maintain genome integrity (Domínguez-Sánchez et al., 2011; García-Benítez, Gaillard and Aguilera, 2017; Salas-Armenteros et al., 2017). Moreover, THOC1 depletion has been shown to induce R-loop dependent DNA damage and genomic instability (Domínguez-Sánchez et al., 2011; García-Benítez, Gaillard and Aguilera, 2017; Salas-Armenteros et al., 2017). Thus, potential interactions with THOC1 may present one potential mechanism for ZFP36L1's role in limiting R-loop-dependent replication stress and genome instability. DDX and DHX ATP-dependent RNA helicases belong to a large family of RNA processing factors involved in binding or remodelling RNA substrates, RNA secondary structures, or RNP complexes (Zhang and Li, 2021). Our results demonstrated that ZFP36L1 potentially interacts with multiple DDX and DHX ATP-dependent RNA helicases suggesting ZFP36L1's involvement in various aspects of RNA metabolism. Interestingly, many members of the DDX RNA helicases such as DDX1, DDX5, DDX21, DDX23 (Li et al., 2016; Song et al., 2017; Sridhara et al., 2017;(Mersaoui et al., 2019) and DHX RNA helicase DHX9 (Cristini et al., 2018) have been reported to resolve persistent R-loops to maintain genome integrity. Although we did not detect these members at significant levels, other members identified through MS such as DDX18, DDX24 and DHX37 have been reported to bind R-loops in human cells (Cristini et al., 2018; Wang et al., 2018; Mosler et al., 2021). We also found that ZFP36L1 potentially interacts with the RecQ family of DNA helicase member RECQ1 which is reported to be enriched at stalled replications forks at CFS loci following APH treatment (Lu et al., 2013). Moreover, RECQ1 depletion sensitises cells to DNA damage and chromosomal fragility in APH-induced replication stress conditions, thus highlighting a potential mechanism for increased DNA damage and chromosomal aberrations in ZFP36L1 ablated cells (Lu et al., 2013). Although beyond the scope of this study, interaction with MLH1 further strengthens a role for ZFP36L1 in the maintenance of genome integrity, due to MLH1's predominant role in the MMR pathway (Cannavo et al., 2007). We have elucidated both previously established and potential novel interactors for ZFP36L1, while our approach minimises false identification of non-specific interactors by utilising EV control groups, it is possible that some non-specific proteins are still identified. Therefore, follow-up investigations utilising co-IP followed by western blot for detection of proteins identified by MS are required to validate ZFP36L1 protein interactions reported in this study. Moreover, adapting this method to assess potential ZFP36L1 protein interactions described in the study under conditions of replication stress could uncover mechanisms associated with the maintenance of genome stability. Nonetheless, the detection of the proteins involved in deterring R-loop formation and maintenance of genome integrity even in unperturbed conditions presents a novel insight into potential pathways that may be abrogated in the absence of ZFP36L1.

9. General discussion

Cells are in a constant battle to ensure correct genome duplication and faithful transmission of genetic information to progeny cells. Processes that impede the timely progression of DNA replication machinery such as replication stress can prove deleterious to genomic integrity resulting in chromosomal breaks and recombination events observed in cancers (Gaillard, García-Muse and Aguilera, 2015; Macheret and Halazonetis, 2015). Furthermore, DNA structures such as R-loops are a major source of replication stress leading to genomic instability. Evidence has implicated AU-RBPs in the maintenance of genome integrity and has recently been highlighted to interact with or deter the formation of R-loops (Cristini et al., 2018; Wang et al., 2018; Alfano et al., 2019), thus presenting potential mechanisms for their emergence as key players in the maintenance of genome stability (Chapter 1). In line with the emerging roles of AU-RBPs in genome maintenance, this study aimed to uncover a role for ZFP36L1 in maintaining genome integrity during episodes of replication stress. Here, we have provided several lines of evidence for ZFP36L1's role in maintaining genome integrity by limiting replication stress-induced genomic instability and potential R-loop accumulation that could be extended to understand its potential role in human diseases such as cancers (Figure 9).

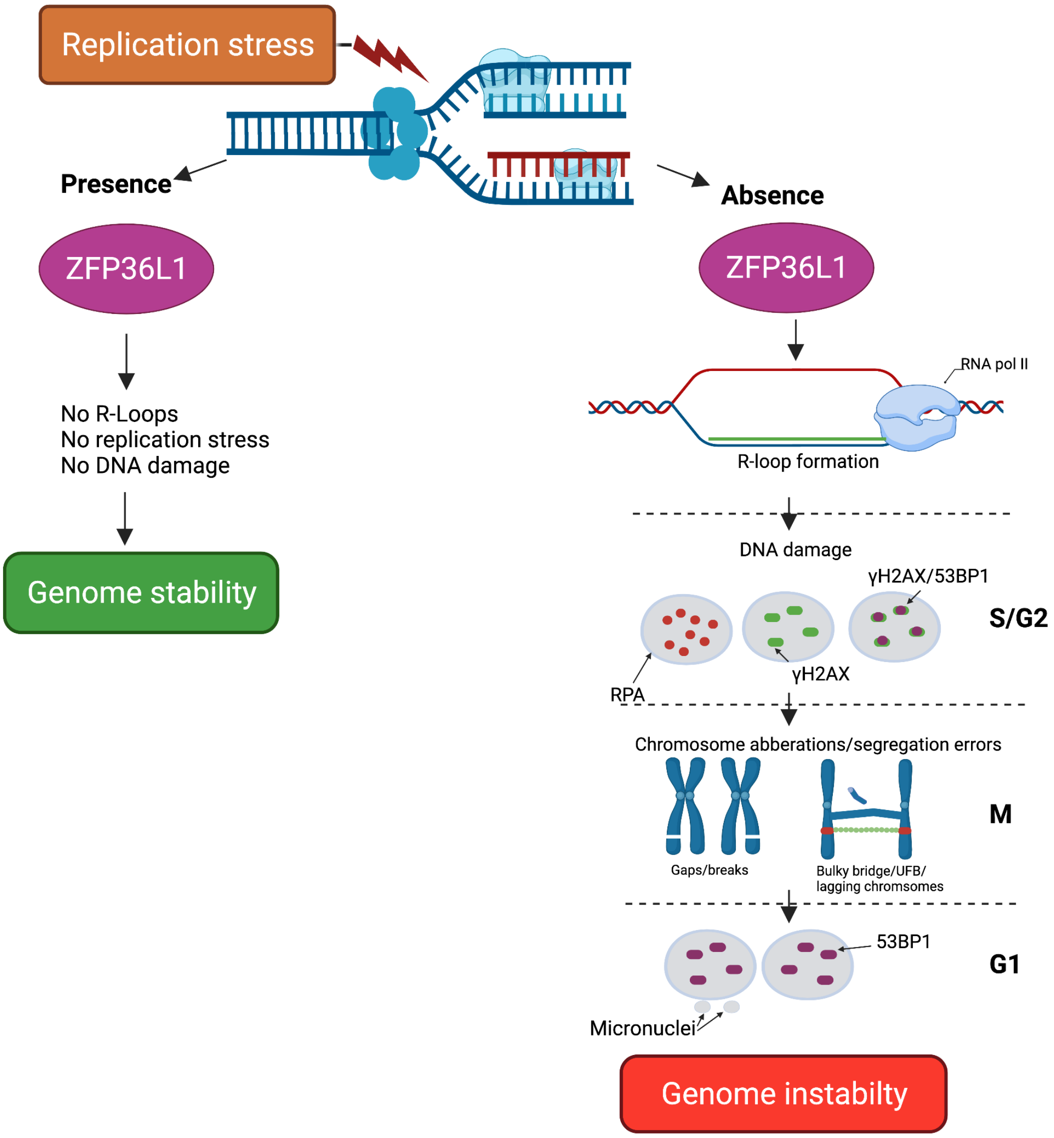
Replication stress
Presence
Absence
ZFP36L1
ZFP36L1
No R-Loops
No replication stress
No DNA damage
Genome stability
RNA pol II
R-loop formation
DNA damage
γH2AX/53BP1
S/G2
RPA
γH2AX
Chromosome abberations/segregation errors
M
Gaps/breaks
Bulky bridge/UFB/
lagging chromsomes
53BP1
G1
Micronuclei
Genome instabilty

Figure 9. Proposed model for ZFP36L1's role in maintaining genome integrity in conditions of replication stress.
In ZFP36L1's presence, the formation of R-loops is suppressed thus limiting replication stress and DNA damage leading to genome stability. Loss of ZFP36L1 leads to the formation of R-loops which is further exacerbated under conditions of replication stress. When R-loops remain unresolved they can lead to DNA damage in the S/G2 phase, chromosomal aberrations/segregation errors in M-phase and micronuclei and 53BP1 NB formation in the subsequent G1 phase leading to genome instability.

We first set out to develop a model system to study the role of ZFP36L1 in maintaining genome integrity during episodes of mild replication stress. We created a ZFP36L1 ablated T-REx U-2OS system utilising CRISPR-Cas9 technology. For this purpose, we utilised the all-in-one CRISPR plasmid to target exon 2 of the *ZFP36L1* gene

(Figure 3.2-3.3). Our approach resulted in high editing efficiency (>85%) as indicated by PCR amplification and NGS analysis of the *ZFP36L1* target site (Figure 3.4). Importantly, these observations corresponded to changes in ZFP36L1 protein expression following western blot analysis (Figure 3.5). We were able to generate a clone that demonstrated no detectable ZFP36L1 expression suggesting successful CRISPR-Cas9 disruption of the *ZFP36L1* target locus which was further verified by NGS amplicon sequencing (Figure 3.6). Sequence reads generated by amplicon sequencing demonstrated that 99.53% of reads were modified and corresponded to heterozygous mutations leading to ablation of ZFP36L1 expression (Figure 3.6). Thus, for the first time in literature, we were able to successfully target and abolish ZFP36L1 expression in a T-REx U-2OS system. Importantly, this cellular model enabled controlled re-expression of recombinant ZFP36L1. We found that loss of ZFP36L1 significantly reduced cell growth in T-REx U-2OS cells (Figure 3.7). Recent evidence supporting our observations shows that CRISPR-Cas9 mediated ablation of ZFP36L1 in chronic myeloid leukaemia cells negatively impacts cell growth (Kaehler et al., 2021). Although this is the only report to date that assesses cell growth through CRISPR-Cas9 permanent disruption of ZFP36L1 expression, transient knockdown of ZFP36L1 showed a contrasting effect on cellular proliferation. shRNA or siRNA-mediated knockdown of ZFP36L1 in human colorectal cancer cells or bladder cancer cells respectively increased cellular proliferation (Suk et al., 2018; Loh et al., 2019). How loss of ZFP36L1 impacts cell growth is beyond the scope of this study, however, we speculate that one of the reasons might be associated with ZFP36L1's ability to regulate proteins that control cell cycle progression through post-transcriptional control of mRNA stability. Future work could assess cell cycle progression in ZFP36L1 ablated T-REx U-2OS cells or asses for changes in cell cycle-related mRNAs such as *cyclin*

D or *CDKN1A* which are known targets of ZFP36L1 which would enable a better understanding between ZFP36L1's role in cellular proliferation (Suk et al., 2018; Kaehler et al., 2021).

Secondly, replication stress-associated DNA lesions that remain unresolved in mitosis have been demonstrated to lead to defects in chromosome segregation and genomic instability (Gan et al., 2011). We investigated the impact of the loss of ZFP36L1 by assessing for phenotypic markers of mitotic defects and genomic instability (Chapter 4). We demonstrated that loss of ZFP36L1 increases the prevalence of chromosomal aberrations (Figure 4.2) and segregation errors in the form of DAPI-stained bulky bridges and lagging chromosomes (Figure 4.3) which were further exacerbated under replication stress conditions. Replication stress has been demonstrated to exacerbate conditions within intrinsically unstable genomic loci known as CFS leading to gaps and breaks on metaphase chromosomes in multiple cancer types, we, therefore, speculated that the observed chromosomal aberrations could correlate to increased CFS instability in the absence of ZFP36L1 (Durkin et al., 2006; Chan et al., 2009; Di Marco et al., 2017; Helmrich, Ballarino and Tora, 2011; Hamperl et al., 2017). To this end, we assessed the formation of a distinct type of anaphase bridge known as UFBs that are marked by FANCD2 foci that arise intrinsically unstable CFS loci and are enriched at stalled replication forks (Chan et al., 2009; Sirbu et al., 2013). Our results demonstrated that loss of ZFP36L1 increased the prevalence of FANCD2-associated UFBs which was exacerbated in mild replication stress conditions with no effect on centromeric UFBs suggesting that loss of ZFP36L1 potentially increases replication stress at CFS loci leading to replication fork stalling (Figure 4.4). When segregation defects remain unresolved, they can be converted into 53BP1 NBs in the subsequent

G1 phase or lead to the formation of micronuclei, a maker of CIN and genomic instability (Okamoto et al., 2018). We provided evidence that loss of ZFP36L1 induces the accumulation of both micronuclei (Figure 4.5) and 53BP1 NBs (Figure 4.6) which are exacerbated in mild replication stress conditions. Together, this provides evidence that under replication stress conditions loss of ZFP36L1 induces the increased prevalence of chromosomal segregation errors that are transmitted to G1-phase cells as lesions where they are shielded in 53BP1 NBs or form as micronuclei, thus leading to genomic instability.

AU-RBPs ZFP36, AUF1 and TIAR have emerged as key players in maintaining chromosome integrity in response to replication stress or DNA damage. Specifically, loss of ZFP36, AUF1 and TIAR was shown to increase susceptibility to chromosomal aberrations (Pont et al., 2012; Lafarga et al., 2018; Alfano et al., 2019; Lee et al., 2020). In the case of ZFP36 and AUF1 aberrations on metaphase chromosomes were attributed to defects in DNA repair pathways (Alfano et al., 2019; Lee et al., 2020), whereas mild replication stress in TIAR deficient Hela cells induced chromosomal aberrations due to unprocessed lesions entering mitosis (Lafarga et al., 2018). Strikingly, TIAR loss was also found to lead to chromatid bridging in anaphase in response to low doses of APH (Lafarga et al., 2018). Taken together, this suggests that ZFP36L1 may exhibit functions closer to TIAR than ZFP36 and AUF1 in respect to suppressing the entry of lesions into mitosis that lead to chromosomal segregation errors.

The molecular mechanisms associated with ZFP36L1 loss resulting in FANCD2-associated UFBs presented an opportunity for further insight into its role in maintaining genomic integrity. Importantly, reports have implicated FANCD2 to be required for efficient replication of the genome dependent on R-loop resolution in response to replication stress (García-Rubio et al., 2015; Schwab et al., 2015). Moreover, FANCD2 is important to maintain CFS stability protecting replication fork stalling at CFS loci FRA16D and FRA6E and its deficiency increased R-loops at CFS (Howlett et al., 2005; Madireddy et al., 2016). Thus, taken together these reports suggest that ZFP36L1 could be important for the maintenance of CFS stability and genome integrity by limiting the accumulation of R-loop structures. Interestingly, mild replication stress conditions in TIAR defective cells were reported to increase replication fork stalling and accumulation of FANCD2 foci (Lafarga et al., 2018). Moreover, TIAR has been reported to interact with R-loops in human cells (Cristini et al., 2018; Wang et al., 2018). Therefore, this implies that ZFP36L1 may be involved in limiting the occurrence of such structures that are susceptible to forming at intrinsically unstable CFS loci leading to genomic instability.

Thirdly, multiple studies have elucidated the occurrence of replication stress-induced chromosome segregation errors to be associated with DNA lesions or structures in the S-phase that remain unresolved at the onset of mitosis (Ichijima et al., 2010; Chan, Fugger and West, 2017). To this end, we investigated if loss of ZFP36L1 resulted in replication stress-induced DNA damage (Chapter 5). Consistent with our observations associating loss of ZFP36L1 to increased chromosome segregation errors in mitosis, we found that loss of ZFP36L1 increases S/G2 phase-related RPA (Figure 5.2) and γH2AX (Figure 5.3) the surrogate markers of ssDNA and DNA damage respectively. In ZFP36L1 ablated cells the prevalence of both RPA and γH2AX foci increased in response to APH-induced replication stress suggesting that ZFP36L1 is required to suppress the formation of ssDNA and DNA damage. Moreover, we associated the increase in RPA and γH2AX foci with increased incidence of DSBs as demonstrated through increased 53BP1 and γH2AX colocalisation (Figure 5.4) under conditions of mild replication stress suggesting ZFP36L1 is required to limit the formation of DSBs. Importantly, we cannot exclude that DSBs are formed as an active process of nucleolytic cleavage to mediate DNA repair and not because of fork collapse (Pepe and West, 2014). However, mechanisms that underly DSBs formed following nucleolytic cleavage also arise from stalled replication forks (Pepe and West, 2014). Thus, taken together we implicate ZFP36L1 to protect cells from replication stress-associated DNA damage and subsequent DSB formation.

In line with this potential protective role for ZFP36L1 against DSB formation, AU-RBPs ZFP36, TIAR, AUF1 and HuR have been reported to suppress the formation of DSBs through distinct pathways (Lafarga et al., 2018; Alfano et al., 2019; Lee et al., 2020; Jain et al., 2022). Perhaps the most closely related indicator for ZFP36L1 ‘s role in limiting replication stress-associated DSBs was elucidated in ZFP36 deficient cells that displayed increased 53BP1 and γH2AX colocalisation in response to HU and cisplatin-induced replication stress (Lee et al., 2020). However, the mechanisms associated with replication stress in HU or cisplatin conditions are vastly different to that of low-dose APH (Vesela et al., 2017), suggesting a distinct mechanism associated with ZFP36L1’s role in the maintenance of genomic integrity in comparison to ZFP36. Recent evidence from our collaborator utilising chromatin immunoprecipitation (ChIP) indicates that loss of ZFP36L1 results in the enrichment of RPA, γH2AX and 53BP1 at CFS loci FRA3B, FRA16D and FRA7H (Solaiman et al, manuscript under progress).

Importantly, the degree of DNA damage has been demonstrated to correlate with S-phase progression, resulting in the slowing of replication to coordinate DNA repair (Willis and Rhind, 2009). Cell cycle analysis demonstrated loss of leads to accumulation of cells in the S-phase following APH-induced replication stress further supporting observations of S-phase related DNA damage (Figure 5.5 A and B). Moreover, loss of ZFP36L1 only slightly increased CHK1 phosphorylation in mild replication conditions, indicative of a functional replication stress response in ZFP36L1 ablated cells (Figure 5.5C). Our results are supported by reports implicating APH-induced replication stress in U-2OS cells to increase the number of cells in the S-phase and induce low levels of CHK1 S345 phosphorylation, without resulting in cell cycle arrest (Courtot et al., 2021). Nonetheless even in the presence of CHK1 activation cells can enter mitosis with unrepaired DNA resulting in chromosomal instability (Lebrec et al., 2022), therefore, lesions may remain unrepaired during S-phase where they enter mitosis resulting in mitotic defects and genome instability. This is further supported by our results demonstrating that APH-induced replication stress in ZFP36L1 KO cells did not result in apoptosis (Figure 5.6). Thus, taken together we speculate that CHK1 activation initiates DNA repair mechanisms in S-phase to suppress cells from undergoing apoptosis (Gagou, Zuazua-Villar and Meuth, 2010).

In this study, we demonstrate ZFP36L1 bound to chromatin fractions in human cells (Figure 5.7A) both in the presence and absence of APH-induced replication stress conditions (Figure 5.7C). Moreover, we found that replication stress potentially increases ZFP36L1 chromatin binding as observed through increased expression of ZFP36L1 in chromatin fractions and a reduction of ZFP36L1 expression in cytoplasmic containing soluble fractions (Figure 5.7C). Overall, these results suggested the potential translocation of ZFP36L1 from the cytoplasm to the nucleus under conditions of replication stress. Although, we were able to detect ZFP36L1 in RNase A treated chromatin fractions, we cannot exclude that ZFP36L1 may be bound to chromatin through RNA interactions as RNase A has no activity on RNA that is hybridised to DNA (Huertas and Aguilera, 2003). The significance of ZFP36L1's chromatin binding ability is currently unknown; however, MS data from this study has elucidated that ZFP36L1 potentially interacts with histone proteins (Appendix D; Table1). Furthermore, reports have revealed that proteins containing zinc fingers are enriched on chromatin proximal to R-loops (Yan et al., 2022). Therefore, these findings present further opportunities to identify novel ZFP36L1 interactions within the nucleus.

In this study, we were able to demonstrate that the observed phenotypes associated with CRISPR-Cas9 mediated ablation of ZFP36L1 were due to specific targeting of ZFP36L1 (Chapter 6). Specifically, we were able to generate a stable system for controlled tetracycline-induced expression of exogenous ZFP36L1 in ZFP36L1 KO cells (Figures 6.2). Utilising this stable system, we first demonstrated that the inducible expression of ZFP36L1 limited the formation of micronuclei in APH-induced replication stress conditions (Figure 6.3). These findings were further extended to a reduction of G1-associated 53BP1 NBs following tetracycline-induced expression of ZFP36L1 (Figure 6.4). Importantly, the increased prevalence of micronuclei and 53BP1 NBs in untreated conditions were also reduced to WT levels suggesting that ZFP36L1 is required in the event of endogenous replication stress conditions. In agreement with the specificity of our ZFP36L1 KO system, siRNA-mediated knockdown of ZFP36L1 in U-2OS, Hela and MCF-7 cells increased the frequency of G1-associated 53BP1 in unperturbed and APH-induced replication stress conditions (Solaiman et al, manuscript under progress).

R-loops can lead to replication stress and if unresolved these R-loop structures can result in DNA damage and genomic instability (Gan et al., 2011; Helmrich, Ballarino and Tora, 2011; Sollier et al., 2014; Costantino and Koshland, 2018). Importantly, highly transcribed regions or CFS loci have been attributed to an increase in R-loops and their presence at these sites has been attributed to the FA pathway (García-Rubio et al., 2015). (Helmrich, Ballarino and Tora, 2011). Specifically, FANCD2 has been reported to protect replication forks from stalling when they encounter R-loops, suppressing DNA damage formation (García-Rubio et al., 2015). Since our results implicated potential CFS instability through observations of chromosomal aberrations and FANCD2-associated UFBs, we speculated if the associated phenotypic abnormalities in ZFP36L1 ablated cells were due to unscheduled R-loop formation. Our results demonstrate for the first time a potential link between loss of ZFP36L1 and replication stress-associated R-loop formation that potentially leads to increased susceptibility to genomic instability (Chapter 7). Overexpression of GFP-RNase H1 D210N in ZFP36L1 abolished cells, revealed a significant increase in R-loop formation in unperturbed and APH-induced replication stress conditions (Figure 7.2). Thus, these results indicated that ZFP36L1 is required to limit the formation of R-loops in response to mild replication stress. Importantly, our approach to detecting R-loops through GFP-RNase H1 D210N has been extensively utilised to visualise R-loops in human cells by fluorescent microscopy (Bhatia et al., 2014; Britton et al., 2014; Nguyen et al., 2017; Nascakova et al., 2021). Due to the increased presence of replication stress-associated R-loops in ZFP36L1 cells, we speculated that if unresolved they could prove deleterious to genome integrity resulting in the observed phenotype associated with loss of ZFP36L1. Supporting increased R-loops as a cause of increased replication stress, R-loop resolution in ZFP36L1 abolished cells suppressed the formation of G1 associated 53BP1 NBs (Figure 7.3) and RPA foci in S/G2 cells in unperturbed and under APH-induced replication stress conditions (Figure 7.4). Significantly, overexpression expression of catalytically inactive RNase H1 D210N did not reduce the prevalence of 53BP1 NBs (Figure 7.3) or RPA (Figure 7.4). Taken together, our results indicate that increased R-loops pose a potential block to replication fork progression leading to an increase in ssDNA formation in S/G2 cells. In line with our findings reports mapping interactions with R-loops have demonstrated the interaction of AU-RBPs TIAR, KSHRP, HuR and AUF1 with R-loops in human cells (Cristini et al., 2018; Wang et al., 2018). Specifically, depletion of AUF1 was shown to increase the formation of R-loops impairing DNA repair and resulting in genomic instability, however, resolution of R-loops in AUF1 depleted cells overexpressing RNase H1 was shown to rescue DNA repair mechanisms, suggesting R-loops were a major cause of DNA repair deficiencies (Alfano et al., 2019).

Finally, we highlight novel protein interactions for ZFP36L1 through IP-MS some of which have reported function in the maintenance of genome integrity and deterring unscheduled R-loop formation (Chapter 8). Our approach identified known interactors of ZFP36L1 involved in RNA degradation including CNOT1 and XRN1 and highlighted novel interactions with proteins involved in RNA splicing, RNA helicases and proteins involved in translation. Interestingly, some of the proteins identified through MS such as THOC1 have been highlighted as a key factor in suppressing R-loop-dependent genomic instability (Luna et al., 2019). Moreover, the detection of ATP- dependent

RNA helicases such as the DDX and DHX family with reported function in R-loop removal to prevent replication stress and genomic instability (Hodroj et al., 2017), presents further opportunity to understand the molecular mechanisms by which ZFP36L1 maintains genomic instability. Although interactions between these identified proteins need to be further explored particularly under replicative stress conditions, we speculate that ZFP36L1 could form protein interactions required for the suppression of deleterious R-loops. Therefore, further characterising protein interactions identified in this study could elucidate the molecular mechanisms associated with ZFP36L1's role in suppressing replication stress-associated genomic instability.

10. Conclusion and future work

Our findings have provided multiple lines of evidence supporting the emerging roles of AU-RBPs as key players in the maintenance of genome integrity. We have demonstrated a clear link between loss of ZFP36L1 and replication stress-associated chromosomal segregation errors, DNA damage and genomic instability. We further provide evidence for the increased prevalence of R-loops that we suspect are a major cause of the defects associated with the loss of ZFP36L1. Therefore, we speculate that ZFP36L1 could be an important regulator deterring the formation of unscheduled R-loops that pose a threat to genome integrity. How ZFP36L1 deters the formation of R-loops is unclear. However, our findings demonstrating ZFP36L1 to potentially interact with proteins with known function in R-loop homeostasis presents an interesting area of future work. Further characterising these interactions through Co-IP or demonstrating ZFP36L1's ability to colocalise with these proteins at sites of replication stress-induced DNA damage could reveal the molecular mechanisms associated with the maintenance of genome integrity under conditions of replication stress. Collectively, our results have elucidated ZFP36L1's integral role in suppressing replication stress-associated genomic instability that can be extended to understand its function as a novel tumour suppressor highlighted in multiple cancer types, with the potential to act as a future therapeutic target.

11. Appendices

Appendix A

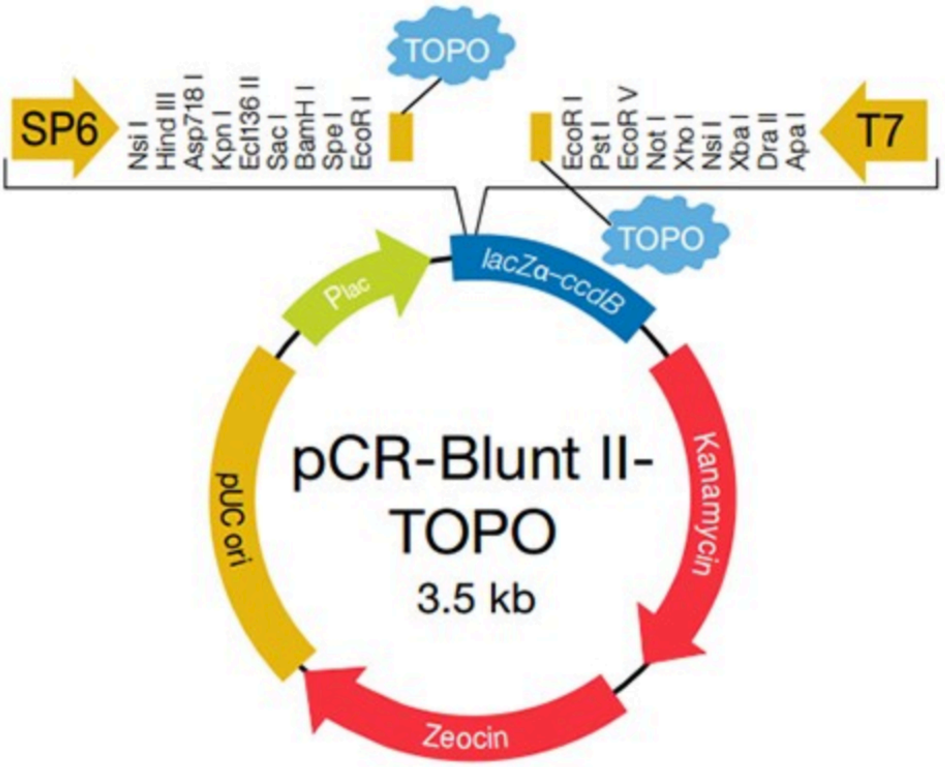
SP6
Nsi I
Hind III
Asp718 I
Kpn I
Ecl136 II
Sac I
BamH I
Spe I
EcoR I
TOPO
TOPO
EcoR I
Pst I
EcoR V
Not I
Xho I
Nsi I
Xba I
Dra II
Apa I
T7
Plac
lacZα-ccdB
Kanamycin
Zeocin
pUC ori
pCR-Blunt II-TOPO
3.5 kb

Figure 1 Vector map for pCR-Blunt II-TOPO
pCR-Blunt II-TOPO contains covalently bound topoisomerase I (TOPO) for cloning of blunt-ended PCR products flanked by EcoRI sites. Kanamycin-resistant gene enabled antibiotic selection in *E.coli*. Vector image from Thermofisher scientific.

Appendix B

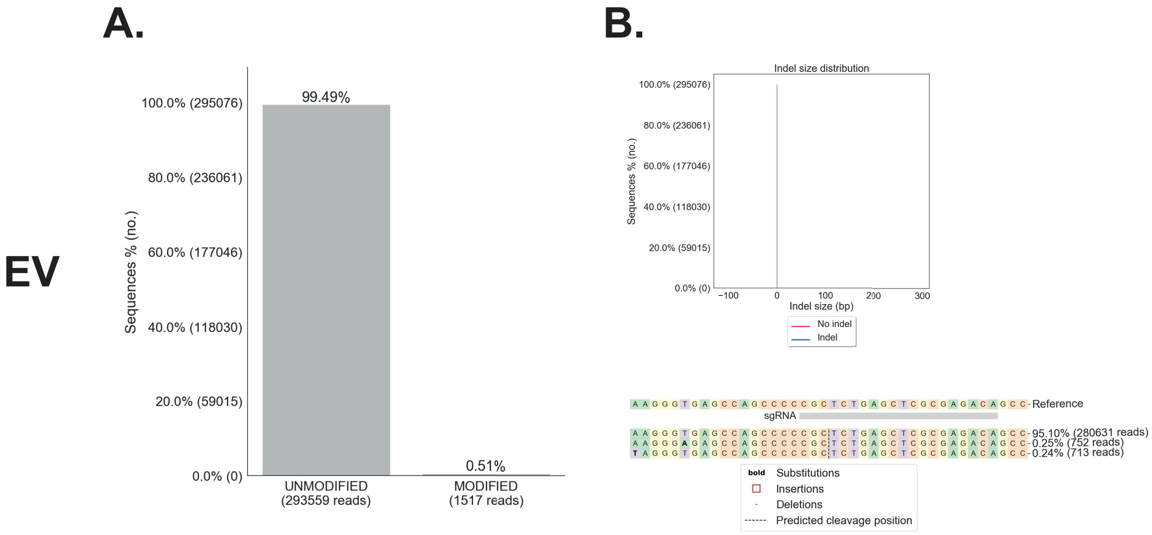

Figure 1 NGS analysis of T-REx U-2OS empty vector-transfected clone

A. CRISPresso2 generated alignment and editing frequency determined by the percentage and number of sequence reads with unmodified/modified alleles from the empty vector (EV) transfected T-REx U-2OS cells. **B.** Indel distribution and visualisation of identified alleles around gRNA cleave site from EV transfected cells (Clement et al., 2019).

Appendix C

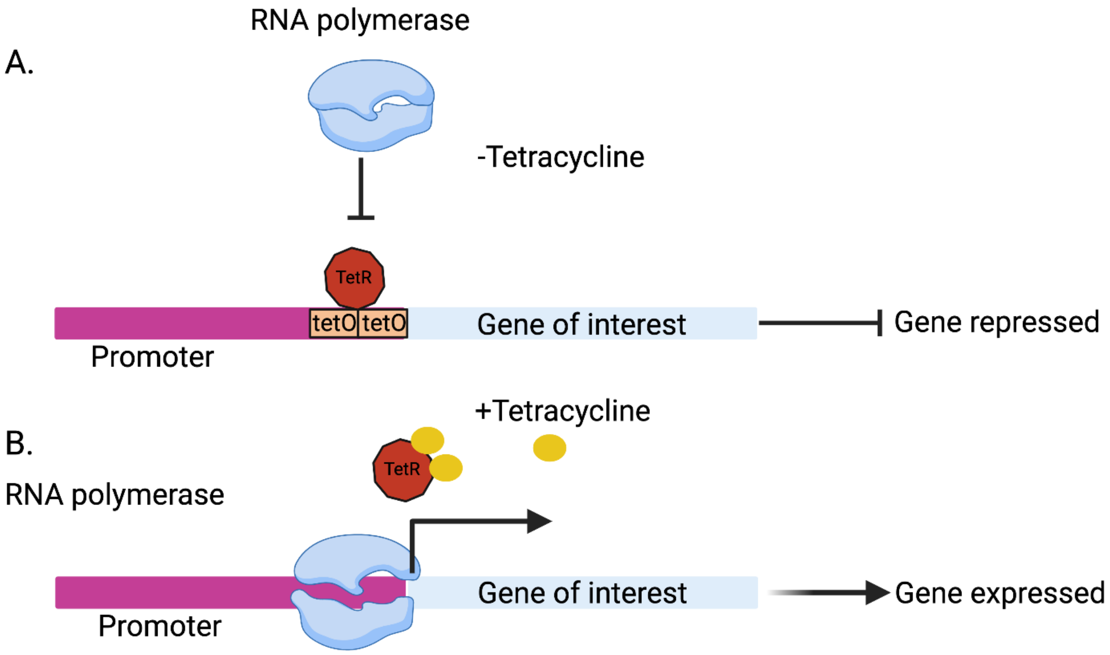
A.
RNA polymerase
-Tetracycline
TetR
tetO
tetO
Gene of interest
Gene repressed
Promoter
B.
+Tetracycline
RNA polymerase
TetR
Gene of interest
Gene expressed
Promoter

Figure 1 Mechanism of gene repression and expression utilising the T-REx system. A. In the absence of tetracycline (-tetracycline), the tetracycline repressor (TetR) binds the tetracycline operator (tetO) sites within a promoter with high affinity inhibiting transcription of a gene of interest by RNA polymerase and subsequent gene expression. **B**. In the presence of tetracycline (+Tetracycline), TetR binds to tetracycline causing dissociation from the tetO sites enabling RNA polymerase to mediate transcription of a gene of interest and subsequent gene expression (Created with Biorender.com).

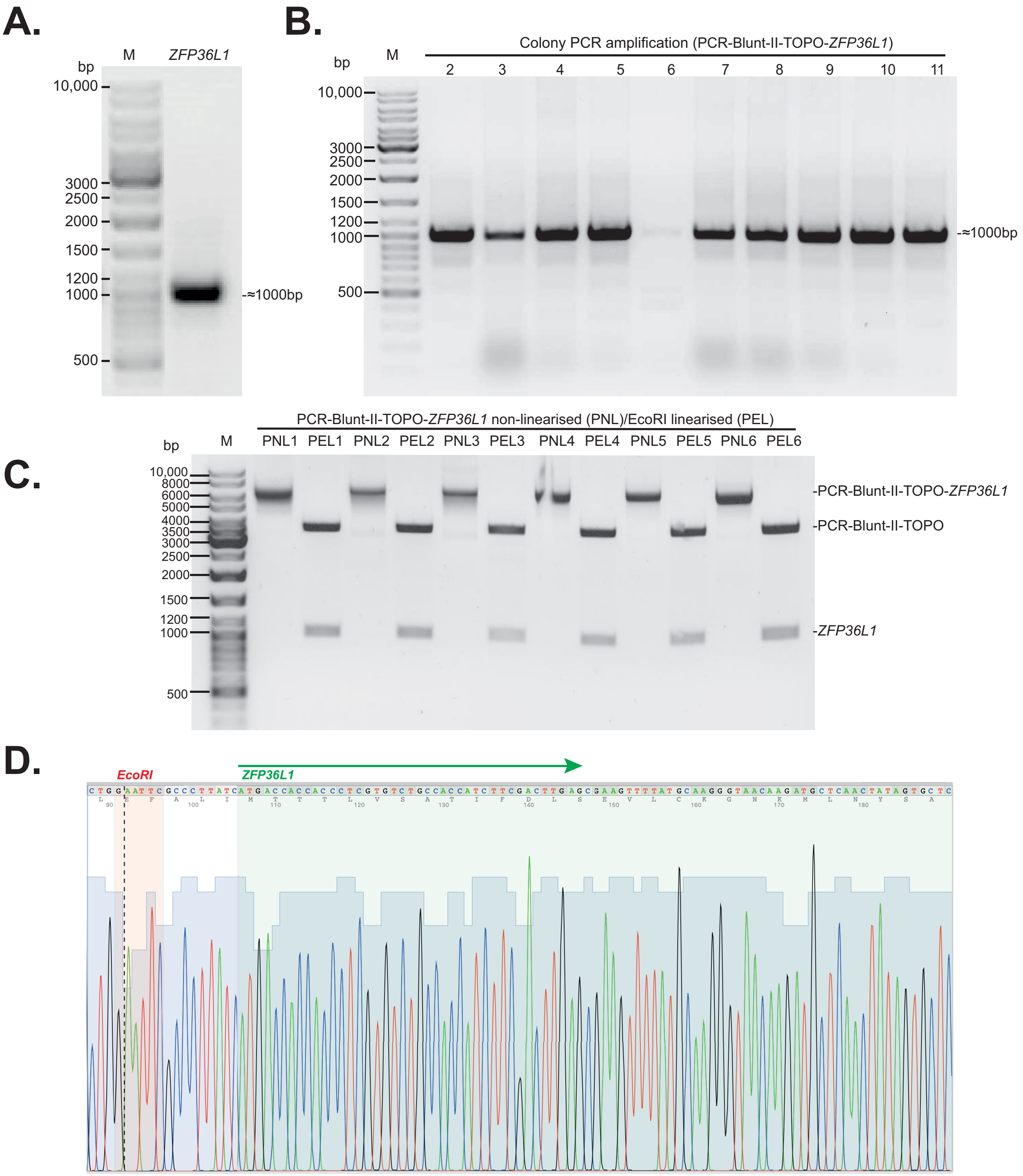

Figure 2 PCR-Blunt II-topo-ZFP36L1 construction and sequence verification. **A.** PCR amplification of *ZFP36L1* ORF (1017bp) from PCDNA6-His-ZFP36L1~1000bp. **B**. Colony PCR amplification of *ZFP36L1* from *E.coli* transformed with PCR-Blunt-II-topo-*ZFP36L1*, exhibiting a DNA fragment of approximately 1000bp. **C**. Gel electrophoresis of non-linearised PCR-Blunt II-topo-*ZFP36L1* (PNL1-6) with EcoRI digested PCR-Blunt II-topo-*ZFP36L1* (PEL1-6) releasing the *ZFP36L1* insert Maker (M) corresponds to a 10,000 bp DNA ladder. **D**. Chromatogram from Sanger sequencing of PCR-Blunt II-topo-*ZFP36L1* demonstrating successful insertion *ZFP36L1* with a start codon (indicated by green arrow and box) within EcoRI cloning site (Red box).

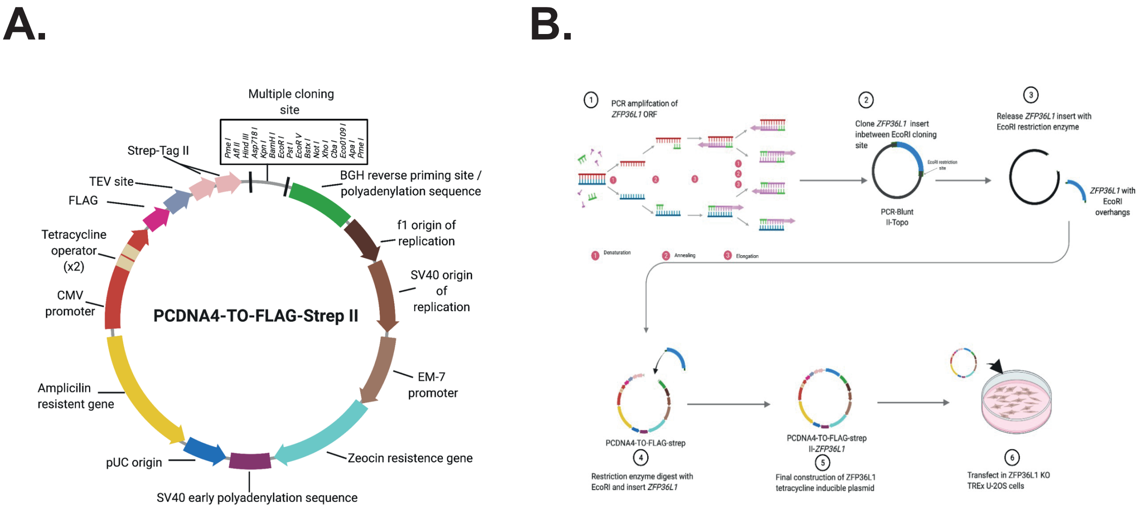
A.
Multiple cloning site
Pme I
Afl II
Hind III
Asp718 I
Kpn I
BamH I
EcoR I
Pst I
EcoR V
Bstx I
Not I
Xho I
Cba I
Eco0109 I
Apa I
Pme I
Strep-Tag II
TEV site
FLAG
Tetracycline operator (x2)
CMV promoter
BGH reverse priming site / polyadenylation sequence
f1 origin of replication
SV40 origin of replication
PCDNA4-TO-FLAG-Strep II
EM-7 promoter
Amplicilin resistent gene
Zeocin resistence gene
pUC origin
SV40 early polyadenylation sequence
B.
① PCR amplifcation of ZFP36L1 ORF
② Clone ZFP36L1 insert inbetween EcoRI cloning site
EcoRI restriction site
PCR-Blunt II-Topo
③ Release ZFP36L1 insert with EcoRI restriction enzyme
ZFP36L1 with EcoRI overhangs
1 Denaturation
2 Annealing
3 Elongation
PCDNA4-TO-FLAG-strep
④ Restriction enzyme digest with EcoRI and insert ZFP36L1
PCDNA4-TO-FLAG-strep II-ZFP36L1
⑤ Final construction of ZFP36L1 tetracycline inducible plasmid
⑥ Transfect in ZFP36L1 KO TREx U-2OS cells

Figure 3 Subcloning of a ZFP36L1 inducible expression plasmid. A. Vector map for PCDNA4-TO-FLAG-Strep II. **B.** Experimental workflow including steps 1-6 for subcloning *ZFP36L1* ORF into PCDNA4-TO-FLAG-Strep II. (1) *ZFP36l1* ORF is PCR amplified utilising Q5 DNA polymerase. (2) *ZFP36L1* insert is cloned in between the EcoRI cloning site of PCR-Blunt II-Topo. (3) *ZFP36L1* insert is released utilising EcoRI restriction enzyme generating a *ZFP36L1* insert with EcoRI overhangs compatible for insertion within an EcoRI cloning site. (4) PCDNA4-TO-FLAG-Strep II is digested with EcoRI enabling insertion of the *ZFP36L1*. (5) and (6) Completed PCDNA4-TO-FLAG-Strep II-*ZFP36L1* construct which can be transfected into ZFP36L1 KO T-REx-U-2OS cells for genetic complementation (Created with Biorender.com).

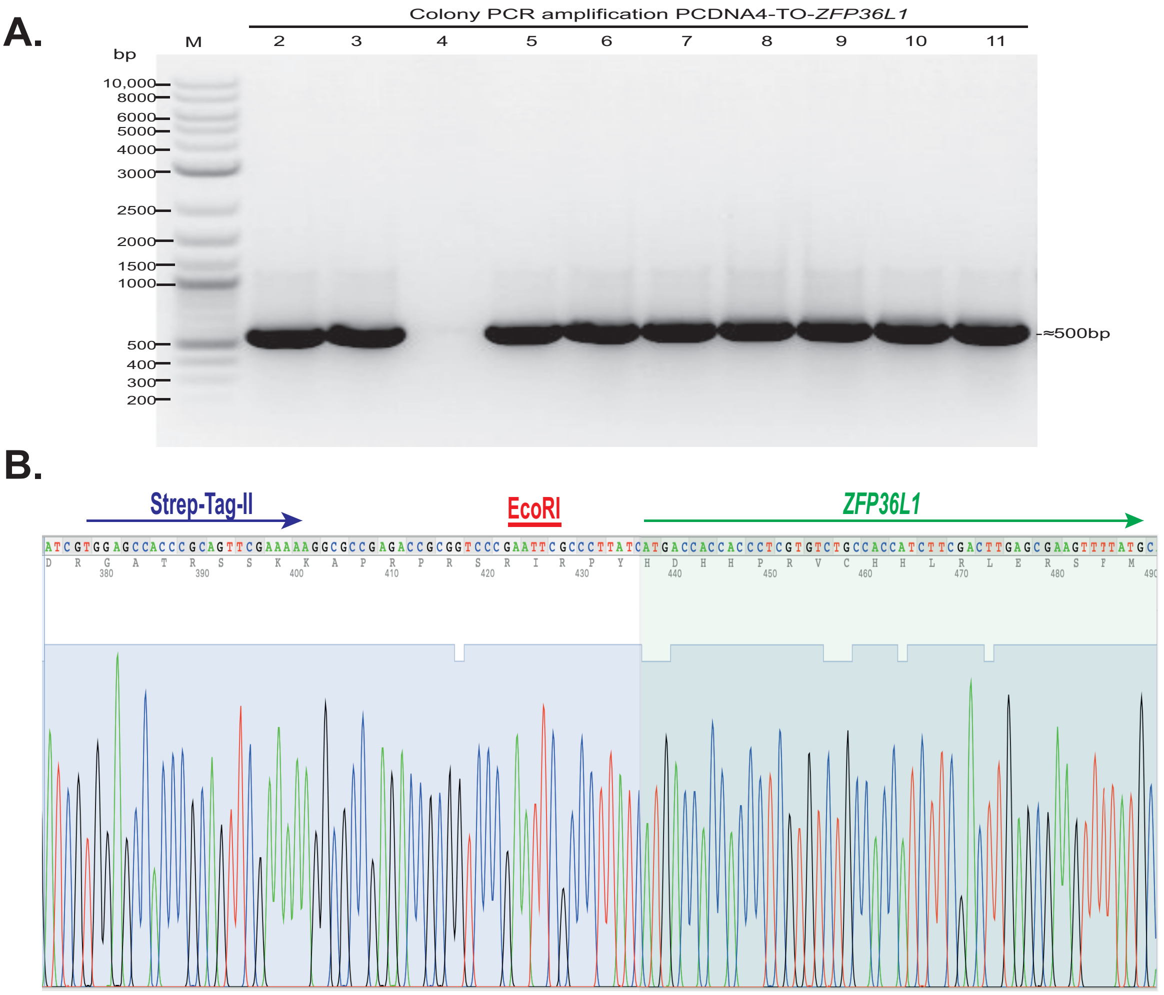

Figure 4 Sequence validation of PCDNA4-TO-FLAG-Strep II-ZFP36L1.
A. PCR amplification of the first 500bp of *ZFP36L1* from *E.coli* transformed with PCDNA4-TO-FLAG-Strep II-*ZFP36L1*, exhibiting a DNA fragment of approximately 500bp. **B**. Chromatogram from Sanger sequencing of PCDNA4-TO-FLAG-Strep II-*ZFP36L1* demonstrating successful insertion *ZFP36L1* with indicated start codon (green arrow and box) downstream of Strep-Tag-II (Purple arrow) and EcoRI cloning site (Red line).

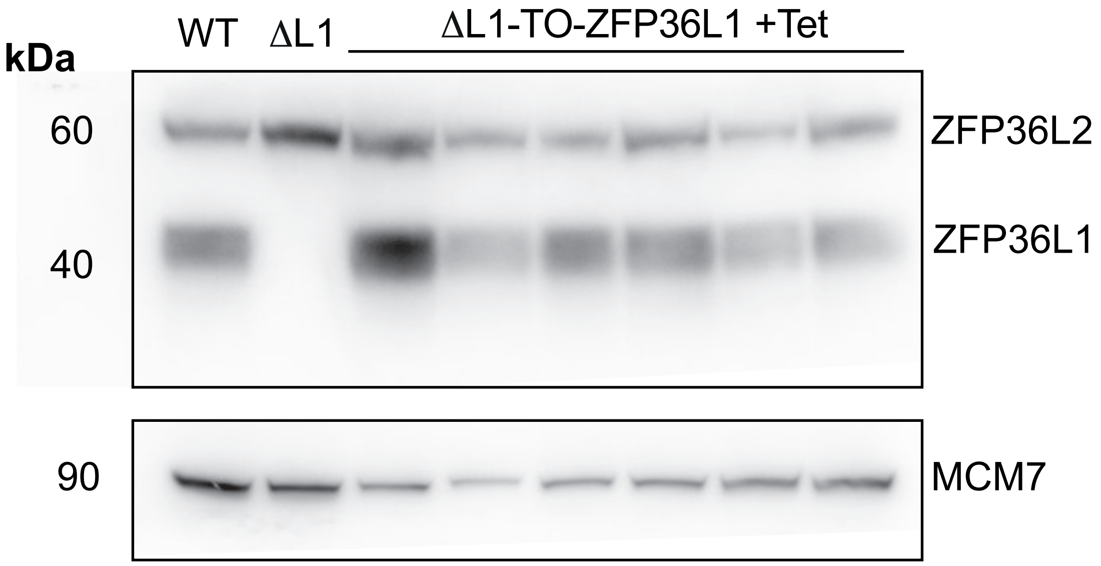
WT
ΔL1
ΔL1-TO-ZFP36L1 +Tet
kDa
60
40
90
ZFP36L2
ZFP36L1
MCM7

Figure 5 Monoclonal screen for stable tetracycline induction of ZFP36L1

A. Western blot analysis of ZFP36L1 (40 kDa) and ZFP36L2 (60 kDa) from WT, ΔL1-T-REx and ΔL1-T-REx clones stably expressing inducible ZFP36L1 (ΔL1-TO-ZFP36L1). Western blot results indicated the addition of tetracycline (+Tet) induced expression of ZFP36L1 in all ΔL1-TO-ZFP36L1 clones. MCM7 (90Kda) was used as a loading control

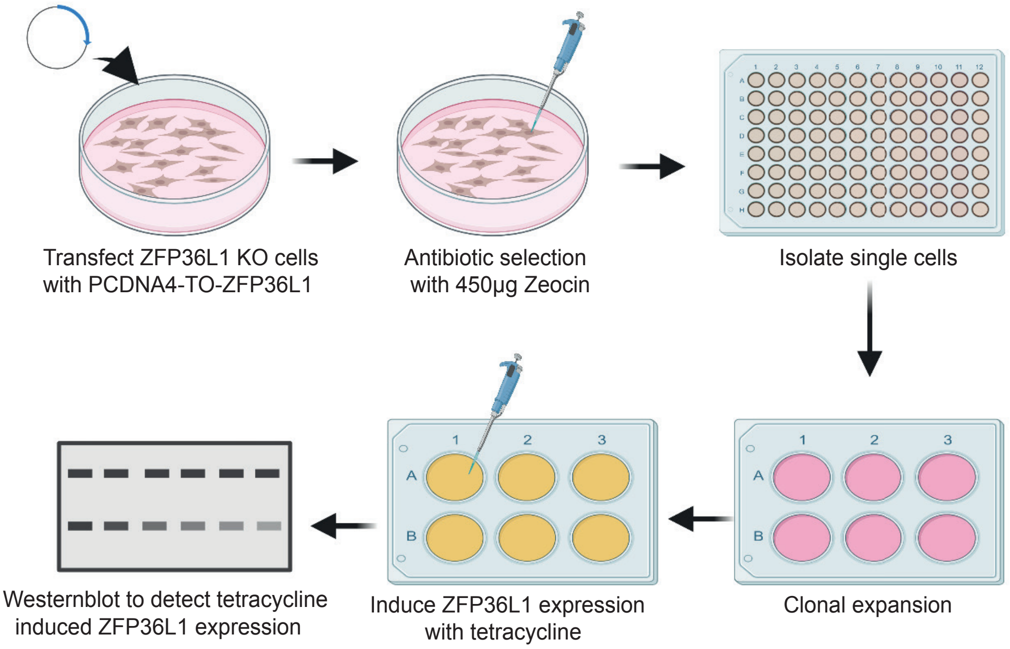
Transfect ZFP36L1 KO cells with PCDNA4-TO-ZFP36L1
Antibiotic selection with 450µg Zeocin
Isolate single cells
A
B
C
D
E
F
G
H
1 2 3 4 5 6 7 8 9 10 11 12
Clonal expansion
Induce ZFP36L1 expression with tetracycline
1 2 3
A
B
Westernblot to detect tetracycline induced ZFP36L1 expression

Figure 6 Workflow for generation of a stable inducible ZFP36L1 expression system. Workflow for generation of ΔL1-T-REx cells stably expressing inducible ZFP36L1 (ΔL1-TO-ZFP36L1). Cells transfected with PCDNA4-TO-ZFP36L1 were selected with 450µg/ml zeocin. Following zeocin selection, single cells were isolated in 96-well plates and expanded to test for tetracycline-induced expression of ZFP36L1 by western blot.

Appendix D

Table 1 Full list of ZFP36L1 interacting proteins identified by MS

List of proteins	Uni prot accession	[a]Score	Matching Peptides (Flag-ZFP36L1)	Matching peptides (Flag-EV)	Protein mass (Da)
ZFP36L1_HUMAN	Q07352	672	71	1	36747
STAU2_HUMAN	Q9NUL3	554	12	0	62797
CNOT1_HUMAN	A5YKK6	537	11	0	269105
PABP3_HUMAN	Q9H361	536	15	0	70214
K1C15_HUMAN	P19012	512	11	0	49409
HUWE1_HUMAN	Q7Z6Z7	485	8	0	485523
RRBP1_HUMAN	Q9P2E9	444	7	0	152763
ARH40_HUMAN	Q8TER5	438	8	0	166265
RLA2_HUMAN	P05387	403	9	0	11657
HELZ_HUMAN	P42694	376	7	0	220600
RRP12_HUMAN	Q5JTH9	356	7	0	145036
H2B1B_HUMAN	P33778	339	30	0	13941
HNRC1_HUMAN	O60812	308	7	0	32179
4ET_HUMAN	Q9NRA8	305	8	0	108476
1433F_HUMAN	Q04917	294	6	0	28372
TNR6A_HUMAN	Q8NDV7	267	5	0	210966
ELP3_HUMAN	Q9H9T3	217	5	0	62789
RECQ1_HUMAN	P46063	210	3	0	74436
PTBP3_HUMAN	O95758	200	4	0	59937
ZNFX1_HUMAN	Q9P2E3	194	3	0	225102
CELF1_HUMAN	Q92879	184	4	0	52429
1433E_HUMAN	P62258	175	4	0	29326
RM02_HUMAN	Q5T653	174	2	0	33564
MESD_HUMAN	Q14696	174	4	0	26231
AGO2_HUMAN	Q9UKV8	167	3	0	98400
RBP56_HUMAN	Q92804	166	3	0	62021
PLPL6_HUMAN	Q8IY17	164	2	0	152341
RAB8A_HUMAN	P61006	160	4	0	23824
KI18A_HUMAN	Q8NI77	158	2	0	103413
LENG1_HUMAN	Q96BZ8	157	3	0	30510
SUGP2_HUMAN	Q8IX01	156	4	0	121044
GNL3_HUMAN	Q9NVN8	155	3	0	62467
AMOL2_HUMAN	Q9Y2J4	153	3	0	85940
MAGT1_HUMAN	Q9H0U3	153	3	0	38410
HELZ2_HUMAN	Q9BYK8	152	3	0	298285
RT18B_HUMAN	Q9Y676	152	3	0	29719
DNJB5_HUMAN	O75953	149	2	0	39337
RU2B_HUMAN	P08579	143	3	0	25470
SYYM_HUMAN	Q9Y2Z4	142	4	0	53393
LORF1_HUMAN	Q9UN81	141	4	0	40258
SMAG1_HUMAN	Q9UPU9	140	2	0	80049

LUZP1_HUMAN	Q86V48	140	2	0	120772
FAKD2_HUMAN	Q9NYY8	138	3	0	82379
RT05_HUMAN	P82675	137	3	0	48489
MLH1_HUMAN	P40692	137	3	0	85175
DHB4_HUMAN	P51659	136	3	0	80092
RM22_HUMAN	Q9NWU5	136	2	0	23796
CNO10_HUMAN	Q9H9A5	136	2	0	83397
UTP4_HUMAN	Q969X6	135	3	0	77525
TRI32_HUMAN	Q13049	134	2	0	73539
NSUN5_HUMAN	Q96P11	133	3	0	47289
FA50A_HUMAN	Q14320	129	3	0	40216
CNOT3_HUMAN	O75175	128	3	0	82049
RPB1_HUMAN	P24928	127	4	0	218407
RPB2_HUMAN	P30876	125	3	0	135236
SBP2L_HUMAN	Q93073	125	2	0	122783
CLP1L_HUMAN	Q96KA5	125	2	0	62531
STK3_HUMAN	Q13188	125	3	0	56550
PTSS1_HUMAN	P48651	124	3	0	56175
RT21_HUMAN	P82921	123	2	0	10909
PPIL1_HUMAN	Q9Y3C6	123	2	0	18339
ZCHC3_HUMAN	Q9NUD5	122	3	0	44318
DDX18_HUMAN	Q9NVP1	122	2	0	75701
SMCA4_HUMAN	P51532	122	3	0	185100
PAP1M_HUMAN	Q5JQF8	122	2	0	22955
RBM15_HUMAN	Q96T37	121	2	0	107352
IRAK1_HUMAN	P51617	120	2	0	77457
RNC_HUMAN	Q9NRR4	120	2	0	160810
ZCHC8_HUMAN	Q6NZY4	119	3	0	79155
PEX16_HUMAN	Q9Y5Y5	119	2	0	38661
NT5D2_HUMAN	Q9H857	118	2	0	61021
DHX8_HUMAN	Q14562	117	2	0	140081
PINX1_HUMAN	Q96BK5	117	2	0	37183
RL7L_HUMAN	Q6DKI1	113	2	0	29821
TRI25_HUMAN	Q14258	113	2	0	72581
NCBP1_HUMAN	Q09161	110	2	0	92863
SNX8_HUMAN	Q9Y5X2	109	2	0	52935
ABC3F_HUMAN	Q8IUX4	108	2	0	45845
EST1A_HUMAN	Q86US8	105	2	0	161502
KIFC1_HUMAN	Q9BW19	105	3	0	74272
NSE2_HUMAN	Q96MF7	105	2	0	28257
EXOC3_HUMAN	O60645	103	2	0	85969
TOE1_HUMAN	Q96GM8	101	2	0	57367

USP9Y_HUMAN	O00507	101	3	0	294369
ZMAT2_HUMAN	Q96NC0	100	2	0	23768
LSM1_HUMAN	O15116	100	2	0	15170
GPN3_HUMAN	Q9UHW5	99	2	0	33195
GRSF1_HUMAN	Q12849	99	2	0	53605
S10A8_HUMAN	P05109	99	2	0	44967
RM38_HUMAN	Q96DV4	99	2	0	44967
H2A2B_HUMAN	Q8IUE6	99	3	0	13986
DNJA3_HUMAN	Q96EY1	98	2	0	53082
CP131_HUMAN	Q9UPN4	98	2	0	122531
NDUS5_HUMAN	O43920	97	3	0	12737
RPAC1_HUMAN	O15160	97	2	0	39453
BRAT1_HUMAN	Q6PJG6	96	2	0	89773
XPR1_HUMAN	Q9UBH6	95	2	0	82167
CEP78_HUMAN	Q5JTW2	95	3	0	77203
CDK4_HUMAN	P11802	94	2	0	33936
ELP1_HUMAN	O95163	94	2	0	151812
ARMX2_HUMAN	Q7L311	93	2	0	65927
SPTB2_HUMAN	Q01082	93	2	0	275236
RCC1L_HUMAN	Q96I51	93	2	0	50706
PRR11_HUMAN	Q96HE9	92	2	0	40572
TYK2_HUMAN	P29597	92	2	0	135389
XRN1_HUMAN	Q8IZH2	92	2	0	195524
QCR8_HUMAN	O14949	92	2	0	9900
FA98B_HUMAN	Q52LJ0	92	2	0	45917
H2AY_HUMAN	O75367	92	3	0	39763
UFL1_HUMAN	O94874	91	2	0	89995
SMC2_HUMAN	O95347	91	2	0	136085
LA_HUMAN	P05455	91	2	0	54487
CEP55_HUMAN	Q53EZ4	90	2	0	54487
SMG5_HUMAN	Q9UPR3	89	2	0	115451
AKP8L_HUMAN	Q9ULX6	88	2	0	72050
DNJC2_HUMAN	Q99543	88	2	0	72464
BRX1_HUMAN	Q8TDN6	87	2	0	41660
RBPS2_HUMAN	Q6ZRY4	87	2	0	22539
MSI2H_HUMAN	Q96DH6	86	2	0	35345
SYF2_HUMAN	O95926	86	2	0	28761
GPTC4_HUMAN	Q5T3I0	85	2	0	50578
RM49_HUMAN	Q13405	84	2	0	19242
MBB1A_HUMAN	Q9BQG0	82	2	0	149730
AKAP8_HUMAN	O43823	82	2	0	76631
CARF_HUMAN	Q9NXV6	82	2	0	61544
CLK2_HUMAN	P49760	81	2	0	60509

CPSF3_HUMAN	Q9UKF6	80	2	0	78120
DHX37_HUMAN	Q8IY37	80	2	0	130546
MA1B1_HUMAN	Q9UKM7	79	2	0	79814
HNRL2_HUMAN	Q1KMD3	79	2	0	85622
TBL2_HUMAN	Q9Y4P3	78	2	0	50393
UT14A_HUMAN	Q9BVJ6	78	2	0	88095
MTEF3_HUMAN	Q96E29	78	3	0	48055
SH3B4_HUMAN	Q9P0V3	78	2	0	108397
MTCH1_HUMAN	Q9NZJ7	77	2	0	41859
MIC27_HUMAN	Q6UXV4	77	2	0	29311
NOG2_HUMAN	Q13823	76	2	0	83831
KTN1_HUMAN	Q86UP2	76	3	0	156464
NUSAP_HUMAN	Q9BXS6	75	2	0	49592
NOC4L_HUMAN	Q9BVI4	75	2	0	58829
EXOC2_HUMAN	Q96KP1	75	2	0	105083
THOC1_HUMAN	Q96FV9	75	2	0	76359
MELK_HUMAN	Q14680	75	2	0	75506
RT10_HUMAN	P82664	74	2	0	23099
ERH_HUMAN	P84090	74	2	0	12422
MYO1A_HUMAN	Q9UBC5	74	2	0	119238
EI2BE_HUMAN	Q13144	72	2	0	81070
RFC3_HUMAN	P40938	72	2	0	41328
T126A_HUMAN	Q9H061	71	3	0	21741
SFSWA_HUMAN	Q12872;	71	2	0	105156
DDX24_HUMAN	Q9GZR7	71	2	0	96898
DCA13_HUMAN	Q9NV06	70	2	0	51996
RPF2_HUMAN	Q9H7B2	70	2	0	35731

[a]Mascot protein score >70 was considered significant ($p < 0.05$). Results are from two independent experiments (N=2).

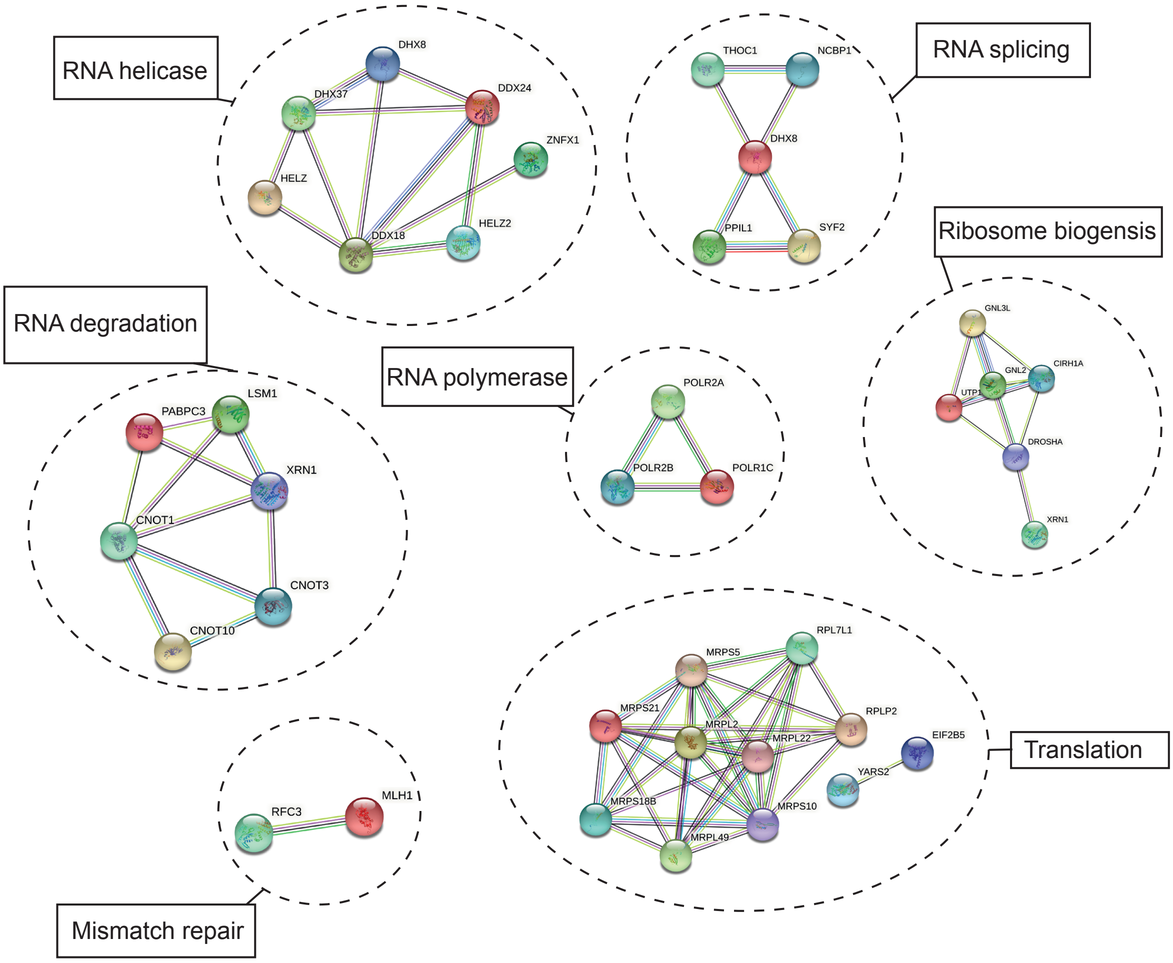
RNA helicase
DHX8
DDX24
DHX37
ZNFX1
HELZ
HELZ2
DDX18
RNA splicing
THOC1
NCBP1
DHX8
PPIL1
SYF2
Ribosome biogensis
GNL3L
GNL2
CIRH1A
UTP1
DROSHA
XRN1
RNA degradation
LSM1
PABPC3
XRN1
CNOT1
CNOT3
CNOT10
RNA polymerase
POLR2A
POLR2B
POLR1C
RPL7L1
MRPS5
MRPS21
RPLP2
MRPL2
MRPL22
EIF2B5
Translation
YARS2
MRPS18B
MRPS10
MRPL49
RFC3
MLH1
Mismatch repair

Figure 1. Network of functional interactions for a selection of proteins identified in FLAG-Strep II-ZFP36L1 eluates. Genes were annotated based on GO terms (Biological process and Molecular function). Manual annotation was used to generate clusters, edges between nodes indicate STRING interactions with a confidence score above 0.4.

12. Glossary

aa Amino acid
Adenine A
APH Aphidicolin
ARE adenylate/uridylate rich element
Arg Arginine
AUF1 AU-Rich Element RNA Binding Protein 1
AU-RBP Adenylate-Uridylate-rich element RNA binding protein
ATM Ataxia telangiectasia mutated
ATR Ataxia telangiectasia and Rad3-related
BP Base pair
Cas9 CRISPR-associated protein 9
CPT Camptothecin
CDK Cyclin-dependent kinase
CFS Common fragile site
CHK1 Checkpoint kinase 1
CHK2 Checkpoint kinase 2
CIN Chromosomal instability
CMV Cytomegalovirus
CRISPR Clustered regularly interspaced short palindromic repeats
CTD C-terminal domain
Cys Cysteine
DAPI 4,6-diamidino-2-phenylindole
DDR DNA damage response
DNA-PK DNA-dependent protein kinase
DSB DNA double-strand breaks
ERFS early replicating fragile site
EV Empty vector
FA Fanconi anaemia
FANCD2 FA Complementation Group D2

FS Fragile site
GMG G2/M transition granule
GOI Gene of interest
GRNA Guide RNA
His Histidine
H2AX Histone H2A variant X phosphorylated at Serine 139
HR Homologous recombination
HU Hydroxyurea
HuR Hu Antigen R
IP Immunoprecipitation
KHSRP KH-Type Splicing Regulatory Protein
KO Knock out
MCM7 – Minichromosome maintenance complex component 7
MCS Multiple cloning site
NC Negative control
NES Nuclear export sequence
NGS Next generation sequencing
NHEJ Non-homologous end joining
NLS Nuclear localisation sequence
NTD N-terminal domain
NB Nuclear body
PC Positive control
PCR Polymerase chain reaction
PI Propidium iodide
PICH Plk1-interacting checkpoint helicase
P bodies Processing bodies
RBD RNA binding domain
RBP RNA binding protein
RNase H1 Ribonuclease H1
RNP Ribonucleoprotein
RPA Replication protein A
RRM RNA recognition motif
R-loop RNA:DNA hybrid
RS Replication stress

Ser Serine
SgRNA single guide RNA
SsDNA Single-stranded DNA
SsRNA single-stranded RNA
SG Stress granules
TET Tetracycline
TetO Tetracycline operon
TetR Tetracycline repressor
TZF Tandem zinc finger
Thr Threonine
TIA-1 T-cell-restricted intracellular antigen-1
TIAR TIA1 related
UFB Ultra fine bridge
UTR Untranslated region
WT Wild type
ZFP36 Zinc finger protein 36
ZFP36L1 Zinc finger protein 36-like 1
ZFP36L2 Zinc finger protein 36-like 2
53BP1 p53-binding protein 1
α Alpha
δ Delta
ΔL1 ZFP36L1 knockout
ε Epsilon
γ Gamma
γH2AX Histone H2A variant X phosphorylated at Serine 139
µg Microgram
µL Microlitre
µm Micrometre
µM Micromolar

13. Bibliography

Abugable, A., Morris, J., Palminha, N., Zaksauskaite, R., Ray, S. and El-Khamisy, S. (2019). DNA repair and neurological disease: From molecular understanding to the development of diagnostics and model organisms. *DNA Repair*, 81, 102669. Available from 10.1016/j.dnarep.2019.102669 [Accessed 30 June 2022].

Adachi, S., Homoto, M., Tanaka, R., Hioki, Y., Murakami, H., Suga, H., Matsumoto, M., Nakayama, K., Hatta, T., Iemura, S. and Natsume, T. (2014). ZFP36L1 and ZFP36L2 control LDLR mRNA stability via the ERK–RSK pathway. *Nucleic Acids Research*, 42 (15), 10037-10049. Available from 10.1093/nar/gku652 [Accessed 5 May 2022].

Aguilera, A. and García-Muse, T. (2012). R Loops: From Transcription Byproducts to Threats to Genome Stability. *Molecular Cell*, 46 (2), 115-124. Available from 10.1016/j.molcel.2012.04.009 [Accessed 30 April 2022].

Alexander, J. and Orr-Weaver, T. (2016). Replication fork instability and the consequences of fork collisions from rereplication. *Genes &amp; Development*, 30 (20), 2241-2252. Available from 10.1101/gad.288142.116 [Accessed 10 June 2022].

Alfano, L., Caporaso, A., Altieri, A., Dell'Aquila, M., Landi, C., Bini, L., Pentimalli, F. and Giordano, A. (2019). Depletion of the RNA binding protein HNRNPD impairs homologous recombination by inhibiting DNA-end resection and inducing R-loop accumulation. *Nucleic Acids Research*, 47 (8), 4068-4085. Available from 10.1093/nar/gkz076 [Accessed 12 April 2022].

Al-Haj, L., Blackshear, P. and Khabar, K. (2012). Regulation of p21/CIP1/WAF-1 mediated cell-cycle arrest by RNase L and tristetraprolin, and involvement of AU-rich elements. *Nucleic Acids Research*, 40 (16), 7739-7752. Available from 10.1093/nar/gks545 [Accessed 12 May 2022].

Al-Khalaf, H. and Aboussekhra, A. (2013). <i>ATR</i> controls the UV-related upregulation of the <i>CDKN1A</i> mRNA in a Cdk1/HuR-dependent manner. *Molecular Carcinogenesis*, 53 (12), 979-987. Available from 10.1002/mc.22066 [Accessed 14 May 2022].

Allison, D. and Wang, G. (2019). R-loops: formation, function, and relevance to cell stress. *Cell Stress*, 3 (2), 38-46. Available from 10.15698/cst2019.02.175 [Accessed 17 June 2022].

Al-Souhibani, N., Al-Ahmadi, W., Hesketh, J., Blackshear, P. and Khabar, K. (2010). The RNA-binding zinc-finger protein tristetraprolin regulates AU-rich mRNAs involved in breast cancer-related processes. *Oncogene*, 29 (29), 4205-4215. Available from 10.1038/onc.2010.168 [Accessed 8 July 2022].

Álvarez-Quilón, A., Serrano-Benítez, A., Ariel Lieberman, J., Quintero, C., Sánchez-Gutiérrez, D., Escudero, L. and Cortés-Ledesma, F. (2014). ATM specifically mediates repair of double-strand breaks with blocked DNA ends. *Nature Communications*, 5 (1). Available from 10.1038/ncomms4347 [Accessed 10 May 2022].

Anantha, R., Alcivar, A., Ma, J., Cai, H., Simhadri, S., Ule, J., König, J. and Xia, B. (2013). Requirement of Heterogeneous Nuclear Ribonucleoprotein C for BRCA Gene Expression and Homologous Recombination. *PLoS ONE*, 8 (4), e61368. Available from 10.1371/journal.pone.0061368 [Accessed 17 April 2022].

Anderson, P. and Kedersha, N. (2002). Stressful initiations. *Journal of Cell Science*, 115 (16), 3227-3234. Available from 10.1242/jcs.115.16.3227 [Accessed 4 May 2022].

Anderson, P., Kedersha, N. and Ivanov, P. (2015). Stress granules, P-bodies and cancer. *Biochimica et Biophysica Acta (BBA) - Gene Regulatory Mechanisms*, 1849 (7), 861-870. Available from 10.1016/j.bbagrm.2014.11.009 [Accessed 8 May 2022].

Andrade, D., Mehta, M., Griffith, J., Oh, S., Corbin, J., Babu, A., De, S., Chen, A., Zhao, Y., Husain, S., Roy, S., Xu, L., Aube, J., Janknecht, R., Gorospe, M., Herman, T., Ramesh, R. and Munshi, A. (2019). HuR Reduces Radiation-Induced DNA Damage by Enhancing Expression of ARID1A. *Cancers*, 11 (12), 2014. Available from 10.3390/cancers11122014 [Accessed 13 May 2022].

Andres, S. and Williams, R. (2017). CtIP/Ctp1/Sae2, molecular form fit for function. *DNA Repair*, 56, 109-117. Available from 10.1016/j.dnarep.2017.06.013 [Accessed 18 April 2022].

Arlt, M., Durkin, S., Ragland, R. and Glover, T. (2006). Common fragile sites as targets for chromosome rearrangements. *DNA Repair*, 5 (9-10), 1126-1135. Available from 10.1016/j.dnarep.2006.05.010 [Accessed 16 May 2022].

Audic, Y. and Hartley, R. (2004). Post-transcriptional regulation in cancer. *Biology of the Cell*, 96 (7), 479-498. Available from 10.1016/j.biolcel.2004.05.002 [Accessed 17 June 2022].

Awate, S. and De Benedetti, A. (2016). TLK1B mediated phosphorylation of Rad9 regulates its nuclear/cytoplasmic localization and cell cycle checkpoint. *BMC Molecular Biology*, 17 (1). Available from 10.1186/s12867-016-0056-x [Accessed 9 July 2022].

Azzalin, C. and Lingner, J. (2006). The Human RNA Surveillance Factor UPF1 Is Required for S Phase Progression and Genome Stability. *Current Biology*, 16 (4), 433-439. Available from 10.1016/j.cub.2006.01.018 [Accessed 22 June 2022].

Babbe, H., McMenamin, J., Hobeika, E., Wang, J., Rodig, S., Reth, M. and Leder, P. (2008). Genomic Instability Resulting from Blm Deficiency Compromises Development, Maintenance, and Function of the B Cell Lineage. *The Journal of Immunology*, 182 (1), 347-360. Available from 10.4049/jimmunol.182.1.347 [Accessed 30 June 2022].

Badura, M., Braunstein, S., Zavadil, J. and Schneider, R. (2012). DNA damage and eIF4G1 in breast cancer cells reprogram translation for survival and DNA repair mRNAs. *Proceedings of the National Academy of Sciences*, 109 (46), 18767-18772. Available from 10.1073/pnas.1203853109 [Accessed 11 May 2022].

Bakheet, T., Hitti, E. and Khabar, K. (2017). ARED-Plus: an updated and expanded database of AU-rich element-containing mRNAs and pre-mRNAs. *Nucleic Acids Research*, 46 (D1), D218-D220. Available from 10.1093/nar/gkx975 [Accessed 3 May 2022].

Bakheet, T., Hitti, E., Al-Saif, M., Moghrabi, W. and Khabar, K. (2018). The AU-rich element landscape across human transcriptome reveals a large proportion in introns and regulation by ELAVL1/HuR. *Biochimica et Biophysica Acta (BBA) - Gene Regulatory Mechanisms*, 1861 (2), 167-177. Available from 10.1016/j.bbagrm.2017.12.006 [Accessed 13 May 2022].

Bakheet, T. (2001). ARED: human AU-rich element-containing mRNA database reveals an unexpectedly diverse functional repertoire of encoded proteins. *Nucleic Acids Research*, 29 (1), 246-254. Available from 10.1093/nar/29.1.246 [Accessed 4 May 2022].

Bakheet, T. (2003). ARED 2.0: an update of AU-rich element mRNA database. *Nucleic Acids Research*, 31 (1), 421-423. Available from 10.1093/nar/gkg023.

Balasubramanian, S., Andreani, M., Andrade, J., Saha, T., Garzón, J., Zhang, W., Rahjouei, A., Rosen, D., Chait, B., Donaldson, A. and Di Virgilio, M. (2021). Protection of nascent DNA at stalled replication forks is mediated by phosphorylation of RIF1 intrinsically disordered region. Available from 10.1101/2021.11.04.467328 [Accessed 18 April 2022].

Bamford, S., Dawson, E., Forbes, S., Clements, J., Pettett, R., Dogan, A., Flanagan, A., Teague, J., Futreal, P., Stratton, M. and Wooster, R. (2004). The COSMIC (Catalogue of Somatic Mutations in Cancer) database and website. *British Journal of Cancer*, 91 (2), 355-358. Available from 10.1038/sj.bjc.6601894 [Accessed 28 May 2022].

Baou, M., Jewell, A. and Murphy, J. (2009). TIS11 Family Proteins and Their Roles in Posttranscriptional Gene Regulation. *Journal of Biomedicine and Biotechnology*, 2009, 1-11. Available from 10.1155/2009/634520 [Accessed 30 June 2022].

Baou, M., Jewell, A., Muthurania, A., Wickremasinghe, R., Yong, K., Carr, R., Marsh, P. and Murphy, J. (2008). Involvement of Tis11b, an AU-rich binding protein, in induction of apoptosis by rituximab in B cell chronic lymphocytic leukemia cells. *Leukemia*, 23 (5), 986-989. Available from 10.1038/leu.2008.340 [Accessed 15 June 2022].

Barlow, J., Faryabi, R., Callén, E., Wong, N., Malhowski, A., Chen, H., Gutierrez-Cruz, G., Sun, H., McKinnon, P., Wright, G., Casellas, R., Robbiani, D., Staudt, L., Fernandez-Capetillo, O. and Nussenzweig, A. (2013). Identification of Early Replicating Fragile Sites that Contribute to Genome Instability. *Cell*, 152 (3), 620-632. Available from 10.1016/j.cell.2013.01.006.

Barman, A., Deb, B. and Chakraborty, S. (2019). A glance at genome editing with CRISPR–Cas9 technology. *Current Genetics*, 66 (3), 447-462. Available from 10.1007/s00294-019-01040-3 [Accessed 18 July 2022].

Barreau, C. (2005). AU-rich elements and associated factors: are there unifying principles?. *Nucleic Acids Research*, 33 (22), 7138-7150. Available from 10.1093/nar/gki1012 [Accessed 4 May 2022].

Bartek, J. and Lukas, J. (2007). DNA damage checkpoints: from initiation to recovery or adaptation. *Current Opinion in Cell Biology*, 19 (2), 238-245. Available from 10.1016/j.ceb.2007.02.009 [Accessed 10 May 2022].

Bartkova, J., Hořejší, Z., Koed, K., Krämer, A., Tort, F., Zieger, K., Guldberg, P., Sehested, M., Nesland, J., Lukas, C., Ørntoft, T., Lukas, J. and Bartek, J. (2005). DNA damage response as a candidate anti-cancer barrier in early human tumorigenesis. *Nature*, 434 (7035), 864-870. Available from 10.1038/nature03482 [Accessed 4 June 2022].

Basile, G., Leuzzi, G., Pichierri, P. and Franchitto, A. (2014). Checkpoint-dependent and independent roles of the Werner syndrome protein in preserving genome integrity in response to mild replication stress. *Nucleic Acids Research*, 42 (20), 12628-12639. Available from 10.1093/nar/gku1022 [Accessed 27 April 2022].

Baumann, C., Körner, R., Hofmann, K. and Nigg, E. (2007). PICH, a Centromere-Associated SNF2 Family ATPase, Is Regulated by Plk1 and Required for the Spindle Checkpoint. *Cell*, 128 (1), 101-114. Available from 10.1016/j.cell.2006.11.041 [Accessed 4 June 2022].

Benjamin, D., Schmidlin, M., Min, L., Gross, B. and Moroni, C. (2006). BRF1 Protein Turnover and mRNA Decay Activity Are Regulated by Protein Kinase B at the Same Phosphorylation Sites. *Molecular and Cellular Biology*, 26 (24), 9497-9507. Available from 10.1128/mcb.01099-06 [Accessed 5 May 2022].

Berglind, H., Pawitan, Y., Kato, S., Ishioka, C. and Soussi, T. (2008). Analysis of p53 mutation status in human cancer cell lines: a paradigm for cell line cross-contamination. *Cancer Biology &amp; Therapy*, 7 (5), 699-708. Available from 10.4161/cbt.7.5.5712 [Accessed 28 May 2022].

Bhatia, V., Barroso, S., García-Rubio, M., Tumini, E., Herrera-Moyano, E. and Aguilera, A. (2014). BRCA2 prevents R-loop accumulation and associates with TREX-2 mRNA export factor PCID2. *Nature*, 511 (7509), 362-365. Available from 10.1038/nature13374 [Accessed 3 June 2022].

Biebricher, A., Hirano, S., Enzlin, J., Wiechens, N., Streicher, W., Huttner, D., Wang, L., Nigg, E., Owen-Hughes, T., Liu, Y., Peterman, E., Wuite, G. and Hickson, I. (2013). PICH: A DNA Translocase Specially Adapted for Processing Anaphase Bridge DNA. *Molecular Cell*, 51 (5), 691-701. Available from 10.1016/j.molcel.2013.07.016 [Accessed 5 June 2022].

Bignell, G., Greenman, C., Davies, H., Butler, A., Edkins, S., Andrews, J., Buck, G., Chen, L., Beare, D., Latimer, C., Widaa, S., Hinton, J., Fahey, C., Fu, B., Swamy, S., Dalgliesh, G., Teh, B., Deloukas, P., Yang, F., Campbell, P., Futreal, P. and Stratton, M. (2010). Signatures of mutation and selection in the cancer genome. *Nature*, 463 (7283), 893-898. Available from 10.1038/nature08768 [Accessed 16 May 2022].

Bizard, A., Nielsen, C. and Hickson, I. (2017). Detection of Ultrafine Anaphase Bridges. *Methods in Molecular Biology*, 495-508. Available from 10.1007/978-1-4939-7306-4_33 [Accessed 25 May 2022].

Blackford, A. and Jackson, S. (2017). ATM, ATR, and DNA-PK: The Trinity at the Heart of the DNA Damage Response. *Molecular Cell*, 66 (6), 801-817. Available from 10.1016/j.molcel.2017.05.015 [Accessed 10 May 2022].

Blackshear, P. and Perera, L. (2014). Phylogenetic Distribution and Evolution of the Linked RNA-Binding and NOT1-Binding Domains in the Tristetraprolin Family of Tandem CCCH Zinc Finger Proteins. *Journal of Interferon &amp; Cytokine Research*, 34 (4), 297-306. Available from 10.1089/jir.2013.0150 [Accessed 5 May 2022].

Blackshear, P., Lai, W., Kennington, E., Brewer, G., Wilson, G., Guan, X. and Zhou, P. (2003). Characteristics of the Interaction of a Synthetic Human Tristetraprolin Tandem Zinc Finger Peptide with AU-rich Element-containing RNA Substrates. *Journal of Biological Chemistry*, 278 (22), 19947-19955. Available from 10.1074/jbc.m301290200 [Accessed 6 May 2022].

Blanco, F., Sanduja, S., Deane, N., Blackshear, P. and Dixon, D. (2014). Transforming Growth Factor β Regulates P-Body Formation through Induction of the mRNA Decay Factor Tristetraprolin. *Molecular and Cellular Biology*, 34 (2), 180-195. Available from 10.1128/mcb.01020-13 [Accessed 9 May 2022].

Borel, F., Lacroix, F. and Margolis, R. (2002). Prolonged arrest of mammalian cells at the G1/S boundary results in permanent S phase stasis. *Journal of Cell Science*, 115 (14), 2829-2838. Available from 10.1242/jcs.115.14.2829 [Accessed 9 July 2022].

Braunstein, S., Badura, M., Xi, Q., Formenti, S. and Schneider, R. (2009). Regulation of Protein Synthesis by Ionizing Radiation. *Molecular and Cellular Biology*, 29 (21), 5645-5656. Available from 10.1128/mcb.00711-09 [Accessed 11 May 2022].

Brennan, S., Kuwano, Y., Alkharouf, N., Blackshear, P., Gorospe, M. and Wilson, G. (2009). The mRNA-Destabilizing Protein Tristetraprolin Is Suppressed in Many Cancers, Altering Tumorigenic Phenotypes and Patient Prognosis. *Cancer Research*, 69 (12), 5168-5176. Available from 10.1158/0008-5472.can-08-4238 [Accessed 7 May 2022].

Brewer, G. (1991). An A + U-rich element RNA-binding factor regulates c-myc mRNA stability in vitro. *Molecular and Cellular Biology*, 11 (5), 2460-2466. Available from 10.1128/mcb.11.5.2460-2466.1991 [Accessed 4 May 2022].

Briata, P., Chen, C., Ramos, A. and Gherzi, R. (2013). Functional and molecular insights into KSRP function in mRNA decay. *Biochimica et Biophysica Acta (BBA) - Gene Regulatory Mechanisms*, 1829 (6-7), 689-694. Available from 10.1016/j.bbagrm.2012.11.003 [Accessed 4 May 2022].

Britton, S., Dernoncourt, E., Delteil, C., Froment, C., Schiltz, O., Salles, B., Frit, P. and Calsou, P. (2014). DNA damage triggers SAF-A and RNA biogenesis factors exclusion from chromatin coupled to R-loops removal. *Nucleic Acids Research*, 42 (14), 9047-9062. Available from 10.1093/nar/gku601 [Accessed 3 June 2022].

Brook, M., Tchen, C., Santalucia, T., McIlrath, J., Arthur, J., Saklatvala, J. and Clark, A. (2006). Posttranslational Regulation of Tristetraprolin Subcellular Localization and Protein Stability by p38 Mitogen-Activated Protein Kinase and Extracellular Signal-Regulated Kinase Pathways. *Molecular and Cellular Biology*, 26 (6), 2408-2418. Available from 10.1128/mcb.26.6.2408-2418.2006 [Accessed 8 May 2022].

Bruno, S., Giaretti, W. and Darzynkiewicz, Z. (1992). Effect of camptothecin on mitogenic stimulation of human lymphocytes: Involvement of DNA topoisomerase I in cell transition from G0 to G1 phase of the cell cycle and in DNA replication. *Journal of Cellular Physiology*, 151 (3), 478-486. Available from 10.1002/jcp.1041510306 [Accessed 9 July 2022].

Burrell, R., McClelland, S., Endesfelder, D., Groth, P., Weller, M., Shaikh, N., Domingo, E., Kanu, N., Dewhurst, S., Gronroos, E., Chew, S., Rowan, A., Schenk, A., Sheffer, M., Howell, M., Kschischo, M., Behrens, A., Helleday, T., Bartek, J., Tomlinson, I. and Swanton, C. (2013). Replication stress links structural and numerical cancer chromosomal instability. *Nature*, 494 (7438), 492-496. Available from 10.1038/nature11935 [Accessed 25 June 2022].

Caldon, C. and Musgrove, E. (2010). Distinct and redundant functions of cyclin E1 and cyclin E2 in development and cancer. *Cell Division*, 5 (1), 2. Available from 10.1186/1747-1028-5-2 [Accessed 12 May 2022].

Cammas, A., Sanchez, B., Lian, X., Dormoy-Raclet, V., van der Giessen, K., de Silanes, I., Ma, J., Wilusz, C., Richardson, J., Gorospe, M., Millevoi, S., Giovarelli, M., Gherzi, R., Di Marco, S. and Gallouzi, I. (2014). Destabilization of nucleophosmin mRNA by the HuR/KSRP complex is required for muscle fibre formation. *Nature Communications*, 5 (1). Available from 10.1038/ncomms5190 [Accessed 30 June 2022].

Campillos, M., Cases, I., Hentze, M. and Sanchez, M. (2010). SIREs: searching for iron-responsive elements. *Nucleic Acids Research*, 38 (Web Server), W360-W367. Available from 10.1093/nar/gkq371 [Accessed 4 May 2022].

Cannavo, E., Gerrits, B., Marra, G., Schlapbach, R. and Jiricny, J. (2007). Characterization of the Interactome of the Human MutL Homologues MLH1, PMS1, and PMS2. *Journal of Biological Chemistry*, 282 (5), 2976-2986. Available from 10.1074/jbc.m609989200 [Accessed 7 July 2022].

Canzoneri, R., Naipauer, J., Stedile, M., Rodriguez Peña, A., Lacunza, E., Gandini, N., Curino, A., Facchinetti, M., Coso, O., Kordon, E. and Abba,

M. (2020). Identification of an AP1-ZFP36 Regulatory Network Associated with Breast Cancer Prognosis. *Journal of Mammary Gland Biology and Neoplasia*, 25 (2), 163-172. Available from 10.1007/s10911-020-09448-1 [Accessed 7 May 2022].

Cao, H. and Lin, R. (2007). Phosphorylation of Recombinant Tristetraprolin In vitro. *The Protein Journal*, 27 (3), 163-169. Available from 10.1007/s10930-007-9119-7 [Accessed 5 May 2022].

Cao, H., Deterding, L. and Blackshear, P. (2014). Identification of a Major Phosphopeptide in Human Tristetraprolin by Phosphopeptide Mapping and Mass Spectrometry. *PLoS ONE*, 9 (7), e100977. Available from 10.1371/journal.pone.0100977 [Accessed 5 May 2022].

Cao, H., Deterding, L., Venable, J., Kennington, E., Yates, J., Tomer, K. and Blackshear, P. (2006). Identification of the anti-inflammatory protein tristetraprolin as a hyperphosphorylated protein by mass spectrometry and site-directed mutagenesis. *Biochemical Journal*, 394 (1), 285-297. Available from 10.1042/bj20051316 [Accessed 5 May 2022].

Cao, H., Dzineku, F. and Blackshear, P. (2003). Expression and purification of recombinant tristetraprolin that can bind to tumor necrosis factor-α mRNA and serve as a substrate for mitogen-activated protein kinases. *Archives of Biochemistry and Biophysics*, 412 (1), 106-120. Available from 10.1016/s0003-9861(03)00012-2 [Accessed 5 May 2022].

Cao, H., Tuttle, J. and Blackshear, P. (2004). Immunological Characterization of Tristetraprolin as a Low Abundance, Inducible, Stable Cytosolic Protein. *Journal of Biological Chemistry*, 279 (20), 21489-21499. Available from 10.1074/jbc.m400900200 [Accessed 5 May 2022].

Carballo, E. and Blackshear, P. (2001). Roles of tumor necrosis factor-α receptor subtypes in the pathogenesis of the tristetraprolin-deficiency syndrome. *Blood*, 98 (8), 2389-2395. Available from 10.1182/blood.v98.8.2389 [Accessed 13 June 2022].

Carballo, E., Gilkeson, G. and Blackshear, P. (1997). Bone marrow transplantation reproduces the tristetraprolin-deficiency syndrome in recombination activating gene-2 (-/-) mice. Evidence that monocyte/macrophage progenitors may be responsible for TNFalpha overproduction. *Journal of Clinical Investigation*, 100 (5), 986-995. Available from 10.1172/jci119649 [Accessed 6 May 2022].

Carballo, E., Lai, W. and Blackshear, P. (1998). Feedback Inhibition of Macrophage Tumor Necrosis Factor-α Production by

Tristetraprolin. *Science*, 281 (5379), 1001-1005. Available from 10.1126/science.281.5379.1001 [Accessed 6 May 2022].

Carrick, D. and Blackshear, P. (2007). Comparative expression of tristetraprolin (TTP) family member transcripts in normal human tissues and cancer cell lines. *Archives of Biochemistry and Biophysics*, 462 (2), 278-285. Available from 10.1016/j.abb.2007.04.011 [Accessed 4 May 2022].

Casado, P., Rodriguez-Prados, J., Cosulich, S., Guichard, S., Vanhaesebroeck, B., Joel, S. and Cutillas, P. (2013). Kinase-Substrate Enrichment Analysis Provides Insights into the Heterogeneity of Signaling Pathway Activation in Leukemia Cells. *Science Signaling*, 6 (268). Available from 10.1126/scisignal.2003573 [Accessed 21 July 2022].

Castello, A., Fischer, B., Frese, C., Horos, R., Alleaume, A., Foehr, S., Curk, T., Krijgsveld, J. and Hentze, M. (2016). Comprehensive Identification of RNA-Binding Domains in Human Cells. *Molecular Cell*, 63 (4), 696-710. Available from 10.1016/j.molcel.2016.06.029 [Accessed 23 June 2022].

Cazzalini, O., Scovassi, A., Savio, M., Stivala, L. and Prosperi, E. (2010). Multiple roles of the cell cycle inhibitor p21CDKN1A in the DNA damage response. *Mutation Research/Reviews in Mutation Research*, 704 (1-3), 12-20. Available from 10.1016/j.mrrev.2010.01.009 [Accessed 13 June 2022].

Cecchini, M., Amiri, M. and Dick, F. (2012). Analysis of Cell Cycle Position in Mammalian Cells. *Journal of Visualized Experiments*, (59). Available from 10.3791/3491 [Accessed 28 April 2022].

Cerritelli, S. and Crouch, R. (2009). Ribonuclease H: the enzymes in eukaryotes. *FEBS Journal*, 276 (6), 1494-1505. Available from 10.1111/j.1742-4658.2009.06908.x [Accessed 21 April 2022].

Chakraborty, P. and Grosse, F. (2011). Human DHX9 helicase preferentially unwinds RNA-containing displacement loops (R-loops) and G-quadruplexes. *DNA Repair*, 10 (6), 654-665. Available from 10.1016/j.dnarep.2011.04.013 [Accessed 15 May 2022].

Chan, K., North, P. and Hickson, I. (2007). BLM is required for faithful chromosome segregation and its localization defines a class of ultrafine anaphase bridges. *The EMBO Journal*, 26 (14), 3397-3409. Available from 10.1038/sj.emboj.7601777 [Accessed 4 June 2022].

Chan, K., Palmai-Pallag, T., Ying, S. and Hickson, I. (2009). Replication stress induces sister-chromatid bridging at fragile site loci in mitosis. *Nature Cell Biology,* 11 (6), 753-760. Available from 10.1038/ncb1882 [Accessed 28 April 2022].

Chan, Y. and West, S. (2018). A new class of ultrafine anaphase bridges generated by homologous recombination. *Cell Cycle*, 17 (17), 2101-2109. Available from 10.1080/15384101.2018.1515555 [Accessed 21 June 2022].

Chan, Y., Fugger, K. and West, S. (2017). Unresolved recombination intermediates lead to ultra-fine anaphase bridges, chromosome breaks and aberrations. *Nature Cell Biology*, 20 (1), 92-103. Available from 10.1038/s41556-017-0011-1 [Accessed 30 June 2022].

Chan, Y., Hieter, P. and Stirling, P. (2014). Mechanisms of genome instability induced by RNA-processing defects. *Trends in Genetics*, 30 (6), 245-253. Available from 10.1016/j.tig.2014.03.005 [Accessed 12 June 2022].

Chand, S., Zarei, M., Schiewer, M., Kamath, A., Romeo, C., Lal, S., Cozzitorto, J., Nevler, A., Scolaro, L., Londin, E., Jiang, W., Meisner-Kober, N., Pishvaian, M., Knudsen, K., Yeo, C., Pascal, J., Winter, J. and Brody, J. (2017). Posttranscriptional Regulation of <i>PARG</i> mRNA by HuR Facilitates DNA Repair and Resistance to PARP Inhibitors. *Cancer Research*, 77 (18), 5011-5025. Available from 10.1158/0008-5472.can-16-2704 [Accessed 14 May 2022].

Chao, H., Poovey, C., Privette, A., Grant, G., Chao, H., Cook, J. and Purvis, J. (2017). Orchestration of DNA Damage Checkpoint Dynamics across the Human Cell Cycle. *Cell Systems*, 5 (5), 445-459.e5. Available from 10.1016/j.cels.2017.09.015 [Accessed 9 June 2022].

Chen, C., Gherzi, R., Ong, S., Chan, E., Raijmakers, R., Pruijn, G., Stoecklin, G., Moroni, C., Mann, M. and Karin, M. (2001). AU Binding Proteins Recruit the Exosome to Degrade ARE-Containing mRNAs. *Cell*, 107 (4), 451-464. Available from 10.1016/s0092-8674(01)00578-5 [Accessed 4 May 2022].

Chen, L., Alexe, G., Dharia, N., Ross, L., Iniguez, A., Conway, A., Wang, E., Veschi, V., Lam, N., Qi, J., Gustafson, W., Nasholm, N., Vazquez, F., Weir, B., Cowley, G., Ali, L., Pantel, S., Jiang, G., Harrington, W., Lee, Y., Goodale, A., Lubonja, R., Krill-Burger, J., Meyers, R., Tsherniak, A., Root, D., Bradner, J., Golub, T., Roberts, C., Hahn, W., Weiss, W., Thiele, C. and Stegmaier, K. (2017). CRISPR-Cas9 screen reveals a MYCN-amplified neuroblastoma dependency on EZH2. *Journal of Clinical Investigation*, 128 (1), 446-462. Available from 10.1172/jci90793 [Accessed 17 July 2022].

Chen, M., Dong, L., Zhang, X., Yin, X., Ning, H., Shen, C., Su, R., Li, F., Song, L., Ma, Y., Wang, F., Zhao, H., Yu, J. and Zhang, J. (2015).

ZFP36L1 promotes monocyte/macrophage differentiation by repressing CDK6. *Scientific Reports*, 5 (1). Available from 10.1038/srep16229 [Accessed 12 June 2022].

Chen, W., Chen, M., Zhao, Z., Weng, Q., Song, J., Fang, S., Wu, X., Wang, H., Zhang, D., Yang, W., Wang, Z., Xu, M. and Ji, J. (2020). ZFP36 Binds With PRC1 to Inhibit Tumor Growth and Increase 5-Fu Chemosensitivity of Hepatocellular Carcinoma. *Frontiers in Molecular Biosciences*, 7. Available from 10.3389/fmolb.2020.00126 [Accessed 8 July 2022].

Cherradi, N., Lejczak, C., Desroches-Castan, A. and Feige, J. (2006). Antagonistic Functions of Tetradecanoyl Phorbol Acetate-Inducible-Sequence 11b and HuR in the Hormonal Regulation of Vascular Endothelial Growth Factor Messenger Ribonucleic Acid Stability by Adrenocorticotropin. *Molecular Endocrinology*, 20 (4), 916-930. Available from 10.1210/me.2005-0121 [Accessed 4 May 2022].

Chiu, H., Chiu, H., Yu, H., Lin, L., Chen, Z., Lin, Y. and Lin, R. (2022). Zinc Finger Protein ZFP36L1 Inhibits Flavivirus Infection by both 5′-3′ XRN1 and 3′-5′ RNA-Exosome RNA Decay Pathways. *Journal of Virology*, 96 (1). Available from 10.1128/jvi.01665-21 [Accessed 3 May 2022].

Chrestensen, C., Schroeder, M., Shabanowitz, J., Hunt, D., Pelo, J., Worthington, M. and Sturgill, T. (2004). MAPKAP Kinase 2 Phosphorylates Tristetraprolin on in Vivo Sites Including Ser178, a Site Required for 14-3-3 Binding. *Journal of Biological Chemistry*, 279 (11), 10176-10184. Available from 10.1074/jbc.m310486200 [Accessed 17 June 2022].

Christmann, M. and Kaina, B. (2013). Transcriptional regulation of human DNA repair genes following genotoxic stress: trigger mechanisms, inducible responses and genotoxic adaptation. *Nucleic Acids Research*, 41 (18), 8403-8420. Available from 10.1093/nar/gkt635 [Accessed 13 May 2022].

Clark, A. and Dean, J. (2016). The control of inflammation via the phosphorylation and dephosphorylation of tristetraprolin: a tale of two phosphatases. *Biochemical Society Transactions*, 44 (5), 1321-1337. Available from 10.1042/bst20160166 [Accessed 8 May 2022].

Clement, K., Rees, H., Canver, M., Gehrke, J., Farouni, R., Hsu, J., Cole, M., Liu, D., Joung, J., Bauer, D. and Pinello, L. (2019). CRISPResso2 provides accurate and rapid genome editing sequence analysis. *Nature Biotechnology*, 37 (3), 224-226. Available from 10.1038/s41587-019-0032-3 [Accessed 23 May 2022].

Coelho, M., de Carné Trécesson, S., Rana, S., Zecchin, D., Moore, C., Molina-Arcas, M., East, P., Spencer-Dene, B., Nye, E., Barnouin, K., Snijders, A., Lai, W., Blackshear, P. and Downward, J. (2017). Oncogenic RAS Signaling Promotes Tumor Immunoresistance by Stabilizing PD-L1 mRNA. *Immunity*, 47 (6), 1083-1099.e6. Available from 10.1016/j.immuni.2017.11.016 [Accessed 7 May 2022].

Corbett, A. (2018). Post-transcriptional regulation of gene expression and human disease. *Current Opinion in Cell Biology*, 52, 96-104. Available from 10.1016/j.ceb.2018.02.011 [Accessed 23 June 2022].

Corcoran, D., Georgiev, S., Mukherjee, N., Gottwein, E., Skalsky, R., Keene, J. and Ohler, U. (2011). PARalyzer: definition of RNA binding sites from PAR-CLIP short-read sequence data. *Genome Biology*, 12 (8), R79. Available from 10.1186/gb-2011-12-8-r79 [Accessed 2 May 2022].

Costantino, L. and Koshland, D. (2018). Genome-wide Map of R-Loop-Induced Damage Reveals How a Subset of R-Loops Contributes to Genomic Instability. *Molecular Cell*, 71 (4), 487-497.e3. Available from 10.1016/j.molcel.2018.06.037 [Accessed 11 June 2022].

Courtot, L., Bournique, E., Maric, C., Guitton-Sert, L., Madrid-Mencía, M., Pancaldi, V., Cadoret, J., Hoffmann, J. and Bergoglio, V. (2021). Low Replicative Stress Triggers Cell-Type Specific Inheritable Advanced Replication Timing. *International Journal of Molecular Sciences*, 22 (9), 4959. Available from 10.3390/ijms22094959 [Accessed 28 April 2022].

Coussens, L. and Werb, Z. (2002). Inflammation and cancer. *Nature*, 420 (6917), 860-867. Available from 10.1038/nature01322 [Accessed 7 May 2022].

Cramer, P. (2019). Organization and regulation of gene transcription. *Nature*, 573 (7772), 45-54. Available from 10.1038/s41586-019-1517-4 [Accessed 30 June 2022].

Cristini, A., Groh, M., Kristiansen, M. and Gromak, N. (2018). RNA/DNA Hybrid Interactome Identifies DXH9 as a Molecular Player in Transcriptional Termination and R-Loop-Associated DNA Damage. *Cell Reports*, 23 (6), 1891-1905. Available from 10.1016/j.celrep.2018.04.025 [Accessed 21 April 2022].

Crossley, M., Bocek, M. and Cimprich, K. (2019). R-Loops as Cellular Regulators and Genomic Threats. *Molecular Cell*, 73 (3), 398-411. Available from 10.1016/j.molcel.2019.01.024 [Accessed 19 June 2022].

Crossley, M., Brickner, J., Song, C., Zar, S., Maw, S., Chédin, F., Tsai, M. and Cimprich, K. (2021). Catalytically inactive, purified RNase H1: A specific and sensitive probe for RNA–DNA hybrid imaging. *Journal of Cell Biology*, 220 (9). Available from 10.1083/jcb.202101092 [Accessed 24 June 2022].

Dang, C. (2012). MYC on the Path to Cancer. *Cell*, 149 (1), 22-35. Available from 10.1016/j.cell.2012.03.003 [Accessed 4 May 2022].

Das, S., Bano, S., Kapse, P. and Kundu, G. (2022). CRISPR based therapeutics: a new paradigm in cancer precision medicine. *Molecular Cancer*, 21 (1). Available from 10.1186/s12943-022-01552-6 [Accessed 11 July 2022].

Debnath, S. and Sharma, S. (2020). RECQ1 Helicase in Genomic Stability and Cancer. *Genes*, 11 (6), 622. Available from 10.3390/genes11060622 [Accessed 21 July 2022].

Di Marco, S., Hasanova, Z., Kanagaraj, R., Chappidi, N., Altmannova, V., Menon, S., Sedlackova, H., Langhoff, J., Surendranath, K., Hühn, D., Bhowmick, R., Marini, V., Ferrari, S., Hickson, I., Krejci, L. and Janscak, P. (2017). RECQ5 Helicase Cooperates with MUS81 Endonuclease in Processing Stalled Replication Forks at Common Fragile Sites during Mitosis. *Molecular Cell*, 66 (5), 658-671.e8. Available from 10.1016/j.molcel.2017.05.006 [Accessed 20 May 2022].

Díaz-Muñoz, M., Kiselev, V., Le Novère, N., Curk, T., Ule, J. and Turner, M. (2017). Tia1 dependent regulation of mRNA subcellular location and translation controls p53 expression in B cells. *Nature Communications*, 8 (1). Available from 10.1038/s41467-017-00454-2 [Accessed 4 May 2022].

Dietlein, F., Thelen, L. and Reinhardt, H. (2014). Cancer-specific defects in DNA repair pathways as targets for personalized therapeutic approaches. *Trends in Genetics*, 30 (8), 326-339. Available from 10.1016/j.tig.2014.06.003 [Accessed 10 May 2022].

Domínguez-Sánchez, M., Barroso, S., Gómez-González, B., Luna, R. and Aguilera, A. (2011). Genome Instability and Transcription Elongation Impairment in Human Cells Depleted of THO/TREX. *PLoS Genetics*, 7 (12), e1002386. Available from 10.1371/journal.pgen.1002386 [Accessed 17 July 2022].

DuBois, R., McLane, M., Ryder, K., Lau, L. and Nathans, D. (1990). A growth factor-inducible nuclear protein with a novel cysteine/histidine repetitive sequence. *Journal of Biological Chemistry*, 265 (31), 19185-19191. Available from 10.1016/s0021-9258(17)30642-7.

Dueva, R. and Iliakis, G. (2020). Replication protein A: a multifunctional protein with roles in DNA replication, repair and beyond. *NAR Cancer*, 2 (3). Available from 10.1093/narcan/zcaa022 [Accessed 6 June 2022].

Durkin, S., Arlt, M., Howlett, N. and Glover, T. (2006). Depletion of CHK1, but not CHK2, induces chromosomal instability and breaks at common fragile sites. *Oncogene*, 25 (32), 4381-4388. Available from 10.1038/sj.onc.1209466 [Accessed 12 March 2022].

Dutertre, M., Lambert, S., Carreira, A., Amor-Guéret, M. and Vagner, S. (2014). DNA damage: RNA-binding proteins protect from near and far. *Trends in Biochemical Sciences*, 39 (3), 141-149. Available from 10.1016/j.tibs.2014.01.003 [Accessed 11 May 2022].

Engstrom, J. and Kmiec, E. (2008). DNA Replication, cell cycle progression and the targeted gene repair reaction. *Cell Cycle*, 7 (10), 1402-1414. Available from 10.4161/cc.7.10.5826 [Accessed 9 July 2022].

Eykelenboom, J., Harte, E., Canavan, L., Pastor-Peidro, A., Calvo-Asensio, I., Llorens-Agost, M. and Lowndes, N. (2013). ATR Activates the S-M Checkpoint during Unperturbed Growth to Ensure Sufficient Replication Prior to Mitotic Onset. *Cell Reports*, 5 (4), 1095-1107. Available from 10.1016/j.celrep.2013.10.027 [Accessed 7 June 2022].

Fabian, M., Frank, F., Rouya, C., Siddiqui, N., Lai, W., Karetnikov, A., Blackshear, P., Nagar, B. and Sonenberg, N. (2013). Structural basis for the recruitment of the human CCR4–NOT deadenylase complex by tristetraprolin. *Nature Structural &amp; Molecular Biology*, 20 (6), 735-739. Available from 10.1038/nsmb.2572 [Accessed 3 May 2022].

Fallahi, M., Amelio, A., Cleveland, J. and Rounbehler, R. (2014). CREB Targets Define the Gene Expression Signature of Malignancies Having Reduced Levels of the Tumor Suppressor Tristetraprolin. *PLoS ONE*, 9 (12), e115517. Available from 10.1371/journal.pone.0115517 [Accessed 8 July 2022].

Fan, J., Yang, X., Wang, W., Wood, W., Becker, K. and Gorospe, M. (2002). Global analysis of stress-regulated mRNA turnover by using cDNA arrays. *Proceedings of the National Academy of Sciences*, 99 (16), 10611-10616. Available from 10.1073/pnas.162212399 [Accessed 11 May 2022].

Fenech, M., Knasmueller, S., Bolognesi, C., Holland, N., Bonassi, S. and Kirsch-Volders, M. (2020). Micronuclei as biomarkers of DNA damage, aneuploidy, inducers of chromosomal hypermutation and as sources of pro-inflammatory DNA in humans. *Mutation Research/Reviews in Mutation Research*, 786, 108342. Available from 10.1016/j.mrrev.2020.108342 [Accessed 5 June 2022].

Fernández-Casañas, M. and Chan, K. (2018). The Unresolved Problem of DNA Bridging. *Genes*, 9 (12), 623. Available from 10.3390/genes9120623 [Accessed 5 June 2022].

Förch, P., Puig, O., Kedersha, N., Martínez, C., Granneman, S., Séraphin, B., Anderson, P. and Valcárcel, J. (2000). The Apoptosis-Promoting Factor TIA-1 Is a Regulator of Alternative Pre-mRNA Splicing. *Molecular Cell*, 6 (5), 1089-1098. Available from 10.1016/s1097-2765(00)00107-6 [Accessed 14 May 2022].

Fragkos, M. and Naim, V. (2017). Rescue from replication stress during mitosis. *Cell Cycle*, 16 (7), 613-633. Available from 10.1080/15384101.2017.1288322 [Accessed 21 June 2022].

Franks, T. and Lykke-Andersen, J. (2007). TTP and BRF proteins nucleate processing body formation to silence mRNAs with AU-rich elements. *Genes &amp; Development*, 21 (6), 719-735. Available from 10.1101/gad.1494707 [Accessed 8 May 2022].

Gaba, A., Grivennikov, S., Do, M., Stumpo, D., Blackshear, P. and Karin, M. (2012). Cutting Edge: IL-10–Mediated Tristetraprolin Induction Is Part of a Feedback Loop That Controls Macrophage STAT3 Activation and Cytokine Production. *The Journal of Immunology*, 189 (5), 2089-2093. Available from 10.4049/jimmunol.1201126 [Accessed 13 June 2022].

Gagou, M., Zuazua-Villar, P. and Meuth, M. (2010). Enhanced H2AX Phosphorylation, DNA Replication Fork Arrest, and Cell Death in the Absence of Chk1. *Molecular Biology of the Cell*, 21 (5), 739-752. Available from 10.1091/mbc.e09-07-0618 [Accessed 6 June 2022].

Gaillard, H., García-Muse, T. and Aguilera, A. (2015). Replication stress and cancer. *Nature Reviews Cancer*, 15 (5), 276-289. Available from 10.1038/nrc3916 [Accessed 17 June 2022].

Gaj, T., Gersbach, C. and Barbas, C. (2013). ZFN, TALEN, and CRISPR/Cas-based methods for genome engineering. Trends in Biotechnology, 31 (7), 397-405. Available from 10.1016/j.tibtech.2013.04.004 [Accessed 31 July 2022].

Galloway, A., Saveliev, A., Łukasiak, S., Hodson, D., Bolland, D., Balmanno, K., Ahlfors, H., Monzón-Casanova, E., Mannurita, S., Bell, L., Andrews, S., Díaz-Muñoz, M., Cook, S., Corcoran, A. and Turner, M. (2016). RNA-binding proteins ZFP36L1 and ZFP36L2 promote cell quiescence. *Science*, 352 (6284), 453-459. Available from 10.1126/science.aad5978 [Accessed 12 May 2022].

Gan, W., Guan, Z., Liu, J., Gui, T., Shen, K., Manley, J. and Li, X. (2011). R-loop-mediated genomic instability is caused by impairment of replication fork progression. *Genes &amp; Development*, 25 (19), 2041-2056. Available from 10.1101/gad.17010011 [Accessed 15 May 2022].

García-Benítez, F., Gaillard, H. and Aguilera, A. (2017). Physical proximity of chromatin to nuclear pores prevents harmful R loop accumulation contributing to maintain genome stability. *Proceedings of the National Academy of Sciences*, 114 (41), 10942-10947. Available from 10.1073/pnas.1707845114 [Accessed 17 July 2022].

García-Mauriño, S., Rivero-Rodríguez, F., Velázquez-Cruz, A., Hernández-Vellisca, M., Díaz-Quintana, A., De la Rosa, M. and Díaz-Moreno, I. (2017). RNA Binding Protein Regulation and Cross-Talk in the Control of AU-rich mRNA Fate. *Frontiers in Molecular Biosciences*, 4. Available from 10.3389/fmolb.2017.00071 [Accessed 4 May 2022].

García-Rubio, M., Pérez-Calero, C., Barroso, S., Tumini, E., Herrera-Moyano, E., Rosado, I. and Aguilera, A. (2015). The Fanconi Anemia Pathway Protects Genome Integrity from R-loops. *PLOS Genetics*, 11 (11), e1005674. Available from 10.1371/journal.pgen.1005674 [Accessed 11 June 2022].

Georgakilas, A., Tsantoulis, P., Kotsinas, A., Michalopoulos, I., Townsend, P. and Gorgoulis, V. (2014). Are common fragile sites merely structural domains or highly organized “functional” units susceptible to oncogenic stress?. *Cellular and Molecular Life Sciences*, 71 (23), 4519-4544. Available from 10.1007/s00018-014-1717-x [Accessed 16 May 2022].

Gerstberger, S., Hafner, M. and Tuschl, T. (2014). A census of human RNA-binding proteins. *Nature Reviews Genetics*, 15 (12), 829-845. Available from 10.1038/nrg3813 [Accessed 1 May 2022].

Gherzi, R., Lee, K., Briata, P., Wegmüller, D., Moroni, C., Karin, M. and Chen, C. (2004). A KH Domain RNA Binding Protein, KSRP, Promotes ARE-Directed mRNA Turnover by Recruiting the Degradation Machinery. *Molecular Cell*, 14 (5), 571-583. Available from 10.1016/j.molcel.2004.05.002 [Accessed 4 May 2022].

Ghosh, S. and Jacobson, A. (2010). RNA decay modulates gene expression and controls its fidelity. *Wiley Interdisciplinary Reviews: RNA*, 1 (3), 351-361. Available from 10.1002/wrna.25 [Accessed 23 June 2022].

Glisovic, T., Bachorik, J., Yong, J. and Dreyfuss, G. (2008). RNA-binding proteins and post-transcriptional gene regulation. *FEBS Letters*, 582 (14), 1977-1986. Available from 10.1016/j.febslet.2008.03.004 [Accessed 30 June 2022].

Goddio, M., Gattelli, A., Slomiansky, V., Lacunza, E., Gingerich, T., Tocci, J., Facchinetti, M., Curino, A., LaMarre, J., Abba, M. and Kordon, E. (2012). Mammary differentiation induces expression of Tristetraprolin, a tumor suppressor AU-rich mRNA-binding protein. *Breast Cancer*

Research and Treatment, 135 (3), 749-758. Available from 10.1007/s10549-012-2216-0 [Accessed 8 July 2022].

Goldfarb, D., Corbett, A., Mason, D., Harreman, M. and Adam, S. (2004). Importin α: a multipurpose nuclear-transport receptor. *Trends in Cell Biology*, 14 (9), 505-514. Available from 10.1016/j.tcb.2004.07.016 [Accessed 15 July 2022].

Gómez-González, B. and Aguilera, A. (2007). Activation-induced cytidine deaminase action is strongly stimulated by mutations of the THO complex. *Proceedings of the National Academy of Sciences*, 104 (20), 8409-8414. Available from 10.1073/pnas.0702836104 [Accessed 15 May 2022].

Gomperts, M., C.Pascall, J. and D.Brown, K. (1990). The nucleotide sequence of a cDNA encoding an EGF-inducible gene indicates the existence of a new family of mitogen-induced genes. *Oncogene*, 5 (7), 1081-3.

Gorgoulis, V., Vassiliou, L., Karakaidos, P., Zacharatos, P., Kotsinas, A., Liloglou, T., Venere, M., DiTullio, R., Kastrinakis, N., Levy, B., Kletsas, D., Yoneta, A., Herlyn, M., Kittas, C. and Halazonetis, T. (2005). Activation of the DNA damage checkpoint and genomic instability in human precancerous lesions. *Nature*, 434 (7035), 907-913. Available from 10.1038/nature03485 [Accessed 4 June 2022].

Gratacós, F. and Brewer, G. (2010). The role of AUF1 in regulated mRNA decay. *Wiley Interdisciplinary Reviews: RNA*, 1 (3), 457-473. Available from 10.1002/wrna.26 [Accessed 30 June 2022].

Griseri, P., Bourcier, C., Hieblot, C., Essafi-Benkhadir, K., Chamorey, E., Touriol, C. and Pagès, G. (2011). A synonymous polymorphism of the Tristetraprolin (TTP) gene, an AU-rich mRNA-binding protein, affects translation efficiency and response to Herceptin treatment in breast cancer patients. *Human Molecular Genetics*, 20 (23), 4556-4568. Available from 10.1093/hmg/ddr390 [Accessed 15 June 2022].

Groh, M., Lufino, M., Wade-Martins, R. and Gromak, N. (2014). R-loops Associated with Triplet Repeat Expansions Promote Gene Silencing in Friedreich Ataxia and Fragile X Syndrome. *PLoS Genetics*, 10 (5), e1004318. Available from 10.1371/journal.pgen.1004318 [Accessed 29 April 2022].

Gruber, A., Fallmann, J., Kratochvill, F., Kovarik, P. and Hofacker, I. (2010). AREsite: a database for the comprehensive investigation of AU-rich elements. *Nucleic Acids Research*, 39 (Database), D66-D69. Available from 10.1093/nar/gkq990 [Accessed 3 May 2022].

Haahr, P., Hoffmann, S., Tollenaere, M., Ho, T., Toledo, L., Mann, M., Bekker-Jensen, S., Räschle, M. and Mailand, N. (2016). Activation of the ATR kinase by the RPA-binding protein ETAA1. *Nature Cell Biology*, 18 (11), 1196-1207. Available from 10.1038/ncb3422 [Accessed 10 May 2022].

Halász, L., Karányi, Z., Boros-Oláh, B., Kuik-Rózsa, T., Sipos, É., Nagy, É., Mosolygó-L, Á., Mázló, A., Rajnavölgyi, É., Halmos, G. and Székvölgyi, L. (2017). RNA-DNA hybrid (R-loop) immunoprecipitation mapping: an analytical workflow to evaluate inherent biases. *Genome Research*, 27 (6), 1063-1073. Available from 10.1101/gr.219394.116 [Accessed 3 June 2022].

Halees, A., El-Badrawi, R. and Khabar, K. (2007). ARED Organism: expansion of ARED reveals AU-rich element cluster variations between human and mouse. *Nucleic Acids Research*, 36 (Database), D137-D140. Available from 10.1093/nar/gkm959 [Accessed 3 May 2022].

Halees, A., Hitti, E., Al-Saif, M., Mahmoud, L., Vlasova-St. Louis, I., Beisang, D., Bohjanen, P. and Khabar, K. (2011). Global assessment of GU-rich regulatory content and function in the human transcriptome. *RNA Biology*, 8 (4), 681-691. Available from 10.4161/rna.8.4.16283 [Accessed 4 May 2022].

Hamperl, S. and Cimprich, K. (2014). The contribution of co-transcriptional RNA:DNA hybrid structures to DNA damage and genome instability. *DNA Repair*, 19, 84-94. Available from 10.1016/j.dnarep.2014.03.023 [Accessed 26 May 2022].

Hamperl, S., Bocek, M., Saldivar, J., Swigut, T. and Cimprich, K. (2017). Transcription-Replication Conflict Orientation Modulates R-Loop Levels and Activates Distinct DNA Damage Responses. *Cell*, 170 (4), 774-786.e19. Available from 10.1016/j.cell.2017.07.043 [Accessed 30 April 2022].

Han, C., Wan, G., Langley, R., Zhang, X. and Lu, X. (2012). Crosstalk between the DNA damage response pathway and microRNAs. *Cellular and Molecular Life Sciences*, 69 (17), 2895-2906. Available from 10.1007/s00018-012-0959-8 [Accessed 15 May 2022].

Han, Y., Zheng, Q., Tian, Y., Ji, Z. and Ye, H. (2019). Identification of a nine-gene panel as a prognostic indicator for recurrence with muscle-invasive bladder cancer. *Journal of Surgical Oncology*, 119 (8), 1145-1154. Available from 10.1002/jso.25446 [Accessed 8 July 2022].

Hanahan, D. and Weinberg, R. (2011). Hallmarks of Cancer: The Next Generation. *Cell*, 144 (5), 646-674. Available from 10.1016/j.cell.2011.02.013 [Accessed 16 June 2022].

Harrigan, J., Belotserkovskaya, R., Coates, J., Dimitrova, D., Polo, S., Bradshaw, C., Fraser, P. and Jackson, S. (2011). Replication stress induces 53BP1-containing OPT domains in G1 cells. *Journal of Cell Biology*, 193 (1), 97-108. Available from 10.1083/jcb.201011083 [Accessed 17 April 2022].

Hau, H., Walsh, R., Ogilvie, R., Williams, D., Reilly, C. and Bohjanen, P. (2007). Tristetraprolin recruits functional mRNA decay complexes to ARE sequences. *Journal of Cellular Biochemistry*, 100 (6), 1477-1492. Available from 10.1002/jcb.21130 [Accessed 9 May 2022].

Hellman, A., Zlotorynski, E., Scherer, S., Cheung, J., Vincent, J., Smith, D., Trakhtenbrot, L. and Kerem, B. (2002). A role for common fragile site induction in amplification of human oncogenes. *Cancer Cell*, 1 (1), 89-97. Available from 10.1016/s1535-6108(02)00017-x [Accessed 16 May 2022].

Helmrich, A., Ballarino, M. and Tora, L. (2011). Collisions between Replication and Transcription Complexes Cause Common Fragile Site Instability at the Longest Human Genes. *Molecular Cell*, 44 (6), 966-977. Available from 10.1016/j.molcel.2011.10.013 [Accessed 29 April 2022].

Hentze, M., Castello, A., Schwarzl, T. and Preiss, T. (2018). A brave new world of RNA-binding proteins. *Nature Reviews Molecular Cell Biology*, 19 (5), 327-341. Available from 10.1038/nrm.2017.130 [Accessed 1 May 2022].

HEXIMER, S. and FORSDYKE, D. (1993). A Human Putative Lymphocyte G<sub>0</sub>/G<sub>1</sub>Switch Gene Homologous to a Rodent Gene Encoding a Zinc-Binding Potential Transcription Factor. *DNA and Cell Biology*, 12 (1), 73-88. Available from 10.1089/dna.1993.12.73 [Accessed 6 May 2022].

Hinman, M. and Lou, H. (2008). Diverse molecular functions of Hu proteins. *Cellular and Molecular Life Sciences*, 65 (20), 3168-3181. Available from 10.1007/s00018-008-8252-6 [Accessed 4 May 2022].

Hodroj, D., Recolin, B., Serhal, K., Martinez, S., Tsanov, N., Abou Merhi, R. and Maiorano, D. (2017). An ATR -dependent function for the Ddx19 RNA helicase in nuclear R-loop metabolism. *The EMBO Journal*, 36 (9), 1182-1198. Available from 10.15252/embj.201695131 [Accessed 23 July 2022].

Hodson, D., Janas, M., Galloway, A., Bell, S., Andrews, S., Li, C., Pannell, R., Siebel, C., MacDonald, H., De Keersmaecker, K., Ferrando, A., Grutz, G. and Turner, M. (2010). Deletion of the RNA-binding proteins ZFP36L1 and ZFP36L2 leads to perturbed thymic development and T lymphoblastic leukemia. *Nature Immunology*, 11 (8), 717-724. Available from 10.1038/ni.1901 [Accessed 7 May 2022].

Holcomb, V., Rodier, F., Choi, Y., Busuttil, R., Vogel, H., Vijg, J., Campisi, J. and Hasty, P. (2008). Ku80 Deletion Suppresses Spontaneous Tumors and Induces a p53-Mediated DNA Damage Response. *Cancer Research*, 68 (22), 9497-9502. Available from 10.1158/0008-5472.can-08-2085 [Accessed 6 June 2022].

Hong, S. (2017). RNA Binding Protein as an Emerging Therapeutic Target for Cancer Prevention and Treatment. *Journal of Cancer Prevention*, 22 (4), 203-210. Available from 10.15430/jcp.2017.22.4.203 [Accessed 1 May 2022].

Howlett, N., Taniguchi, T., Durkin, S., D'Andrea, A. and Glover, T. (2005). The Fanconi anemia pathway is required for the DNA replication stress response and for the regulation of common fragile site stability. *Human Molecular Genetics*, 14 (5), 693-701. Available from 10.1093/hmg/ddi065 [Accessed 15 June 2022].

Huen, M. and Chen, J. (2007). The DNA damage response pathways: at the crossroad of protein modifications. *Cell Research*, 18 (1), 8-16. Available from 10.1038/cr.2007.109 [Accessed 10 May 2022].

Huertas, P. and Aguilera, A. (2003). Cotranscriptionally Formed DNA:RNA Hybrids Mediate Transcription Elongation Impairment and Transcription-Associated Recombination. *Molecular Cell*, 12 (3), 711-721. Available from 10.1016/j.molcel.2003.08.010 [Accessed 15 May 2022].

Huertas, P. (2010). DNA resection in eukaryotes: deciding how to fix the break. *Nature Structural &amp; Molecular Biology*, 17 (1), 11-16. Available from 10.1038/nsmb.1710 [Accessed 15 May 2022].

Hyatt, L., Wasserman, G., Rah, Y., Matsuura, K., Coleman, F., Hilliard, K., Pepper-Cunningham, Z., Ieong, M., Stumpo, D., Blackshear, P., Quinton, L., Mizgerd, J. and Jones, M. (2014). Myeloid ZFP36L1 Does Not Regulate Inflammation or Host Defense in Mouse Models of Acute Bacterial Infection. *PLoS ONE*, 9 (10), e109072. Available from 10.1371/journal.pone.0109072 [Accessed 13 June 2022].

Ibrahim, H., Wilusz, J. and Wilusz, C. (2008). RNA recognition by 3′-to-5′ exonucleases: The substrate perspective. *Biochimica et Biophysica Acta (BBA) - Gene Regulatory Mechanisms*, 1779 (4), 256-265. Available from 10.1016/j.bbagrm.2007.11.004 [Accessed 30 May 2022].

Ichijima, Y., Yoshioka, K., Yoshioka, Y., Shinohe, K., Fujimori, H., Unno, J., Takagi, M., Goto, H., Inagaki, M., Mizutani, S. and Teraoka, H. (2010). DNA Lesions Induced by Replication Stress Trigger Mitotic Aberration and Tetraploidy Development. *PLoS ONE*, 5 (1), e8821. Available from 10.1371/journal.pone.0008821 [Accessed 30 June 2022].

Igarashi, M. and Okuda, S. (2019). Evolutionary analysis of proline-directed phosphorylation sites in the mammalian growth cone identified using phosphoproteomics. *Molecular Brain*, 12 (1). Available from 10.1186/s13041-019-0476-x [Accessed 5 May 2022].

Jackson, S. and Bartek, J. (2009). The DNA-damage response in human biology and disease. *Nature*, 461 (7267), 1071-1078. Available from 10.1038/nature08467 [Accessed 10 May 2022].

Jackson, S. (2002). Sensing and repairing DNA double-strand breaks. *Carcinogenesis*, 23 (5), 687-696. Available from 10.1093/carcin/23.5.687 [Accessed 10 May 2022].

Jain, A., McCoy, M., Coats, C., Brown, S., Addya, S., Pelz, C., Sears, R., Yeo, C. and Brody, J. (2022). HuR Plays a Role in Double-Strand Break Repair in Pancreatic Cancer Cells and Regulates Functional BRCA1-Associated-Ring-Domain-1(BARD1) Isoforms. *Cancers*, 14 (7), 1848. Available from 10.3390/cancers14071848 [Accessed 11 June 2022].

Jamil, S., Lam, I., Majd, M., Tsai, S. and Duronio, V. (2015). Etoposide induces cell death via mitochondrial-dependent actions of p53. *Cancer Cell International*, 15 (1). Available from 10.1186/s12935-015-0231-z [Accessed 9 July 2022].

Jang, Y., Elsayed, Z., Eki, R., He, S., Du, K., Abbas, T. and Kai, M. (2020). Intrinsically disordered protein RBM14 plays a role in generation of RNA:DNA hybrids at double-strand break sites. *Proceedings of the National Academy of Sciences*, 117 (10), 5329-5338. Available from 10.1073/pnas.1913280117 [Accessed 18 April 2022].

Jayasooriya, R., Choi, Y., Hyun, J. and Kim, G. (2014). Camptothecin sensitizes human hepatoma Hep3B cells to TRAIL-mediated apoptosis via ROS-dependent death receptor 5 upregulation with the involvement of MAPKs. *Environmental Toxicology and Pharmacology*, 38 (3), 959-967. Available from 10.1016/j.etap.2014.10.012 [Accessed 9 July 2022].

Jiang, W., Zhu, D., Wang, C. and Zhu, Y. (2020). Tumor suppressing effects of tristetraprolin and its small double-stranded RNAs in bladder cancer. *Cancer Medicine*, 10 (1), 269-285. Available from 10.1002/cam4.3622 [Accessed 8 July 2022].

Jo, M., Kusano, Y. and Hirota, T. (2021). Unraveling pathologies underlying chromosomal instability in cancers. *Cancer Science*, 112 (8), 2975-2983. Available from 10.1111/cas.14989 [Accessed 23 June 2022].

Johnson, B., Geha, M. and Blackwell, T. (2000). Similar but distinct effects of the tristetraprolin/TIS11 immediate-early proteins on cell survival. *Oncogene*, 19 (13), 1657-1664. Available from 10.1038/sj.onc.1203474 [Accessed 15 June 2022].

Johnson, B., Stehn, J., Yaffe, M. and Blackwell, T. (2002). Cytoplasmic Localization of Tristetraprolin Involves 14-3-3-dependent and -independent Mechanisms. *Journal of Biological Chemistry*, 277 (20), 18029-18036. Available from 10.1074/jbc.m110465200 [Accessed 8 May 2022].

Joyal, J., Jiang, J. and Israel, D. (2006). Synthesis of DNA Libraries: Use of PCR to Analyze Ligation Substrates and Products. *Cold Spring Harbor Protocols*, 2006 (1), pdb.prot4136. Available from 10.1101/pdb.prot4136 [Accessed 26 May 2022].

Jungmichel, S., Rosenthal, F., Altmeyer, M., Lukas, J., Hottiger, M. and Nielsen, M. (2013). Proteome-wide Identification of Poly(ADP-Ribosyl)ation Targets in Different Genotoxic Stress Responses. *Molecular Cell*, 52 (2), 272-285. Available from 10.1016/j.molcel.2013.08.026 [Accessed 13 May 2022].

Kaehler, M., Dworschak, M., Rodin, J., Ruemenapp, J., Vater, I., Penas, E., Liu, C., Cascorbi, I. and Nagel, I. (2021). ZFP36L1 plays an ambiguous role in the regulation of cell expansion and negatively regulates CDKN1A in chronic myeloid leukemia cells. *Experimental Hematology*, 99, 54-64.e7. Available from 10.1016/j.exphem.2021.05.006 [Accessed 7 May 2022].

Kastan, M. and Bartek, J. (2004). Cell-cycle checkpoints and cancer. *Nature*, 432 (7015), 316-323. Available from 10.1038/nature03097 [Accessed 10 May 2022].

Kedar, V., Zucconi, B., Wilson, G. and Blackshear, P. (2012). Direct Binding of Specific AUF1 Isoforms to Tandem Zinc Finger Domains of Tristetraprolin (TTP) Family Proteins. *Journal of Biological Chemistry*, 287 (8), 5459-5471. Available from 10.1074/jbc.m111.312652 [Accessed 4 May 2022].

Kedersha, N., Cho, M., Li, W., Yacono, P., Chen, S., Gilks, N., Golan, D. and Anderson, P. (2000). Dynamic Shuttling of Tia-1 Accompanies the Recruitment of mRNA to Mammalian Stress Granules. *Journal of Cell Biology*, 151 (6), 1257-1268. Available from 10.1083/jcb.151.6.1257 [Accessed 4 May 2022].

Kedersha, N., Stoecklin, G., Ayodele, M., Yacono, P., Lykke-Andersen, J., Fritzler, M., Scheuner, D., Kaufman, R., Golan, D. and Anderson, P. (2005). Stress granules and processing bodies are dynamically linked sites of mRNP remodeling. *Journal of Cell Biology*, 169 (6), 871-884. Available from 10.1083/jcb.200502088 [Accessed 8 May 2022].

Khabar, K. (2005). The AU-Rich Transcriptome: More Than Interferons and Cytokines, and Its Role in Disease. *Journal of Interferon &amp; Cytokine Research*, 25 (1), 1-10. Available from 10.1089/jir.2005.25.1 [Accessed 4 May 2022].

Khanna, K. and Jackson, S. (2001). DNA double-strand breaks: signaling, repair and the cancer connection. *Nature Genetics*, 27 (3), 247-254. Available from 10.1038/85798 [Accessed 9 May 2022].

Kilchert, C., Wittmann, S. and Vasiljeva, L. (2016). The regulation and functions of the nuclear RNA exosome complex. *Nature Reviews Molecular Cell Biology*, 17 (4), 227-239. Available from 10.1038/nrm.2015.15 [Accessed 17 June 2022].

Kim, H. and Gorospe, M. (2008). Phosphorylated HuR shuttles in cycles. *Cell Cycle*, 7 (20), 3124-3126. Available from 10.4161/cc.7.20.6884 [Accessed 14 May 2022].

Kim, H., Abdelmohsen, K. and Gorospe, M. (2010). Regulation of HuR by DNA Damage Response Kinases. *Journal of Nucleic Acids*, 2010, 1-8. Available from 10.4061/2010/981487 [Accessed 13 May 2022].

Kim, Y., Furman, C., Manhart, C., Alani, E. and Finkelstein, I. (2018). Intrinsically disordered regions regulate both catalytic and non-catalytic activities of the MutLα mismatch repair complex. *Nucleic Acids Research*. Available from 10.1093/nar/gky1244 [Accessed 18 April 2022].

Kishore, S., Jaskiewicz, L., Burger, L., Hausser, J., Khorshid, M. and Zavolan, M. (2011). A quantitative analysis of CLIP methods for identifying binding sites of RNA-binding proteins. *Nature Methods*, 8 (7), 559-564. Available from 10.1038/nmeth.1608 [Accessed 8 May 2022].

Klaric, J., Wüst, S. and Panier, S. (2021). New Faces of old Friends: Emerging new Roles of RNA-Binding Proteins in the DNA Double-Strand Break Response. *Frontiers in Molecular Biosciences*, 8. Available from 10.3389/fmolb.2021.668821 [Accessed 21 April 2022].

Kleiman, F. and Manley, J. (2001). The BARD1-CstF-50 Interaction Links mRNA 3′ End Formation to DNA Damage and Tumor Suppression. *Cell*, 104 (5), 743-753. Available from 10.1016/s0092-8674(01)00270-7 [Accessed 11 May 2022].

Kondo, M., Noguchi, A., Matsuura, Y., Shimada, M., Yokota, N. and Kawahara, H. (2018). Novel phosphorelay-dependent control of ZFP36L1 protein during the cell cycle. *Biochemical and Biophysical*

Research Communications, 501 (2), 387-393. Available from 10.1016/j.bbrc.2018.04.212 [Accessed 8 May 2022].

Kontoyiannis, D., Pasparakis, M., Pizarro, T., Cominelli, F. and Kollias, G. (1999). Impaired On/Off Regulation of TNF Biosynthesis in Mice Lacking TNF AU-Rich Elements. *Immunity*, 10 (3), 387-398. Available from 10.1016/s1074-7613(00)80038-2 [Accessed 13 June 2022].

Kotsantis, P., Petermann, E. and Boulton, S. (2018). Mechanisms of Oncogene-Induced Replication Stress: Jigsaw Falling into Place. *Cancer Discovery*, 8 (5), 537-555. Available from 10.1158/2159-8290.cd-17-1461 [Accessed 10 May 2022].

Kröhler, T., Kessler, S., Hosseini, K., List, M., Barghash, A., Patial, S., Laggai, S., Gemperlein, K., Haybaeck, J., Müller, R., Helms, V., Schulz, M., Hoppstädter, J., Blackshear, P. and Kiemer, A. (2019). The mRNA-binding Protein TTP/ZFP36 in Hepatocarcinogenesis and Hepatocellular Carcinoma. *Cancers*, 11 (11), 1754. Available from 10.3390/cancers11111754 [Accessed 7 May 2022].

Kruiswijk, F., Yuniati, L., Magliozzi, R., Low, T., Lim, R., Bolder, R., Mohammed, S., Proud, C., Heck, A., Pagano, M. and Guardavaccaro, D. (2012). Coupled Activation and Degradation of eEF2K Regulates Protein Synthesis in Response to Genotoxic Stress. *Science Signaling*, 5 (227). Available from 10.1126/scisignal.2002718 [Accessed 11 May 2022].

Kumar, M., Matta, A., Masui, O., Srivastava, G., Kaur, J., Thakar, A., Shukla, N., RoyChoudhury, A., Sharma, M., Walfish, P., Michael Siu, K., Chauhan, S. and Ralhan, R. (2015). Nuclear heterogeneous nuclear ribonucleoprotein D is associated with poor prognosis and interactome analysis reveals its novel binding partners in oral cancer. *Journal of Translational Medicine*, 13 (1). Available from 10.1186/s12967-015-0637-3 [Accessed 15 May 2022].

Kumar, R., Nagpal, G., Kumar, V., Usmani, S., Agrawal, P. and Raghava, G. (2019). HumCFS: a database of fragile sites in human chromosomes. *BMC Genomics*, 19 (S9). Available from 10.1186/s12864-018-5330-5 [Accessed 16 May 2022].

Kumaraswamy, S., Chinnaiyan, P., Shankavaram, U., Lü, X., Camphausen, K. and Tofilon, P. (2008). Radiation-Induced Gene Translation Profiles Reveal Tumor Type and Cancer-Specific Components. *Cancer Research*, 68 (10), 3819-3826. Available from 10.1158/0008-5472.can-08-0016 [Accessed 11 May 2022].

Lafarga, V., Sung, H., Haneke, K., Roessig, L., Pauleau, A., Bruer, M., Rodriguez-Acebes, S., Lopez-Contreras, A., Gruss, O., Erhardt, S., Mendez, J., Fernandez-Capetillo, O. and Stoecklin, G. (2018).

<scp>TIAR</scp> marks nuclear G2/M transition granules and restricts <scp>CDK</scp> 1 activity under replication stress. *EMBO reports*, 20 (1). Available from 10.15252/embr.201846224 [Accessed 13 May 2022].

Lai, W., Carballo, E., Strum, J., Kennington, E., Phillips, R. and Blackshear, P. (1999). Evidence that Tristetraprolin Binds to AU-Rich Elements and Promotes the Deadenylation and Destabilization of Tumor Necrosis Factor Alpha mRNA. *Molecular and Cellular Biology*, 19 (6), 4311-4323. Available from 10.1128/mcb.19.6.4311 [Accessed 13 June 2022].

Lai, W., Carballo, E., Thorn, J., Kennington, E. and Blackshear, P. (2000). Interactions of CCCH Zinc Finger Proteins with mRNA. *Journal of Biological Chemistry*, 275 (23), 17827-17837. Available from 10.1074/jbc.m001696200 [Accessed 12 April 2022].

Lai, W., Kennington, E. and Blackshear, P. (2002). Interactions of CCCH Zinc Finger Proteins with mRNA. *Journal of Biological Chemistry*, 277 (11), 9606-9613. Available from 10.1074/jbc.m110395200 [Accessed 3 May 2022].

Lai, W., Kennington, E. and Blackshear, P. (2003). Tristetraprolin and Its Family Members Can Promote the Cell-Free Deadenylation of AU-Rich Element-Containing mRNAs by Poly(A) Ribonuclease. *Molecular and Cellular Biology*, 23 (11), 3798-3812. Available from 10.1128/mcb.23.11.3798-3812.2003 [Accessed 3 May 2022].

Lai, W., Stumpo, D. and Blackshear, P. (1990). Rapid insulin-stimulated accumulation of an mRNA encoding a proline-rich protein. *Journal of Biological Chemistry*, 265 (27), 16556-16563. Available from 10.1016/s0021-9258(17)46259-4 [Accessed 6 May 2022].

Lai, W., Stumpo, D., Wells, M., Gruzdev, A., Hicks, S., Nicholson, C., Yang, Z., Faccio, R., Webster, M., Passmore, L. and Blackshear, P. (2019). Importance of the Conserved Carboxyl-Terminal CNOT1 Binding Domain to Tristetraprolin Activity <i>In Vivo</i>. *Molecular and Cellular Biology*, 39 (13). Available from 10.1128/mcb.00029-19 [Accessed 30 May 2022].

Lal, A., Abdelmohsen, K., Pullmann, R., Kawai, T., Galban, S., Yang, X., Brewer, G. and Gorospe, M. (2006). Posttranscriptional Derepression of GADD45α by Genotoxic Stress. *Molecular Cell*, 22 (1), 117-128. Available from 10.1016/j.molcel.2006.03.016 [Accessed 13 May 2022].

Lebedeva, S., Jens, M., Theil, K., Schwanhäusser, B., Selbach, M., Landthaler, M. and Rajewsky, N. (2011). Transcriptome-wide Analysis of Regulatory Interactions of the RNA-Binding Protein HuR. *Molecular Cell*, 43 (3), 340-352. Available from 10.1016/j.molcel.2011.06.008 [Accessed 13 May 2022].

Lebrec, V., Poteau, M., Morretton, J. and Gavet, O. (2022). Chk1 dynamics in G2 phase upon replication stress predict daughter cell outcome. *Developmental Cell*, 57 (5), 638-653.e5. Available from 10.1016/j.devcel.2022.02.013 [Accessed 11 June 2022].

Lee, H., Lee, S. and Leem, S. (2014). Tristetraprolin Regulates Prostate Cancer Cell Growth Through Suppression of E2F1. *Journal of Microbiology and Biotechnology*, 24 (2), 287-294. Available from 10.4014/jmb.1309.09070 [Accessed 7 May 2022].

Lee, T., Choi, J., Park, J. and Kang, T. (2020). Posttranscriptional control of the replication stress response via TTP-mediated Claspin mRNA stabilization. *Oncogene*, 39 (16), 3245-3257. Available from 10.1038/s41388-020-1220-9 [Accessed 12 May 2022].

Lezaja, A., Panagopoulos, A., Wen, Y., Carvalho, E., Imhof, R. and Altmeyer, M. (2021). RPA shields inherited DNA lesions for post-mitotic DNA synthesis. *Nature Communications*, 12 (1). Available from 10.1038/s41467-021-23806-5 [Accessed 8 June 2022].

Li, L., Germain, D., Poon, H., Hildebrandt, M., Monckton, E., McDonald, D., Hendzel, M. and Godbout, R. (2016). DEAD Box 1 Facilitates Removal of RNA and Homologous Recombination at DNA Double-Strand Breaks. *Molecular and Cellular Biology*, 36 (22), 2794-2810. Available from 10.1128/mcb.00415-16 [Accessed 17 July 2022].

Li, S. and Wu, X. (2020). Common fragile sites: protection and repair. *Cell &amp; Bioscience*, 10 (1). Available from 10.1186/s13578-020-00392-5 [Accessed 17 June 2022].

Li, X., Han, M., Zhang, H., Liu, F., Pan, Y., Zhu, J., Liao, Z., Chen, X. and Zhang, B. (2022). Structures and biological functions of zinc finger proteins and their roles in hepatocellular carcinoma. *Biomarker Research*, 10 (1). Available from 10.1186/s40364-021-00345-1.

Liang, J., Lei, T., Song, Y., Yanes, N., Qi, Y. and Fu, M. (2009). RNA-destabilizing Factor Tristetraprolin Negatively Regulates NF-κB Signaling. *Journal of Biological Chemistry*, 284 (43), 29383-29390. Available from 10.1074/jbc.m109.024745 [Accessed 8 May 2022].

Lin, R., Huang, C., Liu, P., Lin, I., Huang, Y., Chen, A., Chiu, H., Shih, S., Lin, L., Lien, S., Yen, L. and Liao, C. (2020). Zinc finger protein ZFP36L1 inhibits influenza A virus through translational repression by targeting HA, M and NS RNA transcripts. *Nucleic Acids Research*. Available from 10.1093/nar/gkaa458 [Accessed 12 April 2022].

LINDAHL, T. and BARNES, D. (2000). Repair of Endogenous DNA Damage. *Cold Spring Harbor Symposia on Quantitative Biology*, 65 (0), 127-134. Available from 10.1101/sqb.2000.65.127 [Accessed 9 May 2022].

Liu, P., Barkley, L., Day, T., Bi, X., Slater, D., Alexandrow, M., Nasheuer, H. and Vaziri, C. (2006). The Chk1-mediated S-phase Checkpoint Targets Initiation Factor Cdc45 via a Cdc25A/Cdk2-independent Mechanism. *Journal of Biological Chemistry*, 281 (41), 30631-30644. Available from 10.1074/jbc.m602982200 [Accessed 28 April 2022].

Liu, X. and Hu, C. (2020). Novel Potential Therapeutic Target for E2F1 and Prognostic Factors of E2F1/2/3/5/7/8 in Human Gastric Cancer. *Molecular Therapy - Methods &amp; Clinical Development*, 18, 824-838. Available from 10.1016/j.omtm.2020.07.017 [Accessed 7 May 2022].

Loh, X., Ding, L. and Koeffler, H. (2017). Abstract 4494: Tumor suppressive role of ZFP36L1 by suppressing HIF1α and Cyclin D1 in bladder and breast cancer. *Cancer Research*, 77 (13_Supplement), 4494-4494. Available from 10.1158/1538-7445.am2017-4494 [Accessed 8 July 2022].

Loh, X., Sun, Q., Ding, L., Mayakonda, A., Venkatachalam, N., Yeo, M., Silva, T., Xiao, J., Doan, N., Said, J., Ran, X., Zhou, S., Dakle, P., Shyamsunder, P., Koh, A., Huang, R., Berman, B., Tan, S., Yang, H., Lin, D. and Koeffler, H. (2019). RNA-Binding Protein <i>ZFP36L1</i> Suppresses Hypoxia and Cell-Cycle Signaling. *Cancer Research*, 80 (2), 219-233. Available from 10.1158/0008-5472.can-18-2796 [Accessed 7 May 2022].

Lou, D., Kim, E., Meyerson, N., Pancholi, N., Mohni, K., Enard, D., Petrov, D., Weller, S., Weitzman, M. and Sawyer, S. (2016). An Intrinsically Disordered Region of the DNA Repair Protein Nbs1 Is a Species-Specific Barrier to Herpes Simplex Virus 1 in Primates. *Cell Host &amp; Microbe*, 20 (2), 178-188. Available from 10.1016/j.chom.2016.07.003 [Accessed 18 April 2022].

Lu, X., Parvathaneni, S., Hara, T., Lal, A. and Sharma, S. (2013). Replication stress induces specific enrichment of RECQ1 at common fragile sites FRA3B and FRA16D. *Molecular Cancer*, 12 (1). Available from 10.1186/1476-4598-12-29 [Accessed 16 July 2022].

Lukas, C., Savic, V., Bekker-Jensen, S., Doil, C., Neumann, B., Sølvhøj Pedersen, R., Grøfte, M., Chan, K., Hickson, I., Bartek, J. and Lukas, J. (2011). 53BP1 nuclear bodies form around DNA lesions generated by mitotic transmission of chromosomes under replication stress. *Nature Cell Biology*, 13 (3), 243-253. Available from 10.1038/ncb2201 [Accessed 27 April 2022].

Luna, R., Rondón, A., Pérez-Calero, C., Salas-Armenteros, I. and Aguilera, A. (2019). The THO Complex as a Paradigm for the Prevention of Cotranscriptional R-Loops. *Cold Spring Harbor Symposia on Quantitative Biology*, 84, 105-114. Available from 10.1101/sqb.2019.84.039594 [Accessed 13 July 2022].

Lunde, B., Moore, C. and Varani, G. (2007). RNA-binding proteins: modular design for efficient function. *Nature Reviews Molecular Cell Biology*, 8 (6), 479-490. Available from 10.1038/nrm2178 [Accessed 23 June 2022].

Lykke-Andersen, J. and Wagner, E. (2005). Recruitment and activation of mRNA decay enzymes by two ARE-mediated decay activation domains in the proteins TTP and BRF-1. *Genes &amp; Development*, 19 (3), 351-361. Available from 10.1101/gad.1282305 [Accessed 3 May 2022].

Ma, H., Kim, A., Kafai, N., Earnest, J., Shah, A., Case, J., Basore, K., Gilliland, T., Sun, C., Nelson, C., Thackray, L., Klimstra, W., Fremont, D. and Diamond, M. (2020). LDLRAD3 is a receptor for Venezuelan equine encephalitis virus. *Nature*, 588 (7837), 308-314. Available from 10.1038/s41586-020-2915-3 [Accessed 17 July 2022].

Ma, W. and Mayr, C. (2018). A Membraneless Organelle Associated with the Endoplasmic Reticulum Enables 3′UTR-Mediated Protein-Protein Interactions. *Cell*, 175 (6), 1492-1506.e19. Available from 10.1016/j.cell.2018.10.007 [Accessed 9 May 2022].

Macheret, M. and Halazonetis, T. (2015). DNA Replication Stress as a Hallmark of Cancer. *Annual Review of Pathology: Mechanisms of Disease*, 10 (1), 425-448. Available from 10.1146/annurev-pathol-012414-040424 [Accessed 17 June 2022].

Madireddy, A., Kosiyatrakul, S., Boisvert, R., Herrera-Moyano, E., García-Rubio, M., Gerhardt, J., Vuono, E., Owen, N., Yan, Z., Olson, S., Aguilera, A., Howlett, N. and Schildkraut, C. (2016). FANCD2 Facilitates Replication through Common Fragile Sites. *Molecular Cell*, 64 (2), 388-404. Available from 10.1016/j.molcel.2016.09.017 [Accessed 15 June 2022].

Maffia, A., Ranise, C. and Sabbioneda, S. (2020). From R-Loops to G-Quadruplexes: Emerging New Threats for the Replication Fork. *International Journal of Molecular Sciences*, 21 (4), 1506. Available from 10.3390/ijms21041506 [Accessed 17 June 2022].

Maitra, S., Chou, C., Luber, C., Lee, K., Mann, M. and Chen, C. (2008). The AU-rich element mRNA decay-promoting activity of BRF1 is regulated by mitogen-activated protein kinase-activated protein kinase 2. *RNA*, 14 (5), 950-959. Available from 10.1261/rna.983708 [Accessed 5 May 2022].

Makita, S., Takatori, H. and Nakajima, H. (2021). Post-Transcriptional Regulation of Immune Responses and Inflammatory Diseases by RNA-Binding ZFP36 Family Proteins. *Frontiers in Immunology*, 12. Available from 10.3389/fimmu.2021.711633 [Accessed 22 July 2022].

Mankouri, H., Huttner, D. and Hickson, I. (2013). How unfinished business from S-phase affects mitosis and beyond. *The EMBO Journal*, 32 (20), 2661-2671. Available from 10.1038/emboj.2013.211.

Marchese, F., Aubareda, A., Tudor, C., Saklatvala, J., Clark, A. and Dean, J. (2010). MAPKAP Kinase 2 Blocks Tristetraprolin-directed mRNA Decay by Inhibiting CAF1 Deadenylase Recruitment. *Journal of Biological Chemistry*, 285 (36), 27590-27600. Available from 10.1074/jbc.m110.136473 [Accessed 3 May 2022].

Marderosian, M., Sharma, A., Funk, A., Vartanian, R., Masri, J., Jo, O. and Gera, J. (2006). Tristetraprolin regulates Cyclin D1 and c-Myc mRNA stability in response to rapamycin in an Akt-dependent manner via p38 MAPK signaling. *Oncogene*, 25 (47), 6277-6290. Available from 10.1038/sj.onc.1209645 [Accessed 13 June 2022].

Marechal, A. and Zou, L. (2013). DNA Damage Sensing by the ATM and ATR Kinases. *Cold Spring Harbor Perspectives in Biology*, 5 (9), a012716-a012716. Available from 10.1101/cshperspect.a012716 [Accessed 10 May 2022].

Maréchal, A. and Zou, L. (2014). RPA-coated single-stranded DNA as a platform for post-translational modifications in the DNA damage response. *Cell Research*, 25 (1), 9-23. Available from 10.1038/cr.2014.147 [Accessed 8 June 2022].

Martínez-Calle, N., Pascual, M., Ordoñez, R., Enériz, E., Kulis, M., Miranda, E., Guruceaga, E., Segura, V., Larráyoz, M., Bellosillo, B., Calasanz, M., Besses, C., Rifón, J., Martín-Subero, J., Agirre, X. and Prosper, F. (2019). Epigenomic profiling of myelofibrosis reveals widespread DNA methylation changes in enhancer elements and <i>ZFP36L1</i> as a potential tumor suppressor gene that is epigenetically regulated. *Haematologica*, 104 (8), 1572-1579. Available from 10.3324/haematol.2018.204917 [Accessed 8 July 2022].

Masuda, K., Abdelmohsen, K., Kim, M., Srikantan, S., Lee, E., Tominaga, K., Selimyan, R., Martindale, J., Yang, X., Lehrmann, E., Zhang, Y., Becker, K., Wang, J., Kim, H. and Gorospe, M. (2011). Global dissociation of HuR-mRNA complexes promotes cell survival after ionizing radiation. *The EMBO Journal*, 30 (6), 1040-1053. Available from 10.1038/emboj.2011.24 [Accessed 14 May 2022].

Matoulkova, E., Michalova, E., Vojtesek, B. and Hrstka, R. (2012). The role of the 3' untranslated region in post-transcriptional regulation of protein expression in mammalian cells. *RNA Biology*, 9 (5), 563-576. Available from 10.4161/rna.20231 [Accessed 4 May 2022].

Matsunaga, T. and Yamashita, J. (2014). Single-step generation of gene knockout-rescue system in pluripotent stem cells by promoter insertion with CRISPR/Cas9. *Biochemical and Biophysical Research Communications*, 444 (2), 158-163. Available from 10.1016/j.bbrc.2014.01.037 [Accessed 17 July 2022].

Matsuoka, S., Ballif, B., Smogorzewska, A., McDonald, E., Hurov, K., Luo, J., Bakalarski, C., Zhao, Z., Solimini, N., Lerenthal, Y., Shiloh, Y., Gygi, S. and Elledge, S. (2007). ATM and ATR Substrate Analysis Reveals Extensive Protein Networks Responsive to DNA Damage. *Science*, 316 (5828), 1160-1166. Available from 10.1126/science.1140321 [Accessed 10 May 2022].

Matsuura, Y., Noguchi, A., Sakai, S., Yokota, N. and Kawahara, H. (2020). Nuclear accumulation of ZFP36L1 is cell cycle-dependent and determined by a C-terminal serine-rich cluster. *The Journal of Biochemistry*, 168 (5), 477-489. Available from 10.1093/jb/mvaa072 [Accessed 17 April 2022].

Maura, F., Bolli, N., Angelopoulos, N., Dawson, K., Leongamornlert, D., Martincorena, I., Mitchell, T., Fullam, A., Gonzalez, S., Szalat, R., Abascal, F., Rodriguez-Martin, B., Samur, M., Glodzik, D., Roncador, M., Fulciniti, M., Tai, Y., Minvielle, S., Magrangeas, F., Moreau, P., Corradini, P., Anderson, K., Tubio, J., Wedge, D., Gerstung, M., Avet-Loiseau, H., Munshi, N. and Campbell, P. (2019). Genomic landscape and chronological reconstruction of driver events in multiple myeloma. *Nature Communications*, 10 (1). Available from 10.1038/s41467-019-11680-1 [Accessed 7 May 2022].

Maya-Mendoza, A., Moudry, P., Merchut-Maya, J., Lee, M., Strauss, R. and Bartek, J. (2018). High speed of fork progression induces DNA replication stress and genomic instability. *Nature*, 559 (7713), 279-284. Available from 10.1038/s41586-018-0261-5 [Accessed 6 June 2022].

Mazan-Mamczarz, K., Hagner, P., Zhang, Y., Dai, B., Lehrmann, E., Becker, K., Keene, J., Gorospe, M., Liu, Z. and Gartenhaus, R. (2011). ATM regulates a DNA damage response posttranscriptional RNA operon in lymphocytes. *Blood*, 117 (8), 2441-2450. Available from 10.1182/blood-2010-09-310987 [Accessed 14 May 2022].

Mersaoui, S., Yu, Z., Coulombe, Y., Karam, M., Busatto, F., Masson, J. and Richard, S. (2019). Arginine methylation of the DDX 5 helicase RGG /

RG motif by PRMT 5 regulates resolution of RNA:DNA hybrids. *The EMBO Journal*, 38 (15). Available from 10.15252/embj.2018100986 [Accessed 17 July 2022].

Mirkin, N., Fonseca, D., Mohammed, S., Cevher, M., Manley, J. and Kleiman, F. (2008). The 3' processing factor CstF functions in the DNA repair response. *Nucleic Acids Research*, 36 (6), 1792-1804. Available from 10.1093/nar/gkn005 [Accessed 11 May 2022].

Mocanu, C., Karanika, E., Fernández-Casañas, M., Herbert, A., Olukoga, T., Özgürses, M. and Chan, K. (2022). DNA replication is highly resilient and persistent under the challenge of mild replication stress. *Cell Reports*, 39 (3), 110701. Available from 10.1016/j.celrep.2022.110701 [Accessed 20 May 2022].

Momma, T., Gonda, K., Akama, Y., Endo, E., Ujiie, D., Fujita, S., Maejima, Y., Horita, S., Shimomura, K., Saji, S., Kono, K., Yashima, R., Watanabe, F., Sugano, K. and Nomizu, T. (2019). MLH1 germline mutation associated with Lynch syndrome in a family followed for more than 45 years. *BMC Medical Genetics*, 20 (1). Available from 10.1186/s12881-019-0792-0 [Accessed 22 July 2022].

Montecucco, A., Rossi, R., Ferrari, G., Scovassi, A., Prosperi, E. and Biamonti, G. (2001). Etoposide Induces the Dispersal of DNA Ligase I from Replication Factories. *Molecular Biology of the Cell*, 12 (7), 2109-2118. Available from 10.1091/mbc.12.7.2109 [Accessed 9 July 2022].

Moore, S., Järvelin, A., Davis, I., Bond, G. and Castello, A. (2018). Expanding horizons: new roles for non-canonical RNA-binding proteins in cancer. *Current Opinion in Genetics &amp; Development*, 48, 112-120. Available from 10.1016/j.gde.2017.11.006 [Accessed 2 May 2022].

Moreno, A., Carrington, J., Albergante, L., Al Mamun, M., Haagensen, E., Komseli, E., Gorgoulis, V., Newman, T. and Blow, J. (2016). Unreplicated DNA remaining from unperturbed S phases passes through mitosis for resolution in daughter cells. *Proceedings of the National Academy of Sciences*, 113 (39). Available from 10.1073/pnas.1603252113 [Accessed 5 June 2022].

Moskwa, P., Buffa, F., Pan, Y., Panchakshari, R., Gottipati, P., Muschel, R., Beech, J., Kulshrestha, R., Abdelmohsen, K., Weinstock, D., Gorospe, M., Harris, A., Helleday, T. and Chowdhury, D. (2011). miR-182-Mediated Downregulation of BRCA1 Impacts DNA Repair and Sensitivity to PARP Inhibitors. *Molecular Cell*, 41 (2), 210-220. Available from 10.1016/j.molcel.2010.12.005 [Accessed 15 May 2022].

Mosler, T., Conte, F., Longo, G., Mikicic, I., Kreim, N., Möckel, M., Petrosino, G., Flach, J., Barau, J., Luke, B., Roukos, V. and Beli, P. (2021). R-loop proximity proteomics identifies a role of DDX41 in transcription-associated genomic instability. *Nature Communications*, 12 (1). Available from 10.1038/s41467-021-27530-y [Accessed 23 July 2022].

Mukherjee, N., Corcoran, D., Nusbaum, J., Reid, D., Georgiev, S., Hafner, M., Ascano, M., Tuschl, T., Ohler, U. and Keene, J. (2011). Integrative Regulatory Mapping Indicates that the RNA-Binding Protein HuR Couples Pre-mRNA Processing and mRNA Stability. *Molecular Cell*, 43 (3), 327-339. Available from 10.1016/j.molcel.2011.06.007 [Accessed 13 May 2022].

Mukherjee, N., Jacobs, N., Hafner, M., Kennington, E., Nusbaum, J., Tuschl, T., Blackshear, P. and Ohler, U. (2014). Global target mRNA specification and regulation by the RNA-binding protein ZFP36. *Genome Biology*, 15 (1), R12. Available from 10.1186/gb-2014-15-1-r12 [Accessed 8 May 2022].

Murata, T., Morita, N., Hikita, K., Kiuchi, K., Kiuchi, K. and Kaneda, N. (2005). Recruitment of mRNA-destabilizing protein TIS11 to stress granules is mediated by its zinc finger domain. *Experimental Cell Research*, 303 (2), 287-299. Available from 10.1016/j.yexcr.2004.09.031 [Accessed 8 May 2022].

Murata, T., Yoshino, Y., Morita, N. and Kaneda, N. (2002). Identification of nuclear import and export signals within the structure of the zinc finger protein TIS11. *Biochemical and Biophysical Research Communications*, 293 (4), 1242-1247. Available from 10.1016/s0006-291x(02)00363-7 [Accessed 3 May 2022].

Musgrove, E., Caldon, C., Barraclough, J., Stone, A. and Sutherland, R. (2011). Cyclin D as a therapeutic target in cancer. *Nature Reviews Cancer*, 11 (8), 558-572. Available from 10.1038/nrc3090 [Accessed 7 May 2022].

Myers, K., Gagou, M., Zuazua-Villar, P., Rodriguez, R. and Meuth, M. (2009). ATR and Chk1 Suppress a Caspase-3–Dependent Apoptotic Response Following DNA Replication Stress. *PLoS Genetics*, 5 (1), e1000324. Available from 10.1371/journal.pgen.1000324 [Accessed 28 April 2022].

Naim, V. and Rosselli, F. (2009). The FANC pathway and BLM collaborate during mitosis to prevent micro-nucleation and chromosome abnormalities. *Nature Cell Biology*, 11 (6), 761-768. Available from 10.1038/ncb1883 [Accessed 30 April 2022].

Nascakova, Z., Boleslavska, B., Urban, V., Oravetzova, A., Vlachova, E., Janscak, P. and Dobrovolna, J. (2021). RAD51 Inhibition Induces R-Loop Formation in Early G1 Phase of the Cell Cycle. *International*

Journal of Molecular Sciences, 22 (7), 3740. Available from 10.3390/ijms22073740 [Accessed 16 April 2022].

Newman, R., Ahlfors, H., Saveliev, A., Galloway, A., Hodson, D., Williams, R., Besra, G., Cook, C., Cunningham, A., Bell, S. and Turner, M. (2017). Maintenance of the marginal-zone B cell compartment specifically requires the RNA-binding protein ZFP36L1. *Nature Immunology*, 18 (6), 683-693. Available from 10.1038/ni.3724 [Accessed 13 June 2022].

Newman, R., McHugh, J. and Turner, M. (2015). RNA binding proteins as regulators of immune cell biology. *Clinical and Experimental Immunology*, 183 (1), 37-49. Available from 10.1111/cei.12684 [Accessed 3 May 2022].

Ngo, H., Lovely, G., Phillips, R. and Chan, D. (2014). Distinct structural features of TFAM drive mitochondrial DNA packaging versus transcriptional activation. *Nature Communications*, 5 (1). Available from 10.1038/ncomms4077 [Accessed 14 May 2022].

Nguyen, G., Dexheimer, T., Rosenthal, A., Chu, W., Singh, D., Mosedale, G., Bachrati, C., Schultz, L., Sakurai, M., Savitsky, P., Abu, M., McHugh, P., Bohr, V., Harris, C., Jadhav, A., Gileadi, O., Maloney, D., Simeonov, A. and Hickson, I. (2013). A Small Molecule Inhibitor of the BLM Helicase Modulates Chromosome Stability in Human Cells. *Chemistry &amp; Biology*, 20 (1), 55-62. Available from 10.1016/j.chembiol.2012.10.016 [Accessed 9 July 2022].

Nguyen, H., Yadav, T., Giri, S., Saez, B., Graubert, T. and Zou, L. (2017). Functions of Replication Protein A as a Sensor of R Loops and a Regulator of RNaseH1. *Molecular Cell*, 65 (5), 832-847.e4. Available from 10.1016/j.molcel.2017.01.029 [Accessed 16 April 2022].

Noguchi, A., Adachi, S., Yokota, N., Hatta, T., Natsume, T. and Kawahara, H. (2018). ZFP36L2 is a cell cycle-regulated CCCH protein necessary for DNA lesion-induced S-phase arrest. *Biology Open*. Available from 10.1242/bio.031575 [Accessed 15 May 2022].

Okamoto, Y., Iwasaki, W., Kugou, K., Takahashi, K., Oda, A., Sato, K., Kobayashi, W., Kawai, H., Sakasai, R., Takaori-Kondo, A., Yamamoto, T., Kanemaki, M., Taoka, M., Isobe, T., Kurumizaka, H., Innan, H., Ohta, K., Ishiai, M. and Takata, M. (2018). Replication stress induces accumulation of FANCD2 at central region of large fragile genes. *Nucleic Acids Research*, 46 (6), 2932-2944. Available from 10.1093/nar/gky058 [Accessed 30 April 2022].

Olazabal-Herrero, A., Green, A., Chen, X., Sung, P., Pillai, M. and Kupfer, G. (2020). Binding of FANCD2 to SRSF1 Splicing Factor Prevents Genomic Instability through R Loop Regulation. *Blood*, 136 (Supplement

1), 19-19. Available from 10.1182/blood-2020-141369 [Accessed 2 June 2022].

Oldfield, C. and Dunker, A. (2014). Intrinsically Disordered Proteins and Intrinsically Disordered Protein Regions. *Annual Review of Biochemistry*, 83 (1), 553-584. Available from 10.1146/annurev-biochem-072711-164947 [Accessed 18 April 2022].

Ota, M., Gonja, H., Koike, R. and Fukuchi, S. (2016). Multiple-Localization and Hub Proteins. *PLOS ONE*, 11 (6), e0156455. Available from 10.1371/journal.pone.0156455 [Accessed 16 July 2022].

Otsuka, H., Fukao, A., Funakami, Y., Duncan, K. and Fujiwara, T. (2019). Emerging Evidence of Translational Control by AU-Rich Element-Binding Proteins. *Frontiers in Genetics*, 10. Available from 10.3389/fgene.2019.00332 [Accessed 23 June 2022].

Otsuka, H., Fukao, A., Tomohiro, T., Adachi, S., Suzuki, T., Takahashi, A., Funakami, Y., Natsume, T., Yamamoto, T., Duncan, K. and Fujiwara, T. (2020). ARE-binding protein ZFP36L1 interacts with CNOT1 to directly repress translation via a deadenylation-independent mechanism. *Biochimie*, 174, 49-56. Available from 10.1016/j.biochi.2020.04.010 [Accessed 15 July 2022].

Ottaviano, L., Schaefer, K., Gajewski, M., Huckenbeck, W., Baldus, S., Rogel, U., Mackintosh, C., de Alava, E., Myklebost, O., Kresse, S., Meza-Zepeda, L., Serra, M., Cleton-Jansen, A., Hogendoorn, P., Buerger, H., Aigner, T., Gabbert, H. and Poremba, C. (2010). Molecular characterization of commonly used cell lines for bone tumor research: A trans-European EuroBoNet effort. *Genes, Chromosomes and Cancer*, 49 (1), 40-51. Available from 10.1002/gcc.20717 [Accessed 28 May 2022].

Otto, T. and Sicinski, P. (2017). Cell cycle proteins as promising targets in cancer therapy. *Nature Reviews Cancer*, 17 (2), 93-115. Available from 10.1038/nrc.2016.138 [Accessed 25 June 2022].

Ozeri-Galai, E., Bester, A. and Kerem, B. (2012). The complex basis underlying common fragile site instability in cancer. *Trends in Genetics*, 28 (6), 295-302. Available from 10.1016/j.tig.2012.02.006 [Accessed 16 May 2022].

Palakodeti, A., Han, Y., Jiang, Y. and Le Beau, M. (2003). The role of late/slow replication of the FRA16D in common fragile site induction. *Genes, Chromosomes and Cancer*, 39 (1), 71-76. Available from 10.1002/gcc.10290 [Accessed 30 April 2022].

Papadaki, O., Milatos, S., Grammenoudi, S., Mukherjee, N., Keene, J. and Kontoyiannis, D. (2009). Control of Thymic T Cell Maturation, Deletion and Egress by the RNA-Binding Protein HuR. *The Journal of Immunology*, 182 (11), 6779-6788. Available from 10.4049/jimmunol.0900377 [Accessed 3 May 2022].

Park, S., Chung, C., Gonzalez, E. and Yoo, C. (2018). Causal Inference Network of Genes Related with Bone Metastasis of Breast Cancer and Osteoblasts Using Causal Bayesian Networks. *Journal of Bone Metabolism*, 25 (4), 251. Available from 10.11005/jbm.2018.25.4.251 [Accessed 8 July 2022].

Park, S., Lee, J., Jeong, W., Kim, Y., Cha, H., Joe, Y., Chung, H., Cho, W., Do, J., Lee, B., Park, J. and Ko, B. (2015). TTP mediates cisplatin-induced apoptosis of head and neck cancer cells by down-regulating the expression of<i>Bcl-2</i>. *Journal of Chemotherapy*, 27 (3), 174-180. Available from 10.1179/1973947814y.0000000234 [Accessed 7 May 2022].

Paulsen, R., Soni, D., Wollman, R., Hahn, A., Yee, M., Guan, A., Hesley, J., Miller, S., Cromwell, E., Solow-Cordero, D., Meyer, T. and Cimprich, K. (2009). A Genome-wide siRNA Screen Reveals Diverse Cellular Processes and Pathways that Mediate Genome Stability. *Molecular Cell*, 35 (2), 228-239. Available from 10.1016/j.molcel.2009.06.021 [Accessed 12 June 2022].

Pepe, A. and West, S. (2014). MUS81-EME2 Promotes Replication Fork Restart. *Cell Reports*, 7 (4), 1048-1055. Available from 10.1016/j.celrep.2014.04.007 [Accessed 11 June 2022].

Perkins, D., Pappin, D., Creasy, D. and Cottrell, J. (1999). Probability-based protein identification by searching sequence databases using mass spectrometry data. *Electrophoresis*, 20 (18), 3551-3567. Available from 10.1002/(sici)1522-2683(19991201)20:18<3551::aid-elps3551>3.0.co;2-2 [Accessed 20 July 2022].

Petermann, E., Orta, M., Issaeva, N., Schultz, N. and Helleday, T. (2010). Hydroxyurea-Stalled Replication Forks Become Progressively Inactivated and Require Two Different RAD51-Mediated Pathways for Restart and Repair. *Molecular Cell*, 37 (4), 492-502. Available from 10.1016/j.molcel.2010.01.021 [Accessed 25 June 2022].

Peterson, L. and Zhang, D. (2004). The 8;21 translocation in leukemogenesis. *Oncogene*, 23 (24), 4255-4262. Available from 10.1038/sj.onc.1207727 [Accessed 30 May 2022].

Phillips, R., Ramos, S. and Blackshear, P. (2002). Members of the Tristetraprolin Family of Tandem CCCH Zinc Finger Proteins Exhibit

CRM1-dependent Nucleocytoplasmic Shuttling. *Journal of Biological Chemistry*, 277 (13), 11606-11613. Available from 10.1074/jbc.m111457200 [Accessed 8 May 2022].

Polo, S. and Jackson, S. (2011). Dynamics of DNA damage response proteins at DNA breaks: a focus on protein modifications. *Genes &amp; Development*, 25 (5), 409-433. Available from 10.1101/gad.2021311 [Accessed 17 April 2022].

Polo, S., Blackford, A., Chapman, J., Baskcomb, L., Gravel, S., Rusch, A., Thomas, A., Blundred, R., Smith, P., Kzhyshkowska, J., Dobner, T., Taylor, A., Turnell, A., Stewart, G., Grand, R. and Jackson, S. (2012). Regulation of DNA-End Resection by hnRNPU-like Proteins Promotes DNA Double-Strand Break Signaling and Repair. *Molecular Cell*, 45 (4), 505-516. Available from 10.1016/j.molcel.2011.12.035 [Accessed 17 April 2022].

Pont, A., Sadri, N., Hsiao, S., Smith, S. and Schneider, R. (2012). mRNA Decay Factor AUF1 Maintains Normal Aging, Telomere Maintenance, and Suppression of Senescence by Activation of Telomerase Transcription. *Molecular Cell*, 47 (1), 5-15. Available from 10.1016/j.molcel.2012.04.019 [Accessed 5 June 2022].

Potapova, T. and Gorbsky, G. (2017). The Consequences of Chromosome Segregation Errors in Mitosis and Meiosis. *Biology*, 6 (4), 12. Available from 10.3390/biology6010012 [Accessed 21 June 2022].

Powley, I., Kondrashov, A., Young, L., Dobbyn, H., Hill, K., Cannell, I., Stoneley, M., Kong, Y., Cotes, J., Smith, G., Wek, R., Hayes, C., Gant, T., Spriggs, K., Bushell, M. and Willis, A. (2009). Translational reprogramming following UVB irradiation is mediated by DNA-PKcs and allows selective recruitment to the polysomes of mRNAs encoding DNA repair enzymes. *Genes &amp; Development*, 23 (10), 1207-1220. Available from 10.1101/gad.516509 [Accessed 11 May 2022].

Priestley, P., Baber, J., Lolkema, M., Steeghs, N., de Bruijn, E., Shale, C., Duyvesteyn, K., Haidari, S., van Hoeck, A., Onstenk, W., Roepman, P., Voda, M., Bloemendal, H., Tjan-Heijnen, V., van Herpen, C., Labots, M., Witteveen, P., Smit, E., Sleijfer, S., Voest, E. and Cuppen, E. (2019). Pan-cancer whole-genome analyses of metastatic solid tumours. *Nature*, 575 (7781), 210-216. Available from 10.1038/s41586-019-1689-y [Accessed 7 May 2022].

Pullmann, R., Kim, H., Abdelmohsen, K., Lal, A., Martindale, J., Yang, X. and Gorospe, M. (2007). Analysis of Turnover and Translation Regulatory RNA-Binding Protein Expression through Binding to Cognate mRNAs. *Molecular and Cellular Biology*, 27 (18), 6265-6278. Available from 10.1128/mcb.00500-07 [Accessed 4 May 2022].

Radke, J., Ishaque, N., Koll, R., Gu, Z., Schumann, E., Sieverling, L., Uhrig, S., Hübschmann, D., Toprak, U., López, C., Hostench, X., Borgoni, S., Juraeva, D., Pritsch, F., Paramasivam, N., Balasubramanian, G., Schlesner, M., Sahay, S., Weniger, M., Pehl, D., Radbruch, H., Osterloh, A., Korfel, A., Misch, M., Onken, J., Faust, K., Vajkoczy, P., Moskopp, D., Wang, Y., Jödicke, A., Trümper, L., Anagnostopoulos, I., Lenze, D., Küppers, R., Hummel, M., Schmitt, C., Wiestler, O., Wolf, S., Unterberg, A., Eils, R., Herold-Mende, C., Brors, B., Siebert, R., Wagner, S., Haake, A., Richter, J., Richter, G., Eils, R., Lawerenz, C., Eils, J., Kerssemakers, J., Jaeger-Schmidt, C., Scholz, I., Bergmann, A., Borst, C., Braulke, F., Burkhardt, B., Claviez, A., Dreyling, M., Eberth, S., Einsele, H., Frickhofen, N., Haas, S., Hansmann, M., Karsch, D., Klepl, N., Kneba, M., Lisfeld, J., Mantovani-Löffler, L., Rohde, M., Ott, G., Stadler, C., Staib, P., Stilgenbauer, S., Zenz, T., Hansmann, M., Kube, D., Haas, S., Klapper, W., Kostezka, U., Möller, P., Rosenwald, A., Ott, G., Szczepanowski, M., Ammerpohl, O., Aukema, S., Binder, V., Borkhardt, A., Haake, A., Hoell, J., Leich, E., Lichter, P., López, C., Nagel, I., Pischimariov, J., Radlwimmer, B., Richter, J., Rosenstiel, P., Rosenwald, A., Schilhabel, M., Schreiber, S., Vater, I., Wagener, R., Siebert, R., Bernhart, S., Binder, H., Doose, G., Eils, R., Hoffmann, S., Hopp, L., Kleinheinz, K., Kretzmer, H., Kreuz, M., Korbel, J., Langenberger, D., Loeffler, M., Rosolowski, M., Stadler, P., Sungalee, S., Siebert, R., Wiemann, S. and Heppner, F. (2022). The genomic and transcriptional landscape of primary central nervous system lymphoma. *Nature Communications*, 13 (1). Available from 10.1038/s41467-022-30050-y [Accessed 12 May 2022].

Rajeeve, V., Vendrell, I., Wilkes, E., Torbett, N. and Cutillas, P. (2014). Cross-species Proteomics Reveals Specific Modulation of Signaling in Cancer and Stromal Cells by Phosphoinositide 3-kinase (PI3K) Inhibitors. *Molecular &amp; Cellular Proteomics*, 13 (6), 1457-1470. Available from 10.1074/mcp.m113.035204 [Accessed 21 July 2022].

Ray Chaudhuri, A., Hashimoto, Y., Herrador, R., Neelsen, K., Fachinetti, D., Bermejo, R., Cocito, A., Costanzo, V. and Lopes, M. (2012). Topoisomerase I poisoning results in PARP-mediated replication fork reversal. *Nature Structural &amp; Molecular Biology*, 19 (4), 417-423. Available from 10.1038/nsmb.2258 [Accessed 9 July 2022].

Regairaz, M., Zhang, Y., Fu, H., Agama, K., Tata, N., Agrawal, S., Aladjem, M. and Pommier, Y. (2011). Mus81-mediated DNA cleavage resolves replication forks stalled by topoisomerase I–DNA complexes. *Journal of*

Cell Biology, 195 (5), 739-749. Available from 10.1083/jcb.201104003 [Accessed 9 July 2022].

Rehfeld, A., Plass, M., Krogh, A. and Friis-Hansen, L. (2013). Alterations in Polyadenylation and Its Implications for Endocrine Disease. *Frontiers in Endocrinology*, 4. Available from 10.3389/fendo.2013.00053 [Accessed 4 May 2022].

Reinhardt, H., Hasskamp, P., Schmedding, I., Morandell, S., van Vugt, M., Wang, X., Linding, R., Ong, S., Weaver, D., Carr, S. and Yaffe, M. (2010). DNA Damage Activates a Spatially Distinct Late Cytoplasmic Cell-Cycle Checkpoint Network Controlled by MK2-Mediated RNA Stabilization. *Molecular Cell*, 40 (1), 34-49. Available from 10.1016/j.molcel.2010.09.018 [Accessed 14 May 2022].

Rigby, W., Roy, K., Collins, J., Rigby, S., Connolly, J., Bloch, D. and Brooks, S. (2005). Structure/Function Analysis of Tristetraprolin (TTP): p38 Stress-Activated Protein Kinase and Lipopolysaccharide Stimulation Do Not Alter TTP Function. *The Journal of Immunology*, 174 (12), 7883-7893. Available from 10.4049/jimmunol.174.12.7883 [Accessed 17 June 2022].

Rinaldi, C., Pizzul, P., Longhese, M. and Bonetti, D. (2021). Sensing R-Loop-Associated DNA Damage to Safeguard Genome Stability. *Frontiers in Cell and Developmental Biology*, 8. Available from 10.3389/fcell.2020.618157 [Accessed 6 June 2022].

Roberts, S. and Gordenin, D. (2014). Hypermutation in human cancer genomes: footprints and mechanisms. *Nature Reviews Cancer*, 14 (12), 786-800. Available from 10.1038/nrc3816 [Accessed 5 June 2022].

Rounbehler, R., Fallahi, M., Yang, C., Steeves, M., Li, W., Doherty, J., Schaub, F., Sanduja, S., Dixon, D., Blackshear, P. and Cleveland, J. (2012). Tristetraprolin Impairs Myc-Induced Lymphoma and Abolishes the Malignant State. *Cell*, 150 (3), 563-574. Available from 10.1016/j.cell.2012.06.033.

Sadri, N., Lu, J., Badura, M. and Schneider, R. (2010). AUF1 is involved in splenic follicular B cell maintenance. *BMC Immunology*, 11 (1). Available from 10.1186/1471-2172-11-1 [Accessed 3 May 2022].

Saini, Y., Chen, J. and Patial, S. (2020). The Tristetraprolin Family of RNA-Binding Proteins in Cancer: Progress and Future Prospects. *Cancers*, 12 (6), 1539. Available from 10.3390/cancers12061539 [Accessed 7 May 2022].

Salas-Armenteros, I., Pérez-Calero, C., Bayona-Feliu, A., Tumini, E., Luna, R. and Aguilera, A. (2017). Human THO –Sin3A interaction reveals new mechanisms to prevent R-loops that cause genome instability. *The EMBO Journal*, 36 (23), 3532-3547. Available from 10.15252/embj.201797208 [Accessed 17 July 2022].

Salas-Armenteros, I., Pérez-Calero, C., Bayona-Feliu, A., Tumini, E., Luna, R. and Aguilera, A. (2017). Human THO –Sin3A interaction reveals new mechanisms to prevent R-loops that cause genome instability. *The EMBO Journal*, 36 (23), 3532-3547. Available from 10.15252/embj.201797208 [Accessed 21 July 2022].

Sanchez, A., de Vivo, A., Tonzi, P., Kim, J., Huang, T. and Kee, Y. (2020). Transcription-replication conflicts as a source of common fragile site instability caused by BMI1-RNF2 deficiency. *PLOS Genetics*, 16 (3), e1008524. Available from 10.1371/journal.pgen.1008524 [Accessed 16 April 2022].

Santos-Pereira, J. and Aguilera, A. (2015). R loops: new modulators of genome dynamics and function. *Nature Reviews Genetics*, 16 (10), 583-597. Available from 10.1038/nrg3961 [Accessed 15 May 2022].

Santos-Pereira, J., Herrero, A., García-Rubio, M., Marín, A., Moreno, S. and Aguilera, A. (2013). The Npl3 hnRNP prevents R-loop-mediated transcription–replication conflicts and genome instability. *Genes &amp; Development*, 27 (22), 2445-2458. Available from 10.1101/gad.229880.113 [Accessed 12 June 2022].

Saunus, J., French, J., Edwards, S., Beveridge, D., Hatchell, E., Wagner, S., Stein, S., Davidson, A., Simpson, K., Francis, G., Leedman, P. and Brown, M. (2008). Posttranscriptional Regulation of the Breast Cancer Susceptibility Gene <i>BRCA1</i> by the RNA Binding Protein HuR. *Cancer Research*, 68 (22), 9469-9478. Available from 10.1158/0008-5472.can-08-1159 [Accessed 12 May 2022].

Schichl, Y., Resch, U., Hofer-Warbinek, R. and de Martin, R. (2009). Tristetraprolin Impairs NF-κB/p65 Nuclear Translocation. *Journal of Biological Chemistry*, 284 (43), 29571-29581. Available from 10.1074/jbc.m109.031237 [Accessed 3 May 2022].

Schmidlin, M., Lu, M., Leuenberger, S., Stoecklin, G., Mallaun, M., Gross, B., Gherzi, R., Hess, D., Hemmings, B. and Moroni, C. (2004). The ARE-dependent mRNA-destabilizing activity of BRF1 is regulated by protein kinase B. *The EMBO Journal*, 23 (24), 4760-4769. Available from 10.1038/sj.emboj.7600477 [Accessed 3 May 2022].

Schonn, I., Hennesen, J. and Dartsch, D. (2009). Cellular responses to etoposide: cell death despite cell cycle arrest and repair of DNA damage. *Apoptosis*, 15 (2), 162-172. Available from 10.1007/s10495-009-0440-9 [Accessed 9 July 2022].

Schultz, L., Chehab, N., Malikzay, A. and Halazonetis, T. (2000). P53 Binding Protein 1 (53bp1) Is an Early Participant in the Cellular Response to DNA Double-Strand Breaks. *Journal of Cell Biology*, 151 (7), 1381-1390. Available from 10.1083/jcb.151.7.1381 [Accessed 27 April 2022].

Schwab, R., Nieminuszczy, J., Shah, F., Langton, J., Lopez Martinez, D., Liang, C., Cohn, M., Gibbons, R., Deans, A. and Niedzwiedz, W. (2015). The Fanconi Anemia Pathway Maintains Genome Stability by Coordinating Replication and Transcription. *Molecular Cell*, 60 (3), 351-361. Available from 10.1016/j.molcel.2015.09.012 [Accessed 10 June 2022].

Sedlyarov, V., Fallmann, J., Ebner, F., Huemer, J., Sneezum, L., Ivin, M., Kreiner, K., Tanzer, A., Vogl, C., Hofacker, I. and Kovarik, P. (2016). Tristetraprolin binding site atlas in the macrophage transcriptome reveals a switch for inflammation resolution. *Molecular Systems Biology*, 12 (5), 868. Available from 10.15252/msb.20156628 [Accessed 8 May 2022].

Sherman, B., Hao, M., Qiu, J., Jiao, X., Baseler, M., Lane, H., Imamichi, T. and Chang, W. (2022). DAVID: a web server for functional enrichment analysis and functional annotation of gene lists (2021 update). *Nucleic Acids Research*, 50 (W1), W216-W221. Available from 10.1093/nar/gkac194 [Accessed 20 July 2022].

Shimada, H., Ichikawa, H. and Ohki, M. (2002). Potential involvement of the AML1-MTG8 fusion protein in the granulocytic maturation characteristic of the t(8;21) acute myelogenous leukemia revealed by microarray analysis. *Leukemia*, 16 (5), 874-885. Available from 10.1038/sj.leu.2402465 [Accessed 7 May 2022].

Sidali, A., Teotia, V., Solaiman, N., Bashir, N., Kanagaraj, R., Murphy, J. and Surendranath, K. (2021). AU-Rich Element RNA Binding Proteins: At the Crossroads of Post-Transcriptional Regulation and Genome Integrity. *International Journal of Molecular Sciences*, 23 (1), 96. Available from 10.3390/ijms23010096 [Accessed 27 July 2022].

Sidi, S., Sanda, T., Kennedy, R., Hagen, A., Jette, C., Hoffmans, R., Pascual, J., Imamura, S., Kishi, S., Amatruda, J., Kanki, J., Green, D., D'Andrea, A. and Look, A. (2008). Chk1 Suppresses a Caspase-2 Apoptotic Response to DNA Damage that Bypasses p53, Bcl-2, and Caspase-3. *Cell*, 133 (5), 864-877. Available from 10.1016/j.cell.2008.03.037 [Accessed 28 April 2022].

Singh, D., Pandita, R., Singh, M., Chakraborty, S., Hambarde, S., Ramnarain, D., Charaka, V., Ahmed, K., Hunt, C. and Pandita, T. (2018). MOF Suppresses Replication Stress and Contributes to Resolution of

Stalled Replication Forks. *Molecular and Cellular Biology*, 38 (6). Available from 10.1128/mcb.00484-17 [Accessed 15 May 2022].

Sirbu, B., Couch, F., Feigerle, J., Bhaskara, S., Hiebert, S. and Cortez, D. (2011). Analysis of protein dynamics at active, stalled, and collapsed replication forks. *Genes &amp; Development*, 25 (12), 1320-1327. Available from 10.1101/gad.2053211 [Accessed 6 June 2022].

Sirbu, B., McDonald, W., Dungrawala, H., Badu-Nkansah, A., Kavanaugh, G., Chen, Y., Tabb, D. and Cortez, D. (2013). Identification of Proteins at Active, Stalled, and Collapsed Replication Forks Using Isolation of Proteins on Nascent DNA (iPOND) Coupled with Mass Spectrometry. *Journal of Biological Chemistry*, 288 (44), 31458-31467. Available from 10.1074/jbc.m113.511337 [Accessed 10 June 2022].

Skourti-Stathaki, K., Proudfoot, N. and Gromak, N. (2011). Human Senataxin Resolves RNA/DNA Hybrids Formed at Transcriptional Pause Sites to Promote Xrn2-Dependent Termination. *Molecular Cell*, 42 (6), 794-805. Available from 10.1016/j.molcel.2011.04.026 [Accessed 21 April 2022].

Smith, J., Mun Tho, L., Xu, N. and A. Gillespie, D. (2010). The ATM–Chk2 and ATR–Chk1 Pathways in DNA Damage Signaling and Cancer. *Advances in Cancer Research*, 73-112. Available from 10.1016/b978-0-12-380888-2.00003-0 [Accessed 10 May 2022].

Sollier, J., Stork, C., García-Rubio, M., Paulsen, R., Aguilera, A. and Cimprich, K. (2014). Transcription-Coupled Nucleotide Excision Repair Factors Promote R-Loop-Induced Genome Instability. *Molecular Cell*, 56 (6), 777-785. Available from 10.1016/j.molcel.2014.10.020 [Accessed 21 April 2022].

Son, Y., Kim, H., Choi, W., Chun, C. and Chun, J. (2019). RNA-binding protein ZFP36L1 regulates osteoarthritis by modulating members of the heat shock protein 70 family. *Nature Communications*, 10 (1). Available from 10.1038/s41467-018-08035-7 [Accessed 15 June 2022].

Song, C., Hotz-Wagenblatt, A., Voit, R. and Grummt, I. (2017). SIRT7 and the DEAD-box helicase DDX21 cooperate to resolve genomic R loops and safeguard genome stability. *Genes &amp; Development*, 31 (13), 1370-1381. Available from 10.1101/gad.300624.117 [Accessed 17 July 2022].

Spagnolo, L., Rivera-Calzada, A., Pearl, L. and Llorca, O. (2006). Three-Dimensional Structure of the Human DNA-PKcs/Ku70/Ku80 Complex Assembled on DNA and Its Implications for DNA DSB Repair. *Molecular Cell*, 22 (4), 511-519. Available from 10.1016/j.molcel.2006.04.013 [Accessed 15 May 2022].

Spies, J., Lukas, C., Somyajit, K., Rask, M., Lukas, J. and Neelsen, K. (2019). 53BP1 nuclear bodies enforce replication timing at under-replicated DNA to limit heritable DNA damage. *Nature Cell Biology*, 21 (4), 487-497. Available from 10.1038/s41556-019-0293-6 [Accessed 27 April 2022].

Sridhara, S., Carvalho, S., Grosso, A., Gallego-Paez, L., Carmo-Fonseca, M. and de Almeida, S. (2017). Transcription Dynamics Prevent RNA-Mediated Genomic Instability through SRPK2-Dependent DDX23 Phosphorylation. *Cell Reports*, 18 (2), 334-343. Available from 10.1016/j.celrep.2016.12.050 [Accessed 17 July 2022].

Stirling, P. and Hieter, P. (2017). Canonical DNA Repair Pathways Influence R-Loop-Driven Genome Instability. *Journal of Molecular Biology*, 429 (21), 3132-3138. Available from 10.1016/j.jmb.2016.07.014 [Accessed 15 May 2022].

Stirling, P., Chan, Y., Minaker, S., Aristizabal, M., Barrett, I., Sipahimalani, P., Kobor, M. and Hieter, P. (2012). R-loop-mediated genome instability in mRNA cleavage and polyadenylation mutants. *Genes &amp; Development*, 26 (2), 163-175. Available from 10.1101/gad.179721.111 [Accessed 15 May 2022].

Stoecklin, G., Stubbs, T., Kedersha, N., Wax, S., Rigby, W., Blackwell, T. and Anderson, P. (2004). MK2-induced tristetraprolin:14-3-3 complexes prevent stress granule association and ARE-mRNA decay. *The EMBO Journal*, 23 (6), 1313-1324. Available from 10.1038/sj.emboj.7600163 [Accessed 3 May 2022].

Stoecklin, G., Tenenbaum, S., Mayo, T., Chittur, S., George, A., Baroni, T., Blackshear, P. and Anderson, P. (2008). Genome-wide Analysis Identifies Interleukin-10 mRNA as Target of Tristetraprolin. *Journal of Biological Chemistry*, 283 (17), 11689-11699. Available from 10.1074/jbc.m709657200 [Accessed 13 June 2022].

Stoecklin, G. (2002). Functional cloning of BRF1, a regulator of ARE-dependent mRNA turnover. *The EMBO Journal*, 21 (17), 4709-4718. Available from 10.1093/emboj/cdf444 [Accessed 14 May 2022].

Stork, C., Bocek, M., Crossley, M., Sollier, J., Sanz, L., Chédin, F., Swigut, T. and Cimprich, K. (2016). Co-transcriptional R-loops are the main cause of estrogen-induced DNA damage. *eLife*, 5. Available from 10.7554/elife.17548 [Accessed 9 July 2022].

Stumpo, D., Broxmeyer, H., Ward, T., Cooper, S., Hangoc, G., Chung, Y., Shelley, W., Richfield, E., Ray, M., Yoder, M., Aplan, P. and Blackshear, P. (2009). Targeted disruption of Zfp36l2, encoding a CCCH tandem zinc finger RNA-binding protein, results in defective hematopoiesis. *Blood*, 114 (12), 2401-2410. Available from 10.1182/blood-2009-04-214619 [Accessed 6 May 2022].

Stumpo, D., Byrd, N., Phillips, R., Ghosh, S., Maronpot, R., Castranio, T., Meyers, E., Mishina, Y. and Blackshear, P. (2004). Chorioallantoic Fusion Defects and Embryonic Lethality Resulting from Disruption of <i>Zfp36L1</i> , a Gene Encoding a CCCH Tandem Zinc Finger Protein of the Tristetraprolin Family. *Molecular and Cellular Biology*, 24 (14), 6445-6455. Available from 10.1128/mcb.24.14.6445-6455.2004 [Accessed 6 May 2022].

Su, Y., Wang, S., Chiang, P., Lin, N., Shen, Y., Chang, G. and Chang, C. (2012). Tristetraprolin Inhibits Poly(A)-Tail Synthesis in Nuclear mRNA that Contains AU-Rich Elements by Interacting with Poly(A)-Binding Protein Nuclear 1. *PLoS ONE*, 7 (7), e41313. Available from 10.1371/journal.pone.0041313 [Accessed 8 May 2022].

Suk, F., Chang, C., Lin, R., Lin, S., Liu, S., Jau, C. and Liang, Y. (2018). ZFP36L1 and ZFP36L2 inhibit cell proliferation in a cyclin D-dependent and p53-independent manner. *Scientific Reports*, 8 (1). Available from 10.1038/s41598-018-21160-z [Accessed 12 April 2022].

Sundvold, H. (2020). Triciribine Engages ZFP36L1 and HuR to Stabilize LDLR mRNA. *Molecules*, 25 (19), 4505. Available from 10.3390/molecules25194505 [Accessed 14 May 2022].

Surendranath, K. et al. (2022) “A deep learning workflow for quantification of micronuclei in DNA damage studies in cultured cancer cell lines: A proof of Principle Investigation.” Available from 10.1101/2022.09.18.508405. [Accessed 12 February 2023].

Suswam, E., Li, Y., Zhang, X., Gillespie, G., Li, X., Shacka, J., Lu, L., Zheng, L. and King, P. (2008). Tristetraprolin Down-regulates Interleukin-8 and Vascular Endothelial Growth Factor in Malignant Glioma Cells. *Cancer Research*, 68 (3), 674-682. Available from 10.1158/0008-5472.can-07-2751 [Accessed 7 May 2022].

Suswam, E. (2005). Novel DNA-binding properties of the RNA-binding protein TIAR. *Nucleic Acids Research*, 33 (14), 4507-4518. Available from 10.1093/nar/gki763 [Accessed 14 May 2022].

Tan, S., Chadha, S., Liu, Y., Gabasova, E., Perera, D., Ahmed, K., Constantinou, S., Renaudin, X., Lee, M., Aebersold, R. and Venkitaraman, A. (2017). A Class of Environmental and Endogenous Toxins Induces BRCA2 Haploinsufficiency and Genome Instability. *Cell*, 169 (6), 1105-1118.e15. Available from 10.1016/j.cell.2017.05.010 [Accessed 4 June 2022].

Taupin, J., Tian, Q., Kedersha, N., Robertson, M. and Anderson, P. (1995). The RNA-binding protein TIAR is translocated from the nucleus to the cytoplasm during Fas-mediated apoptotic cell death. *Proceedings of the National Academy of Sciences*, 92 (5), 1629-1633. Available from 10.1073/pnas.92.5.1629 [Accessed 14 May 2022].

Taylor, G., Carballo, E., Lee, D., Lai, W., Thompson, M., Patel, D., Schenkman, D., Gilkeson, G., Broxmeyer, H., Haynes, B. and Blackshear, P. (1996). A Pathogenetic Role for TNFα in the Syndrome of Cachexia, Arthritis, and Autoimmunity Resulting from Tristetraprolin (TTP) Deficiency. *Immunity*, 4 (5), 445-454. Available from 10.1016/s1074-7613(00)80411-2 [Accessed 6 May 2022].

Taylor, G., Lai, W., Oakey, R., Seldin, M., Shows, T., Eddy, R. and Blackshear, P. (1991). The human TTP protein: sequence, alignment with related proteins, and chromosomal localization of the mouse and human genes. *Nucleic Acids Research*, 19 (12), 3454-3454. Available from 10.1093/nar/19.12.3454 [Accessed 6 May 2022].

Thompson, S., Bakhoum, S. and Compton, D. (2010). Mechanisms of Chromosomal Instability. *Current Biology*, 20 (6), R285-R295. Available from 10.1016/j.cub.2010.01.034 [Accessed 21 June 2022].

Thys, R., E. Lehman, C., C. T. Pierce, L. and Wang, Y. (2015). DNA Secondary Structure at Chromosomal Fragile Sites in Human Disease. *Current Genomics*, 16 (1), 60-70. Available from 10.2174/1389202916666150114223205 [Accessed 17 June 2022].

Tiedje, C., Ronkina, N., Tehrani, M., Dhamija, S., Laass, K., Holtmann, H., Kotlyarov, A. and Gaestel, M. (2012). The p38/MK2-Driven Exchange between Tristetraprolin and HuR Regulates AU–Rich Element–Dependent Translation. *PLoS Genetics*, 8 (9), e1002977. Available from 10.1371/journal.pgen.1002977 [Accessed 4 May 2022].

Tiwari, A., Addis Jones, O. and Chan, K. (2018). 53BP1 can limit sister-chromatid rupture and rearrangements driven by a distinct ultrafine DNA bridging-breakage process. *Nature Communications*, 9 (1). Available from 10.1038/s41467-018-03098-y [Accessed 9 July 2022].

Tsantoulis, P., Kotsinas, A., Sfikakis, P., Evangelou, K., Sideridou, M., Levy, B., Mo, L., Kittas, C., Wu, X., Papavassiliou, A. and Gorgoulis, V. (2007). Oncogene-induced replication stress preferentially targets common fragile sites in preneoplastic lesions. A genome-wide study. *Oncogene*, 27 (23), 3256-3264. Available from 10.1038/sj.onc.1210989 [Accessed 16 May 2022].

Tubbs, A. and Nussenzweig, A. (2017). Endogenous DNA Damage as a Source of Genomic Instability in Cancer. *Cell*, 168 (4), 644-656. Available from 10.1016/j.cell.2017.01.002 [Accessed 9 May 2022].

Tudor, C., Marchese, F., Hitti, E., Aubareda, A., Rawlinson, L., Gaestel, M., Blackshear, P., Clark, A., Saklatvala, J. and Dean, J. (2009). The p38 MAPK pathway inhibits tristetraprolin-directed decay of interleukin-10 and pro-inflammatory mediator mRNAs in murine macrophages. *FEBS Letters*, 583 (12), 1933-1938. Available from 10.1016/j.febslet.2009.04.039 [Accessed 23 June 2022].

Uruci, S., Lo, C., Wheeler, D. and Taneja, N. (2021). R-Loops and Its Chro-Mates: The Strange Case of Dr. Jekyll and Mr. Hyde. *International Journal of Molecular Sciences*, 22 (16), 8850. Available from 10.3390/ijms22168850 [Accessed 22 June 2022].

van Andel, E., Roosjen, M., van der Zanden, S., Lange, S., Weijers, D., Smulders, M., Savelkoul, H., Zuilhof, H. and Tijhaar, E. (2022). Highly Specific Protein Identification by Immunoprecipitation–Mass Spectrometry Using Antifouling Microbeads. *ACS Applied Materials &amp; Interfaces*, 14 (20), 23102-23116. Available from 10.1021/acsami.1c22734 [Accessed 16 July 2022].

van der Lee, R., Buljan, M., Lang, B., Weatheritt, R., Daughdrill, G., Dunker, A., Fuxreiter, M., Gough, J., Gsponer, J., Jones, D., Kim, P., Kriwacki, R., Oldfield, C., Pappu, R., Tompa, P., Uversky, V., Wright, P. and Babu, M. (2014). Classification of Intrinsically Disordered Regions and Proteins. *Chemical Reviews*, 114 (13), 6589-6631. Available from 10.1021/cr400525m [Accessed 18 April 2022].

Varnum, B., Ma, Q., Chi, T., Fletcher, B. and Herschman, H. (1991). The TIS11 primary response gene is a member of a gene family that encodes proteins with a highly conserved sequence containing an unusual Cys-His repeat. *Molecular and Cellular Biology*, 11 (3), 1754-1758. Available from 10.1128/mcb.11.3.1754-1758.1991 [Accessed 6 May 2022].

Vesela, E., Chroma, K., Turi, Z. and Mistrik, M. (2017). Common Chemical Inductors of Replication Stress: Focus on Cell-Based Studies. *Biomolecules*, 7 (4), 19. Available from 10.3390/biom7010019 [Accessed 17 May 2022].

Vogel, K., Bell, L., Galloway, A., Ahlfors, H. and Turner, M. (2016). The RNA-Binding Proteins Zfp36l1 and Zfp36l2 Enforce the Thymic β-Selection Checkpoint by Limiting DNA Damage Response Signaling and Cell Cycle Progression. *The Journal of Immunology*, 197 (7), 2673-2685. Available from 10.4049/jimmunol.1600854 [Accessed 12 May 2022].

Voloshanenko, O., Gmach, P., Winter, J., Kranz, D. and Boutros, M. (2017). Mapping of Wnt-Frizzled interactions by multiplex CRISPR targeting of receptor gene families. *The FASEB Journal*, 31 (11), 4832-4844. Available from 10.1096/fj.201700144r [Accessed 17 July 2022].

Voutsinos, V., Munk, S. and Oestergaard, V. (2018). Common Chromosomal Fragile Sites—Conserved Failure Stories. *Genes*, 9 (12), 580. Available from 10.3390/genes9120580 [Accessed 16 May 2022].

Wahba, L., Amon, J., Koshland, D. and Vuica-Ross, M. (2011). RNase H and Multiple RNA Biogenesis Factors Cooperate to Prevent RNA:DNA Hybrids from Generating Genome Instability. *Molecular Cell*, 44 (6), 978-988. Available from 10.1016/j.molcel.2011.10.017 [Accessed 15 May 2022].

Waldmann, H. and Lefkovits, I. (1984). Limiting dilution analysis of cells of the immune system II: What can be learnt?. *Immunology Today*, 5 (10), 295-298. Available from 10.1016/0167-5699(84)90154-3 [Accessed 23 May 2022].

Wan, Y., Zheng, X., Chen, H., Guo, Y., Jiang, H., He, X., Zhu, X. and Zheng, Y. (2015). Splicing function of mitotic regulators links R-loop–mediated DNA damage to tumor cell killing. *Journal of Cell Biology*, 209 (2), 235-246. Available from 10.1083/jcb.201409073 [Accessed 24 June 2022].

Wang, I., Grunseich, C., Fox, J., Burdick, J., Zhu, Z., Ravazian, N., Hafner, M. and Cheung, V. (2018). Human proteins that interact with RNA/DNA hybrids. *Genome Research*, 28 (9), 1405-1414. Available from 10.1101/gr.237362.118 [Accessed 15 May 2022].

Wang, J., Youkharibache, P., Zhang, D., Lanczycki, C., Geer, R., Madej, T., Phan, L., Ward, M., Lu, S., Marchler, G., Wang, Y., Bryant, S., Geer, L. and Marchler-Bauer, A. (2019). iCn3D, a web-based 3D viewer for sharing 1D/2D/3D representations of biomolecular structures. *Bioinformatics*, 36 (1), 131-135. Available from 10.1093/bioinformatics/btz502 [Accessed 2 June 2022].

Wang, K., Wang, H., Wu, Y., Su, Y., Chiang, P., Lin, N., Wang, S., Chang, G. and Chang, C. (2015). Functional regulation of Zfp36l1 and Zfp36l2 in response to lipopolysaccharide in mouse RAW264.7 macrophages. *Journal of Inflammation*, 12 (1). Available from 10.1186/s12950-015-0088-x [Accessed 20 July 2022].

Wang, T., Wei, J., Sabatini, D. and Lander, E. (2014). Genetic Screens in Human Cells Using the CRISPR-Cas9 System. *Science*, 343 (6166), 80-84. Available from 10.1126/science.1246981.

Ward, I. and Chen, J. (2001). Histone H2AX Is Phosphorylated in an ATR-dependent Manner in Response to Replicational Stress. *Journal of Biological Chemistry,* 276 (51), 47759-47762. Available from 10.1074/jbc.c100569200 [Accessed 9 June 2022].

Ward, I., Minn, K. and Chen, J. (2004). UV-induced Ataxia-telangiectasia-mutated and Rad3-related (ATR) Activation Requires Replication Stress. *Journal of Biological Chemistry*, 279 (11), 9677-9680. Available from 10.1074/jbc.c300554200 [Accessed 9 June 2022].

Warren, C. and Shechter, D. (2017). Fly Fishing for Histones: Catch and Release by Histone Chaperone Intrinsically Disordered Regions and Acidic Stretches. *Journal of Molecular Biology*, 429 (16), 2401-2426. Available from 10.1016/j.jmb.2017.06.005 [Accessed 18 April 2022].

Watanabe, R., Ui, A., Kanno, S., Ogiwara, H., Nagase, T., Kohno, T. and Yasui, A. (2014). SWI/SNF Factors Required for Cellular Resistance to DNA Damage Include ARID1A and ARID1B and Show Interdependent Protein Stability. *Cancer Research*, 74 (9), 2465-2475. Available from 10.1158/0008-5472.can-13-3608 [Accessed 13 May 2022].

Weber, A. and Ryan, A. (2015). ATM and ATR as therapeutic targets in cancer. *Pharmacology &amp; Therapeutics*, 149, 124-138. Available from 10.1016/j.pharmthera.2014.12.001 [Accessed 10 May 2022].

Wessel, S., Mohni, K., Luzwick, J., Dungrawala, H. and Cortez, D. (2019). Functional Analysis of the Replication Fork Proteome Identifies BET Proteins as PCNA Regulators. *Cell Reports*, 28 (13), 3497-3509.e4. Available from 10.1016/j.celrep.2019.08.051 [Accessed 8 July 2022].

Wilhelm, T., Olziersky, A., Harry, D., De Sousa, F., Vassal, H., Eskat, A. and Meraldi, P. (2019). Mild replication stress causes chromosome mis-segregation via premature centriole disengagement. *Nature Communications*, 10 (1). Available from 10.1038/s41467-019-11584-0 [Accessed 12 March 2022].

Wilhelm, T., Said, M. and Naim, V. (2020). DNA Replication Stress and Chromosomal Instability: Dangerous Liaisons. *Genes*, 11 (6), 642. Available from 10.3390/genes11060642.

Willis, N. and Rhind, N. (2009). Regulation of DNA replication by the S-phase DNA damage checkpoint. *Cell Division*, 4 (1), 13. Available from 10.1186/1747-1028-4-13 [Accessed 18 July 2022].

Wilusz, C., Wormington, M. and Peltz, S. (2001). The cap-to-tail guide to mRNA turnover. *Nature Reviews Molecular Cell Biology*, 2 (4), 237-246. Available from 10.1038/35067025 [Accessed 4 May 2022].

Wood, M., Quinet, A., Lin, Y., Davis, A., Pasero, P., Ayala, Y. and Vindigni, A. (2020). TDP-43 dysfunction results in R-loop accumulation and DNA replication defects. *Journal of Cell Science*. Available from 10.1242/jcs.244129 [Accessed 23 June 2022].

Wu, H., Lima, W. and Crooke, S. (2001). Investigating the Structure of Human RNase H1 by Site-directed Mutagenesis. *Journal of Biological Chemistry*, 276 (26), 23547-23553. Available from 10.1074/jbc.m009676200 [Accessed 16 April 2022].

Xing, R., Zhou, Y., Yu, J., Yu, Y., Nie, Y., Luo, W., Yang, C., Xiong, T., Wu, W., Li, Z., Bing, Y., Lin, S., Zhang, Y., Hu, Y., Li, L., Han, L., Yang, C., Huang, S., Huang, S., Zhou, R., Li, J., Wu, K., Fan, D., Tang, G., Dou, J., Zhu, Z., Ji, J., Fang, X. and Lu, Y. (2019). Whole-genome sequencing reveals novel tandem-duplication hotspots and a prognostic mutational signature in gastric cancer. *Nature Communications*, 10 (1). Available from 10.1038/s41467-019-09644-6 [Accessed 7 May 2022].

Xu, L., Ning, H., Gu, L., Wang, Q., Lu, W., Peng, H., Cui, W., Ying, B., Ross, C., Wilson, G., Wei, L., Wold, W. and Liu, J. (2015). Tristetraprolin induces cell cycle arrest in breast tumor cells through targeting AP-1/c-Jun and NF-κB pathway. *Oncotarget*, 6 (39), 41679-41691. Available from 10.18632/oncotarget.6149 [Accessed 13 June 2022].

Yan, L., Wei, W., Cao, W., Zhang, X., Xie, Y. and Xiao, Q. (2014). Overexpression of E2F1 in human gastric carcinoma is involved in anti-cancer drug resistance. *BMC Cancer*, 14 (1). Available from 10.1186/1471-2407-14-904 [Accessed 7 May 2022].

Yan, Q., Wulfridge, P., Doherty, J., Fernandez-Luna, J., Real, P., Tang, H. and Sarma, K. (2022). Proximity labeling identifies a repertoire of site-specific R-loop modulators. *Nature Communications*, 13 (1). Available from 10.1038/s41467-021-27722-6 [Accessed 12 June 2022].

Yarden, R., Metsuyanim, S., Pickholtz, I., Shabbeer, S., Tellio, H. and Papa, M. (2012). BRCA1-dependent Chk1 phosphorylation triggers partial chromatin disassociation of phosphorylated Chk1 and facilitates S-phase cell cycle arrest. *The International Journal of Biochemistry &amp; Cell Biology*, 44 (11), 1761-1769. Available from 10.1016/j.biocel.2012.06.026 [Accessed 9 July 2022].

Yonemori, K., Seki, N., Kurahara, H., Osako, Y., Idichi, T., Arai, T., Koshizuka, K., Kita, Y., Maemura, K. and Natsugoe, S. (2017). <i>ZFP36L2</i>promotes cancer cell aggressiveness and is regulated by antitumor<i>microRNA-375</i>in pancreatic ductal adenocarcinoma. *Cancer Science*, 108 (1), 124-135. Available from 10.1111/cas.13119 [Accessed 7 May 2022].

Zekavati, A., Nasir, A., Alcaraz, A., Aldrovandi, M., Marsh, P., Norton, J. and Murphy, J. (2014). Post-Transcriptional Regulation of BCL2 mRNA by the RNA-Binding Protein ZFP36L1 in Malignant B Cells. *PLoS ONE*, 9 (7), e102625. Available from 10.1371/journal.pone.0102625 [Accessed 7 May 2022].

Zeman, M. and Cimprich, K. (2013). Causes and consequences of replication stress. *Nature Cell Biology*, 16 (1), 2-9. Available from 10.1038/ncb2897 [Accessed 30 April 2022].

Zhang, C., Spektor, A., Cornils, H., Francis, J., Jackson, E., Liu, S., Meyerson, M. and Pellman, D. (2015). Chromothripsis from DNA damage in micronuclei. *Nature*, 522 (7555), 179-184. Available from 10.1038/nature14493 [Accessed 5 June 2022].

Zhang, D. and O'Donnell, M. (2016). The Eukaryotic Replication Machine. *DNA Replication Across Taxa*, 191-229. Available from 10.1016/bs.enz.2016.03.004 [Accessed 7 July 2022].

Zhang, L. and Li, X. (2021). DEAD-Box RNA Helicases in Cell Cycle Control and Clinical Therapy. *Cells*, 10 (6), 1540. Available from 10.3390/cells10061540 [Accessed 17 July 2022].

Zhang, R. and Wang, J. (2018). HuR stabilizes TFAM mRNA in an ATM/p38-dependent manner in ionizing irradiated cancer cells. *Cancer Science*, 109 (8), 2446-2457. Available from 10.1111/cas.13657 [Accessed 14 May 2022].

Zhao, H. and Piwnica-Worms, H. (2001). ATR-Mediated Checkpoint Pathways Regulate Phosphorylation and Activation of Human Chk1. *Molecular and Cellular Biology*, 21 (13), 4129-4139. Available from 10.1128/mcb.21.13.4129-4139.2001.

Zheng, W., Zhang, C., Li, Y., Pearce, R., Bell, E. and Zhang, Y. (2021). Folding non-homologous proteins by coupling deep-learning contact maps with I-TASSER assembly simulations. *Cell Reports Methods*, 1 (3), 100014. Available from 10.1016/j.crmeth.2021.100014.

Zhou, B. and Elledge, S. (2000). The DNA damage response: putting checkpoints in perspective. *Nature*, 408 (6811), 433-439. Available from 10.1038/35044005 [Accessed 10 May 2022].

Zucconi, B. and Wilson, G. (2013). Assembly of Functional Ribonucleoprotein Complexes by AU-rich Element RNA-binding Protein 1 (AUF1) Requires Base-dependent and -independent RNA Contacts. *Journal of Biological Chemistry*, 288 (39), 28034-28048. Available from 10.1074/jbc.m113.489559 [Accessed 4 May 2022].